

---

Masters Theses

Student Theses and Dissertations

---

Fall 2014

## Shear behavior of high strength self-consolidating concrete in NU bridge girders

Alexander Michael Griffin

Follow this and additional works at: [https://scholarsmine.mst.edu/masters\\_theses](https://scholarsmine.mst.edu/masters_theses)



Part of the [Civil Engineering Commons](#)

Department:

---

### Recommended Citation

Griffin, Alexander Michael, "Shear behavior of high strength self-consolidating concrete in NU bridge girders" (2014). *Masters Theses*. 7328.

[https://scholarsmine.mst.edu/masters\\_theses/7328](https://scholarsmine.mst.edu/masters_theses/7328)

This thesis is brought to you by Scholars' Mine, a service of the Missouri S&T Library and Learning Resources. This work is protected by U. S. Copyright Law. Unauthorized use including reproduction for redistribution requires the permission of the copyright holder. For more information, please contact [scholarsmine@mst.edu](mailto:scholarsmine@mst.edu).



SHEAR BEHAVIOR OF HIGH STRENGTH SELF-CONSOLIDATING CONCRETE  
IN NU BRIDGE GIRDERS

by

ALEXANDER MICHAEL GRIFFIN

A THESIS

Presented to the Faculty of the Graduate School of the  
MISSOURI UNIVERSITY OF SCIENCE AND TECHNOLOGY

In Partial Fulfillment of the Requirements for the Degree

MASTER OF SCIENCE IN CIVIL ENGINEERING

2014

Approved by

John J. Myers, Advisor  
Mohamed A. ElGawady  
Dimitri Feys



## ABSTRACT

As the nation's infrastructure continues to age, advanced concrete technologies have been developed to both reduce a structure's costs and increase its life expectancy. Since the early 1990's, self-consolidating concrete (SCC) has been one of these technologies. Many, however, have been reluctant to implement SCC in highway girders due to the mixture constituents. One of these concerns is the reduced content and size of the coarse aggregate. These differences in the concrete potentially hinder SCC's mechanical properties and shear resistance. Additionally, for high strength concretes (HSC) with weaker aggregates, shear cracks tend to propagate through the coarse aggregate, reducing the aggregate interlock component of the shear resistance.

This study aimed at assessing the web-shear strength both with and without web reinforcement of two precast-prestressed Nebraska University (NU) 53 girders fabricated with high strength self-consolidating concrete (HS-SCC). The results were compared to the ACI 318 (2011) and AASHTO LRFD (2012) code estimates, and a finite element model (FEM) package, Response 2000. ATENA Engineering, a finite element analysis (FEA) program, was also used to evaluate the qualitative results, specifically crack patterns and the effect of the coarse aggregate content and size. A prestressed concrete database was also constructed to assess the effect of the reduced coarse aggregate content on the shear capacity of HS-SCC in prestressed concrete members. The mechanical properties of the HS-SCC mix were also tested and compared to relevant empirical equations. The HS-SCC mix investigated in this study proves to be a viable cost-saving alternative for bridge superstructure elements.

## ACKNOWLEDGMENTS

First and foremost, I would like to thank my advisor, Dr. John J. Myers. It has been a pleasure working on such an interesting and rewarding project under Dr. Myers. I would also like to thank the members of my committee, Dr. Mohamed ElGawady and Dr. Dimitri Feys for their review of this document.

None of the work could have been completed without the help of fellow graduate students Eli Hernandez, Hayder Alghazali, and Benjamin Gliha and undergraduate students Reed Norphy and Michael Janke. It has been a pleasure getting to know these fellow students throughout the research project. Additional thanks are necessary for Jason Cox and John Bullock of the Center for Infrastructure Engineering Studies (CIES), who helped with the preparation and removal of the test girders in the laboratory. Technical assistance was provided by Gary Abbot and Brian Swift, who were extremely valuable throughout the course of the project.

Special thanks are entitled to the Missouri S&T Office of Graduate Studies for the Chancellor's Fellowship, and the National University Transportation Center (NUTC) for the funding of this project. I would also like to thank the Missouri Department of Transportation for their valuable advice and financial support, and County Materials Corporation for the fabrication of the test girders.

To my parents Michael and Karyn, and my brother Kyle, thank you for all the support and encouragement in both my academics and athletics. And finally, a heartfelt thank you goes out to my wonderful girlfriend, Amanda, who always made sure I never worked too hard.

## TABLE OF CONTENTS

	Page
ABSTRACT .....	iii
ACKNOWLEDGMENTS .....	iv
LIST OF ILLUSTRATIONS .....	x
LIST OF TABLES .....	xiii
NOMENCLATURE .....	xiv
SECTION	
1. INTRODUCTION .....	1
1.1. BACKGROUND .....	1
1.2. RESEARCH OBJECTIVE .....	2
1.3. SCOPE AND LIMITATIONS.....	3
1.4. THESIS ORGANIZATION.....	3
2. LITERATURE REVIEW.....	5
2.1. HIGH STRENGTH SELF-CONSOLIDATING CONCRETE .....	5
2.1.1. Introduction. ....	5
2.1.2. Fresh Material Properties. ....	6
2.1.2.1 Filling ability.....	6
2.1.2.2 Passing ability. ....	6
2.1.2.3 Stability. ....	8
2.1.3. Hardened Material Properties.....	9
2.1.3.1 Compressive strength.....	10
2.1.3.2 Modulus of elasticity.....	10
2.1.3.3 Modulus of rupture. ....	11
2.2. SHEAR BEHAVIOR OF PRESTRESSED CONCRETE.....	11
2.2.1. Shear Transfer Mechanisms. ....	11
2.2.1.1 Uncracked concrete and the flexural compression zone.....	13
2.2.1.2 Interface shear transfer.....	13
2.2.1.3 Dowel action of longitudinal reinforcement. ....	13
2.2.1.4 Residual tensile stresses across cracks.....	13

2.2.1.5 Arch action.....	13
2.2.1.6 Transverse reinforcement.....	14
2.2.2. Prestress Losses.....	14
2.2.3. Modified Compression Field Theory.....	16
2.2.4. Size Effect.....	19
2.3. SHEAR TESTS ON UNREINFORCED PRESTRESSED BEAMS.....	21
2.3.1. Introduction.....	21
2.3.2. Sozen et al. (1959).....	21
2.3.3. Elzanaty et al. (1986).....	22
2.3.4. Shahawy and Batchelor (1996).....	23
2.3.5. Teng et al. (1998b).....	24
2.3.6. Myers et al. (2012).....	24
2.3.7. Conclusions.....	25
2.4. SHEAR BEHAVIOR OF HS-SCC.....	27
2.4.1. Push-Off Test.....	27
2.4.2. Mid-Scale and Full-Scale Beam Tests.....	28
2.4.2.1 Myers et al. (2012).....	29
2.4.2.2 Khayat and Mitchell (2009).....	29
2.4.2.3 Labonte (2004).....	30
2.5. NEBRASKA UNIVERSITY I-GIRDER.....	31
2.5.1. Development.....	31
2.5.2. Implementation in Missouri.....	33
2.6. CURRENT STATE OF SCC.....	34
3. GIRDER DESIGN & FABRICATION.....	37
3.1. INTRODUCTION.....	37
3.2. GIRDER DESIGN.....	38
3.2.1. Member Design.....	38
3.2.2. Mix Design.....	41
3.2.3. Materials.....	41
3.3. GIRDER FABRICATION.....	43
3.3.1. Electrical Resistive Strain Gages.....	43



3.3.1.1 Gauge description. ....	43
3.3.1.2 Installation.....	44
3.3.2. Concrete Batching and Specimen Collection. ....	45
3.3.3. Fresh Properties. ....	47
3.3.4. Storage and Delivery. ....	47
3.4. CIP DECK .....	48
3.4.1. Deck Layout. ....	48
3.4.2. Mix Design. ....	49
3.4.3. Concrete Batching and Specimen Collection. ....	51
3.4.4. Fresh Properties. ....	52
3.5. TEST SETUP .....	53
3.5.1. External Strengthening. ....	53
3.5.2. Crack Reporting Grid. ....	54
3.5.3. Test Setup. ....	55
3.5.4. Test Procedure. ....	57
4. TEST RESULTS & ANALYSIS .....	61
4.1. HARDENED MATERIAL PROPERTIES .....	61
4.1.1. Test Girders. ....	61
4.1.1.1 Compressive strength. ....	61
4.1.1.2 Modulus of elasticity.....	61
4.1.1.3 Modulus of rupture. ....	63
4.1.2. CIP Deck. ....	65
4.2. SHEAR TESTING.....	66
4.2.1. ACI. ....	66
4.2.1.1 Background. ....	66
4.2.1.2 Results.....	69
4.2.2. AASHTO.....	71
4.2.2.1 Background. ....	72
4.2.2.2 Results.....	74
4.2.3. Testing Observations.....	75
4.2.3.1 Longitudinal strain readings. ....	76

4.2.3.2 Crack documentation. ....	77
4.2.3.3 Effect of shear reinforcement on concrete contribution to shear. ....	79
4.2.3.4 Cracking moment. ....	79
4.2.3.5 Description of failure. ....	80
4.3. RESPONSE 2000 ANALYSIS .....	82
4.3.1. Introduction. ....	82
4.3.2. Results. ....	84
4.3.2.1 Shear tests with web reinforcement. ....	85
4.3.2.2 Shear tests without web reinforcement. ....	86
4.4. ATENA ENGINEERING ANALYSIS .....	87
4.4.1. Introduction. ....	87
4.4.2. Results. ....	88
4.4.2.1 Crack Patterns. ....	88
4.4.2.2 Effect of aggregate size. ....	90
4.5. EVALUATION WITH COLLECTED DATABASE .....	93
4.5.1. Introduction. ....	93
4.5.2. Results. ....	95
4.5.3. Summary of Database Results. ....	104
4.6. SUMMARY .....	105
5. SUMMARY & CONCLUSIONS .....	107
5.1. SUMMARY .....	107
5.2. FINDINGS & CONCLUSIONS .....	108
5.2.1. HS-SCC Mechanical Properties. ....	108
5.2.2. Shear Tests. ....	108
5.3. RECOMMENDATIONS .....	110
5.4. FUTURE WORK .....	110
<b>APPENDICES</b>	
A. DESIGN DRAWINGS .....	112
B. MIX DESIGNS .....	115
C. EXCEL SPREADSHEETS .....	118
D. CRACK PATTERNS AND DOCUMENTATION .....	124

E. SHEAR DATABASE .....	155
F. RESPONSE 2000.....	157
G. ATENA ENGINEERING .....	178
REFERENCES .....	183
VITA .....	190

## LIST OF ILLUSTRATIONS

Figure	Page
2.1. Mechanisms of Shear Transfer (Wight and MacGregor, 2009) .....	12
2.2. Proportions of Shear Transfer Mechanisms (Wight and MacGregor, 2009).....	12
2.3. Arch Action via Strut and Tie Model (ACI-ASCE 445, 1999) .....	14
2.4. Failure Modes for Short Shear Spans (Wight and MacGregor, 2009) .....	14
2.5. Mohr’s Circle for Prestressed Concrete at Neutral Axis (Nilson, 1987) .....	15
2.6. Equilibrium Relationships in the MCFT (ACI-ASCE 445, 1999) .....	18
2.7. Orientation of Stresses and Strains in the MCFT (Collins et al., 1996) .....	18
2.8. Stress-Strain Relationships for Cracked Concrete (Bhide and Collins, 1989) .....	19
2.9. Size Effect on Concrete Shear Strength (Kani, 1967) .....	20
2.10. Effect of Shear Span to Depth Ratio on Relative Strength (Kani, 1967) .....	20
2.11. Elzanaty et al. (1986) Investigated Cross-Sections.....	23
2.12. Teng et al. (1998b) Crack Patterns at Failure .....	25
2.13. Push-Off Test (Myers et al., 2012) .....	27
2.14. HS-SCC vs. HSC Ultimate Shear Stress (Myers et al., 2012).....	30
2.15. Pre-tensioned NU Girder (Hanna et al., 2010) .....	33
2.16. NU 53 Cross-Section (MoDOT EPG, 2011) .....	34
3.1. Test Girder Cross-Section.....	39
3.2. NU Test Girder Strand Layout.....	39
3.3. Shear Reinforcement Layout .....	40
3.4. Shear Studs in Region 3.....	41
3.5. Electrical Resistive Strain Gauge.....	43
3.6. Location of Strain Gauges .....	44
3.7. Strain Gauge Installation.....	44
3.8. Fabrication of Test Girders .....	45
3.9. Test Girder Fresh Properties .....	46
3.10. Test Girder QC/QA Specimens .....	46
3.11. Test Girder Delivery Process at Missouri S&T .....	48
3.12. CIP Deck Reinforcement Layout.....	49

3.13. CIP Deck Preparation .....	50
3.14. Test Girder CIP Deck Pour .....	51
3.15. Test Girder CIP Deck QC/QA Specimens .....	51
3.16. Tarping of CIP Deck .....	52
3.17. External Strengthening .....	53
3.18. External Strengthening Layout .....	54
3.19. External Strengthening Schematic .....	55
3.20. Crack Monitoring Grid .....	55
3.21. Test Setup Schematic .....	56
3.22. Overall Test Setup .....	57
3.23. Hydraulic Jack .....	59
3.24. Cracks in Non-Tested Region .....	60
3.25. Demolition and Removal of Test Girders .....	60
4.1. HS-SCC Test Girders Compressive Strength vs. Age .....	62
4.2. HS-SCC Modulus of Elasticity vs. Compressive Strength .....	63
4.3. HS-SCC Modulus of Rupture vs. Compressive Strength .....	64
4.4. CIP Deck Compressive Strength vs. Age .....	65
4.5. Schematic of Web-Shear and Flexure-Shear Cracking (ACI 318, 2011) .....	68
4.6. ACI Load Deflection Response for Test #1 .....	70
4.7. ACI Load Deflection Response for Test #2 .....	70
4.8. AASHTO/MoDOT EPG Load Deflection Response for Test #2 .....	75
4.9. Monitored Prestressing Tendon Strains .....	77
4.10. Crack Comparator Card .....	78
4.11. Effect of Shear Reinforcement on Concrete Contribution to Shear .....	80
4.12. Nominal Moment Capacity Analysis .....	81
4.13. Test Girders at Failure without Web Reinforcement .....	81
4.14. Shear Failure Plane .....	82
4.15. Location of Critical Section for Shear (Bentz, 2000) .....	83
4.16. Predicted Crack Widths at Failure .....	86
4.17. ATENA Crack Patterns at Failure .....	91

4.18. ATENA Relative Capacity by Varying Aggregate Size without Shear Reinforcement .....	92
4.19. ATENA Relative Capacity by Varying Aggregate Size with Shear Reinforcement .....	93
4.20. Distribution of Shear Test Results (Hawkins and Kuchma, 2007).....	94
4.21. Shear Strength Ratio vs. Compressive Strength .....	98
4.22. Shear Strength Ratio vs. Effective Depth .....	99
4.23. Shear Strength Ratio vs. Prestress Level .....	100
4.24. Shear Strength Ratio vs. CA Content by Total Weight of Aggregate .....	101
4.25. Shear Strength Ratio vs. CA Content by Total Weight of Mix .....	102
4.26. Shear Strength Ratio vs. Shear Span to Depth Ratio .....	103

## LIST OF TABLES

Table	Page
2.1. Variables Influencing the Filling Ability of SCC (ACI 237R, 2007).....	7
2.2. Variables Influencing the Passing Ability of SCC (ACI 237R, 2007) .....	8
2.3. Targets for SCC Slump Flow and J-Ring (Khayat and Mitchell, 2009).....	9
2.4. Factors Affecting Stability of SCC Mixes (ACI 237R, 2007).....	10
2.5. Khayat and Mitchell (2009) Investigated Coarse Aggregate Contents .....	31
3.1. NU Test Girders Progression of Events.....	37
3.2. ASTM Standards for Fresh Property Tests and Specimen Fabrication .....	38
3.3. Test Girder Shear Reinforcement .....	40
3.4. Test Girder HS-SCC Mix Design .....	42
3.5. Manufacturer’s Reinforcing and Prestressing Steel Mechanical Properties.....	42
3.6. Test Girder HS-SCC Fresh Properties .....	47
3.7. Test Girder CIP Deck Mix Design.....	50
3.8. TG2 CIP Deck Fresh Properties .....	52
4.1. Compressive Strength of CIP Deck .....	66
4.2. Compressive Strength of HS-SCC on Day of Shear Test.....	66
4.3. ACI Predicted Shear Capacity with Web Reinforcement.....	71
4.4. ACI Predicted Shear Capacity without Web Reinforcement.....	72
4.5. AASHTO Predicted Shear Capacity with Web Reinforcement .....	76
4.6. AASHTO Predicted Shear Capacity without Web Reinforcement .....	76
4.7. Maximum Observed Crack Widths .....	79
4.8. Observed vs. Predicted Moments .....	80
4.9. Response 2000 Concrete Properties.....	84
4.10. Comparisons with Response 2000 with Web Reinforcement.....	85
4.11. Comparisons with Response 2000 without Web Reinforcement .....	87
4.12. Concrete Material Properties for ATENA Analysis .....	89
4.13. Database Concrete Types and Geometries .....	96
4.14. Summary Table of Shear Testing without Web Reinforcement.....	106

## NOMENCLATURE

Symbol	Description
a	Depth of equivalent stress block (in.)
$a_g$	Maximum aggregate size (in.)
$A_c$	Area of concrete section (in. <sup>2</sup> )
$A_{ps}$	Area of prestressing steel (in. <sup>2</sup> )
$A_s$	Area of non-prestressing longitudinal steel (in. <sup>2</sup> )
$A_v$	Area of shear reinforcement (in. <sup>2</sup> )
$b_w$	Web thickness (in.)
$b_v$	Effective web width (in.)
c	Distance from extreme compressive fiber to neutral axis (in.)
$d_p$	Depth from extreme compression fiber to centroid of prestressing tendons (in.)
$d_s$	Distance from extreme compression fiber to centroid of non-prestressed tensile reinforcement (in.)
$d_v$	Effective shear depth, taken as the perpendicular distance between resultants of tensile and compressive forces due to flexure (in.)
$E_c$	Modulus of elasticity of concrete (psi)
$E_{ct}$	Modulus of elasticity of concrete at transfer (psi)
$E_p$	Modulus of elasticity of prestressing steel (ksi)
$E_s$	Modulus of elasticity of non-prestressing steel (ksi)
$f_c$	Specified design concrete compressive strength (ksi)
$f_{ci}$	Compressive strength of concrete at release (psi)
$f_{cgp}$	Concrete stress at centroid of prestressing steel due to prestressing force after elastic losses and member self-weight (ksi)



$f_{pc}$	Compressive stress at the centroid of the concrete section due to the effective prestress force (psi)
$f_{po}$	Locked in difference in strain between the prestressing steel and the surrounding concrete multiplied by the modulus of elasticity of the prestressing steel (ksi)
$f_{pt}$	Stress in prestressing strands immediately after transfer (ksi)
$f_r$	Modulus of rupture of concrete (psi)
$f_y$	Specified yield strength of shear reinforcement (ksi)
$f_{pe}$	Effective stress in the prestressing steel after losses (ksi)
$f_{py}$	Yield stress of prestressing steel (ksi)
$h$	Total depth of member (in.)
$H$	Relative humidity (%)
$h_c$	Total depth of composite member (in.)
$I_c$	Gross moment of inertia of composite section (in. <sup>4</sup> )
$I_g$	Gross moment of inertia of girder (in. <sup>4</sup> )
$k_f$	Factor for strength of concrete at release
$K_{df}$	Transformed section coefficient that accounts for time dependent interaction between concrete and bonded steel for time period between deck placement and final time
$k_{hc}$	Humidity factor for creep
$k_{hs}$	Humidity factor for shrinkage
$K_{id}$	Transformed section coefficient that accounts for time dependent interaction between concrete and bonded steel for time period between transfer and deck placement
$K_L$	Factor for type of prestressing steel
$k_s$	Factor accounting for V/S of concrete section

$k_{td}$	Time development factor
$M_{cr}$	Flexural cracking moment (k-ft)
$M_{cr}$	Flexural cracking moment due to applied loads (k-ft)
$M_{fl}$	Nominal moment capacity as noted in Kani (1967) (k-ft)
$M_{max}$	Maximum applied moment at section due to externally applied loads (k-ft)
$M_u$	Factored moment at section (k-ft)
$N_u$	Factored axial force at section (kips)
$P_e$	Effective prestress force (ksi)
$P_{\Delta}$	Prestress force lost due to long term prestress losses before deck placement (kips)
$r_u$	Relative strength of member
$s$	Center to center spacing of shear reinforcement (in.)
$s_x$	Cracking spacing parameter (in.)
$s_{xe}$	Equivalent value of $s_x$ taking into account the MAS
$t$	Age of specimen (days)
$t_d$	Age of concrete at deck placement (days)
$t_f$	Age of concrete at final time (days)
$t_i$	Age of concrete at transfer (days)
$V/S$	Volume to surface ratio (in.)
$V_c$	Nominal concrete shear resistance (kips)
$V_{ci}$	Nominal shear resistance when diagonal cracking results from applied shear and moment (kips)
$V_{cw}$	Nominal shear resistance when diagonal cracking results from high principle stresses in the web (kips)
$V_d$	Applied shear force at section due to unfactored dead load (kips)

$V_i$	Factored shear force at section due to externally applied loads (kips)
$V_n$	Nominal shear resistance (kips)
$V_p$	Component of prestressing force in the direction of shear force (kips)
$V_s$	Nominal shear reinforcement resistance (kips)
$V_u$	Factored shear force at section (kips)
$w$	AASHTO unit weight of concrete ( $k/ft^3$ )
$w/cm$	Water to cement ratio
$w_c$	ACI unit weight of concrete ( $lb/ft^3$ )
$\alpha$	Angle of inclination of shear reinforcement to longitudinal reinforcement (degree)
$\beta$	Factor indicating ability of diagonally cracked concrete to transmit tension
$\epsilon_{bdf}$	Concrete shrinkage strain of girder between time of deck placement and final time
$\epsilon_{bid}$	Concrete shrinkage strain of girder between time of transfer and deck placement
$\epsilon_{ddf}$	Concrete shrinkage strain of deck between placement and final time
$\epsilon_s$	Net longitudinal strain at centroid of longitudinal reinforcement
$\Delta f_{cd}$	Change in concrete stress at centroid of prestressing strands due to shrinkage of deck concrete (ksi)
$\Delta f_{cdf}$	Change in concrete stress at centroid of prestressing strands due to long term losses between transfer and deck placement combined with deck weight and superimposed loads (ksi)
$\Delta f_{pCD}$	Prestress losses due to creep of CIP deck concrete (ksi)
$\Delta f_{pCR}$	Prestress losses due to creep of girder concrete (ksi)
$\Delta f_{pES}$	Elastic shortening prestress losses (ksi)
$\Delta f_{pR1}$	Prestress losses due to relaxation of tendons before placement of CIP deck (ksi)

$\Delta f_{pR2}$	Prestress losses due to relaxation of tendons after placement of CIP deck (ksi)
$\Delta f_{pSD}$	Prestress losses due to shrinkage of concrete after placement of CIP deck (ksi)
$\Delta f_{pSR}$	Prestress losses due to shrinkage of concrete before placement of CIP deck (ksi)
$\Delta f_{pSR}$	Prestress gain due to shrinkage of CIP deck (ksi)
$\theta$	Angle of inclination of diagonal compressive stress (degrees)
$\lambda$	Reduction factor for lightweight concrete
$\phi$	Shear resistance factor
$\psi(t_1, t_2)$	Creep coefficient at time $t_1$ from due to loads applied at time $t_2$
AASHTO	American Association of State Highway and Transportation Officials
ACI	American Concrete Institute
ASTM	American Society for Testing and Materials
CA	Coarse aggregate
CC	Conventional concrete
CIP	Cast in place
CR	Creep
DOT	Department of transportation
EPG 751	Engineering Policy Guide section 751 from the Missouri Department of Transportation
FA	Fine aggregate
FEA	Finite element analysis
FEM	Finite element model
HS-SCC	High strength self-consolidating concrete

HSC	High strength concrete
HRWR	High range water reducer
HRWRA	High range water reducing admixture
LRFD	Load and resistance factored design
MoDOT	Missouri Department of Transportation
MOE	Modulus of elasticity
MOR	Modulus of rupture
MS	Mild steel shear reinforcement
NCHRP	National Cooperative Highway Research Program
NU	Nebraska University
PC/PS	Precast prestressed concrete
QC/QA	Quality control/quality assurance
R2K	Response 2000
RC	Reinforced concrete
SCC	Self-consolidating concrete
SERL	Structural Engineering Research Laboratory
SH	Shrinkage
T1	First test conducted on each girder, with shear reinforcement
T2	Second test conducted on each girder, without shear reinforcement
TG1	Test girder 1, consisting of WWR shear reinforcement
TG2	Test girder 2, consisting of MS shear reinforcement
WWR	Welded wire mesh shear reinforcement

# 1. INTRODUCTION

## 1.1. BACKGROUND

Recent catastrophes in our nation's aging infrastructure have created a desire to develop resilient concrete mix designs with advanced concrete technology for precast prestressed (PC/PS) bridges that will extend beyond the current 50 year service life.

To accomplish this goal, innovative concrete mix designs have been developed. Self-consolidating concrete (SCC) has been implemented in a number of bridge infrastructures, most notably in Japan and Europe. However, its implementation in PC/PS concrete bridges in the United States has been limited due to insufficient laboratory test data, and a general uneasiness among designers and precast fabricators.

Self-consolidating concrete has been documented to reduce both costs associated with fabrication and long-term maintenance, as well as to expedite the construction process. Since mechanical vibration is not required, there is a reduction in labor cost and a reduced risk for employee injuries. In the case of high strength self-consolidating concrete (HS-SCC), which is the focus of this study, there are additional benefits in terms of increased durability due to the low water to cement ratio and the lack of mechanical vibration.

The modifications required in the mix design to produce a flowable, nonsegregating concrete lead to reluctance in its full-scale application. Reductions in the coarse aggregate's (CA) size and proportions combined with an increase in the paste content hinder some mechanical properties: namely, the modulus of elasticity (MOE), creep (CR), and shrinkage (SH) with respect to conventional concrete (CC). The effects on these mechanical properties can lead to increased deflections and prestress losses in prestressed elements. These material modifications, coupled with a lower water to cement (w/cm) ratio, decrease the interface shear transfer contribution to the concrete's shear strength. This leads to additional concerns when using HS-SCC. This study aims at investigating the concrete contribution to shear of HS-SCC.

In recent years, the use of high strength concrete (HSC), noted as a design strength equal to or greater than 8,000 psi (55 MPa) based upon the American Concrete Institute (ACI) Committee 363 (ACI 363R, 2010), has created a demand for more

economical and efficient cross-sections for use in PC/PS concrete bridge elements. This resulted in the development of the Nebraska University (NU) cross-section at the University of Nebraska-Lincoln in Omaha, Nebraska in the early 1990's. Not only is the cross-section more suitable for HSC, but it also allows a traditional simple-span PC/PS concrete bridge to be easily transformed into a continuous structure. The Missouri Department of Transportation (MoDOT) began implementing the NU Series into their new bridge construction in 2006. To date, MoDOT has only used it in combination with traditional concrete mixtures.

The following thesis describes the fabrication, preparation, and shear testing of the NU 53 girder series constructed with HS-SCC. This study was one task of MoDOT project number TRyy1236, consisting of the full-scale implementation of HS-SCC, SCC, and high volume fly ash concrete (HVFAC) in a three span continuous PC/PS concrete bridge (Bridge no. A7957) near Linn, Missouri. Following the completion and evaluation of the shear testing, construction commenced on Bridge A7957 in the summer of 2013.

## **1.2. RESEARCH OBJECTIVE**

This research study was conducted in an attempt to assess the shear behavior of HS-SCC in a precast-prestressed concrete beam section using the NU 53 girder cross-section both with and without shear reinforcement. The ultimate shear capacity was then validated with the 2011 ACI 318 and the 2012 American Association of State Highway and Transportation Officials (AASHTO) Load and Resistance Factored Design (LRFD) Bridge Design Specifications (AASHTO LRFD, 2012) prediction equations. This study also aimed at starting a new collection of shear tests for SCC. There is limited research of the shear behavior of full-scale I-beams. A new database of I-beams with HSC will enable more accurate design equations for new construction. The next step would include modifications for differences in the concrete constituent materials (of SCC) similar to the reduction factors for lightweight concrete. Once a reliable database for SCC shear tests is established, designers will not be as reluctant to design infrastructure elements with self-consolidating concrete.

Additionally, hardened material properties for HS-SCC were investigated for compressive strength, modulus of elasticity and modulus of rupture, and compared to existing empirical equations.

### **1.3. SCOPE AND LIMITATIONS**

The results, conclusions, and recommendations in this study are applicable to precast-prestressed beam elements using the NU 53 girder series fabricated with high strength self-consolidating concrete. Furthermore, it should be noted that the results of the study are representative of the mixture constituents of the concrete. This includes the type, size, and content of the coarse aggregate in the mix design as these factors delineate HSC from HS-SCC. In addition, other HS-SCC mixes with different CA percentages and constituent materials may yield different results.

In contrast to the consistent and repeatable flexural response of reinforced and prestressed concrete members, shear failures can be quite difficult to predict due to the numerous factors that contribute to shear strength. Since it is not a fully understood concept, all prediction equations, such as the ACI 318 and AASHTO LRFD are based, at least to some extent, on empirical relationships (in contrast to the mechanics based approach for the flexural response). Thus, the test results in this study represent only one small set of data to ultimately evaluate the shear strength of HS-SCC with respect to current prediction equations. To develop a separate set of shear prediction equations or modification factors for SCC, additional test results that form a larger database are needed. This study aims to contribute to this goal to the point where SCC can be confidently implemented in both reinforced and prestressed concrete beam and column elements.

### **1.4. THESIS ORGANIZATION**

This thesis is organized into five sections. Section 1 is an introduction to the study which includes a background of SCC, the research objective, and the scope.

Section 2 contains background information necessary before the study was commenced; this includes the following subject areas: properties of HS-SCC, shear behavior of prestressed concrete, shear characteristics of HS-SCC, a review of previous



shear tests, the background and implementation of the Nebraska University I Girder, and the current state of SCC across the globe.

The girder design and fabrication process is described in Section 3. This discussion includes the girder design, fabrication process at the precast plant, delivery to the Missouri University of Science and Technology (Missouri S&T) Butler-Carlton Hall Structural Engineering Laboratory (SERL), and the design and fabrication of the cast in place (CIP) concrete deck at Missouri S&T. Both the test layout and test setup are also described.

Section 4 includes the test results and analysis with comparisons to the ACI 318 code, and AASHTO's LRFD Bridge Design Specifications. The results are also compared to the expected shear behavior using Response 2000 and ATENA Engineering. The relation of the test results to existing shear tests of prestressed concrete is also discussed. The conclusions reached in this study, as well as future research recommendations, are presented in Section 5. Appendices A through G are located at the end of this thesis, which include supplemental details and information.

## 2. LITERATURE REVIEW

### 2.1. HIGH STRENGTH SELF-CONSOLIDATING CONCRETE

**2.1.1. Introduction.** High strength self-consolidating concrete includes the benefits of SCC with the added strength gain of HSC. ACI 363R defines high strength concrete as concrete with a specified concrete compressive strength for design of 8,000 psi (55 MPa) or greater; however, this benchmark varies across the country (ACI 363R, 2010). Thus, consideration must be taken when applying design equations in the ACI 318 code and AASHTO LRFD Bridge Design Specifications as many empirical relations were developed from data with compressive strengths less than 8,000 psi (55.2 MPa) (ACI 318, 2011; AASHTO LRFD, 2012).

Self-consolidating concrete is defined as “highly flowable, nonsegregating concrete that can spread into place, fill the formwork, and encapsulate the reinforcement without any mechanical consolidation” (ACI 237R, 2007). The advantages as cited in ACI 237R are listed below. A review of the fresh and mechanical properties of HS-SCC is subsequently presented to identify the mechanical differences between traditional concrete and SCC.

- Reduced equipment and labor costs.
- Less need for screeding operations to ensure flat surfaces. This in turn can accelerate construction and reduce overall costs.
- Can be cast with desired mechanical properties independent of the skill of the vibrating crew.
- Accelerated construction.
- Facilitates filling complex formwork or members with congested reinforcement without hindering quality.
- Reduced noise pollution. Mechanical vibration can cause construction delays in urban areas due to limited construction time windows. This enables construction to continue outside of typical working hours.
- Decreased employee injuries.
- Permits more flexible reinforcement detailing and design.

- Creates smooth, aesthetically appealing surfaces free of honeycombing and signs of bleeding and discoloration. This can lead to increased durability properties.

**2.1.2. Fresh Material Properties.** The workability of SCC in the fresh state defines its uniqueness with respect to conventional concrete. The workability of SCC in the precast industry is characterized by filling ability, passing ability, and stability and is evaluated by the American Society for Testing and Materials (ASTM) standard test methods (ACI 237R, 2007).

**2.1.2.1 Filling ability.** The filling ability of SCC is described as the ability of the concrete to flow and completely fill the formwork under its own weight (ACI 237R, 2007). This characteristic differentiates SCC from conventional concrete. Adequate filling ability allows the SCC to encapsulate the formwork without any voids. The flowability of SCC is achieved through a smaller size and proportion of coarse aggregate. The addition of high range water reducers (HRWR) or superplasticizers enhances the flowability.

The slump flow test measures the filling ability of SCC (ASTM C 1611, 2009). It is analogous to the slump test for CC, with the exception that the horizontal spread is measured as opposed to the vertical slump (see Figure 3.9b). The desired slump flow is based upon the geometry and reinforcement level of the structural member. Intricate geometries and congested reinforcement require larger slump flow values. Table 2.1 lists the variables affecting the filling capacity of SCC as reported by ACI 237R (2007). If an excessively large slump flow is selected for a simple cross-section and low reinforcement level, stability and segregation issues can occur (ACI 237R, 2007). The National Cooperative Highway Research Program (NCHRP) Report 628 provides target slump flow values for various reinforcement and geometrical configurations to maintain adequate workability (Khayat and Mitchell, 2009). Slump flow values during the fabrication of the NU girders were recorded and included in this thesis.

**2.1.2.2 Passing ability.** Passing ability is defined as the ease of the concrete to pass obstacles (i.e. reinforcement) without blockage or segregation (ACI 237R, 2007). As the concrete is poured, the aggregate must flow through narrow constrictions, around congested reinforcement, and fill the voids behind the obstacle. This property is tested via the J-ring test (ASTM C 1621, 2009). The test involves a slump cone and a pegged

ring which simulates the reinforcement. The concrete is filled in the cone and allowed to flow (like the slump flow test) out and around the J-ring. The mix is visually inspected if the aggregate flows around and behind the steel pegs. The spread of concrete is then measured and recorded. Since there are obstacles obstructing the flow, the measured J-ring spread is typically less than the slump flow. Khayat and Mitchell (2009) indicated that a desired J-ring spread is approximately 2 to 4 in. (51 to 102 mm) less than the slump flow.

Table 2.1. Variables Influencing the Filling Ability of SCC (ACI 237R, 2007)

Application Variables	Influence
Reinforcement level	High reinforcement level inhibits flow
Intricacy of the element shape	Intricate shapes are more difficult to fill
Wall thickness	Narrow section inhibits flow
Placement technique	Slow, discontinuous pouring decreases placement energy
Element length	Longer distances are more difficult to fill
Mixture Variables	Influence
Fluidity (slump flow) level	High fluidity improves filling ability
Viscosity level	Viscosity that is too high can limit filling ability

The intricacy of the formwork, reinforcement level, viscosity, slump flow, and coarse aggregate size and content affect the passing ability of SCC as described in Table 2.2. NCHRP Report 628 provides suggestions for the spread from the J-ring test (Table 2.3) where shaded regions represent desired characteristics. When a SCC mix can achieve both filling ability and passing ability, the mix is said to exhibit high filling capacity (ACI 237R, 2007). A desire for adequate filling capacity necessitates a smaller size and content of coarse aggregate. However, as the coarse aggregate content declines there are drawbacks in terms of static stability, modulus of elasticity, and the aggregate interlock contribution to shear strength.

Table 2.2. Variables Influencing the Passing Ability of SCC (ACI 237R, 2007)

Application Variables	Influence
Reinforcement level	Tight reinforcement can cause aggregate bridging and blocking of concrete
Narrowing of formwork	Narrow sections in formwork can cause aggregate bridging and blocking of concrete
Mixture Variables	Influence
Fluidity (slump flow) level	Fluidity that is too low may not allow for enough deformability, while fluidity that is too high may cause instability and mixture separation
Viscosity level	Viscosity level should be gauged in light of the fluidity level
Coarse aggregate size	Larger aggregates will increase blocking tendency
Coarse aggregate content	Larger coarse aggregate content will increase blocking tendency

**2.1.2.3 Stability.** The stability of an SCC mix refers to the resistance to bleeding, segregation, and surface settlement (ACI 237R, 2007). Stability consists of both dynamic stability and static stability. Dynamic stability refers to the resistance to segregation during placement of the concrete while static stability focuses on the mix in the plastic state after placement. Segregation of the aggregate particles can affect the performance and mechanical properties of a structural member. Table 2.4 lists the factors that influence the stability of SCC. Sometimes, viscosity modifying admixtures (VMAs) are included in the mix to help maintain the stability of the mixture (ACI 237R, 2007).

Only the static stability was tested following ASTM C 1610 (2010) during the fabrication of the test girders and is briefly described. Concrete is poured into an 8 x 26 in. (203 x 660 mm) mold which is separated into 3 sections. After 15 minutes, two collector plates are inserted at the top and bottom of the column's middle section. The top and bottom sections are then washed separately through a #4 sieve, and the retained aggregate masses are then used to calculate a segregation percentage. ACI 237R (2007) recommends a maximum of 10% for the segregation column, meaning the difference

between the mass of coarse aggregate from the bottom and top sections can be no more than 10%.

Table 2.3. Targets for SCC Slump Flow and J-Ring (Khayat and Mitchell, 2009)

Relative values			Slump flow (ASTM C1611/C1611 M-05)			J-Ring (Slump flow– J-Ring flow) (ASTM C1621)		
			23.5-25 in.	25-27.5 in.	27.5-29 in.	3-4 in.	2-3 in.	≤2 in.
Element characteristics	Low	Reinforcement density						
	Medium							
	High							
	Small	Shape intricacy						
	Moderate							
	Congested							
	Shallow	Depth						
	Moderate							
	Deep							
	Short	Length						
	Moderate							
	Long							
	Thin	Thickness						
	Moderate							
	Thick							
Low	Coarse aggregate content							
Medium								
High								

Conversion: 1 in. = 25.4 mm

**2.1.3. Hardened Material Properties.** By altering the size and content of the coarse aggregate in SCC, the mechanical properties and ultimately the structural performance can be negatively affected. The following sections discuss impact of HS-SCC on the compressive strength, modulus of elasticity, and modulus of rupture.

Table 2.4. Factors Affecting Stability of SCC Mixes (ACI 237R, 2007)

Application Variables	Influence
Placement technique (drop height)	High placement energy can cause materials to separate
Reinforcement level	If concrete falls or flows through reinforcement, separation of the materials can occur
Element height	The depth of an element is proportional to its potential for aggregate settlement and bleeding
Mixture Variables	Influence
Fluidity (slump flow) level	All else held equal, as fluidity level increases, stability decreases
Viscosity level	As viscosity increases, stability increases

**2.1.3.1 Compressive strength.** The use of high range water reducing admixtures (HRWRA) in HS-SCC mixes increases the compressive strength of equivalent HSC mixes (Myers et al., 2012). The HRWR disperses the cement particles, which increases the surface area of the cement particles available for hydration. Myers et al. (2012) also noted that the effect of the HRWR increases with compressive strength. This can be attributed to the lower w/cm ratio in high strength concrete mixes. The aforementioned conclusions consisted of dolomitic limestone coarse aggregate and a CA content by weight of total aggregate of 48%, matching that used in this study. ACI 237R (2007) also notes that, for a given w/cm ratio, SCC can achieve greater compressive strength than CC due to the reduction in bleeding and segregation resulting from mechanical vibration. Without vibration, SCC can achieve a more uniform microstructure with a less porous interfacial bond zone between the paste and aggregate (ACI 237R, 2007).

**2.1.3.2 Modulus of elasticity.** An understanding of the elastic modulus of HS-SCC is necessary to more accurately predict camber, deflections, shrinkage, creep, and prestress losses in pre-tensioned and post-tensioned structural elements. The MOE of HS-SCC has typically been found to be less than that of conventional high-strength concrete. The reduction in stiffness can be attributed to the smaller percentage and size of the coarse aggregate in most HS-SCC mixes. Additionally, the larger paste content in HS-SCC theoretically leads to a reduction in the modulus of elasticity. Domone (2007)

discovered that the reduction in MOE for SCC can vary from 40% to 5% for low to high strength concretes, respectively. Various studies indicate that the AASHTO LRFD model more accurately predicts the MOE for SCC with crushed aggregate over ACI 363R and ACI 318 models (Khayat and Mitchell, 2009; Long et al., 2013). Both ACI 363R and ACI 318 tend to underestimate the modulus of elasticity (Long et al., 2013).

**2.1.3.3 Modulus of rupture.** The tensile strength of concrete can be measured in two ways: either a splitting tensile strength (STS) test and/or a modulus of rupture (MOR) test following ASTMs C 496 (2011) and C 78 (2010), respectively. The flexural strength depends on the w/cm ratio, coarse aggregate volume and the quality of the interface between the aggregate and cement paste. ACI 237R (2007) states for a given set of mixture proportions, the flexural strength of SCC may be higher. However, Myers et al. (2012) found comparable results between HSC and HS-SCC in terms of MOR testing for the mixes they investigated.

## **2.2. SHEAR BEHAVIOR OF PRESTRESSED CONCRETE**

A review of the shear behavior of prestressed concrete is discussed to obtain of better understanding of the results obtained from the shear testing of the NU 53 test girders. The methods of shear transfer for prestressed beams both with and without web reinforcement is included as well as an explanation of the need for accurate estimation of prestress losses in shear computations. This leads to a review of the modified compression field theory (MCFT), which is the basis of the 2012 AASHTO LRFD shear provisions and Response 2000. The issue of the size effect of large concrete beams and the corresponding reduction in the relative shear capacity is also discussed.

**2.2.1. Shear Transfer Mechanisms.** Concrete can resist shear in a variety of ways, both before and after diagonal cracking occurs. The 1999 ACI-ASCE 445 report cites six mechanisms which contribute to the shear strength of concrete, which include: (1) uncracked concrete ( $V_{cz}$ ), (2) interface shear transfer ( $V_a$ ), (3) dowel action ( $V_d$ ), (4) arch action, (5) residual tensile stresses, and when applicable, (6) transverse reinforcement ( $V_s$ ). Modes 1, 2, 3, and 6 are illustrated in Figure 2.1 with their average proportions in Figure 2.2. All six mechanisms of shear transfer are elaborated on in the following sections. If a member has harped prestressing tendons, the vertical component



of the prestress force also helps resist shear. This additional resistance is included separately from the concrete contribution to shear.

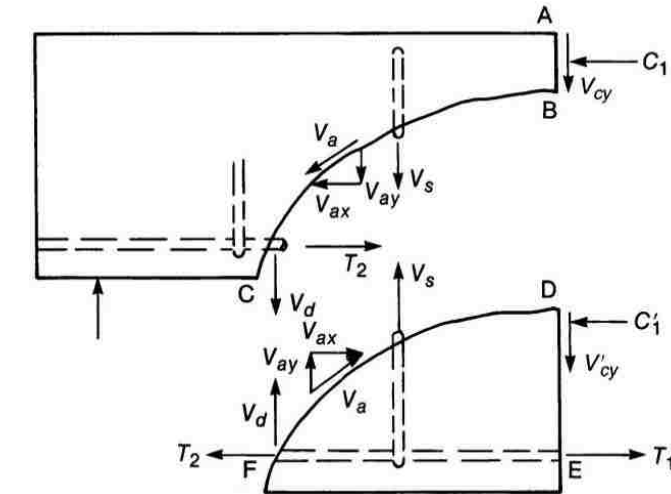


Figure 2.1. Mechanisms of Shear Transfer (Wight and MacGregor, 2009)

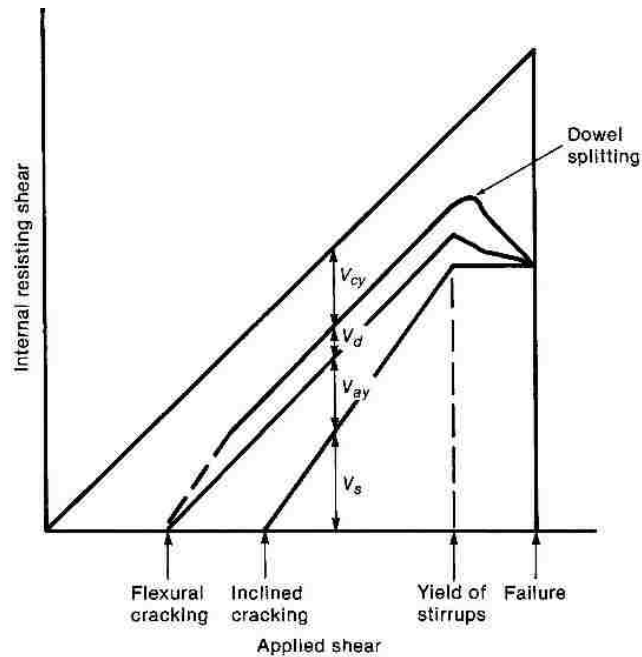


Figure 2.2. Proportions of Shear Transfer Mechanisms (Wight and MacGregor, 2009)

**2.2.1.1 Uncracked concrete and the flexural compression zone.** Shear is transferred through inclined principle tensile and compressive stresses. When the concrete has cracked, the compression block continues to resist shear.

**2.2.1.2 Interface shear transfer.** Four parameters have been identified which affect this mechanism also known as aggregate interlock. These include interface shear stress, normal stress, crack width, and crack slip (ACI-ASCE 445, 1999). In prestressed concrete, this component is amplified due to the increased normal stress from the applied prestressing. As a crack forms around the aggregate, the protruded section creates a friction force that prevents slippage of the crack. When cracks propagate through the aggregate, as is the case with many HSCs, the surface roughness still provides shear resistance for small crack widths. Thus, the material characteristics of the paste and aggregate as well as the surface conditions affect the shear resistance from the concrete.

**2.2.1.3 Dowel action of longitudinal reinforcement.** The longitudinal reinforcement provides a vertical tension force that prevents slippage of the concrete. The contribution due to dowel action can vary, depending on the amount and distribution of the longitudinal reinforcement. Dowel action produces a greater contribution for heavily reinforced beams and when the longitudinal reinforcement is distributed in multiple layers (ACI-ASCE 445, 1999).

**2.2.1.4 Residual tensile stresses across cracks.** For hairline cracks, less than 0.006 in. (0.15 mm), the concrete can still bridge tensile stresses (ACI-ASCE 445, 1999). However, this contribution is small. Additionally, the concrete can still carry tensile stress in-between the inclined cracks.

**2.2.1.5 Arch action.** Although not a direct mechanism of shear transfer, arching action can have a significant contribution to the shear strength when the shear span to depth ratio ( $a/d$ ) ratio is less than roughly 1.0 (ACI-ASCE 445, 1999). This region is also known as a disturbed region (D region), where the assumption of plane sections remains plane is not valid. This phenomenon is illustrated best through the strut and tie model with the load funneled through a compression strut to the support and the longitudinal reinforcement creating the 'tie' at the bottom of the member. The strut and tie model associated with arch action is illustrated in Figure 2.3. The potential failure modes associated with a  $a/d$  ratio less than one are illustrated in Figure 2.4.

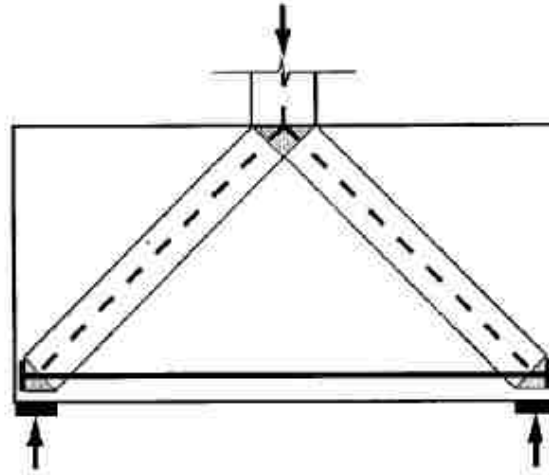


Figure 2.3. Arch Action via Strut and Tie Model (ACI-ASCE 445, 1999)

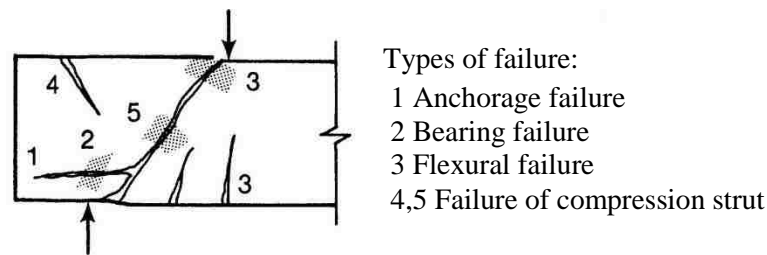


Figure 2.4. Failure Modes for Short Shear Spans (Wight and MacGregor, 2009)

**2.2.1.6 Transverse reinforcement.** The contribution of the web reinforcement was extensively investigated in the 1962 ACI-ASCE 326 report. After the formation of the first inclined crack, the shear reinforcement begins to carry a more significant portion of the shear in the form of an axial tensile force. The steel restricts both the growth and the width of the inclined crack, increasing the concrete contribution to shear in the compression zone and the interface shear transfer at the crack (ACI-ASCE 326, 1962). This trend is not accounted for in the 2011 ACI 318 and 2012 AASHTO LRFD shear provisions as the steel and concrete contributions are added together separately.

**2.2.2. Prestress Losses.** The ability to accurately predict the prestress losses can have significant effects on the predicted shear strength of a prestressed concrete member. A larger effective prestress force directly relates to a larger nominal shear strength. At the neutral axis of the member, there exists both shear and a compressive force in the

longitudinal direction. The added compressive stress creates a larger principal shear stress and an angle of inclination less than 45 degrees in the concrete element as shown in Figure 2.5.

Prestress losses are attributed to anchorage seating losses at the dead and live ends of the prestressing bed, elastic losses, and time dependent losses including shrinkage, creep, and relaxation of the prestressing strands. Anchorage seating losses are considered negligible for large prestressing beds like the one used in this study of almost 300 feet (91.4 m) (AASHTO LRFD, 2012).

Since prestress losses were not monitored in this study, a detailed estimation was conducted using the 2012 AASHTO LRFD Bridge Design Specifications refined method of Section 5.9.5.4. This method, as opposed to the lump sum method, accounts for the time dependent losses before and after a composite deck is poured. This procedure includes updates from the NCHRP Report 496 which incorporates high strength concretes up to 15 ksi (103.4 MPa). Additional research by Brewe and Myers (2010) cites a negligible difference in prestress losses between their investigated HSC and HS-SCC mixes. Schindler et al. (2007) investigated the fresh and hardened mechanical properties of a number of various SCC mixtures with dolomitic limestone. The 28 day compressive strength varied from 8,600 to 12,700 psi (59.3 to 87.6 MPa). The shrinkage strain of the SCC mixes was comparable to the control mixes (Schindler et al. 2007). Therefore, the 2012 AASHTO LRFD refined method was used for estimation of prestress losses of HS-SCC in this study.

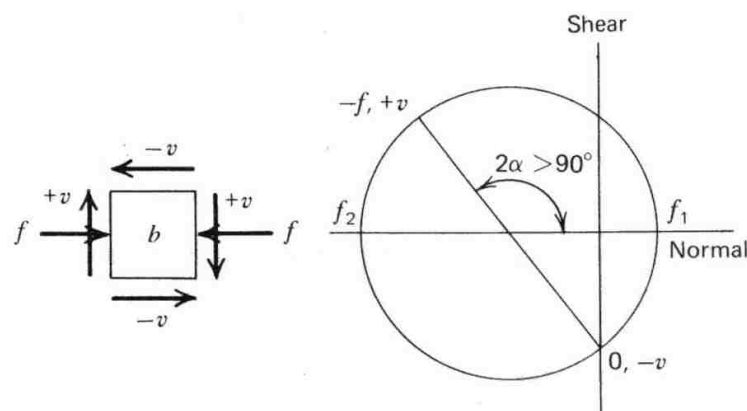


Figure 2.5. Mohr's Circle for Prestressed Concrete at Neutral Axis (Nilson, 1987)

**2.2.3. Modified Compression Field Theory.** A brief review of the MCFT is included in this section as both Response 2000 and the 2012 AASHTO LRFD Bridge Design Specifications use the MCFT to predict the shear strength. The compression field theory (CFT) is analogous to the tension field theory for steel. With steel, excessive shear forces lead to buckling in the direction of the principal compressive stress. The buckling of steel is synonymous to the diagonal cracking of concrete in the direction of the principal tensile stress. When stiffeners (in the case of steel) or shear reinforcement (with concrete) are included, the section can continue to resist load after buckling of the steel or, in this case, cracking of the concrete.

The MCFT uses the conditions of equilibrium, compatibility, and stress-strain relationships of the reinforcement and the diagonally cracked concrete to predict the shear response (Vecchio and Collins, 1986). It is identical to the compression field theory with the exception that the average stresses and strains at a section are used such that tensile stresses can be transmitted in the cracked concrete (see Section 2.2.1.4). Thus, tensile stresses can be transferred in the concrete between diagonal cracks. Equilibrium must be satisfied in terms of average stresses at the section and local stresses at a crack as illustrated in Figure 2.6 with the orientation of the principal stresses and strains shown in Figure 2.7. In the case of prestressed concrete, the initial prestressing force causes a change in the angle ( $\theta$ ) of the diagonally inclined crack (Figure 2.5). The local shear stress at a crack,  $v_{ci}$ , (units of psi) is taken empirically as a function of the crack width ( $w$ ), concrete compressive strength ( $f'_c$ ) and maximum aggregate size ( $a$ ) shown in Equation 2.1 (Vecchio and Collins, 1986).

$$v_{ci} = \frac{2.16\sqrt{f'_c}}{0.31 + \frac{24w}{a + 0.63}} \quad (2.1)$$

The crack width is a function of the principal tensile strain and the crack spacing ( $s_\theta$ ) defined in Equation 2.2 with the crack spacing parameter in Equation 2.3 (Vecchio and Collins, 1986). The parameters  $s_{mx}$  and  $s_{my}$  are the spacing of the x and y direction reinforcement which accounts for the size of the member. In Response 2000, the crack

spacing parameter is calculated following Equation 2.4 where  $c$  is the diagonal distance to the closest reinforcement,  $d_b$  is the diameter of the nearest bar, and  $\rho$  is the reinforcement ratio (Bentz, 2000).

$$w = \varepsilon_1 s_\theta \quad (2.2)$$

$$s_\theta = \frac{1}{\frac{\sin \theta}{s_{mx}} + \frac{\cos \theta}{s_{my}}} \quad (2.3)$$

$$s = 2c + 0.1 \frac{d_b}{\rho} \quad (2.4)$$

Additional constitutive relationships were derived to relate the principal tensile and compressive strains ( $\varepsilon_1$  and  $\varepsilon_2$ , respectively) to the principal stresses ( $f_1$  and  $f_2$ , respectively) at a crack. The stress strain relationships for the diagonally cracked concrete in compression and tension are illustrated in Figure 2.8. The derived models for the cracked concrete in compression and tension are listed as Equations 2.5 and 2.6 (units of psi) where  $\varepsilon'_c$  is the strain at peak uncracked compressive strength and the first term in parentheses must not exceed the uncracked compressive strength (Collins et al., 1996).

$$f_2 = \left( \frac{f'_c}{0.8 + 170\varepsilon_1} \right) \left[ \frac{2\varepsilon_2}{\varepsilon'_c} - \left( \frac{\varepsilon_2}{\varepsilon'_c} \right)^2 \right] \quad (2.5)$$

$$f_1 = \frac{4\sqrt{f'_c}}{1 + \sqrt{500\varepsilon_1}} \quad (2.6)$$

Once the principal stresses are determined at a given section along the height of the member, the corresponding moment, shear and axial force can be calculated from the equilibrium conditions from the average stresses (Figure 2.6).

The 2012 AASHTO LRFD procedure for estimating the shear strength is a simplified version of this model, using a direct procedure to calculate the inclination of the principal compressive stress ( $\theta$ ) and the  $\beta$  factor which accounts for the tensile stress that can be transmitted across a crack. The provisions also provide boundary limits for

the crack spacing parameter and net longitudinal strain for practicality and simplicity in design (AASHTO LRFD, 2012).

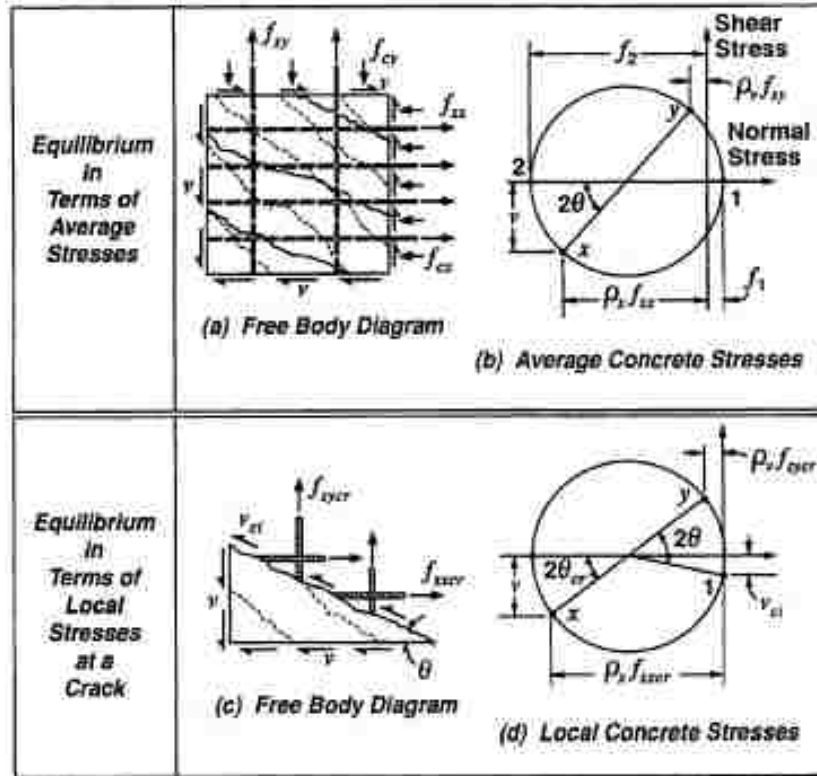


Figure 2.6. Equilibrium Relationships in the MCFT (ACI-ASCE 445, 1999)

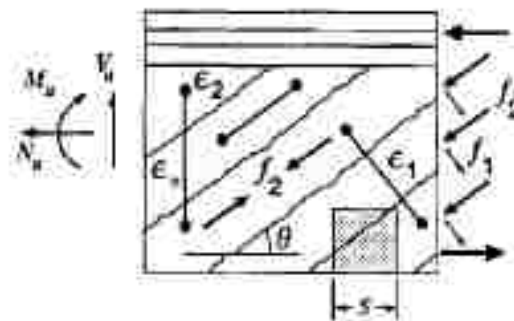


Figure 2.7. Orientation of Stresses and Strains in the MCFT (Collins et al., 1996)

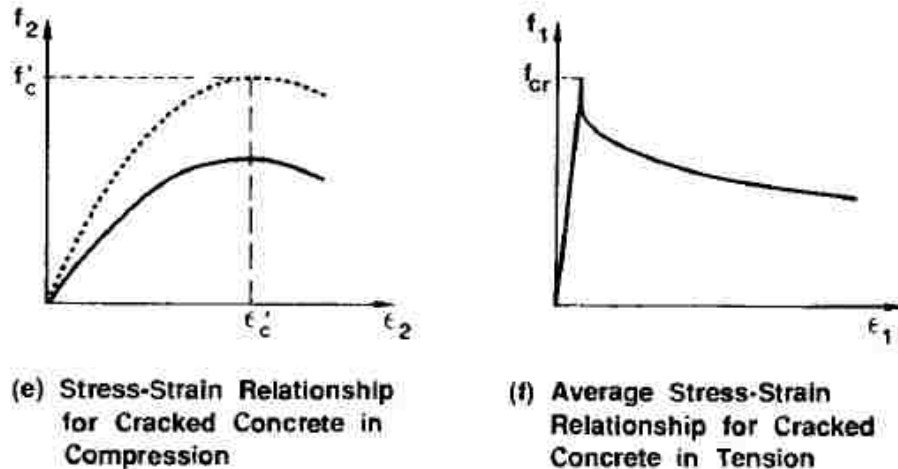


Figure 2.8. Stress-Strain Relationships for Cracked Concrete (Bhide and Collins, 1989)

**2.2.4. Size Effect.** The size effect in the shear strength of reinforced and prestressed concrete beams is described as the reduced shear stress at failure when the beam depth is increased. Kani (1967) examined this when he tested four series of reinforced concrete (RC) beams with heights of 6, 12, 24, and 48 in. (152, 305, 610, 1220 mm). All four beams had equivalent widths and longitudinal reinforcement ratios. The results of his investigation are illustrated in Figure 2.9. The failure shear stress in the large beam can be as much as 40% of the small beam at a critical  $a/d$  ratio of 3.0. As the  $a/d$  ratio increases, this difference in failure shear stress diminishes.

Kani defined the relative strength ( $r_u$ ) of the beams as the failure moment ( $M_u$ ) divided by the nominal moment capacity ( $M_n$ ) to determine the impact of increasing the beam depth. His results showed that the critical shear span to produce the lowest relative strength was approximately three times the effective depth of the member (Figure 2.10). This location is commonly referred to as the “valley of the shear failure.” The  $a/d$  ratio for the NU 53 girders was selected to create the worst case scenario for the relative strength. The actual  $a/d$  ratio in this study was constrained to the 3 ft (914 mm) spacing of the tie down locations in the strong floor of the Butler-Carlton SERL, and so the tested  $a/d$  ratio was 3.2.



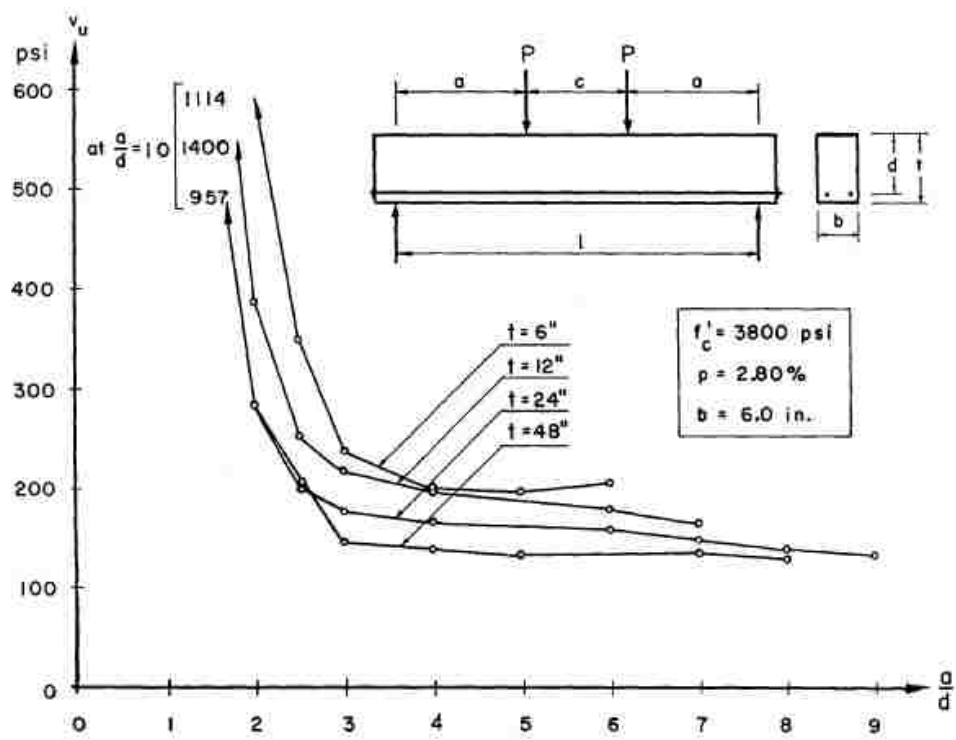


Figure 2.9. Size Effect on Concrete Shear Strength (Kani, 1967)

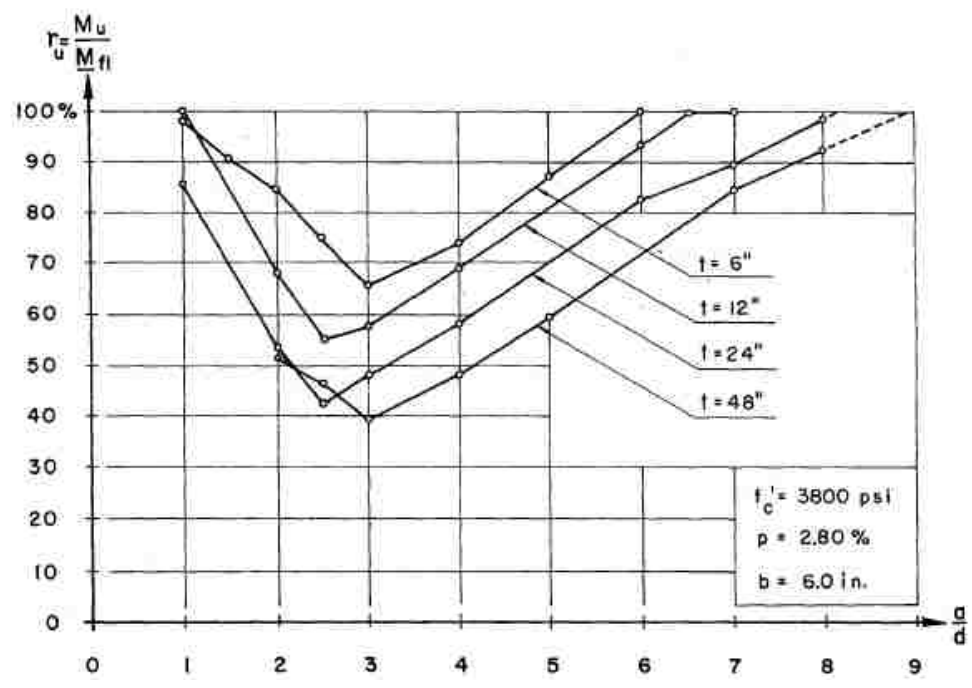


Figure 2.10. Effect of Shear Span to Depth Ratio on Relative Strength (Kani, 1967)

## 2.3. SHEAR TESTS ON UNREINFORCED PRESTRESSED BEAMS

**2.3.1. Introduction.** A review of published results of prestressed concrete shear testing for medium to large beams was conducted to more effectively evaluate the results obtained in this study. Only test results consisting of larger beams (total depth greater than 18 in. (460 mm)) and/or I-beams without web reinforcement were collected. Results from Myers et al. (2012) were also included as a benchmark for a similar HS-SCC mix. In this study, the sections containing web reinforcement were not tested to failure (see Section 3.5.4); for this reason, a literature review of shear tests containing web reinforcement was not conducted. The following researchers tested prestressed beams that were relevant to this study.

**2.3.2. Sozen et al. (1959).** The objective of their study was to obtain a better understanding of prestressed concrete beams subjected to shear failures without web reinforcement. A total of 99 pre-tensioned, post-tensioned, and non-prestressed beams without web reinforcement were tested over a 5 year period. Investigated variables included varying cross-sections, prestress levels, shear spans, longitudinal reinforcement ratios, and concrete compressive strengths. Fifty-six of the 99 beams were I shaped and of those 56, 13 contained no prestressing force and were not evaluated. Cross-sectional dimensions were 6 x 12 in. (152 x 305 mm); web widths of 3 in. and 1.75 in. (76 and 44 mm, respectively) were investigated. The coarse aggregate for all of the 43 relevant I-beams consisted of 0.375 in. (9.53 mm) maximum aggregate size (MAS) Wabash river gravel, and coarse aggregate contents ranged from 49% to 63% by weight of total aggregate. The major constituent of the river gravel was dolomite and limestone, similar to that investigated in this study. The prestressing steel consisted of single wire stress relieved strand with yield and ultimate strengths ranging from 199 to 236 ksi (1372 to 1627 MPa) and 240 to 265 ksi (1655 to 1827 MPa), respectively.

At the conclusion of their tests, they were able to identify two different methods of shear failure: shear compression and web distress. They were able to deduce that when excessive tensile stresses occurred in the web, the mode of failure included either separation of the web from the top or bottom flange, or crushing of the web due to arch action. The results of the study led to them to correlate the assumed tensile strength of the concrete ( $f_t$ ) to the cross-section ( $A_c$ ), level of prestress ( $F_{se}$ ), applied moment to cause

inclined tension cracking ( $M_c$ ), and ratio of web to flange thickness ( $b'/b$ ) shown in Equation 2.7. Albeit an empirical relationship, it was one of the first efforts to develop a mechanically based approach for the shear strength of prestressed concrete members.

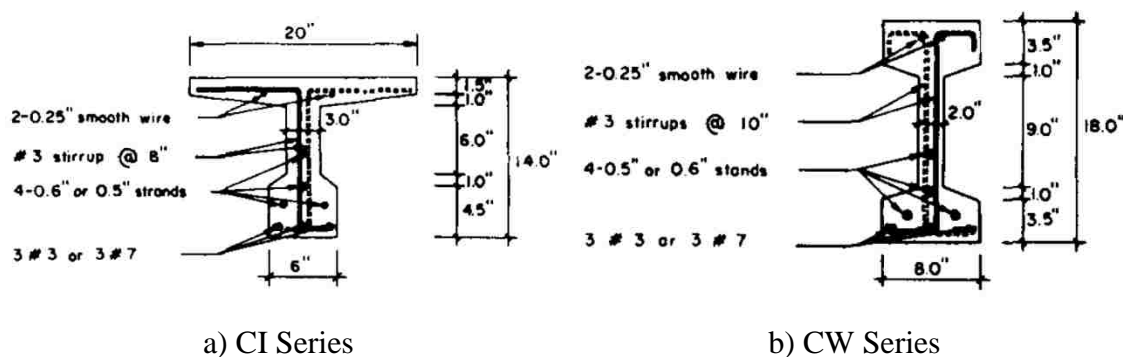
$$\frac{M_c}{f_t b d^2 \sqrt{b'/b}} = 1 + \frac{F_{se}}{A_c f_t} \quad (2.7)$$

**2.3.3. Elzanaty et al. (1986).** Elzanaty, Nilson, and Slate tested 34 prestressed I beams, 18 of which did not include web reinforcement. The focus of the study was on the shear strength of prestressed beams with compressive strengths exceeding 10,000 psi (68.9 MPa). Fourteen of the 18 prestressed beams had compressive strengths of roughly 11,000 psi (75.8 MPa). The coarse aggregate contents by weight of total aggregate of the 6,000 psi (41.4 MPa) and 11,000 psi (75.8 MPa) mixes were 48% and 56%, respectively. They designed two series, the CI (flexure-shear) and CW (web-shear) series to evaluate each component of the ACI 318 prediction equation ( $V_{ci}$  and  $V_{cw}$ , respectively). The shear span to depth ratios for the CI and CW series were 5.8 and 3.8, respectively. The cross-sections for the two series were slightly different to obtain the desired failure mode (Figure 2.11). The heights of the CI and CW series were 14 in. (356 mm) and 18 in. (457 mm), respectively with corresponding web widths of 3 in. (76.2 mm) and 2 in. (50.8 mm).

In addition to varying the concrete compressive strength and a/d ratio, the researchers also examined the influence on varying the prestressing ( $\rho_p$ ) and mild steel ( $\rho$ ) reinforcement ratios. The coarse aggregate was 0.5 in. (12.7 mm) crushed limestone with either 0.5 in. (12.7 mm) or 0.6 in. (15.2 mm) diameter Grade 270 (1861 MPa) low relaxation prestressing steel. Mild steel reinforcement bars had tested yield strengths of 63 ksi (434 MPa).

The researchers documented several observations during testing. The measured-to-predicted ratio of web shear strength (CW series) increased while the same ratio for flexural shear strength (CI series) decreased as the compressive strength was increased from 6,600 to 11,400 psi (45.5 to 78.6 MPa). Increasing the shear span to depth ratio and effective prestress force led to a reduction in the test to predicted shear strength ratio.

They also noted a decreasing effect of the flexural shear strength as the prestressed and non-prestressed longitudinal reinforcement ratios decreased; these variables are not accounted for in the prediction of flexural shear cracking strength (ACI 318, 2011).



Conversion: 1 in. = 25.4 mm

Figure 2.11. Elzanaty et al. (1986) Investigated Cross-Sections

**2.3.4. Shahawy and Batchelor (1996).** Shahawy and Batchelor investigated the shear strength of AASHTO Type II girders both with and without shear reinforcement. All of the tested girders consisted of conventional concrete. Their objective was to evaluate the recent revisions to the AASHTO approach for shear strength of prestressed concrete members. The new revisions at the time reflect the current approach in the 2012 AASHTO LRFD edition, which is based on the modified compression field theory. The researchers tested a total of 40 pre-tensioned AASHTO Type II girders ranging in length from 21 to 41 ft (6.4 to 12.5 m) with varying levels of shear reinforcement. Six of the 40 girders contained no shear reinforcement and were collected for the shear database in this study. The aggregate type was not specified; however, the maximum aggregate size was 0.75 in. (19 mm). Both 0.5 and 0.6 in. (12.7 and 15.2 mm) low relaxation tendons were investigated. The concrete compressive strength varied from 5,500 to 7,000 psi (37.9 to 48.3 MPa). A 42 in. (1.07 m) wide by 8 in. (203 mm) thick CIP deck was poured to simulate a road deck.

Shahawy and Batchelor discovered that the new LRFD method based on the MCFT was more conservative than the 1989 AASHTO specifications which are identical

to today's ACI 318 equations. They also found the LRFD method to overestimate the shear strength when the shear span to depth ratio ( $a/d$ ) was less than 1.5, but underestimate for  $a/d$  ratios greater than 2.0.

The results of Shahawy and Batchelor's study will prove to be the most valuable when comparing to the results of the HS-SCC NU test girders because of the similar height. The AASHTO Type II girder has a height of 36 in. (914 mm) compared to the 53 in. (1346 mm) height of the NU 53 series. The work by Shahawy and Batchelor contained the largest PC/PS beams without web reinforcement in the constructed database.

**2.3.5. Teng et al. (1998b).** Teng, Kong, and Poh tested 34 deep beams, 21 of which were pre-tensioned. Of the prestressed beams, 11 did not contain web reinforcement. The rectangular beams measured roughly 6 x 24 in. (150 x 600 mm) with concrete compressive strengths ranging from 5,600 to 7,000 psi (38.6 to 48.3 MPa). The results of their study were included in the database because of the larger depth. They are the second largest beams in the created database after the specimens from Shahawy and Batchelor (1996). The beams had a shorter  $a/d$  ratio between 1.1 and 1.6, and Grade 270 (1861 MPa) low relaxation tendons were used as the primary method of pretensioning with varying levels of longitudinal mild steel. Since the shear span to depth ratio was so short, the testing ceased when the diagonal compression strut failed (Figure 2.12). The shear strengths of these beams are expected to be higher than similar specimens with larger  $a/d$  ratios due to the observed arch action.

**2.3.6. Myers et al. (2012).** In Appendix A of the Myers et al. (2012) report, Sells and Myers investigated the shear strength in rectangular beams without web reinforcement using both conventional concrete and self-consolidating concrete. Design concrete compressive strengths of 6,000 and 10,000 psi (42.4 and 68.9 MPa) were studied. A total of 4 beams were fabricated, one for each concrete strength and concrete type (CC and SCC). Each beam design allowed for two shear tests, one at each end. All 8 tests were included in the database to evaluate the impact of the coarse aggregate content, and in the case of the 10 ksi (68.9 MPa) HS-SCC beam, to provide a reference point for the NU test girders. Details of the results of the Myers et al. (2012) tests are included in Section 2.4.2.1.

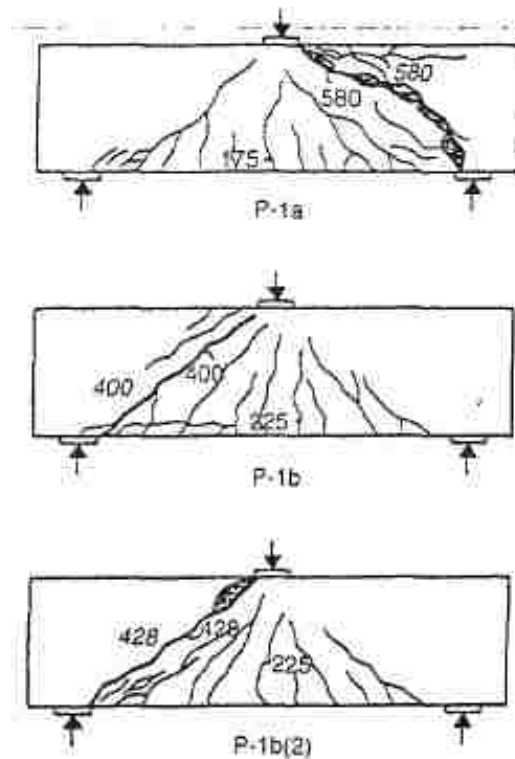


Figure 2.12. Teng et al. (1998b) Crack Patterns at Failure

**2.3.7. Conclusions.** Shear testing on full-scale girders is limited by both fabrication and transportation costs as well as the size of research laboratories across the country. For example, the NU 53 girders in this study were sized to meet the maximum capacity of the overhead crane in the Butler-Carlton Hall SERL. A number of shear tests have been conducted on full-scale girders with shear reinforcement (Haines, 2005; Nagle and Kuchma, 2007; Hawkins and Kuchma, 2007; Runzell et al., 2007; Alejandro et al., 2008; Heckman and Bayrak, 2008; Labib et al., 2013) including SCC (Khayat and Mitchell, 2009; Labonte, 2004). However, to more accurately predict the shear resistance carried by the concrete, the shear behavior of girders without web reinforcement requires additional examination.

Even after the development of a database, there still are concerns when relating laboratory tests to concrete members in the field. Hawkins and Kuchma (2007) cited six differences between shear testing of laboratory members and the actual members in the field:

- Laboratory members are generally shorter and stockier than their field counterparts. Limitations due to weight restrictions in research laboratories and lack of funding for full-scale specimens influence the design of laboratory test specimens.
- Typical laboratory testing consists of three or four point load configurations while field members are typically subjected to distributed loads. The application of point loads in the laboratory setting is often much simpler and cost-effective especially when large scale testing is completed.
- Aside from the last 10 years, the majority of laboratory specimens were constructed without shear reinforcement, while field members nearly always have web reinforcement.
- Due to the cost of fabrication and transportation related issues, laboratory specimens are typically smaller than those in the field and are tested as a simply supported member. For simplicity, these specimens are typically rectangular in cross-section. However, in the field, many structures are continuous with I-shaped beams, especially with the development of more efficient concrete cross-sections for bridge applications.
- Laboratory specimens typically have excess longitudinal reinforcement to ensure a shear failure, while field members are designed to fail in flexure. Excess reinforcement in the laboratory setting can lead to an excessive dowel action contribution to shear that is not encountered in the field.
- Field members are designed for shear across their entire length while laboratory members are designed to fail at predetermined sections.

Despite these discrepancies, the only rational approach to predicting response in the field is through laboratory testing. By testing full-scale specimens similar to those in the field, departments of transportation (DOT) can have more confidence in their designs with reliable results backing it up. Therefore, only with the funding and support from DOTs, will more efficient and economical girders be possible.

## 2.4. SHEAR BEHAVIOR OF HS-SCC

A principal reason for hesitation in the implementation of HS-SCC lies in its potential limiting shear performance. In the case of HS-SCC, modifications in the material proportions hinder the ability of the concrete to transmit shear stresses through aggregate interlock at low coarse aggregate levels. Furthermore, when weaker limestone aggregates (as in the Kim et al., 2010 study) are used in a HSC application, the failure plane can propagate through the aggregate particles, rather than at the paste-aggregate interface zone (Kim et al., 2010). Consequently, the contribution to shear strength from aggregate interlock is expected to be negatively affected in HS-SCC.

**2.4.1. Push-Off Test.** The author identified two researchers who have studied the shear response of HS-SCC in push-off tests. This is a widely recognized, most notably used by Mattock (1969 & 1972), Reinhardt (1981), and Walraven (1981 & 1994) on conventional concrete mixes (Myers et al., 2012). The test involves applying a line load through to “precrack” the specimen, followed by the “push-off” where the shear data is gathered. The horizontal slip, crack width and applied load are measured. A clamping force is applied normal to the crack to prevent excessive crack widths and is measured. Figure 2.13 illustrates the push-off test.



Figure 2.13. Push-Off Test (Myers et al., 2012)

Myers et al. (2012) discovered that the coarse aggregate fraction and concrete type (HS-SCC vs. HSC) showed little impact on the shear resistance of the specimens for



the mixes he investigated. There was a slight trend that showed reduced shear stress for a given crack opening for higher strength concretes. The smoother failure plane in the high-strength specimens explains the results. However, there was no distinguishable difference in shear stress at a given crack opening between the HS-SCC and HSC mixes for a given aggregate type. Since the only significant variable between HS-SCC and HSC is the coarse aggregate content (10% difference in Myers et al. study), the volume of coarse aggregate had a negligible effect of the observed shear stress between the two mixes in the range of aggregate contents studied. The most distinguishable findings related to the aggregate type. The limestone aggregate carried significantly less shear stress across a crack opening than the river gravel, a result of the reduced stiffness of limestone aggregates. This difference in strength of the aggregates led to the formation of cracks around the river gravel but through the limestone. Thus, the river gravel exhibited greater aggregate interlock (Myers et al., 2012).

Kim et al. (2010) observed similar trends regarding push-off tests of high and low strength SCC and CC mixes. Push-off tests revealed a decreasing contribution of aggregate interlock at high compressive strength levels, and an increased contribution of river gravel over limestone aggregates. Unlike Myers et al. (2012) study, Kim et al. (2010) found statistically significant data which showed, for the investigated aggregates, the volume of coarse aggregate influences the contribution of aggregate interlock. Additionally, the researchers noted a lower fraction reduction factor,  $c$ , and friction coefficient,  $\mu$ , for HS-SCC than HSC at maximum shear stress for the mixes investigated. The fraction reduction factor accounts for the reduced contact area at a crack due to particle fracturing. The smaller volume of coarse aggregate in HS-SCC explains this trend (Kim et al., 2010).

**2.4.2. Mid-Scale and Full-Scale Beam Tests.** There is limited evidence regarding beam shear testing on HS-SCC. In the case of SCC, there are mixed results concerning the ultimate shear capacity with respect to CC. Hassan et al. (2010) reported that RC SCC beams showed reduced shear resistance and ductility compared to their CC counterparts. Their beams consisted of 0.375 in. (10 mm) crushed limestone with coarse aggregate contents by weight of total aggregate of 49% and 61% for the SCC and CC mixes, respectively. Lin and Chen (2012) found that for an equivalent CA content, SCC

beams had increased shear resistance; however, for typical SCC beams in which the CA content is lower than a CC mix at a given compressive strength, the shear resistance was found to be less than the CC beam. Their investigated coarse aggregate contents (by weight of total aggregate) ranged from 55% for the CC beams down to 46% for the SCC beams. The aggregate type was not specified; however, the CA size was 0.375 in. (10 mm).

**2.4.2.1 Myers et al. (2012).** Myers and Sells conducted shear tests on mid-size precast-prestressed rectangular beams. The tests included high and low strength SCC and CC beams for a total of 4 specimens. The rectangular beams were 8 x 16 in. (203 x 406 mm) without web reinforcement with a span to depth ratio ( $a/d$ ) of 3.75. The percentage of coarse aggregate content for the mixes varied from 48% for SCC to 58% for CC. Locally available Missouri coarse aggregates were investigated. Due to the thick cross-section (as opposed to an I-beam), the beams were designed to fail in flexure-shear cracking. Each member was tested twice, once at each end. The SCC and HS-SCC beams experienced increased deflections over the CC beams. This could be attributed to the lower modulus of elasticity reported in the SCC mixtures. The failure loads for the HS-SCC beams exceeded the predicted failure from ACI 318 (2011), AASHTO LRFD (2007), and Response 2000 on the order of 50 to 70%. The normalized shear stress for the HS-SCC beams slightly outperformed that of the HSC mix shown in Figure 2.14. The HS-SCC mix is denoted by S10-48L, the HSC mix by C10-5L, the SCC mix by S6-48L, and the CC mix by C6-58L. The two SCC beams exhibited less variation at ultimate failure loads than the CC beams (Myers et al., 2012). This could be attributed to the casting conditions and lack of vibration of the SCC mixtures.

**2.4.2.2 Khayat and Mitchell (2009).** Full-scale structural performance testing on AASHTO Type II girders with web reinforcement was completed by Khayat and Mitchell as part of the NCHRP Report 628. Four girders were fabricated from 8,000 and 10,000 psi (55 and 69 MPa, respectively) SCC as well as CC. Both mixes contained 0.5 in. (12.7 mm) crushed aggregate with coarse aggregate contents listed in Table 2.5. The researchers noted the following in terms of shear performance:

- All four girders exceeded the nominal shear resistance according to the 2007 AASHTO LRFD specifications. However, the HS-SCC maximum shear load was 6.5% less than that of the 10,000 psi (69 MPa) CC girder.
- Both the HSC and HS-SCC girders experienced initial shear cracking at similar loads.
- The HS-SCC girders exhibited less deflection prior to shear failure compared to the other investigated mixes.

The reduced ductility and shear resistance associated with the SCC mixtures could be attributed to the reduction in coarse aggregate volume, thereby reducing the energy absorbing characteristic of aggregate interlock (Khayat and Mitchell, 2009).

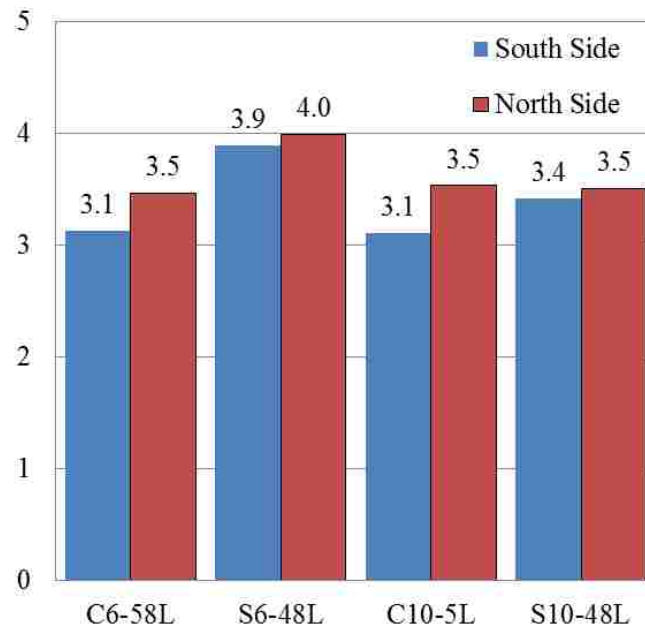


Figure 2.14. HS-SCC vs. HSC Ultimate Shear Stress (Myers et al., 2012)

**2.4.2.3 Labonte (2004).** Under the supervision of Dr. Hamilton at the University of Florida, Labonte tested a collection of AASHTO Type II girders to assess the structural performance. Two girders were fabricated to be tested in shear, one with SCC, and one with CC. Both girders were tested with shear reinforcement, and contained 0.75

in. (19.1 mm) coarse aggregate at 48% by weight of total aggregate. The type of aggregate was not specified. A HRWR was included to achieve the desired SCC fresh properties. The cylinder compressive strength at the time of the testing was 10,000 and 7,500 psi (68.9 and 51.7 MPa) for the SCC and CC girder, respectively. The researcher observed that the CC girder outperformed the SCC girder by 8.7% despite the higher compressive strength of the SCC girder. The SCC girder still exceeded ACI 318 and AASHTO LRFD estimates by at least 50% (Labonte, 2004).

Table 2.5. Khayat and Mitchell (2009) Investigated Coarse Aggregate Contents

	CC	SCC	HSC	HS-SCC
Design $f_c$ (psi)	8,000	8,000	10,000	10,000
CA Content (%)*	59	46	58	53

\*By total weight of aggregate

Conversion: 1 psi = 0.006895 MPa

## 2.5. NEBRASKA UNIVERSITY I-GIRDER

**2.5.1. Development.** The NU I-girder was developed at the University of Nebraska in the early 1990's in an effort to optimize the structural sections that are more material efficient. Standard I sections such as the AASHTO series were developed for concrete strengths lower than conventionally used in design today. More efficient and economical sections in the precast-prestressed industry could lead to longer, lighter, slender elements, reducing the number of intermediate bents, and thus reducing overall costs. Geren and Tadros (1994) developed the NU series cross-section taking into account important factors from state engineers, bridge consultants, and precast manufacturers including costs associated with:

- Concrete and accessories
- Transportation
- Prestressing steel and labor
- Cast in place deck

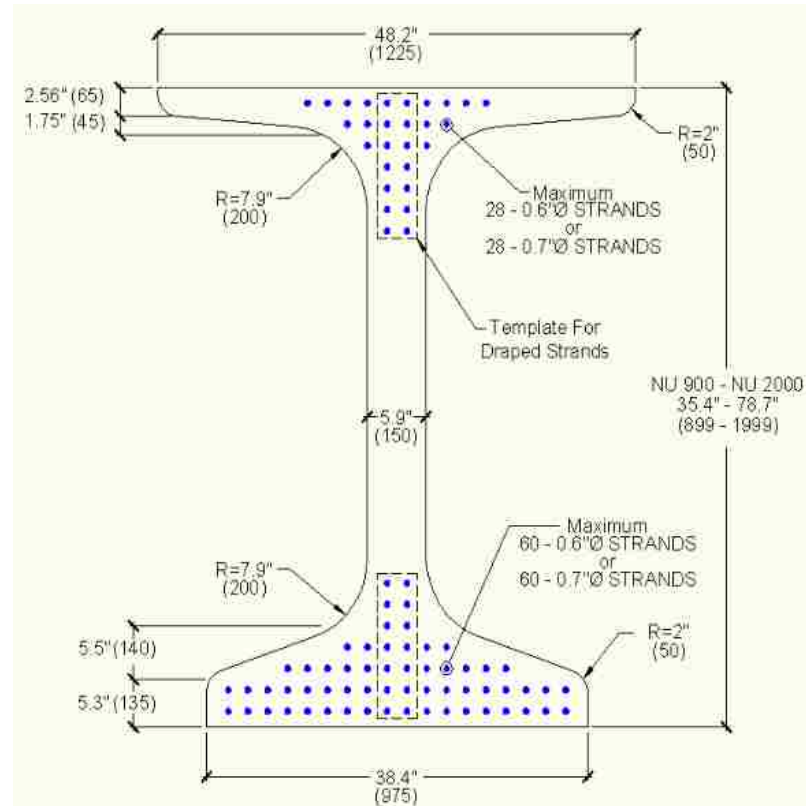
- Post tensioning
- Mild steel reinforcement

In conjunction with these ideas, Geren and Tadros focused on optimizing the I-beam for a continuous span application (others, like the AASHTO series, were designed for a simple span application). Continuity in bridges is gaining momentum to increase span lengths and to eliminate the CIP deck expansion joints which require costly maintenance.

Their parametric study resulted in a cross-section with a wider bottom flange for placement of prestressing strands and to enhance the concrete compressive strength under negative moment. With more strands placed in the bottom row (larger eccentricity), the NU girder excels when designed with high strength concrete. These factors together create a larger moment capacity leading to longer spans and wider girder spacings. The top flange was also widened to allow a smaller effective span length for the CIP deck, reducing the required deck thickness. The web was designed to accommodate a 3 in. (75 mm) post tensioning duct, two 0.5 in. (12.5 mm) draped tendons, 0.5 in. (12.5 mm) diameter stirrups, and 1 in. (25.4 mm) of concrete cover on each side; resulting in a 6.9 in. (175 mm) web. The web was reduced to 5.9 in. (150 mm) for a pre-tensioned system, and can easily be modified through form placement. Rather than sharp angles between the flanges and web as evident in the AASHTO series, all corners were designed with circular curves for an increased aesthetic appearance.

Due to the narrow web and wide bottom flange, it can be difficult to vibrate conventional concrete near the corners of the bottom flange. Therefore, SCC is a perfect match for the NU girder series to reduce the issues associated with the congested steel reinforcement in a wide bottom flange.

The complete NU girder series consists of 8 cross-sections: NU750, NU900, NU1100, NU1350, NU1600, NU1800, NU2000, and NU2400. The numbers represent the girder depth in millimeters and all models have identical web widths and top and bottom flange widths. This standardization makes it easily adaptable for precast manufacturers. The standard shape is shown in Figure 2.15.



Conversion: in. (mm)

Figure 2.15. Pre-tensioned NU Girder (Hanna et al., 2010)

**2.5.2. Implementation in Missouri.** The MoDOT specifies two types of PC/PS concrete I-girders in the design of all projects; the MoDOT Standard Girder, based off of the AASHTO series, and the NU Girder. In an effort to design more structurally efficient concrete bridges, MoDOT adopted the NU girder series in the middle of 2006 (A. Arounpradith, personal communication, January 10, 2014). Of the 8 NU models, MoDOT incorporated the NU900, NU1100, NU1350, NU1600, and NU1800 in their Engineering Policy Guide (EPG) and were relabeled to reflect U.S. customary units: NU 35, NU 43, NU 53, NU 63, and NU 70, respectively. The NU 53 investigated in this study is shown in Figure 2.16 according to MoDOT's EPG Section 751.22.1.2 (2011).

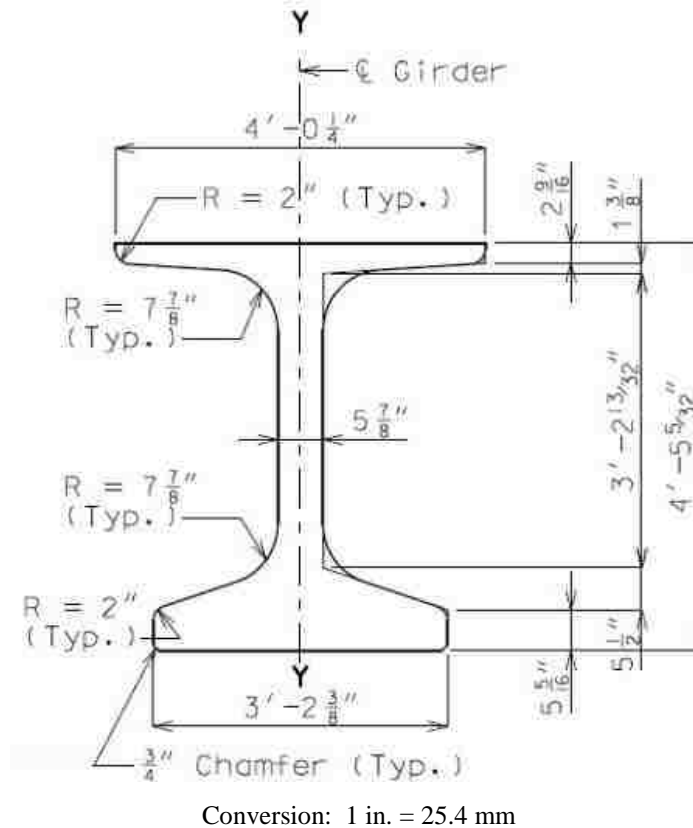


Figure 2.16. NU 53 Cross-Section (MoDOT EPG, 2011)

## 2.6. CURRENT STATE OF SCC

Since its development in Japan in the late 1980's, self-consolidating concrete has been widely implemented across Japan, Europe and the United States (EFNARC, 2005). ACI 237R (2007) cites sixteen references linked to the use of SCC in both the precast and cast-in-place industry in the United States. The production in the precast industry in the United States rose from 17,000 yd<sup>3</sup> (13000 m<sup>3</sup>) in 2000 to 2.3 million yd<sup>3</sup> (1.76 million m<sup>3</sup>) in 2003 and continues to climb to this day (ACI 237R, 2007). The use of SCC has been widespread; however, the implementation of HS-SCC in structural applications is extremely limited. Examples of the implementation of SCC include:

- **Shin-kiba Ohashi Bridge, Japan.** SCC was used in the production of the cable stay bridge towers (Okamura and Ouchi, 2003).
- **Ritto Bridge, Japan.** Due to congested steel reinforcement and the need for high earthquake resistance, SCC was chosen for the pier construction. The specified

compressive strength of the SCC mixture was 7,250 psi (50 MPa) (Ouchi et al., 2003).

- **Higashi-Oozu Viaduct, Japan.** SCC was chosen to produce the precast-prestressed T-girders to alleviate noise complaints from vibration of the concrete and to create a smoother finished surface. The specified compressive strength used in the T-girders was 7,250 psi (50 MPa) (Ouchi et al., 2003).
- **Soda Lanken Project, Sweden.** Difficulties in compaction of conventional concrete in rock lining, wall sections, and arch sections in the tunnel led to project managers choosing SCC. The decision also provided an increased aesthetic appearance. The 28 day cube compressive strength ranged from 10,000 to 11,600 psi (70 to 80 MPa) (Ouchi et al., 2003).
- **Pedestrian Bridges, Rolla, Missouri.** An implementation project comparing the use of HSC and HS-SCC in two pedestrian bridges was conducted in Rolla, MO. Both the hardened properties and time-dependent deformations were studied via load tests (Myers and Bloch, 2011).
- **Bridge A7957, Highway 50, Osage County, Missouri.** A three span precast-prestressed continuous bridge was constructed during the second half of 2013. Each span was designed with a different mix design: span one consisted of 8,000 psi (55.2 MPa) conventional concrete, span two of 10,000 psi (68.9 MPa) HS-SCC, and span three of 8,000 psi (55.2 MPa) SCC. The bridge is the first of its kind in Missouri. The study presented in this thesis was performed for MoDOT prior to the construction of this bridge.
- **Tauranga Harbour Link, Tauranga, New Zealand.** Self-consolidating concrete was chosen to expand the multi-span existing bridge at the Port of Tauranga. The expansion was completed in 2009. SCC was chosen to achieve the goal 100 year design life in a harsh marine environment. Durability models predicted a useful design life ranging from 103 to 156 years depending on the structural element and level of clear cover. The design strength of the pretensioned beams was 8700 psi (60 MPa); however, to achieve the desired durability properties, the two SCC mix designs developed for the project had 28 day cylindrical compressive strengths of 10,400 psi and 12,600 psi (71.5 and 87.0



MPa), respectively. By exploiting HS-SCC's durability and constructability properties, the cost advantage for the design build team was 20% of the bid price, roughly \$20 million dollars. This project provides a prime example of the cost savings associated with SCC (McSaveney et al., 2011).

### 3. GIRDER DESIGN & FABRICATION

#### 3.1. INTRODUCTION

Two girders were investigated, identified as test girder 1 (TG1) and test girder 2 (TG2), and both welded wire reinforcement (WWR) and mild steel (MS) bars were examined as the primary method of shear reinforcement in half of each girder. The first test was conducted on the half with web reinforcement, noted by T1, with the second test, noted by T2, conducted on the portion without web reinforcement. The girders were fabricated at County Materials Corporation in Bonne Terre, Missouri. After delivery to the SERL in Butler-Carlton Hall at Missouri S&T, a 6 in. (152 mm) thick composite cast-in-place (CIP) deck was poured to simulate a road deck. Table 3.1 describes the progression of activities that occurred from fabrication through testing.

Table 3.1. NU Test Girders Progression of Events

Description of Activity	Date
Fabrication of TG1 and TG2	3/8/2013
Delivery of TG1 to Missouri S&T SERL	3/20/2013
CIP deck poured	3/28/2013
Testing of reinforced shear region (TG1-T1)	4/22/2013
Testing of unreinforced shear region (TG1-T2)	4/29/2013
Demolition and removal of TG1	5/2/2013
Delivery of TG2 to Missouri S&T SERL	5/8/2013
CIP deck poured	5/10/2013
Testing of reinforced shear region (TG2-T1)	5/24/2013
Testing of unreinforced shear region (TG2-T2)	6/3/2013
Demolition and removal of TG2	6/4/2013

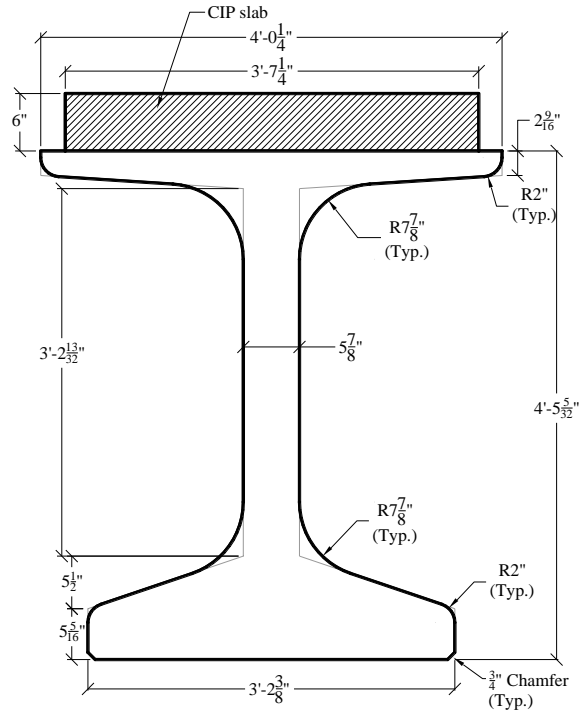
Quality control/quality assurance (QC/QA) specimens (cylinders and MOR beams) were collected during the fabrication of the girders and CIP deck. Table 3.2 lists the ASTM standards followed during specimen collection and performing necessary fresh property tests. ASTM C 31 (2012) includes requirements for rodding the concrete and tapping the sides of the mold during specimen fabrication. In the case of HS-SCC, the molds were only tapped to release entrapped air.

Table 3.2. ASTM Standards for Fresh Property Tests and Specimen Fabrication

		ASTM	Mix
Specimen Collection	QC/QA cylinders	C 31	Deck, HS-SCC
	MOR beams	C 31	Deck, HS-SCC
Fresh Properties	Slump	C 143	Deck
	Air content	C 231	Deck, HS-SCC
	Segregation column	C 1610	HS-SCC
	Slump flow test	C 1611	HS-SCC
	Passing ability (J-ring)	C 1621	HS-SCC

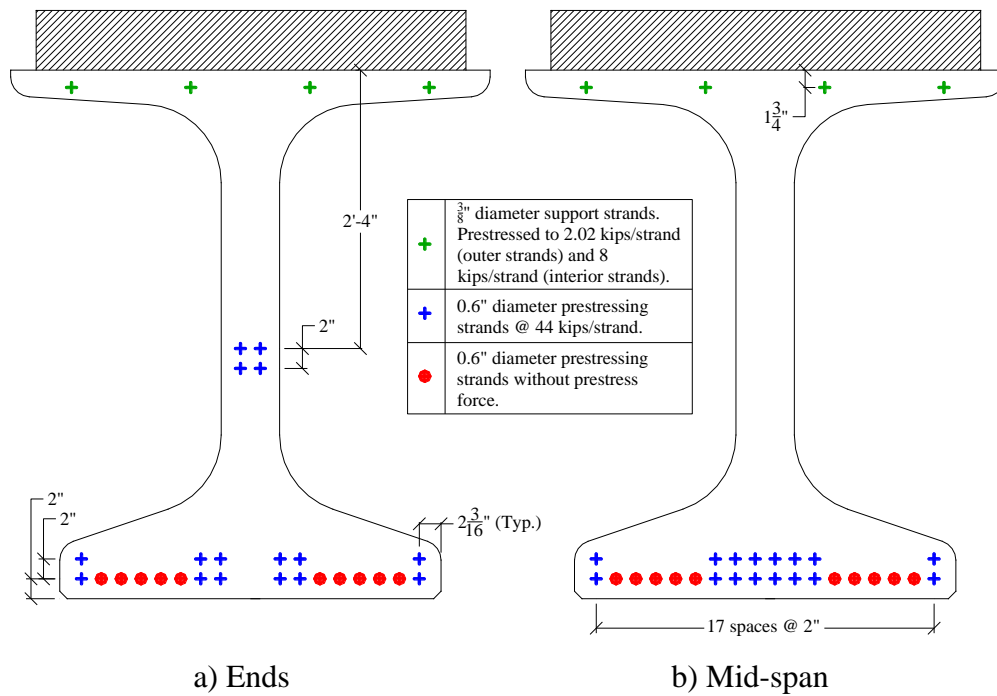
## 3.2. GIRDER DESIGN

**3.2.1. Member Design.** The girders were designed by the research team at Missouri S&T. The cross-section and material properties in span 2 of Bridge A7957 (see Section 1.1) were used for the test girders. Both girders were 40 ft.-10 in. (12.4 m) long, with sixteen 0.6 in. (15.2 mm) Grade 270 (1,862 MPa) low-relaxation prestressed tendons, 4 of which were harped. An additional 10 strands were added for increased flexural resistance. To prevent excessive tensile stresses in the top concrete fibers at release, these additional strands were not prestressed. Figure 3.1 and Figure 3.2 illustrate the cross-sectional dimensions and strand arrangements of the test girders.



Conversion: 1 in. = 25.4 mm

Figure 3.1. Test Girder Cross-Section



a) Ends

b) Mid-span

Conversion: 1 in. = 25.4 mm, 1 kip = 4.448 kN

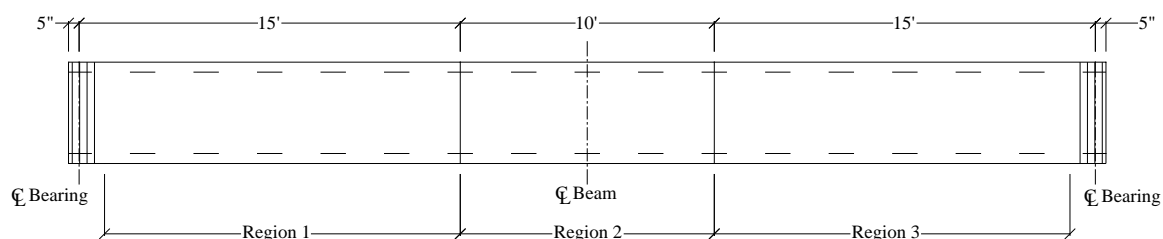
Figure 3.2. NU Test Girder Strand Layout

Each girder had three distinct sections of shear reinforcement described in Table 3.3 and illustrated in Figure 3.3: a middle 10 ft. (3.05 m) region and two 15 ft. (4.57 m) end regions. A central 10 ft. (3.05 m) region of shear reinforcement was added (Table 3.3) to prevent any possible shear failure during testing outside of the “test region.” Test girder 1 consisted of welded wire reinforcement and TG2 contained mild steel bars as the primary method of shear reinforcement. Four pairs of #6 (no. 19) mild steel bars were used within the bearing regions of the test girders. In order for the girder to act as a composite section with the CIP slab, shear studs were installed at 8 in. (203 mm) on center (o.c.) in region 3 as shown in Figure 3.4. Each end region was tested in shear, and external strengthening was provided in the non-tested region during each test. Design drawings provided by MoDOT are located in Appendix A.

Table 3.3. Test Girder Shear Reinforcement

Welded Wire Reinforcement (TG1)						
Region 1			Region 2			Region 3
Bar Size	Spacing	Length	Bar Size	Spacing	Length	No Shear Reinforcement
D20	12"	14'-0"	D20	4"	10'-0"	
Mild Steel Bars Reinforcement (TG2)						
Region 1			Region 2			Region 3
Bar Size	Spacing	Length	Bar Size	Spacing	Length	No Shear Reinforcement
#5	24"	14'-0"	#5	12"	10'-0"	

Conversion: 1 in. = 25.4 mm



Conversion: 1 in. = 25.4 mm

Figure 3.3. Shear Reinforcement Layout



Figure 3.4. Shear Studs in Region 3

**3.2.2. Mix Design.** The mix design for the girders is presented in Table 3.4. The coarse aggregate content for this mix is 48% by weight of total aggregate. Previous investigations at Missouri S&T on development of SCC mixes for MoDOT specified a minimum coarse aggregate content of 48% to preserve stability and mechanical properties of SCC (Myers et al., 2012). Therefore, for this project, the project specifications included this minimum coarse aggregate content requirement. The mix had a 28 day design compressive strength of 10,000 psi (68.9 MPa) and a target release strength of 8,000 psi (55.2 MPa). The target air content was 5.0%. The material constituents and chemical admixtures are included in Appendix B.

**3.2.3. Materials.** A combination of mild steel, welded wire reinforcement, and prestressing steel was used in the test girders. Grade 60 (414 MPa) mild steel was used in both girders at the bearing locations as well as for web reinforcement in test girder 2 (AASHTO M 31, 2007; ASTM A 615, 2012). Welded wire reinforcement was used in test girder 1 for shear reinforcement conforming to AASHTO M 221 (2009) (ASTM A 1064, 2012). Grade 270 (1861 MPa) low relaxation prestressing tendons were

used as the primary method of prestressing as well as for additional non-prestressed longitudinal steel for additional flexural capacity (AASHTO M 203, 2012; ASTM A 416, 2012a). Table 3.5 lists the manufacturer's standard strength properties of steel.

Table 3.4. Test Girder HS-SCC Mix Design

Type	Material	Weight (lb/yd <sup>3</sup> )
Coarse Aggregate	Leadbelt 1/2" Dolomite	1340
Fine Aggregate	Mississippi River Sand	1433
Cementitious Material	Portland Cement Type I	850
Water	--	280
Chemical Admixtures	Air Entraining Agent	17 oz/yd <sup>3</sup>
	High Range Water Reducer	76.5 oz/yd <sup>3</sup>
	Retarder	25.5 oz/yd <sup>3</sup>
w/cm	--	0.329

Conversions: 1 in. = 25.4 mm, 1 lb/yd<sup>3</sup> = 0.5933 kg/m<sup>3</sup>, 1.0 oz/yd<sup>3</sup> = 0.03708 kg/m<sup>3</sup>

Table 3.5. Manufacturer's Reinforcing and Prestressing Steel Mechanical Properties

Component	Yield Strength (ksi)	Ultimate Strength (ksi)	Modulus of Elasticity (ksi)
Mild Steel Bars	60	90	29000
Welded Wire Reinforcement	70	80	29000
Grade 270 Low-Relaxation Tendons	243	270	28500

Conversions: 1 ksi = 6.895 MPa

### 3.3. GIRDER FABRICATION

The test girders were fabricated at County Materials Corporation in Bonne Terre, Missouri on March 8, 2013. The following sections describe the actions taken by Missouri S&T and County Materials Corporation during the fabrication of the test girders.

**3.3.1. Electrical Resistive Strain Gages.** Two strain gauges were installed on the bottom two rows of prestressing tendons to monitor the longitudinal strain during testing. The following two sections describe the gauge and the installation process.

**3.3.1.1 Gauge description.** A linear strain gauge, model EA-06-125BT-120-LE by Micro Measurements, was used in the test girders. The gauge has a constantan foil with a tough, flexible, polyimide backing, with pre-attached leads and encapsulation. The gauge has a resistance of  $120 \pm 0.15\%$  ohms and a usable temperature range of  $-100^{\circ}$  to  $+350^{\circ}\text{F}$  ( $-75^{\circ}$  to  $+175^{\circ}\text{C}$ ). The gauge has an overall length of 0.37 in. (9.4 mm) and an overall width of 0.16 in. (4.1 mm). Two gauges were applied to each girder at mid-span: one on each of the two bottom rows of prestressed tendons. The gauges were used to monitor the stress in the prestressing tendons during the course of the shear testing. The gauge is shown in Figure 3.5 prior to installation.



Figure 3.5. Electrical Resistive Strain Gauge



**3.3.1.2 Installation.** The strain gauges were adhered onto the bottom two layers of prestressing tendons at mid-span of each test girder as shown in Figure 3.6. A standard M-Coat F Coating Kit by Vishay Measurements was used to adhere and protect the gauges from the concrete. The tendons were sanded, wiped clean, and then applied with Teflon<sup>®</sup> tape and a rubber sealant. The leads were then soldered to the electrical wire. A neoprene rubber dough material was molded around the gauge and subsequently wrapped with aluminum tape. A final transparent layer of a nitrile rubber coating was added around the aluminum tape for additional protection from moisture. The complete installation of the gauges is illustrated in Figure 3.7.

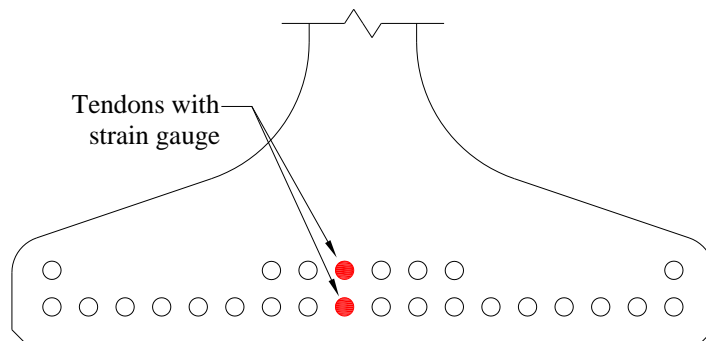


Figure 3.6. Location of Strain Gauges



Figure 3.7. Strain Gauge Installation

**3.3.2. Concrete Batching and Specimen Collection.** The test girders were poured consecutively in four continuous batches; TG2 was batched first with TG1 batched second as shown in Figure 3.8. Air content (ASTM C 231, 2010), slump flow (ASTM C 1611, 2009), and passing ability (J-ring) (ASTM C 1621, 2009) were performed on batches 1 and 3 (Figure 3.9). A segregation column was performed on the first batch.

Quality control/quality assurance specimens were collected for testing of hardened concrete properties through the concrete maturing process as well as on shear test days. Eighteen 4 x 8 in. (100 x 200 mm) cylinders and eight modulus of rupture beams measuring 6 x 6 x 24 in. (150 x 150 x 600 mm) were collected (Figure 3.10). All 18 cylinders were sampled from batch 1, while the modulus of rupture beams were split between batches 1 and 3 for each representative girder. The lower air content in batch 3 could indicate a higher compressive strength than that tested by the cylinders from batch 1. The girders and QC/QA specimens were steam cured at 120°F (49°C) for approximately 72 hours alongside the girders. Specimens were then stored at the Missouri S&T SERL until testing.



Figure 3.8. Fabrication of Test Girders



a) J-Ring (Passing Ability)



b) Slump Flow



c) QC/QA Cylinders and Segregation Column

Figure 3.9. Test Girder Fresh Properties



a) MOR Beams



b) Cylinders

Figure 3.10. Test Girder QC/QA Specimens

**3.3.3. Fresh Properties.** Air content, slump flow, and passing ability were performed on the first and third batches, and a static segregation test was run on the first batch. Fresh properties were recorded for batches 1 (TG2) and 3 (TG1) and are displayed in Table 3.6. The air content from the third batch is 2% less than from the first batch. Thus, the concrete strength in TG1 could be greater than that tested from the QC/QA cylinders collected from the first batch on TG2. The segregation percentage of 7.4% performed on batch 1 meets the ACI 237R (2007) maximum recommended value of 10.0%. Above this threshold, excessive segregation can hinder mechanical properties including compressive strength and modulus of elasticity.

Table 3.6. Test Girder HS-SCC Fresh Properties

		Batch 1 (TG2)	Batch 3 (TG1)
Air		6.3%	4.2%
Slump Flow (in.)		24.5	25
J-Ring (in.)		22	25
Concrete Temp. (°F/°C)		65/18	65/18
Air Temp. (°F/°C)		51/11	51/11
Segregation Column	Top (lb.)	6.14	N/A
	Bottom (lb.)	6.61	N/A
	S (%)	7.4	N/A

Conversions: 1 in. = 25.4 mm, 1 lb. = 0.4536 kg

**3.3.4. Storage and Delivery.** The test girders were stored at the precast plant storage yard at County Materials Corporation until delivered to the Butler-Carlton Hall SERL at Missouri S&T.

The girders were delivered to Missouri S&T on a semi tractor-trailer bed. Test girder 1 was delivered on March 20, 2013, and test girder 2 was delivered on May 8, 2013. Figure 3.11 illustrates the delivery process at Missouri S&T.

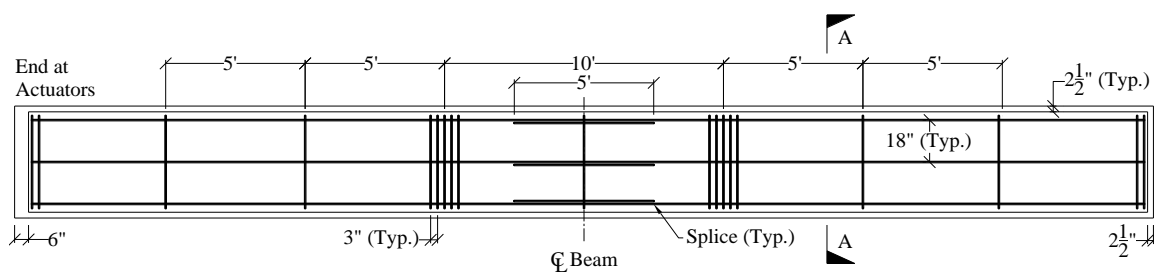


Figure 3.11. Test Girder Delivery Process at Missouri S&T

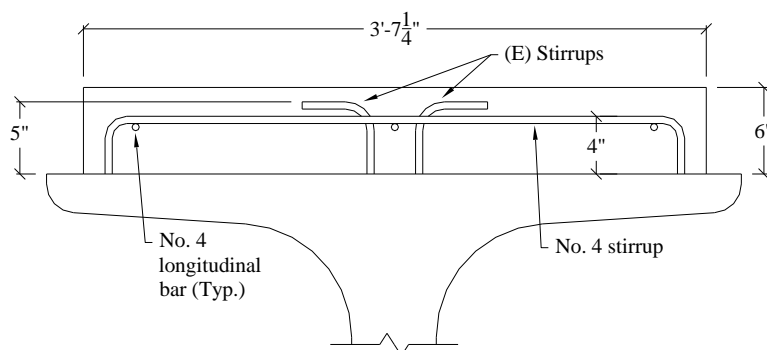
### 3.4. CIP DECK

**3.4.1. Deck Layout.** The deck was 6 in. (152 mm) thick and spanned the entire width of the top flange (minus the thickness of the formwork) for a total width of 43.25 in. (1.10 m). The longitudinal reinforcement included three #4 (no. 13) bars with a 5 ft. (1.52 m) splice at mid-span. Five #4 (no. 13) stirrups were placed at third points of the

girder to support the longitudinal reinforcement. Two #4 (no. 13) stirrups were placed at each end with two intermediate stirrups. Clear cover for the reinforcement was 1.5 in. (38 mm) on all sides and 1.0 in. (25 mm) on the top. The deck reinforcement layout is shown in Figure 3.12 with the formwork in Figure 3.13.



a) Plan



b) Section A-A

Conversion: 1 in. = 25.4 mm

Figure 3.12. CIP Deck Reinforcement Layout

**3.4.2. Mix Design.** The deck mix design was based off of MoDOT's modified B-2 mix, identification no. 12CDMB2A087 to replicate the type of concrete deck mix that would be used in the field. The deck mixes were batched by Ozark Ready Mix Company, Inc. of Rolla, Missouri. The mix design for both girder decks is shown below in Table 3.7; amounts in () indicate values used in test girder 2 deck mix. The mix had a design w/cm ratio of 0.37 with a target air content and slump of 6.0% and 6.0 in. (152

mm), respectively. The mix has a target 28 day compressive strength of 4,000 psi (27.6 MPa).



Figure 3.13. CIP Deck Preparation

Table 3.7. Test Girder CIP Deck Mix Design

Type	Material	Weight (lb/yd <sup>3</sup> )
Coarse Aggregate	Jefferson City 1" Dolomite	1895
Fine Aggregate	Missouri River Sand	1170
Cementitious Material	Portland Cement Type I	450
	Fly Ash Type C	150
Water	--	220
Chemical Admixtures	Air Entraining Agent	4.6 (6.2) oz/yd <sup>3</sup>
	Mid-Range Water Reducer	60 oz/yd <sup>3</sup>
w/cm	--	0.37

Conversions: 1 in. = 25.4 mm, 1 lb/yd<sup>3</sup> = 0.5933 kg/m<sup>3</sup>, 1.0 oz/yd<sup>3</sup> = 0.03708 kg/m<sup>3</sup>

**3.4.3. Concrete Batching and Specimen Collection.** The decks were poured on March 29, 2013 and May 10, 2013 for TG1 and TG2, respectively. Figure 3.14 shows representative images of the pours at the SERL in Butler-Carlton Hall at Missouri S&T. Twenty one 4 x 8 in. (100 x 200 mm) cylinders were collected for compressive strength testing as illustrated in Figure 3.15.



a) CIP Deck Pour

b) Finishing of CIP Deck

Figure 3.14. Test Girder CIP Deck Pour



Figure 3.15. Test Girder CIP Deck QC/QA Specimens



After pouring, the deck was tarped for 14 days (Figure 3.16). The QC/QA cylinders were also placed beneath the tarp to simulate the curing conditions of the deck. Due to time constraints for testing in the laboratory, the second test girder deck was tarped for only 7 days and then subsequently coated with a transparent paint sealant to lock in moisture. Without the tarp in place for the second week, the preparation time of the second test girder was accelerated.



Figure 3.16. Tarping of CIP Deck

**3.4.4. Fresh Properties.** Fresh properties were collected for the CIP deck which was poured on each test girder; however, the fresh properties were not recorded from the first pour. Table 3.8 lists the fresh properties from the CIP deck on TG2.

Table 3.8. TG2 CIP Deck Fresh Properties

Air Temp. (°F/°C)	65/18
Concrete Temp.	not recorded
Air Content (%)	12.0
Slump (in.)	6.5

Conversion: 1 in. = 25.4 mm

### 3.5. TEST SETUP

After curing of the CIP deck, additional testing preparation was completed. This included the application of external strengthening and preparation of a grid for crack documentation. The test setup and procedure are also discussed in this section.

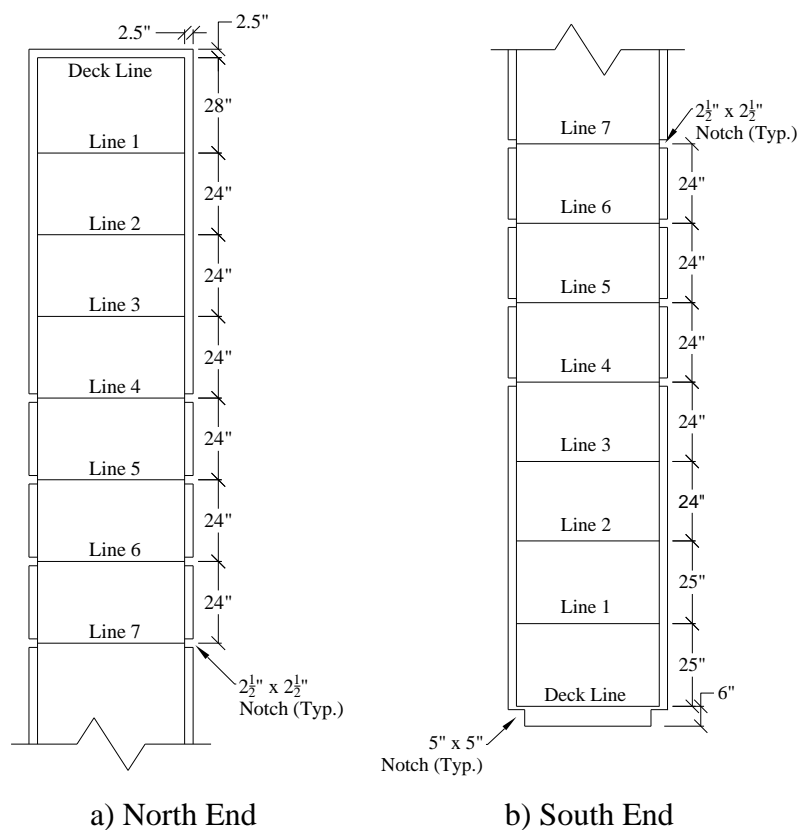
**3.5.1. External Strengthening.** After the tarp was removed from the test girder, external strengthening was applied to the girder in the non-tested region (Figure 3.17). This task was completed to prevent potential damage to the non-tested region while the active test region on the other side of the member was tested. Since the shear reinforcement spacing in the middle 10 ft. (3.05 m) – see Table 3.3 – was half or less than that in the tested region (i.e. additional shear reinforcement), external strengthening was not applied in the central region. External strengthening was applied approximately every 2 ft. (610 mm) from the adjacent support as indicated in Figure 3.18 and was manually tightened. Notches were cut in the top flange of the girder for the actuators and Dywidag bars.



Figure 3.17. External Strengthening

Each stiffener line consisted of a top and bottom beam, consisting of two C-Shape channel sections welded together by 0.5 in. (12.7 mm) thick plates. Stiffeners were also welded to the channels to prevent a buckling failure of the web. They were connected by two #14 (no. 43) Dywidag bars with a yield strength of 75 ksi (517 MPa). The channel

sections ranged in from size C10x30 towards the middle of the girder to size C15x50 at the supports. A schematic of the strengthening system is shown in Figure 3.19 with the stiffener schedule located in Appendix C.



Conversion: 1 in. = 25.4 mm

Figure 3.18. External Strengthening Layout

**3.5.2. Crack Reporting Grid.** The test regions in each girder were painted white, and an 8 x 8 in. (200 x 200 mm) grid was drawn as illustrated in Figure 3.20. Column gridlines were labeled 1 through 25 and row gridlines were labeled A through J. The paint allowed for cracks to be observed more readily as formation occurred. The grid allowed the crack formation to be reproduced more easily and accurately. The cracks were traced in AutoCAD and are included in Appendix D.

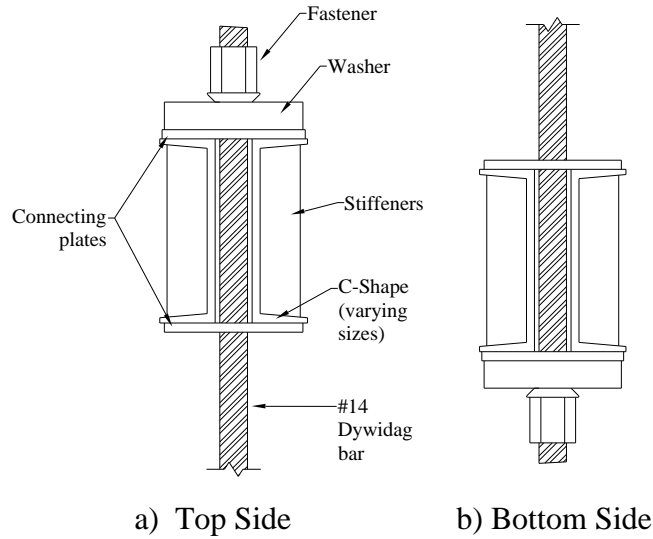


Figure 3.19. External Strengthening Schematic

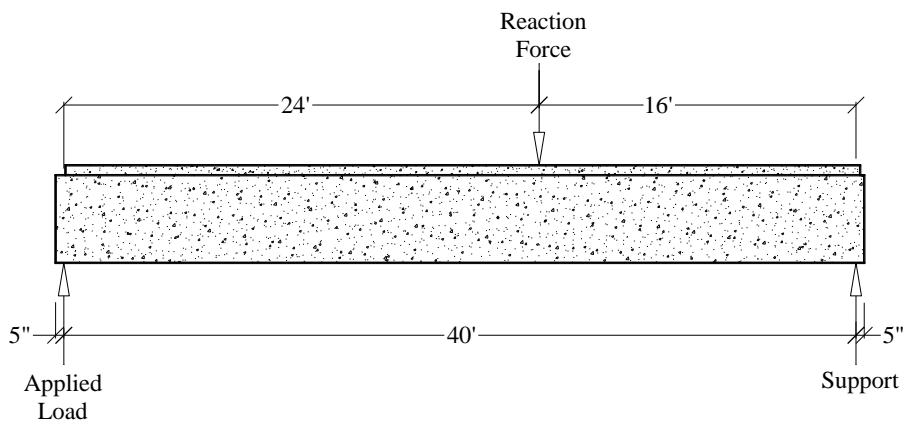


Figure 3.20. Crack Monitoring Grid

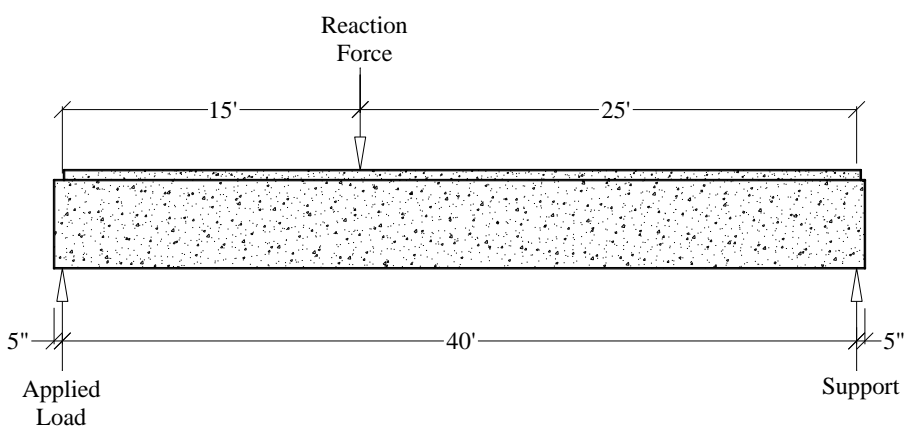
**3.5.3. Test Setup.** The girders were tested under 3 point loading, displayed in Figure 3.21. Two 110 kip (490 kN) capacity actuators were used to apply load to the girder by lifting upward at the south end, creating a downward acting reaction force at the reaction frame. This setup produced a larger moment arm to create a larger shear force in the test region with shear reinforcement. A 500 kip (2224 kN) load cell was used to record the load from the reaction frame. The actuators alone did not supply sufficient force during the test. After they reached full capacity, a 400 kip (1780 kN) capacity hydraulic jack, situated approximately 12 in. (305 mm) on the interior side of the load

frame, was used to apply additional load. Once the girder was situated in the laboratory for testing, its position did not change. After test #1, the reaction frame was moved 9 feet to the south to test the unreinforced section of the girder. Thus, due to the laboratory strongfloor anchor holes located at every 3 ft. (914 mm), the tested shear span varied from 16 ft. (4.88 m) for the first test to 15 ft. (4.57 m) for the second test.

The test set-up is shown in Figure 3.22. The girder rested on two W24x176 I-beams; one at the north end and the other 5 ft. (1.52 m) from the south end. The load frame and reaction frame consisted of two W30x90 beams welded together and supported by W14x90 columns.



a) Test #1 (Reinforced Side)



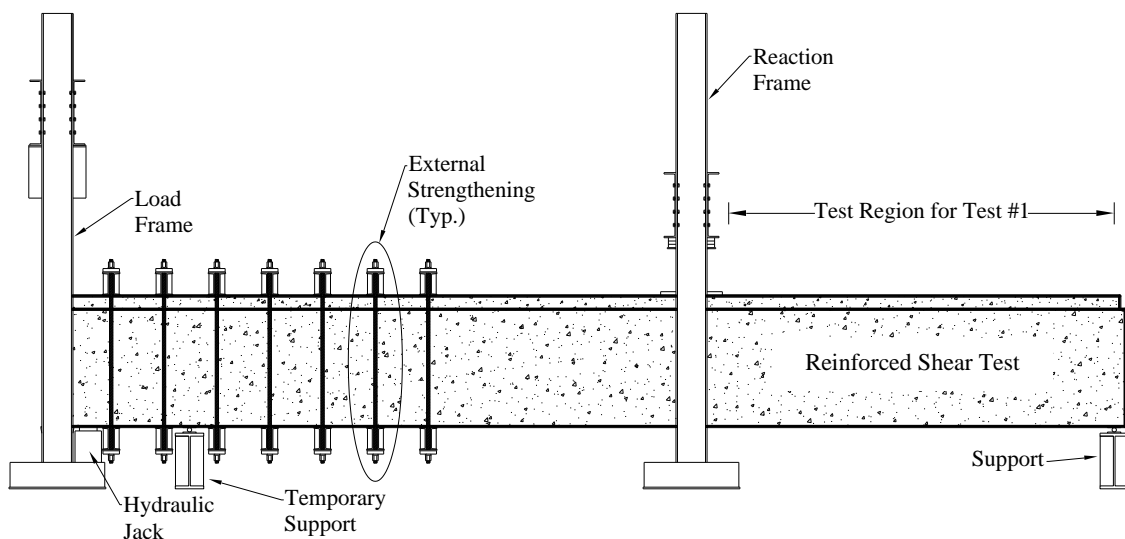
b) Test #2 (Unreinforced Side)

Conversion: 1 ft. = 0.3048 m

Figure 3.21. Test Setup Schematic

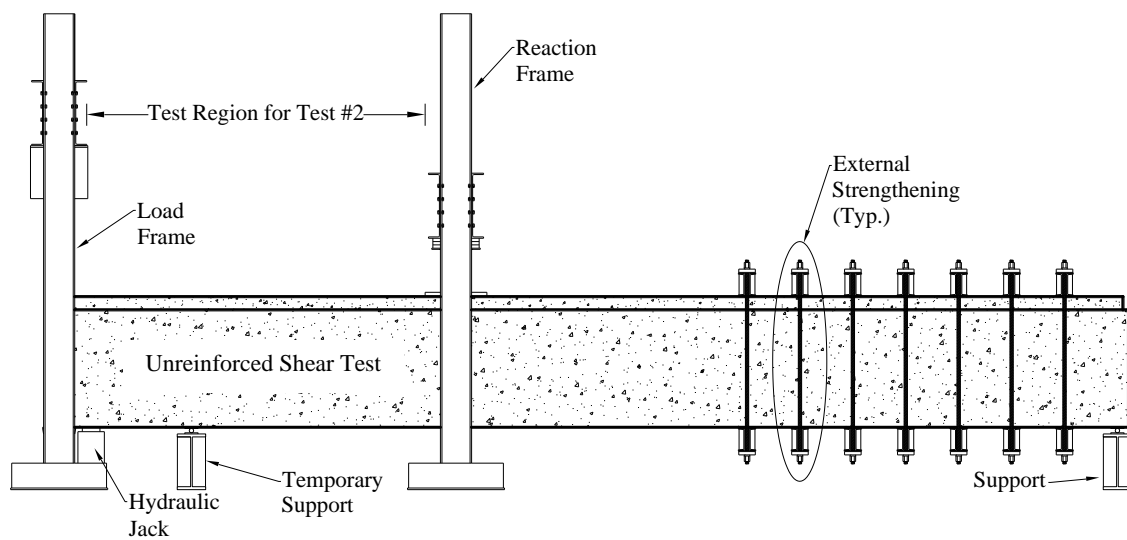
**3.5.4. Test Procedure.** The testing schedule was displayed previously in Table 3.1. The shear reinforced region was tested first due to the ductile behavior, and for the girder to still retain a majority of its stiffness properties for the second test. After the first test concluded, the reaction frame was moved to the south 9 ft. (2.75 m) and the external strengthening was moved to the opposite end.

Each test underwent displacement controlled loading. The actuators lifted the girder at the south end at a rate of 0.1 in./min (2.5 mm/min). Loading continued until approximately 75 kips (334 kN) were read from the load cell at the reaction frame. The girders were then examined for cracks. An additional 20 kips (89 kN) of load was applied and the girder was checked again for cracking. This procedure was repeated until the first sign of cracking. Loading ceased and cracks were marked every 0.2 in. (5.1 mm) of deflection at the actuators. Prior to flexural cracking, this increment of 0.2 in. (5.1 mm) corresponded to an increase in shear of approximately 20 kips (89 kN). After flexural cracking, a 0.2 in. (5.1 mm) deflection correlated to an increase in shear of roughly 10 kips (44.5 kN).

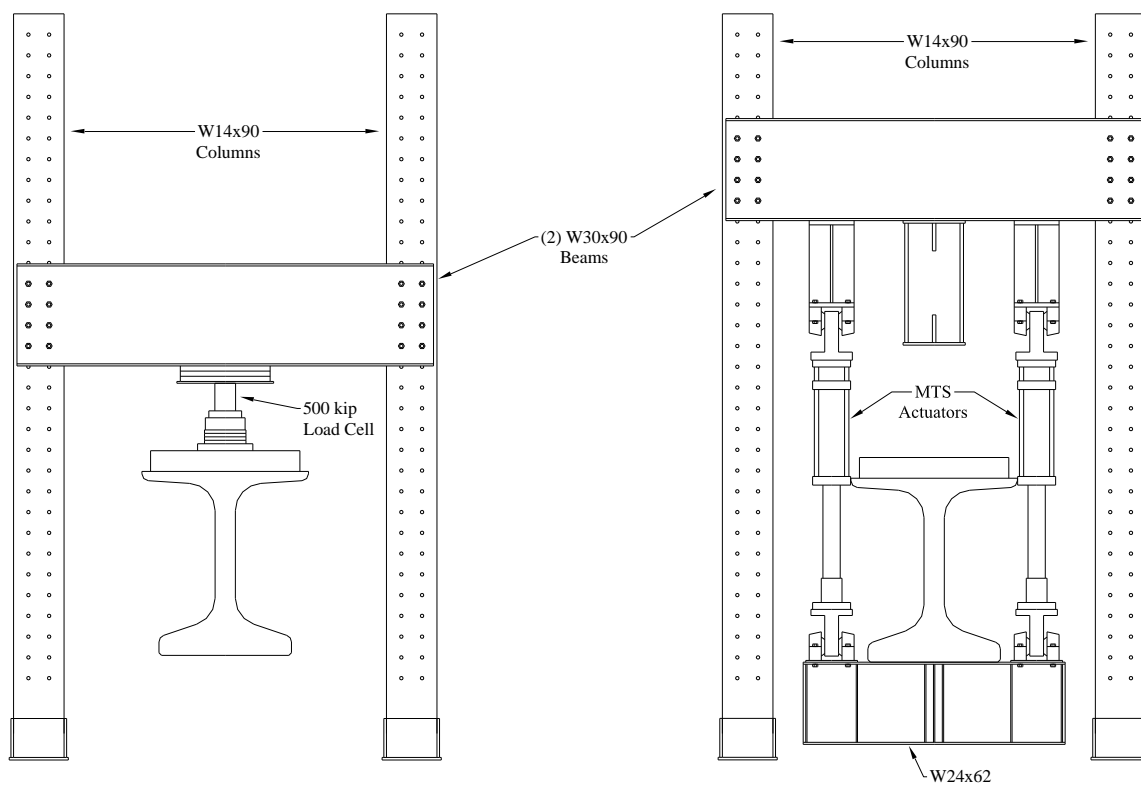


a) Setup for Test #1

Figure 3.22. Overall Test Setup



b) Setup for Test #2



c) Load Frame

d) Reaction Frame

Figure 3.22. Overall Test Setup (cont.)

Once the actuators reached capacity, the 400 kip (1779 kN) hydraulic jack was manually operated as seen in Figure 3.23. The displacement of the actuators was closely monitored while operating the jack to meet the 0.1 in./min (2.5 mm/min) loading rate.

The first test, consisting of shear reinforcement, was not tested to failure. Despite the external strengthening that was applied at the opposite end of the girder, minor hairline cracks still developed in this region in both test girders as shown in Figure 3.24. The Dywidag bars elongated, which resulted in hairline cracking in the externally strengthened region. A higher post-tensioning force in the Dywidag bars could prevent the hairline cracks from occurring in future studies. To prevent excessive damage in this non-tested region during the first test, the region with shear reinforcement was not loaded to failure.

The second test (no shear reinforcement) was tested following the same rate and procedures as the first test. However, this region was tested to failure to obtain the ultimate shear capacity of the section; this corresponded to the shear capacity of the NU girder without shear reinforcement. Following the completion of testing, the girders were demolished into three sections and hauled out of the SERL in Butler-Carlton Hall as shown in Figure 3.25.

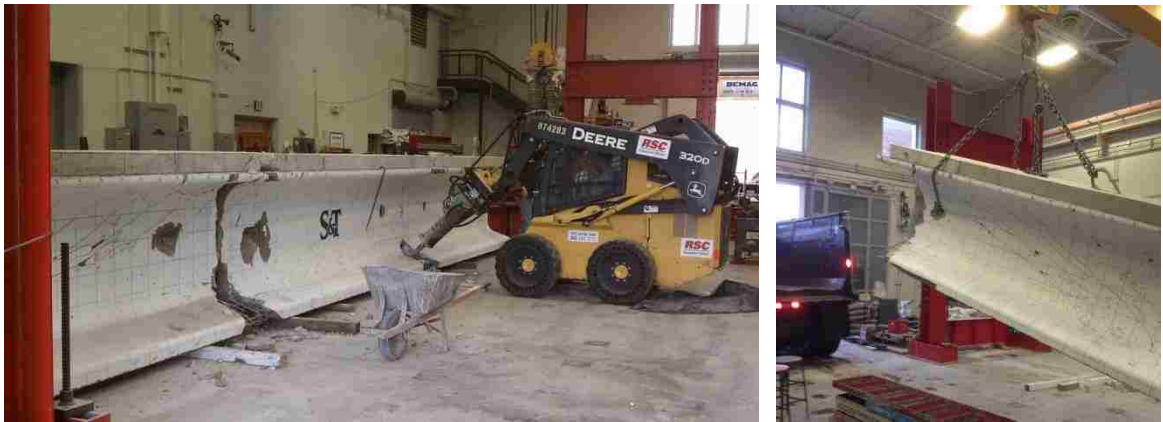


Figure 3.23. Hydraulic Jack





Figure 3.24. Cracks in Non-Tested Region  
(Cracks traced for clarity)



a) Demolition of Test Girder

b) Removal of Test Girder

Figure 3.25. Demolition and Removal of Test Girders

## 4. TEST RESULTS & ANALYSIS

### 4.1. HARDENED MATERIAL PROPERTIES

The QC/QA cylinders and beams were tested and compared to ACI 318 (2011) and ACI 363R (2010) empirical estimates for modulus of elasticity and modulus of rupture as applicable. The compressive strength, modulus of elasticity and modulus of rupture were tested following ASTM C 39 (2012), ASTM C 469 (2010), and ASTM C 78 (2010), respectively. The compressive strength generation over time was also noted for the HS-SCC mix as well as the CIP deck.

**4.1.1. Test Girders.** The following sections discuss the compressive strength, modulus of elasticity, and modulus of rupture test results of the investigated HS-SCC mix.

**4.1.1.1 Compressive strength.** Cylinders were tested for compressive strength at release (3 days), 28 days and on days when laboratory shear tests were performed. The compressive strength was plotted against specimen age in Figure 4.1. The 28 day design compressive strength of 10,000 psi (68.9 MPa) was exceeded by the 28 day test and subsequent days when shear testing was performed. MoDOT recorded compressive strength test results at release (3 days) of 10,490 and 10,660 psi (72.3 and 73.5 MPa) for TG1 and TG2, respectively. Their results exceeded the target release strength of 8,000 psi (55.2 MPa). The difference compared to Missouri S&T's average at 3 days of 7,942 psi (54.8 MPa) could be attributed to the duration of steam curing (the QC/QA cylinders were transported back to Missouri S&T prior to testing), method of capping, as well as the testing machine.

**4.1.1.2 Modulus of elasticity.** The modulus of elasticity (MOE) data was graphed against the square root of compressive strength shown in Figure 4.2. The data was compared to ACI 318 and ACI 363R empirical models. The 2011 ACI 318 Equation 4.1 model is typically not reliable for concrete strengths in excess of 8,000 psi (55 MPa) because the empirical model was developed based on a conventional concrete database (ACI 318, 2011). The ACI 363R (2010) model proposed by Martinez et al. (1982) (Equation 4.2) was implemented as a lower bound for HSC with compressive strengths ranging from 3,000 to 12,000 psi (20.7 to 82.7 MPa). Tomosawa et al. (1993) proposed a

separate ACI 363R model, Equation 4.3, which accounts for the aggregate source as well as type of cementitious material (ACI 363R, 2010). For the listed equations,  $E_c$  is the modulus of elasticity (psi),  $f'_c$  is the compressive strength of concrete (psi), and  $w$  is the concrete unit weight (pcf). The variable  $k_1$  is taken as 1.2 for crushed limestone and calcined bauxite aggregates; 0.95 for crushed quartzite, crushed andesite, crushed basalt, crushed clay slate, and crushed cobble stone aggregates; and 1.0 for other aggregates. The variable  $k_2$  is taken as 0.95 for silica fume, slag cement, and fly ash fume; 1.10 for fly ash; and 1.0 for other types of supplementary cementitious materials (ACI 363R, 2010). The dolomite and Portland cement used in the HS-SCC trial mix correspond to  $k_1$  and  $k_2$  values of 1.0 and 1.0, respectively.

$$E_c = 33w_c^{1.5}\sqrt{f'_c} \quad (4.1)$$

$$E_c = 40,000\sqrt{f'_c} + 10^6 \quad (4.2)$$

$$E_c = 4.86 \times 10^4 k_1 k_2 \left(\frac{w}{150}\right)^2 \left(\frac{f'_c}{8700}\right)^{1/3} \quad (4.3)$$

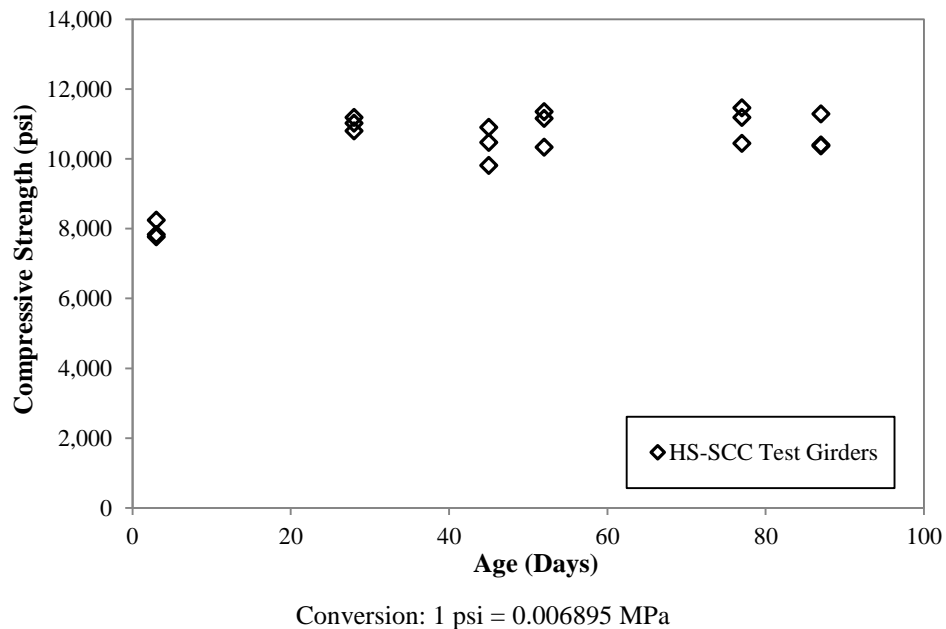


Figure 4.1. HS-SCC Test Girders Compressive Strength vs. Age

The ACI 318 equation overestimates the modulus of elasticity. However, the ACI 363R equation suggested by Martinez et al. (1982) provides an accurate estimate for the MOE of the investigated HS-SCC mix. The Tomosawa et al. (1993) equation of ACI 363R-10 is an accurate lower bound predictor for HS-SCC. Thus, for mix designs of similar aggregate type, size and content, the Tomosawa et al. (1993) equation will provide a conservative, yet accurate estimate of the modulus of elasticity for use in prestress losses and deflection calculations. Other HS-SCC mix designs would yield different results.

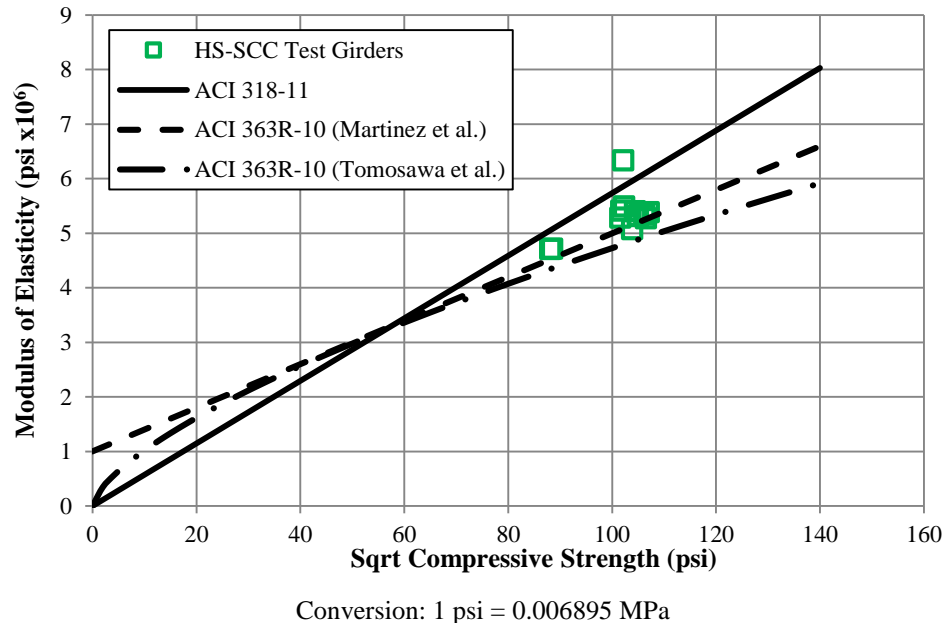


Figure 4.2. HS-SCC Modulus of Elasticity vs. Compressive Strength

**4.1.1.3 Modulus of rupture.** The modulus of rupture (MOR) for HS-SCC was compared to empirical estimates from ACI 318 (2011) (Equation 4.4) and ACI 363R (2010) (Equation 4.5). The results reflect MOR beams sampled from batches 1 and 3 during fabrication. In the below expressions,  $f_r$  is the modulus of rupture (psi),  $\lambda$  is a reduction factor for lightweight concrete, and  $f'_c$  is the compressive strength of concrete (psi). The 2012 AASHTO LRFD model is identical to the 2011 ACI 318 model with the exception of the units considered; AASHTO deals with ksi while ACI 318 regularly uses

psi (ACI 318, 2011, AASHTO LRFD, 2012). For this reason, the AASHTO equation for modulus of rupture was not considered for comparisons. The HSC model proposed by Carrasquillo et al. (1982) considered compressive strengths ranging from 3,000 to 12,000 psi (20.7 to 82.7 MPa).

$$f_r = 7.5\lambda\sqrt{f'_c} \quad (4.4)$$

$$f_r = 11.7\sqrt{f'_c} \quad (4.5)$$

Figure 4.3 displays the modulus of rupture versus the square root of compressive strength for the 8 tests run. Despite the validity of the ACI 318 (2011) empirical model for concrete strengths up to approximately 8,000 psi (55.2 MPa), it appropriately estimates the MOR for the HS-SCC mix investigated. The HSC model in ACI 363R (2010) significantly overestimates the MOR. The failure plane extended through the aggregates indicating that the ACI 363R (2010) equation could be based on mixes with stronger aggregates.

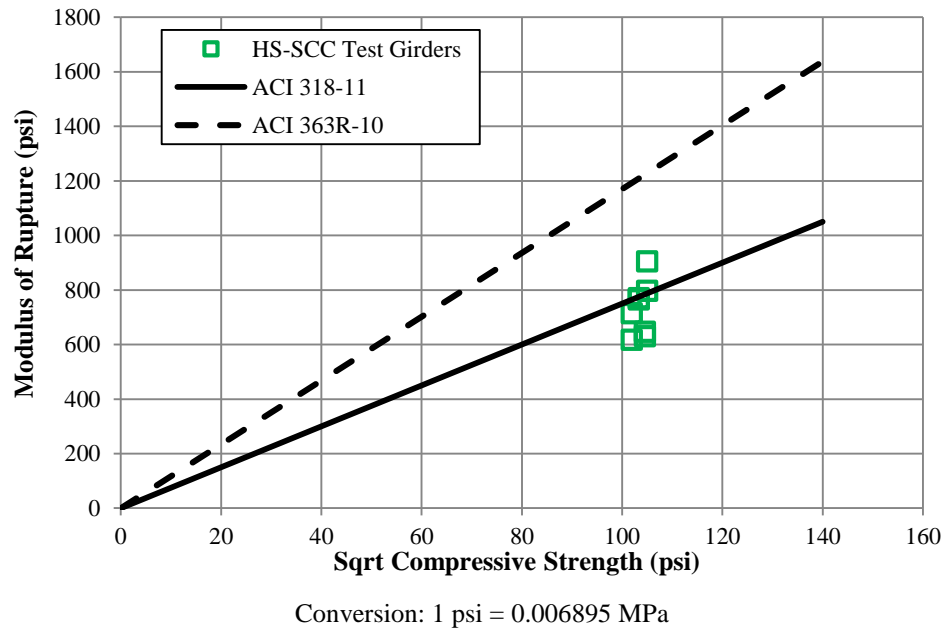
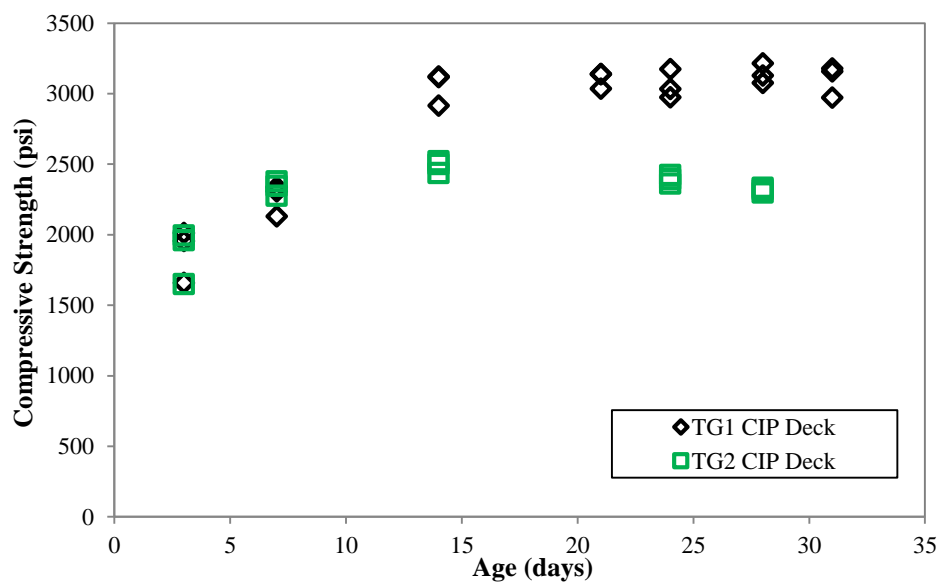


Figure 4.3. HS-SCC Modulus of Rupture vs. Compressive Strength

**4.1.2. CIP Deck.** The CIP deck mix was formulated based upon MoDOT's modified B-2 mix design: mix ID 12CDMB2A087. The design compressive strength at 28 days was 4,000 psi (27.6 MPa). The mix was batched by Ozark Ready Mix Company, Inc. in Rolla, Missouri. Only compressive strength testing was conducted on the deck QC/QA cylinders. The strength generation over time is plotted in Figure 4.4 with average results at 3, 7, 14, 21, 28, and at shear testing days listed in Table 4.1. There is considerable variability in the results between the two batches despite the identical mix designs. The deck on TG2 was only tarped for 7 days and subsequently coated with transparent paint sealant (Section 3.4.3); however, the representative cylinders taken from the second deck mix were not coated with the sealant. Thus, the data points from the TG2 deck mix plateau after the 7 day test, and the actual deck strength in TG2 could be very similar to that in the TG1 deck. Despite this inconsistency between the cylinder strengths and the actual strength in the second CIP deck, the compressive strength tests from the CIP deck on TG2 were assumed to be representative of the deck.



Conversion: 1 psi = 0.006895 MPa

Figure 4.4. CIP Deck Compressive Strength vs. Age

Table 4.1. Compressive Strength of CIP Deck

Age (days)	3	7	14	21	24	28	31
TG1	1,880	2,260	3,050	3,110	3,060 <sup>1</sup>	3,140	3,100 <sup>2</sup>
TG2	1,870	2,330	2,490 <sup>1</sup>	N/A	2,390 <sup>2</sup>	2,320	N/A

1 – Test results performed on day of shear testing for test #1

2 – Test results performed on day of shear testing for test #2

Conversion: 1 psi = 0.006895 MPa

## 4.2. SHEAR TESTING

The ultimate loads from each shear test were compared to both the nominal and factored shear resistances from the 2011 ACI 318 and the 2012 AASHTO LRFD Bridge Design Specifications. Both documents specify an upper limit on the design compressive strength of 10,000 psi (68.9 MPa). The results are compared to code values based on this specified upper limit in addition to the actual compressive strength of the concrete performed on the day of the test; these tested values are listed in Table 4.2. A brief review of each prediction equation is presented followed by results from the destructive shear testing and observed crack patterns.

Table 4.2. Compressive Strength of HS-SCC on Day of Shear Test

	TG1-T1	TG1-T2	TG2-T1	TG2-T2
$f_c$ (psi)	10,390	10,940	11,030	10,680

Conversion: 1 psi = 0.006895 MPa

**4.2.1. ACI.** A brief review of the shear design procedures in the 2011 ACI 318 code is presented followed by comparisons to the shear tests.

**4.2.1.1 Background.** The ACI Building Code Requirements for Structural Concrete (ACI 318, 2011) states the nominal shear strength ( $V_n$ ) of a prestressed concrete member is the summation of the concrete contribution to shear ( $V_c$ ) and the steel reinforcement contribution to shear ( $V_s$ ) shown in Equation 4.6. The factored shear

strength ( $\phi V_n$ ) is then determined by multiplying the nominal shear resistance by a strength reduction factor ( $\phi$ ), which must exceed the ultimate shear force due to external loads (Equation 4.7). The strength reduction factor for shear in the 2011 ACI 318 Section 9.3.2.3 is listed as 0.75. The ultimate shear force ( $V_u$ ) is said to act at a distance  $h/2$  from the support, where  $h$  is the height of the member.

$$V_n = V_c + V_s \quad (4.6)$$

$$\phi V_n \geq V_u \quad (4.7)$$

The 2011 ACI 318 building code provides two methods for computing the concrete contribution to shear of prestressed concrete members. The first is a simplified procedure (Equation 11-9 in ACI 318, 2011) for members with an effective prestress force not less than 40 percent of the tensile strength of the flexural reinforcement. It is most applicable for members subject to uniform loading. The simplified procedure is presented below in Equation 4.8 (ACI 318, 2011). In the below expression,  $V_c$  is the concrete contribution to shear (lb.),  $\lambda$  is a reduction factor for lightweight concrete,  $f'_c$  is the compressive strength of concrete (psi),  $V_u$  is the factored shear force at the section (lb.),  $M_u$  is the factored moment at the section (in.-lb.),  $d$  is the distance from the extreme compression fiber to the centroid of the longitudinal tension reinforcement (in.), and  $b_w$  is the width of the web (in.).

$$V_c = \left( 0.6\lambda\sqrt{f'_c} + 700 \left( \frac{V_u d_p}{M_u} \right) \right) b_w d \quad (4.8)$$

The second procedure is a detailed calculation of the shear resistance which accounts for both web-shear cracking ( $V_{cw}$ ) and flexure-shear cracking ( $V_{ci}$ ) shown in Figure 4.5. To obtain more accurate results, this study compared results to the second (detailed) procedure. The shear contribution provided by the concrete is taken as the lesser of  $V_{cw}$  and  $V_{ci}$ . The critical section investigated was a distance  $h/2$  from the support as stated in ACI 318 (2011). Equations 11-10 and 11-12 in ACI 318 (2011) were used to



determine the shear force to cause flexure-shear and web-shear cracking, respectively. The equations for web-shear and flexure-shear cracking are shown as Equations 4.9 and 4.10. The cracking moment required in Equation 4.10 is listed as Equation 4.11 (ACI 318, 2011). For the listed expressions,  $f_{pc}$  is the compressive stress at the centroid of the concrete section due to the effective prestress force (psi),  $d_p$  is the distance from the extreme compression fiber to the centroid of the prestressing steel (in.),  $V_p$  is the vertical component of the effective prestress force at the section (lb.),  $V_d$  is the shear force at the section due to unfactored dead load (lb.),  $V_i$  is the factored shear force at the section due to externally applied loads (lb.),  $M_{cre}$  is the flexural cracking moment (in.-lb.),  $M_{max}$  is the maximum factored moment at the section due to externally applied loads (in.-lb.),  $I$  is the gross moment of inertia,  $y_t$  is the distance from the centroid to the tension face (in.),  $f_{pe}$  is the compressive stress in concrete due to effective prestress only at the extreme fiber of the section where tensile stress is caused by externally applied loads (psi), and  $f_d$  is the stress due to unfactored dead load at the extreme fiber of the section where tensile stress is caused by externally applied loads (psi).

$$V_{cw} = (3.5\lambda\sqrt{f'_c} + 0.3f_{pc})b_w d_p + V_p \quad (4.9)$$

$$V_{ci} = 0.6\lambda\sqrt{f'_c}b_w d_p + V_d + \left(\frac{V_i M_{cre}}{M_{max}}\right) \quad (4.10)$$

$$M_{cre} = \left(\frac{I}{y_t}\right)(6\lambda\sqrt{f'_c} + f_{pe} - f_d) \quad (4.11)$$

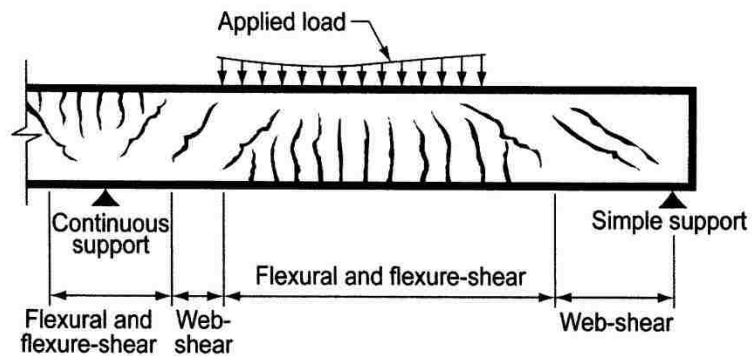


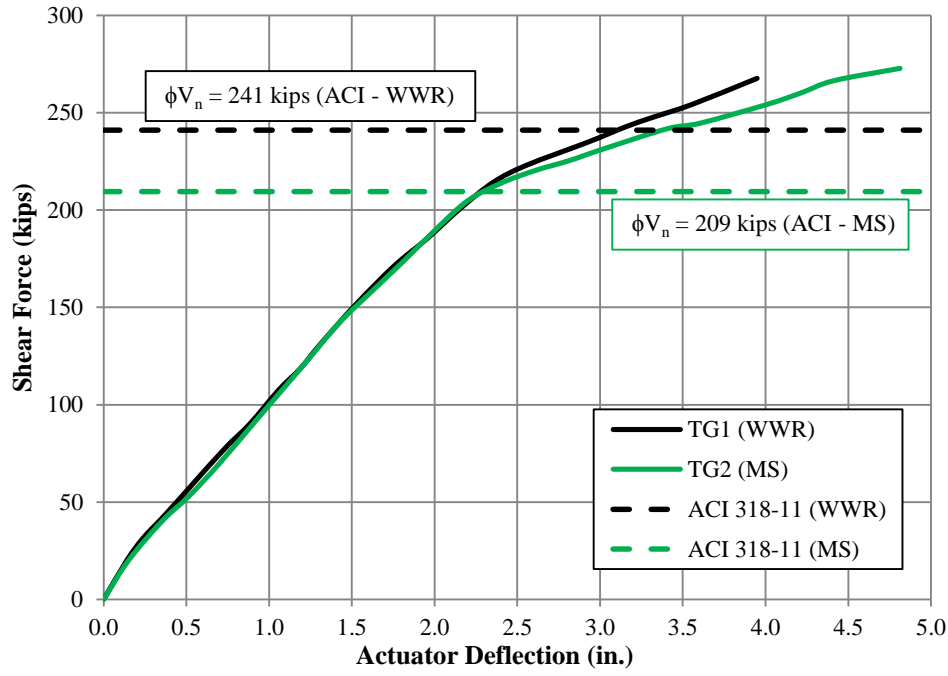
Figure 4.5. Schematic of Web-Shear and Flexure-Shear Cracking (ACI 318, 2011)

The nominal shear strength provided by transverse reinforcement is calculated from ACI 318 (2011) Equation 11-15 for both reinforced and prestressed concrete. This equation is valid when the shear reinforcement is perpendicular to the axis of the member. The equation is presented below as Equation 4.12, where  $V_s$  is the shear contribution from the shear reinforcement (lb.),  $A_v$  is the area of shear reinforcement at spacing  $s$  (in.<sup>2</sup>),  $f_y$  is the specified yield strength of the transverse reinforcement (psi),  $d$  is the distance from the extreme compression fiber to the centroid of the longitudinal tension reinforcement (in.), and  $s$  is the center to center spacing of the transverse reinforcement (in.).

$$V_s = \frac{A_v f_y d}{s} \quad (4.12)$$

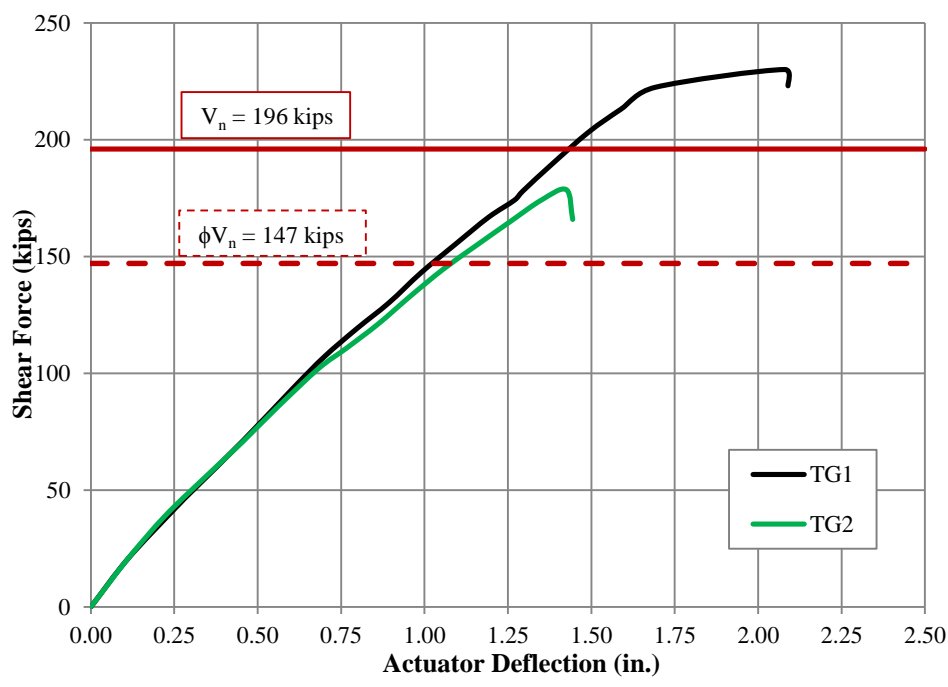
**4.2.1.2 Results.** The load-deflection response was recorded during each test with the deflection measured at the south end of the girder (at the actuators). The shear force was then plotted against this deflection. Figure 4.6 and Figure 4.7 display the load-deflection response for the shear reinforced sections (TG1-T1 and TG2-T1) and non-reinforced sections (TG1-T2 and TG2-T2), respectively. The peak applied shear forces are compared to predicted capacities with the upper limit imposed on the concrete compressive strength.

The shear reinforced region was not tested to complete failure as mentioned in Section 3.5.4. As a result, the nominal shear strength ( $V_n$ ) following ACI 318 (2011) was not plotted, but rather the factored shear strength ( $\phi V_n$ ) in Figure 4.6. Regardless, both types of shear reinforcement (welded wire reinforcement and mild steel bars) exceed the factored shear resistance from ACI 318 (2011). The different predicted factored shear resistance between the WWR and MS of Figure 4.6 can be contributed to the cross-sectional area and spacing of the transverse reinforcement. The WWR had a larger cross-sectional amount of steel per foot length than the MS shear reinforcement.



Conversions: 1 in = 25.4 mm, 1 kip = 4.448 kN

Figure 4.6. ACI Load Deflection Response for Test #1



Conversions: 1 in = 25.4 mm, 1 kip = 4.448 kN

Figure 4.7. ACI Load Deflection Response for Test #2

In Figure 4.7, there is considerable variability between the load-deflection response of the unreinforced tests (TG1-T2 and TG2-T2). This observation is not unusual, since the shear strength of concrete is still not a fully understood concept. Test girder 1 exceeds both the nominal and factored shear strength predicted by ACI 318 (2011). Test girder 2 falls just short of the nominal capacity, but exceeds the calculated factored shear strength.

Table 4.3 and Table 4.4 (in kips) summarize ultimate shear strengths compared to ACI prediction equations. An excel spreadsheet was used to aid in the calculations and is included in Appendix C. Table 4.4 includes ACI 318 comparisons with the concrete compressive strength values from Table 4.2. If the compressive strength of TG1 is increased by approximately 10% reflecting the lower air content in TG1 (see Table 3.6), the tested to predicted ratio drops from 1.14 to 1.13. The average ratio of the two tests still exceeds 1.0. When an upper limit is not placed on the concrete compressive strength, both girders still exceed the factored capacity, and on average, exceed the nominal capacity. However, due to the inherent variability of shear in concrete, additional shear tests on high strength concrete would be necessary to propose any modifications to the upper limit of the concrete compressive strength in the shear provisions.

**4.2.2. AASHTO.** The Missouri Department of Transportation uses their Engineering Policy Guide (EPG), Category 751 LRFD Bridge Design Guidelines for new bridge design (MoDOT EPG, 2011). This document is based on the 2012 AASHTO LRFD Bridge Design Specifications. This section will refer to relevant AASHTO LRFD equations also specified in MoDOT's EPG.

Table 4.3. ACI Predicted Shear Capacity with Web Reinforcement

	Test #1 (kips)				
	$V_c$	$V_s$	$V_n$	$\phi V_n$	$V_{n,test}$
TG1 (WWR)	196	125.4	321.4	241.1	267.6
TG2 (MS)		83.3	279.3	209.5	272.7

Conversion: 1 kip = 4.448 kN

Table 4.4. ACI Predicted Shear Capacity without Web Reinforcement

	$V_{c,test}$	Upper Limit on $f'_c$			No limit on $f'_c$		
		$V_c$	$\phi V_c$	$V_{test}/V_{calc}$	$V_c$	$\phi V_c$	$V_{test}/V_{calc}$
TG1	230.0	196	147	1.17	201	150.7	1.14
TG2	178.5			0.91	200	149.7	0.89
			Average	1.04		Average	1.02

Conversion: 1 kip = 4.448 kN

**4.2.2.1 Background.** The MoDOT EPG follows the general procedure from the 2012 AASHTO LRFD for determination of the nominal shear resistance,  $V_n$ . This procedure is derived from the MCFT developed by Vecchio and Collins (1986). It involves the calculation of the shear resistance at sections along the length of the member based on the applied loads. The AASHTO LRFD cites a critical shear location at a distance  $d_v$  from the support. The effective shear depth,  $d_v$ , is calculated as the distance between the resultant tensile and compressive forces due to flexure (AASHTO LRFD, 2012). For the composite NU girder section, this value is approximately 51 in. (1.30 m). The nominal shear resistance is the summation of the contribution to shear from the concrete ( $V_c$ ), transverse reinforcement ( $V_s$ ), and vertical component of effective prestressing force ( $V_p$ ). AASHTO also specifies a maximum limit on  $V_n$  to prevent crushing of the concrete before yielding of the transverse reinforcement in the web. The nominal shear resistance is then multiplied by the resistance factor,  $\phi$ , to determine the factored shear resistance,  $\phi V_n$ . Unlike ACI 318, AASHTO LRFD uses a resistance factor of 0.9. The nominal shear resistance, maximum limit, and factored shear resistance are presented in Equations 4.13, 4.14 and, 4.15, respectively. In Equation 4.14,  $f'_c$  is the compressive strength (ksi) and  $b_v$  is the effective web width (in.).

$$V_n = V_c + V_s + V_p \quad (4.13)$$

$$V_{n,max} = 0.25 f'_c b_v d_v + V_p \quad (4.14)$$

$$\phi V_n \geq V_u \quad (4.15)$$

The concrete contribution to shear following the general procedure is calculated using Equations 4.16 to 4.20. The  $\beta$  factor, which indicates the ability of the diagonally cracked concrete to transmit tension and shear, depends of the net longitudinal strain at the section at the centroid of the longitudinal reinforcement,  $\epsilon_s$ . The applied moment, axial load, and prestressing influence the net longitudinal strain. Two different equations are used to determine  $\beta$ , depending on the presence of transverse reinforcement. Equation 4.17 is used with shear reinforcement while Equation 4.18 is used without shear reinforcement. When transverse reinforcement is not included, as was the case during the second test, a crack spacing parameter,  $s_{xe}$ , is included to account for the spacing of longitudinal reinforcement and maximum aggregate size; it is to be taken not less than 12.0 in. (305 mm), nor greater than 80.0 in. (2030 mm). For the following expressions,  $M_u$  is the factored moment at the section (in.-kip.),  $V_u$  is the factored shear at the section (kip.),  $N_u$  is the factored axial force (kip.),  $A_{ps}$  is the area of prestressing steel (in.<sup>2</sup>),  $f_{po}$  is the locked in difference in strain between the prestressing steel and the surrounding concrete multiplied by the modulus of elasticity of the prestressing steel (ksi),  $E_s$  is the modulus of elasticity of the non-prestressing steel (ksi),  $A_s$  is the area of non-prestressing steel (in.<sup>2</sup>),  $E_p$  is the modulus of elasticity of the prestressing steel (ksi),  $s_x$  is the crack spacing parameter (in.), and  $a_g$  is the maximum aggregate size (in.).

$$V_c = 0.0316\beta\sqrt{f'_c}b_vd_v \quad (4.16)$$

$$\beta = \frac{4.8}{(1 + 750\epsilon_s)} \quad (4.17)$$

$$\beta = \frac{4.8}{(1 + 750\epsilon_s)} \frac{51}{(39 + s_{xe})} \quad (4.18)$$

$$\epsilon_s = \frac{\left( \frac{|M_u|}{d_v} + 0.5N_u + |V_u - V_p| - A_{ps}f_{po} \right)}{E_sA_s + E_pA_{ps}} \quad (4.19)$$

$$s_{xe} = s_x \left( \frac{1.38}{a_g + 0.63} \right) \quad (4.20)$$

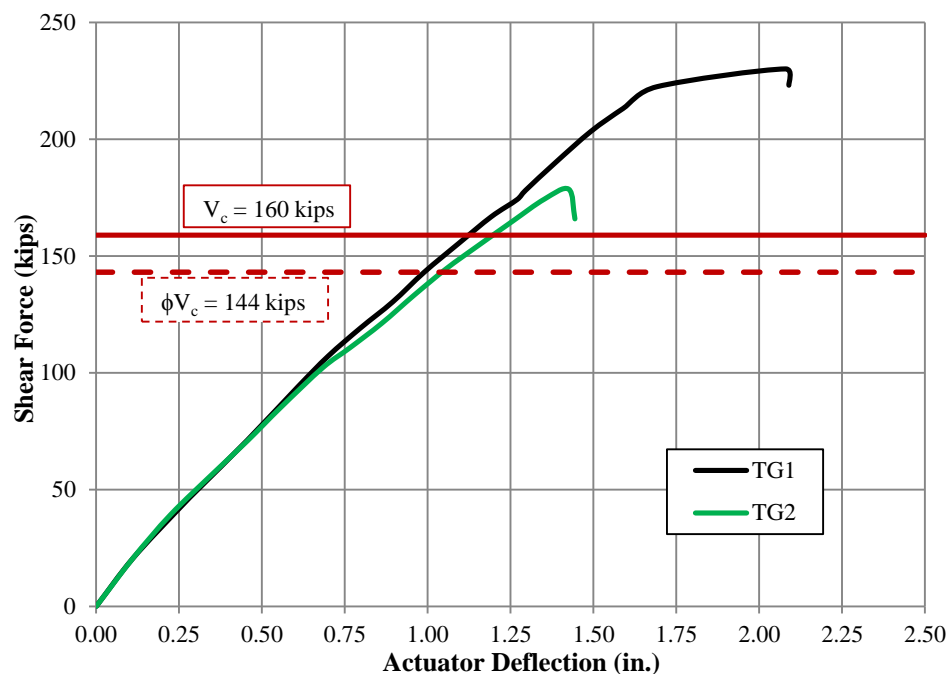
The contribution to shear from the transverse reinforcement from AASHTO LRFD (2012) is taken following Equation 4.21, when the transverse reinforcement is perpendicular to the longitudinal axis of the beam. The variable  $\theta$  is the angle of inclination of the diagonal compressive stress in the concrete (degrees) and is shown in Equation 4.22. In Equation 4.21,  $A_v$  is the area of the transverse reinforcement ( $\text{in.}^2$ ),  $f_y$  is the yield strength of the transverse reinforcement (ksi), and  $s$  is the transverse reinforcement spacing (in.).

$$V_s = \frac{A_v f_y d_v \cot \theta}{s} \quad (4.21)$$

$$\theta = 29 + 3500\varepsilon_s \quad (4.22)$$

**4.2.2.2 Results.** The load-deflection response of the girders was presented in Figure 4.6 and Figure 4.7. The response from the second test (unreinforced region) is presented again as Figure 4.8, but compared to the nominal and factored shear resistance computed from the 2012 AASHTO LRFD. The upper limit on the concrete compressive strength of 10,000 psi (68.9 MPa) is included. The response from the shear test with web reinforcement is not graphed against AASHTO predictions because at the conclusion of the test, they had not reached the factored shear resistance which had occurred with ACI 318 (2011).

Both test girders exceed the nominal and factored shear resistance without transverse reinforcement predicted by the 2012 AASHTO LRFD and the MoDOT EPG. The second test girder exhibited a brief leveling off portion in Figure 4.8, which did not occur with the first test girder. The reason behind the contrast is the ultimate load level. The higher load achieved on TG1 led to the development of flexural cracks, creating the ductile characteristic of the load-deflection curve. No flexural cracking was observed in TG2-T2, and thus the load-deflection curve was approximately linear up until failure.



Conversions: 1 in = 25.4 mm, 1 kip = 4.44822 kN

Figure 4.8. AASHTO/MoDOT EPG Load Deflection Response for Test #2

Table 4.5 and Table 4.6 ( in kips) summarize ultimate shear capacity compared to AASHTO LRFD prediction equations both with and without the upper limit on the compressive strength of 10,000 psi (68.9 MPa). Appendix C contains an excel spreadsheet used for the AASHTO shear calculations. The results indicate that the capacity of the tests with stirrups only reached 71% and 90%, respectively of the predicted capacity. For the tests without web reinforcement, both girders exceeded the nominal capacity by 43% and 11%, respectively. When the actual concrete strength is included, these values fall to 37% and 7%, respectively. Similarly, if the compressive strength of TG1 is increased by 10% to reflect the lower air content, the shear strength ratio drops from 1.37 to 1.31. For large prestressed girders, which are typically designed following AASHTO specifications, HS-SCC proves to be a viable alternative for design.

**4.2.3. Testing Observations.** Additional data was recorded during the shear testing. This includes longitudinal strain readings as well as the shear and flexural crack widths and patterns, all of which are discussed in the subsequent sections. The failure mode of the tested region without shear reinforcement was examined.



Table 4.5. AASHTO Predicted Shear Capacity with Web Reinforcement

	Test #1 (kips)				
	$V_c$	$V_s$	$V_n$	$\phi V_n$	$V_{n,test}$
TG1 (WWR)	159.7	214.7	374.4	337.0	265.7
TG2 (MS)		142.6	302.3	272.1	270.8

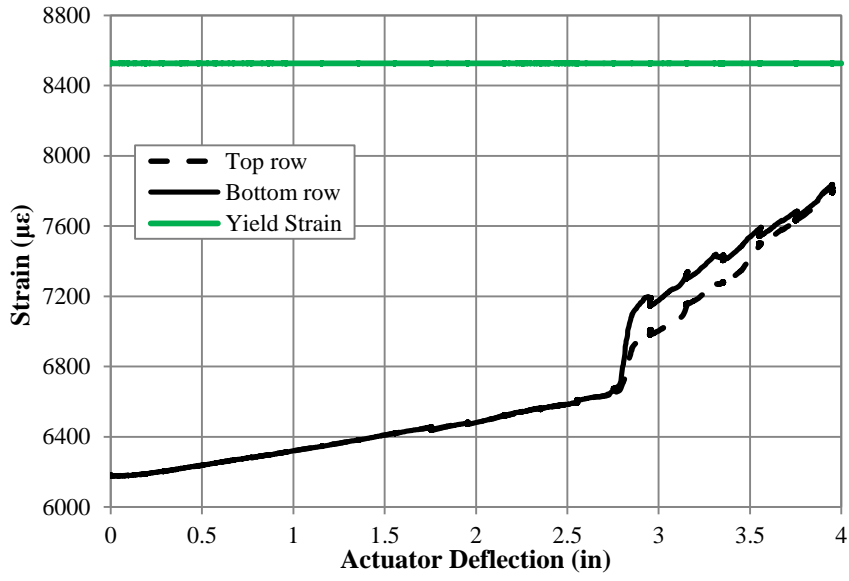
Conversion: 1 kip = 4.448 kN

Table 4.6. AASHTO Predicted Shear Capacity without Web Reinforcement

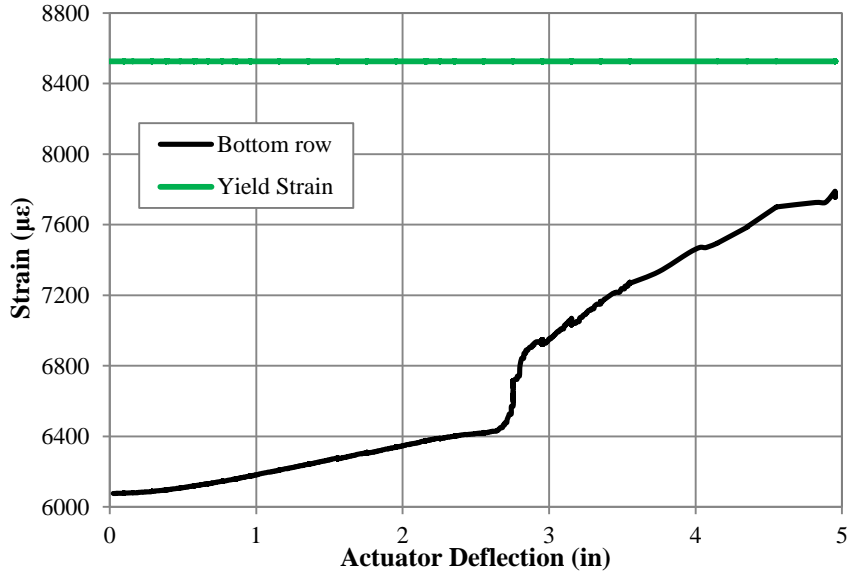
	$V_{c,test}$	Upper Limit on $f'_c$			No limit on $f'_c$		
		$V_c$	$\phi V_c$	$V_{test}/V_{calc}$	$V_c$	$\phi V_c$	$V_{test}/V_{calc}$
TG1	228.1	159.7	143.7	1.43	166.4	149.8	1.37
TG2	176.7			1.11	164.6	148.1	1.07
			Average	1.27		Average	1.22

Conversion: 1 kip = 4.448 kN

**4.2.3.1 Longitudinal strain readings.** The change in strain of the two instrumented prestressing tendons was monitored from the beginning to end of each shear test. The objective of monitoring the prestressing tendons was to evaluate the extent of strain hardening, if any. The strain-deformation plots collected during TG1-T1 and TG2-T1 are displayed in Figure 4.9. The strain readings were shifted up or down to reflect the actual strain in the prestressing tendon; this shift was based on the estimated AASHTO prestress losses and the self-weight of the member. Both figures indicate that during the course of the first tests, the prestressing tendons did not yield at mid-span. The observed “jumps” could be attributed to a local flexural crack at or near the strain gauge. No strain readings were obtained from the top tendon from TG2-T1, a result of possible damage, and were not included in Figure 4.9b.



a) TG1-T1



b) TG2-T1

Figure 4.9. Monitored Prestressing Tendon Strains

**4.2.3.2 Crack documentation.** Crack widths and patterns were recorded throughout each test. Crack widths were measured with a standard crack comparator card shown in Figure 4.10. Appendix D contains the crack patterns and widths documented throughout each test. Five different crack width categories were considered; the first

three were based off of ACI 224R (2001). Cracks less than or equal to 0.004 in. (0.10 mm) were classified as hairline cracks; less than or equal to 0.012 in. (0.30 mm) as acceptable; less than or equal to 0.016 in. (0.41 mm) as moderate; less than or equal to 0.100 in. (2.54 mm) as excessive; and greater than 0.100 in. (2.54 mm) as severe. ACI 224R, no longer included in the 2011 ACI 318 code, lists an upper limit on reasonable crack widths of 0.016 in. (0.41 mm) (ACI 224R, 2001).

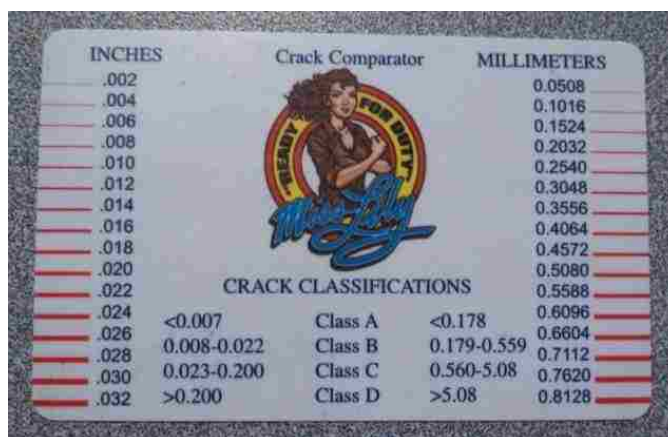


Figure 4.10. Crack Comparator Card

The maximum shear crack widths observed during each test are listed in Table 4.7. During the first tests (reinforced section), the maximum recorded crack width measured 0.018 in. (0.46 mm) and 0.080 in. (2.03 mm) for test girders 1 and 2, respectively. The increased spacing of the transverse reinforcement in TG2 resulted in larger crack widths. Maximum crack widths during the second test (unreinforced section) measured 0.400 in. (10.2 mm) and 0.969 in. (24.6 mm) for test girders 1 and 2, respectively. The shear deformations in TG1-T2 could have been distributed among multiple cracks, reducing the observed crack width at failure and leading to the increased capacity relative to TG2-T2. For TG2-T2, the shear deformation was concentrated along one failure plane, resulting in a larger crack width of nearly 1.0 in. (25.4 mm) at failure and contributing to the lower tested shear strength.

Table 4.7. Maximum Observed Crack Widths

	TG1-T1	TG2-T1	TG1-T2	TG2-T2
Crack width (in.)	0.018	0.080	0.400	0.969

Conversion: 1 in. = 25.4 mm

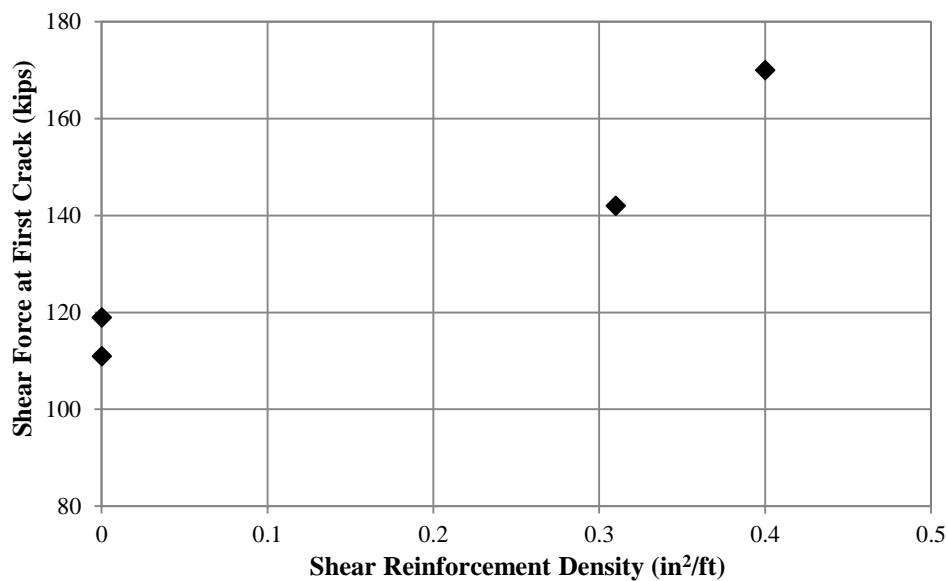
#### 4.2.3.3 Effect of shear reinforcement on concrete contribution to shear.

Although not accounted for in ACI 318 (2011) or AASHTO LRFD (2012), the shear force carried by the concrete increases in the presence of shear reinforcement (see Section 2.2.1.6). For each test, the shear force corresponding to the first inclined shear crack was documented. The results of these observations are illustrated in Figure 4.11. The shear loads are graphed against the density of the transverse reinforcement. Based on the observed loads and cracking of the NU girders, there appears to be a nonlinear increase in the uncracked concrete's contribution to shear as the amount of web reinforcement increases. The ACI 318 (2011) and AASHTO LRFD (2012) attempt to prevent crushing of the concrete before yielding of the transverse reinforcement (i.e. no shear cracking prior to failure) by limiting the amount of shear reinforcement to roughly four times the concrete's shear strength.

**4.2.3.4 Cracking moment.** The flexural cracking moments were also recorded during the first test of each girder and compared to estimates based on fiber stresses. The predicted cracking moment included an estimation for the prestress loss (see Section 2.2.2) and the modulus of rupture which was tested on the day of each shear test. Tested modulus of rupture values for TG1 and TG2 were 665 and 850 psi (4.59 and 5.86 MPa), respectively. An excel spreadsheet for calculation of the prestress losses following the 2012 AASHTO LRFD refined procedure is included in Appendix C. Table 4.8 lists the observed and predicted cracking moments (in kip-ft) as well as the maximum applied moment during the first test of each girder.

The nominal moment capacity of the girders was calculated using Response 2000 using a "no shear" analysis. The nominal moment capacity for the composite cross-section was 6,290 k-ft (8540 kN-m). Figure 4.12 shows the cross-section of the output file from the Response 2000 analysis for the ultimate moment capacity. Tendons

highlighted in red indicate yielding and the dark shaded grey region identifies the compression block. Dark green indicates strain hardening in compression. The maximum applied moments in Table 4.8 are roughly 67% of the nominal capacity, and do not yield the prestressing tendons. The complete flexure analysis computed with Response 2000 can be found in Appendix F.



Conversions: 1 in = 25.4 mm, 1 kip = 4.448 kN

Figure 4.11. Effect of Shear Reinforcement on Concrete Contribution to Shear

Table 4.8. Observed vs. Predicted Moments

	$M_{cr,test}$	$M_{cr,calc}$	$M_{max,applied}$
TG1-T1	3467	3023	4186
TG2-T1	3323	3214	4268

Conversion: 1 k-ft = 1.356 kN-m

**4.2.3.5 Description of failure.** The modes of failure for the unreinforced tests are illustrated in Figure 4.13. Both girders failed as a result of excessive principal tensile stresses in the web. As the load increased, the initial web cracks propagated through the upper and lower flanges towards the supports. Failure occurred when the web shear

cracks contacted the flexural compression zone in the upper flange. Test girder 2 failed in a more brittle manner, evident of the increased crack width at failure. At the conclusion of TG2-T2, the shear crack surface was examined. The crack was relatively smooth, passing through the coarse aggregate particles as pictured in Figure 4.14.

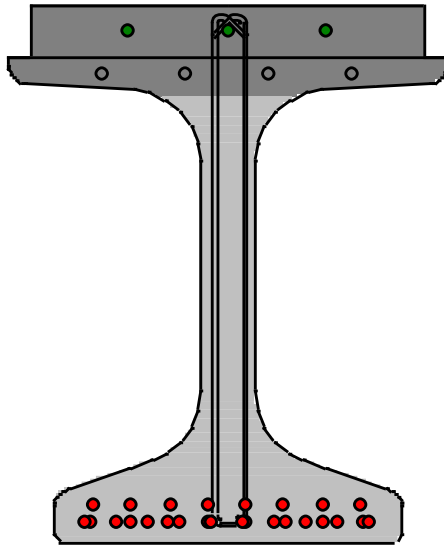
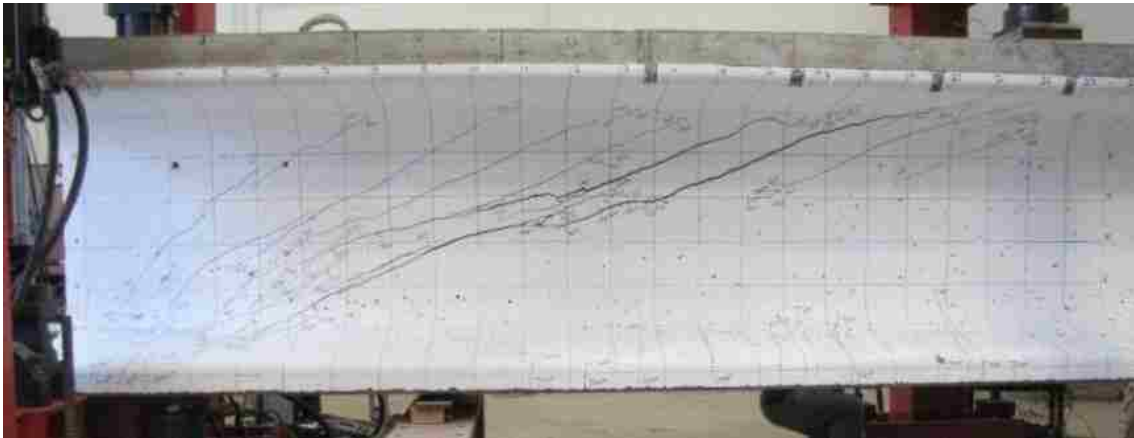
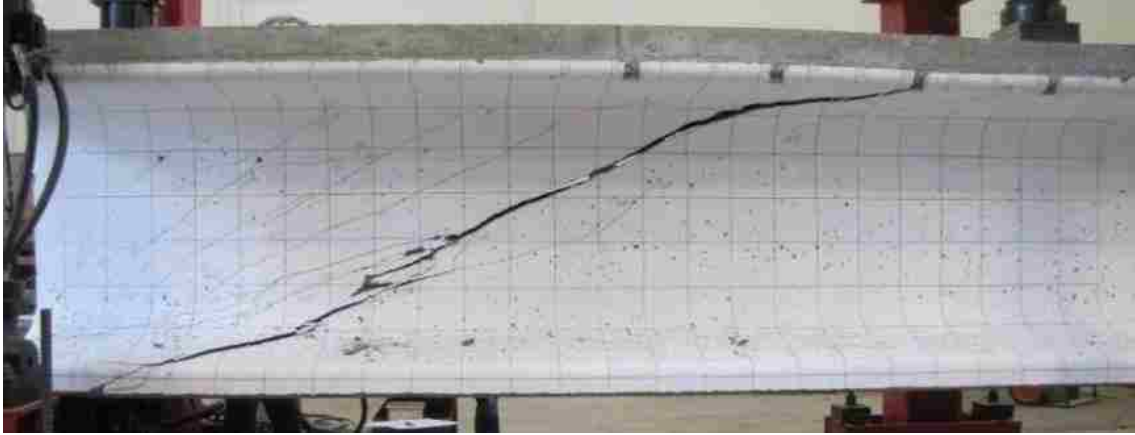


Figure 4.12. Nominal Moment Capacity Analysis



a) TG1-T2

Figure 4.13. Test Girders at Failure without Web Reinforcement



b) TG2-T2

Figure 4.13. Test Girders at Failure without Web Reinforcement (cont.)

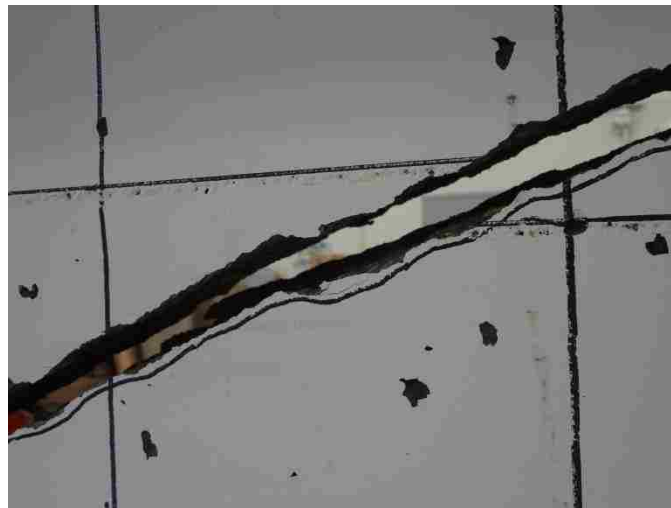


Figure 4.14. Shear Failure Plane

### 4.3. RESPONSE 2000 ANALYSIS

**4.3.1. Introduction.** Response 2000 (R2K) was employed to analyze the results of the shear testing. The software was developed by Evan Bentz at the University of Toronto under the guidance of Michael Collins. It is a sectional analysis tool derived from the MCFT to predict the response of reinforced and prestressed concrete beams and columns. The results are expected to predict the shear capacity more accurately than the 2012 AASHTO LRFD equations since AASHTO is a simplified version of the MCFT

and contains boundary values for several of the variables (see Section 2.2.3). The program has been shown to be a very accurate prediction model for the shear response of prestressed concrete (Hawkins and Kuchma, 2007). For more information regarding the program, see Bentz (2000).

Response 2000 is limited to sections located at least a distance  $d_v$  away from the applied load or support. In these Bernoulli regions (B-regions), the assumption of plane sections remain plane is valid, and the MCFT excels. Within a distance  $0.5d_v \cot \theta$  from support locations or application of loads, the distribution of stresses and strains is not linear, so these sections are commonly known as disturbed regions (D-regions). Here, the flow of forces can be more accurately predicted using strut and tie analyses. For the case of a point load test, the critical section for shear was taken at a distance of  $0.5d_v \cot \theta$  from the applied load. Section S-S' illustrates this location in Figure 4.15. At location S, the assumption of plane sections remain plane is valid and the moment is maximum. A larger applied moment at a section will reduce the axial force due to prestressing, thus reducing the shear component due to interface shear transfer.

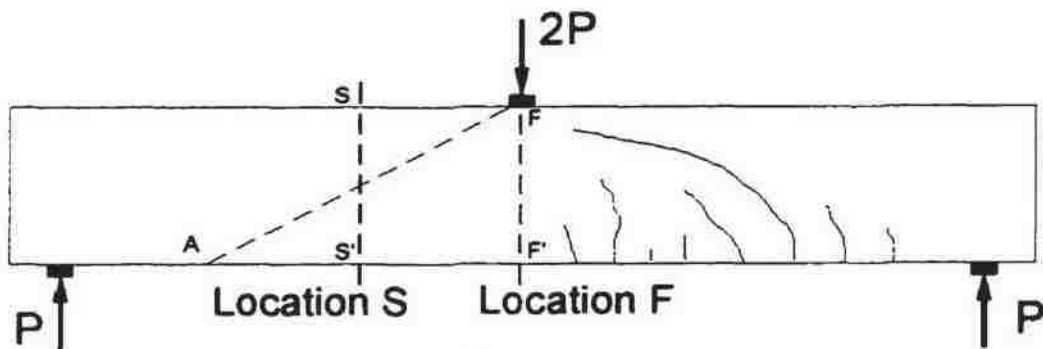


Figure 4.15. Location of Critical Section for Shear (Bentz, 2000)

A strain discontinuity was input to the program to define the interaction between the PC/PS girder and the CIP slab. This step was completed because the deck was not subjected to the prestressing operation. The top fiber strain of the girder was calculated based on fiber stresses multiplied by the 28 day modulus of elasticity of the girder. The input strain discontinuity values were calculated with the aid of an excel spreadsheet



included in Appendix C. The spreadsheet also lists additional input data for each analysis performed. The compressive strength testing of the girders and CIP deck was performed on the day of each test and included in the program. The representative  $f'_c$  values are listed in Table 4.9.

Table 4.9. Response 2000 Concrete Properties

	TG1-T1	TG1-T2	TG2-T1	TG2-T2
Girder (psi)	10,390	10,940	11,030	10,680
Deck (psi)	3,060	3,100	2,490	2,390

Conversion: 1 psi = 0.006895 MPa

**4.3.2. Results.** The results of the analysis for each test are discussed and compared to the experimental test results where applicable. For the first tests including web reinforcement, the sections were not tested to failure; however, the section capacities were still calculated and compared to code estimates.

Response 2000 accounts for HSC by linearly reducing the maximum aggregate size from the input value to 0 as the compressive strength increases from 8,700 to 11,600 psi (60 to 80 MPa) (Bentz, 2000). During testing, the failure surface was relatively smooth, i.e. the cracks propagated through the aggregate as shown in Figure 4.14. As a result of this observation, Response 2000 was run twice for each test; once with the aggregate size set to 0 in. and once with the aggregate size set to the MAS of 0.5 in. (12.7 mm). The difference between the two aggregate settings was negligible for the unreinforced test (test #2). For the first tests (including web reinforcement), the difference was approximately 3 kips and 1 kip (13.3 and 4.4 kN) for TG1 and TG2, respectively. The difference is less in the case of TG2 because the spacing of the shear reinforcement was double that of TG1. The larger spacing equated to a wider crack width, resulting in a lower shear stress transferred at the crack due to aggregate interlock. Appendix F contains the input and output files from each analysis performed.

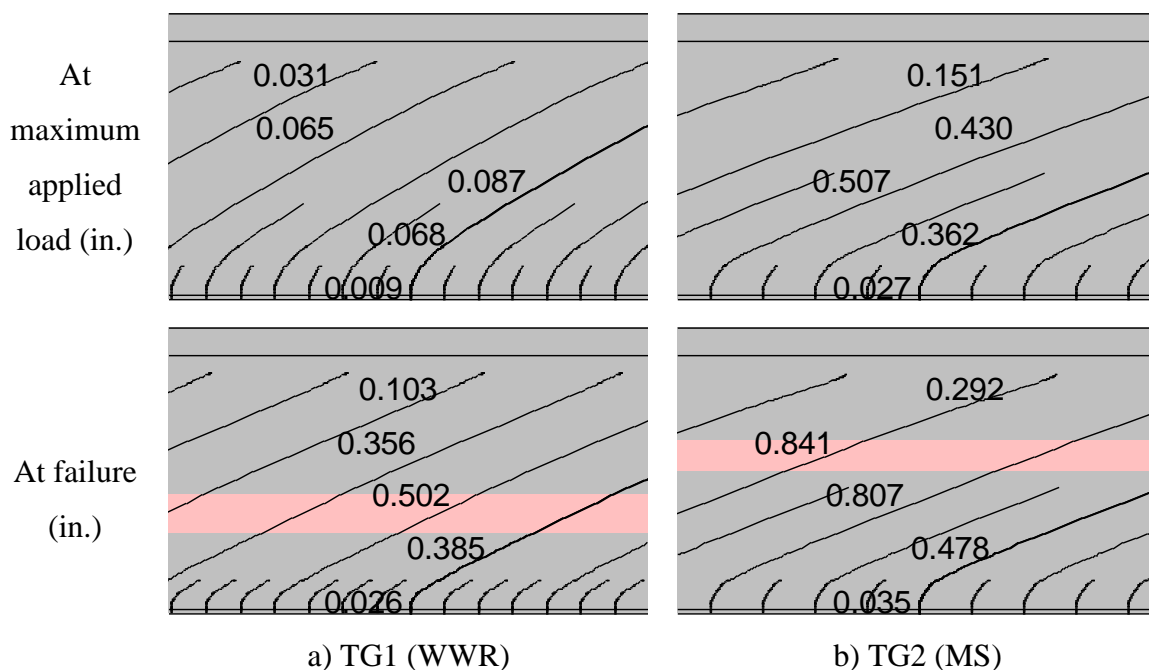
**4.3.2.1 Shear tests with web reinforcement.** The first tests performed on TG1 and TG2 were not completed to failure (Section 3.5.4). The maximum applied shear loads for these tests were 266 kips and 271 kips (1183 and 1205 kN), respectively. The ultimate shear capacities predicted by Response 2000 for the shear reinforced tests are presented in Table 4.10. The capacity predicted by Response 2000 nearly matches the nominal shear strength as predicted by ACI 318 (2011) (Table 4.3), but predicts roughly 85-90% of the nominal capacity estimated by the 2012 AASHTO LRFD model (Table 4.5).

The final shear load for TG2 almost meets the ultimate capacity predicted by Response 2000 while TG1 falls below the predicted shear capacity by almost 20%. Further examination into the proximity to failure of the test girders is illustrated in Figure 4.16. The predicted crack widths at failure range from 0.5 to 0.8 in. (12.7 to 20.3 mm) for TG1 and TG2, respectively. Regions in bright red indicate locations of stirrup yielding. Response 2000 was also performed at the peak applied load and compared to the observed cracking patterns. The observed crack widths at the peak applied load measured 0.018 and 0.080 in. (0.46 and 2.03 mm) for TG1 and TG2, respectively. These are 21% and 16% less than what is predicted by Response 2000, respectively. Various models have been suggested to predict shear crack widths. However, there is significant scatter when assessing the accuracy of crack width models as coefficient of variations range from 37 to 53% (De Silva et al., 2008). A combination of the variability of crack width formulas and the underestimated capacity of Response 2000 attributes to the inconsistency.

Table 4.10. Comparisons with Response 2000 with Web Reinforcement

	$V_{\text{test}}$	$V_{R2K} (a_g=0 \text{ in.})$	$V_{R2K} (a_g=0.5 \text{ in.})$
TG1 (kips)	265.7	317.4	320.2
TG2 (kips)	270.8	275.6	276.2

Conversion: 1 kip = 4.448 kN, 1 in. = 25.4 mm



Conversion: 1 in. 25.4 mm

Figure 4.16. Predicted Crack Widths at Failure

**4.3.2.2 Shear tests without web reinforcement.** The results of the Response 2000 analysis for the unreinforced shear tests provided helpful insight into the reliability of HS-SCC in precast construction. Table 4.11 lists the tested shear capacity against the Response 2000 model and the corresponding shear strength ratio. The slight differences between the predicted values can be attributed to the concrete compressive strength. If the girder compressive strength in TG1 is increased 10% to reflect the lower air content, the predicted capacity increases from 172 kips (766 kN) to 175 kips (778 kN). This reduces the shear strength ratio from 1.32 to 1.30. The predicted shear capacity by Response 2000 is slightly more accurate than AASHTO LRFD (2012) (Table 4.5) since the latter is a simplified version of the MCFT. The generated output plots in Appendix F reveal that flexural cracking has not yet occurred at the section. Flexural cracking was not observed in TG2-T2, but was observed in the bottom flange at the critical section in TG1-T2.

The degree of accuracy of Response 2000 can be traced to the plot of the principal tensile stress, where failure occurs when the principal tensile stress reaches the tensile

stress of the concrete. Numerous factors contribute to the tensile strength of concrete, causing significant variability at a given compressive strength. These include w/cm ratio, type of cement, aggregate, quality of mixing water, curing conditions, age of concrete, maturity of concrete, and rate of loading (Wight and MacGregor, 2009). In Response 2000, the tensile strength of concrete is automatically assumed from Equation 4.23 (Bentz, 2000).

$$f_t = 8.91(f'_c)^{0.4} \quad (4.23)$$

For a compressive strength of 10,000 psi (68.9 MPa), the estimated tensile strength is 355 psi (2.45 MPa). An increase of the tensile strength to 500 psi (3.45 MPa) leads to a shear capacity of 201.1 kips (895 kN), an increase of 17%. Therefore, the tensile strength empirical estimate could contribute to the difference between the tested and predicted shear strengths. A Response 2000 output with  $f_t$  equal to 500 psi (3.45 MPa) is included in Appendix F.

Table 4.11. Comparisons with Response 2000 without Web Reinforcement

	$V_{\text{test}}$ (kips)	$V_{\text{R2K}}$ (kips)	$V_{\text{test}}/V_{\text{R2K}}$
TG1	228.1	172.2	1.32
TG2	176.7	169.6	1.04

Conversion: 1 kip = 4.448 kN

#### 4.4. ATENA ENGINEERING ANALYSIS

**4.4.1. Introduction.** The test girders were examined via ATENA Engineering v5.0.3, a non-linear finite element analysis software specializing in reinforced and prestressed concrete and developed by Cervenka Consulting (Cervenka Consulting, 2013). The program was used to evaluate the qualitative results of the testing, specifically crack patterns and the effect of varying the coarse aggregate size in the HS-SCC mix. Since SCC typically contains a reduced aggregate size which creates the

unique flowability characteristic in the fresh state, this property was investigated. Additionally, the effect of high strength concrete in shear was also examined by reducing the coarse aggregate size to zero.

Tested material properties on the day of each test were input into the program including compressive strength and modulus of elasticity. The modulus of elasticity of the CIP deck was estimated following ACI 318 (2011) Section 8.5.1. The tensile strength of the concrete was calculated with the Response 2000 empirical estimate, Equation 4.23, to maintain consistency in the results. Table 4.12 lists the material properties for each test. In attempt to simulate the “clamping effect” that the external strengthening applied to each non-tested region, these regions were substituted with excess shear reinforcement in the model. This enabled the failure to occur where expected during each shear test. Images of the reinforcement details for each model are included in Appendix G.

**4.4.2. Results.** Four models were created, one for each load test performed. Each model was run three times, with three different MAS coarse aggregate sizes: 0, 0.5 and 1.0 in. (0, 12.7, and 25.4 mm, respectively) to reflect the differences between CC and SCC and the combination of HSC and SCC. All models consisted of approximately 63,000 finite elements and were loaded in the same configuration and at the same rate as the investigated girders. The analysis was terminated if a solution could not be obtained at a discrete applied displacement. However in an actual testing scenario, failure could occur between the load steps. Thus, the results obtained could have slight natural variations because of the displacement controlled loading method, in which data was saved only when a displacement level was successfully analyzed. These variations in the analysis are illustrated through error bars in Section 4.4.2.2. The error bars indicate the percent change in capacity between load steps.

**4.4.2.1 Crack Patterns.** The crack patterns at each load increment were recorded throughout the analysis. The propagation of cracks at the final completed analysis step in each test is presented in Figure 4.17. The tests without web reinforcement are presented in Figures a & b, with c & d including shear reinforcement. To provide a more dynamic visual scale of the crack widths, the CIP deck is not shown in the below images. Regions in red indicate larger crack widths.

Table 4.12. Concrete Material Properties for ATENA Analysis

	Compressive Strength (psi)		Modulus of Elasticity (ksi)		HS-SCC Tensile Strength (psi)
	Girder	Deck	Girder	Deck	
TG1-T1	10,390	3,060	5,445	3,153	360
TG1-T2	10,940	3,100	5,278	3,174	368
TG2-T1	11,030	2,490	5,857	2,844	369
TG2-T2	10,680	2,390	5,377	2,787	364

Conversion: 1 psi = 0.006895 MPa

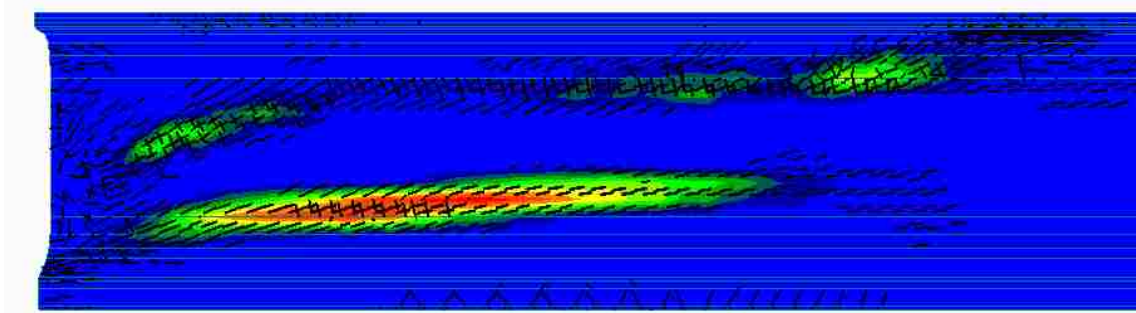
The observed crack patterns from the shear tests are presented in Appendix D. The ATENA predicted crack patterns without reinforcement vary slightly from the actual cracking behavior. For TG1-T2 (Figure 4.17a), the first shear crack initiated in the top of the web near the flange. Here, the internal compressive stress due to prestressing and applied loads is minimized. As the load increased, the axial compressive stress from prestressing and applied loads increased where the first crack originated, and decreased at the bottom of the web, thus creating a second crack. The second test girder without shear reinforcement (Figure 4.17b) followed a similar pattern; however, the second shear crack at the junction of the web and lower flange never completely formed due to the lower ultimate shear force in the model. The observed crack patterns formed at approximately a 30 degree diagonal (see Figure 4.13) rather than propagating at the junction of the web and flange. Maximum predicted crack widths in ATENA for these two analyses were 0.11 and 0.10 in. (2.8 and 2.5 mm) for TG1-T2 and TG2-T2, respectively. These values are less than the observed 0.400 and 0.969 in. (10.2 and 24.6 mm) for test girders 1 and 2, respectively. The difference in crack patterns and the ability to accurately predict shear crack widths reflect these numerical differences.

Figure 4.17c & d illustrate the predicted crack patterns with shear reinforcement. When welded wire reinforcement is used (Figure 4.17c), cracks form at approximately a 30 degree diagonal, similar to those observed during testing. Yet, the model does not predict the same extent of flexure-shear cracking as was observed during testing. A majority of the internal deformations are concentrated through web-shear cracking. When the reinforcement spacing increases to 24 in. (610 mm), the predicted crack

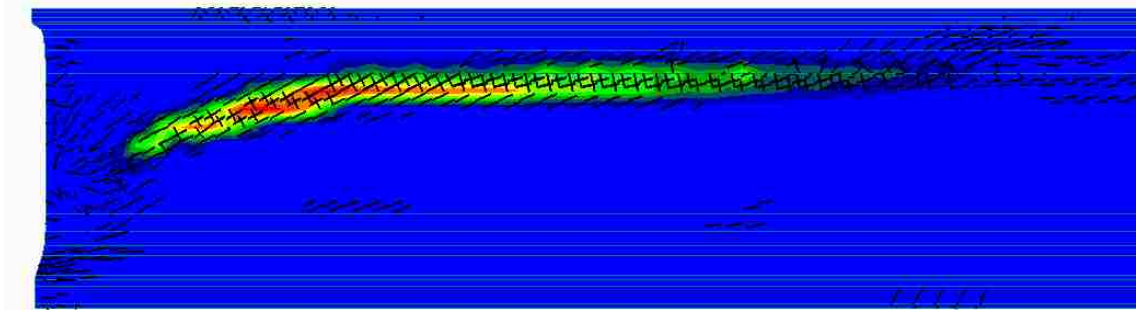
behavior deviates from what was observed (Figure 4.17d). The initial shear crack in the upper portion of the web leads to steep inclined shear cracking between the shear reinforcement bars. The shear cracks tend to “bypass” the reinforcement, finding a path of lesser resistance to the bottom flange. Based on this observation, it is recommended to avoid stirrup spacings of 24 in. (610 mm) or larger. A smaller reinforcing bar at a closer spacing will help distribute the shear cracks more uniformly similar to Figure 4.17c. The predicted crack widths at failure including shear reinforcement measured 0.012 and 0.043 in. (0.30 and 1.10 mm) for test girders 1 and 2, respectively. The larger crack width in TG2 appears to result from the increased spacing to the point at which the stirrups no longer help to limit the crack width. These predicted values agree comparably to the measured crack widths of 0.018 and 0.080 in. (0.46 and 2.03 mm) from TG1 and TG2, respectively despite the fact that the measured values occurred at a shear force less than the failure load. The actual crack widths at failure would exceed those predicted by ATENA Engineering.

**4.4.2.2 Effect of aggregate size.** The results of the analysis were normalized to the predicted capacity with the maximum coarse aggregate size of 0.5 in. (12.7 mm) to create a relative strength. The following figures indicate a percent capacity of each as-built HS-SCC NU test girder. Error bars are included to account for the effect of the discrete load steps as discussed previously in Section 4.4.2.

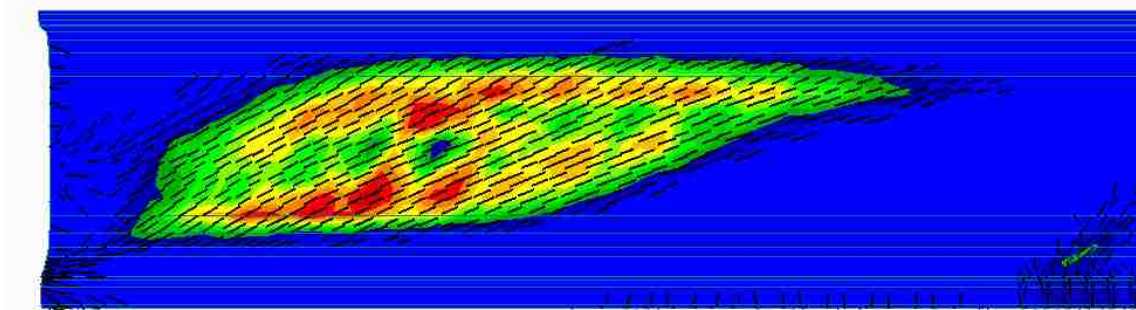
Figure 4.18 displays the reduction in capacity of the prestressed girder without web reinforcement by varying the aggregate size. Both girders show a decrease in capacity when the aggregate size is reduced to zero. As the aggregate size decreases, the aggregate interlock component of the shear carried by the concrete diminishes. Yet when the aggregate size increases, the results show a negligible effect on the shear capacity. Test girder 1 shows an additional increase when the MAS is increased to 1 in. (25.4 mm) while TG2 decreases. From the observations of this analysis, it is not the size of the aggregate that influences the capacity, but rather the presence of the coarse aggregate. The reduced capacity in the TG2 model can be explained by the natural variation in the analysis, which is visualized through the error bars.



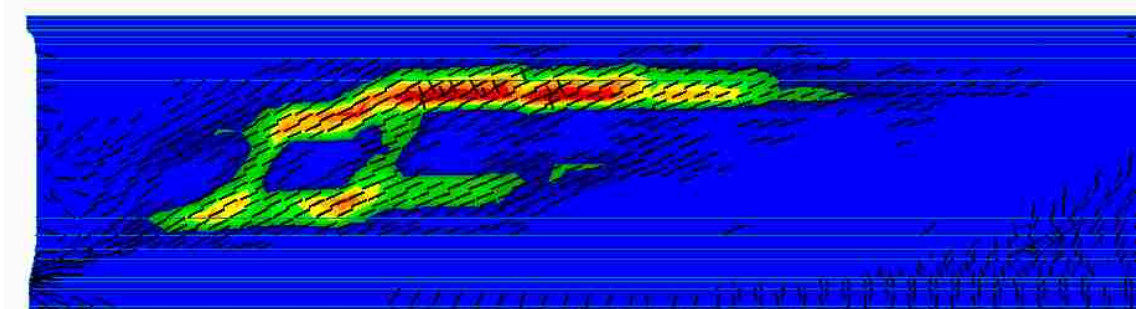
a) TG1-T2



b) TG2-T2



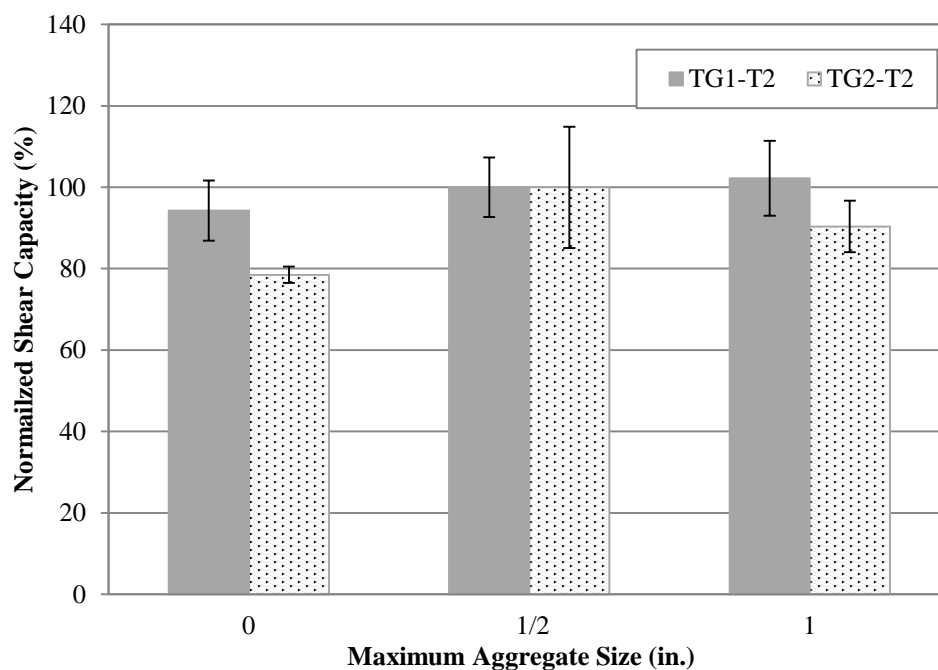
c) TG1-T1



d) TG2-T1

Figure 4.17. ATENA Crack Patterns at Failure

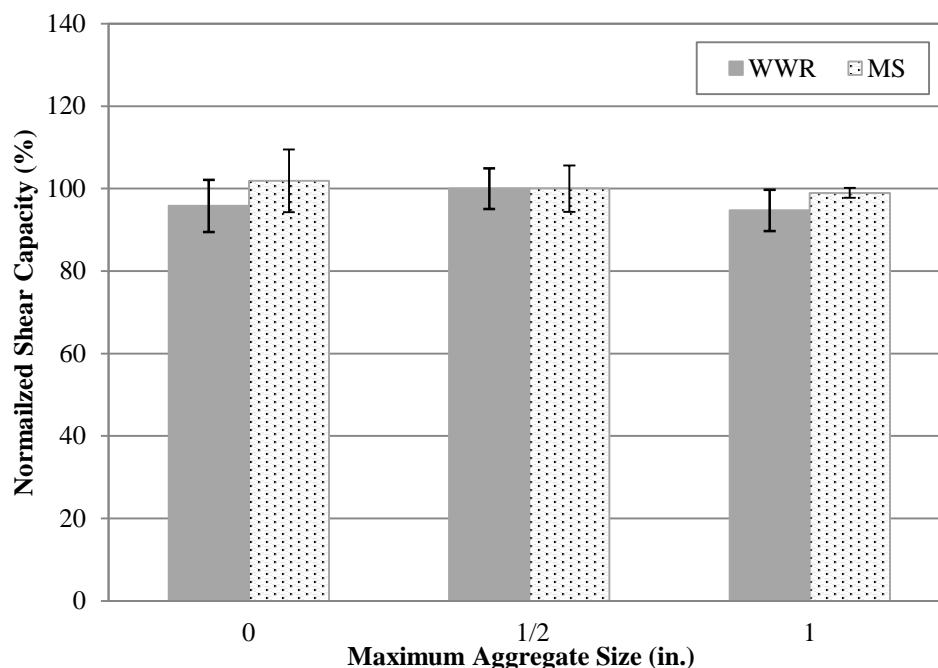




Conversion: 1 in. = 25.4 mm

Figure 4.18. ATENA Relative Capacity by Varying Aggregate Size without Shear Reinforcement

When shear reinforcement is included, the impact of the coarse aggregate size is not as evident (Figure 4.19). When the aggregate size is reduced to zero for TG1, the capacity is reduced by approximately 4 to 5 percent. This result is similar to that encountered in Response 2000 (Section 4.3.2.1). In general, the models show a negligible effect on the shear capacity as the size of the aggregate increases. When reinforcement is included, the crack widths are limited such that the surface roughness provides sufficient interface shear transfer to resist part of the shear load. For larger crack widths occurring without shear reinforcement, the presence of aggregate plays a more significant role (Figure 4.18). For shear beams containing transverse reinforcement, other factors contribute more to the shear strength.



Conversion: 1 in. = 25.4 mm

Figure 4.19. ATENA Relative Capacity by Varying Aggregate Size with Shear Reinforcement

## 4.5. EVALUATION WITH COLLECTED DATABASE

**4.5.1. Introduction.** A database of prestressed concrete members was developed from the literature review discussed in Section 2.3. The collected database focused solely on prestressed members without web reinforcement. Since this study did not include any full-scale tests with conventional concrete of an equivalent compressive strength, a database was necessary to evaluate the results.

Currently, there is not a publicly available database for prestressed concrete members without web reinforcement as there is for reinforced concrete (Reineck et al., 2003). Researchers at the University of Texas at Austin have recently developed an extensive prestressed concrete database covering 1696 tests across the world from 1954 to 2010 to evaluate current prediction equations and models. Their database includes tests both with and without web reinforcement. However, in their report, the researchers focused on members with at least the minimum code required shear reinforcement. The

results of the database indicated that the MCFT was the most accurate predictor of the shear strength (Nakamura et al., 2013).

The NCHRP Report 579 documented the shear strength in HSC members to assess if the 2007 AASHTO LRFD specifications were accurate for concrete strengths exceeding 10,000 psi (68.9 MPa). Their collected database included specimens with a compressive strength in excess of 12,000 psi (82.7 MPa). They concluded that the sectional design model in the AASHTO provisions predicted similar shear capacities for high strength concrete. The results showed a similar level of accuracy and conservativeness for high strength concrete as well as normal strength concretes (Hawkins and Kuchma, 2007). Despite the findings in the report, the 2012 AASHTO LRFD Bridge Design Specifications have not raised the limit on the concrete compressive strength above 10,000 psi (68.9 MPa) in part due to the limited number of shear tests with high strength concrete (AASHTO LRFD, 2012). Hawkins and Kuchma (2007) identified this lack of test data with high strength concrete via Figure 4.20, which shows a large concentration of data points for compressive strengths less than roughly 7,000 psi (48.3 MPa), with scattered results up to 12,000 psi (82.7 MPa). Thus, additional shear tests with higher compressive strengths are necessary.

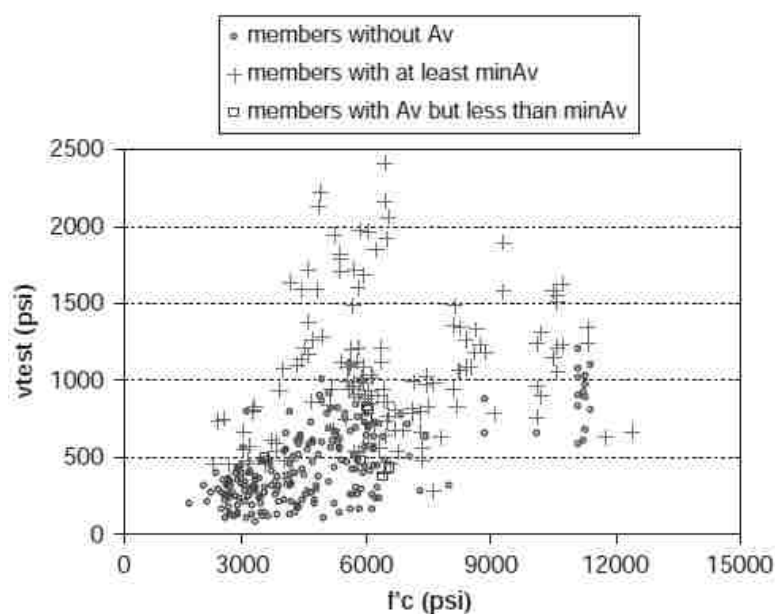


Figure 4.20. Distribution of Shear Test Results (Hawkins and Kuchma, 2007)

**4.5.2. Results.** A total of 85 shear test results were included in the database. The depth of the members in the database ranged from 12 to 44 in. (305 to 1118 mm), excluding the NU girders tested in this study. Table 4.13 lists the studies included in the database as well as the types of concrete and geometrical cross-sections. Concrete compressive strengths ranged from 2,000 to 11,400 psi (13.8 to 78.6 MPa), in which 16 of the 85 tests included compressive strengths exceeding 10,000 psi (68.9 MPa). When calculating the predicted shear strength,  $V_{ACI}$  or  $V_{AASHTO}$ , the actual compressive strength at the time of testing was used. Since a majority of the test data consisted of smaller scale specimens typically used in non-transportation related infrastructure, both the 2011 ACI 318 and the 2012 AASHTO LRFD were investigated. It is expected that the test girders will yield less conservative results when compared to ACI 318 because the size effect in shear is not included in the prediction equations (see Section 2.2.4). The constructed database includes the shear strength ratio, defined as the tested-to-predicted shear strength for the 2011 ACI 318 and the 2012 AASHTO LRFD codes, respectively. Values greater than one indicate conservative results. The shear strength ratio is compared to the concrete compressive strength ( $f'_c$ ), effective depth ( $d$ ), level of prestress ( $P_e/A_c$ ), proportion of coarse aggregate by total weight of aggregate, proportion of coarse aggregate by total weight of mix, and the shear span to depth ratio ( $a/d$ ) to evaluate the impact of HS-SCC in shear. Tabulated results of the database are included in Appendix E.

Figure 4.21 illustrates the shear strength ratio as a function of the compressive strength. There is a slight decrease in the conservativeness of the ACI 318 prediction as the compressive strength increases; however, this trend is not observed for AASHTO LRFD as additional factors are taken into account in the prediction equation (aggregate size, crack spacing parameter) which could influence the results (AASHTO LRFD, 2012). The shear strength ratio of the HS-SCC test girders does not appear to be significantly different from specimens with similar compressive strengths. All test results with compressive strengths in excess of 10,000 psi (68.9 MPa) included limestone aggregates. Thus, at high compressive strengths, the failure plane often extends through the aggregate, limiting the effect of the different coarse aggregate contents between HS-SCC and HSC; a common explanation for the expected reduced shear strength of SCC.

Table 4.13. Database Concrete Types and Geometries

Study	Concrete Type	Member Shape
NU Test Girders	HS-SCC	I
Elzanaty et al. (1986)	HSC	I
Myers et al. (2012)	CC,HSC, SCC, HS-SCC	Rectangle
Shahawy and Batchelor (1996)	CC	I
Sozen et al. (1959)	CC	I
Teng et al. (1998b)	CC	Rectangle

The shear strength ratio is evaluated against the effective depth in Figure 4.22. As expected, there is a decreasing trend in the conservativeness of the results when evaluated with ACI 318 (2011). This is a result of the “size effect” in shear since ACI assumes a linear increase in the shear capacity with member depth. This assumption causes the data points of the test girders in all of the ACI database figures to appear lower than their smaller sized counterparts. The 2012 AASHTO LRFD provisions do not illustrate this trend as the crack spacing parameter,  $s_{xc}$ , accounts for the size of the member. After examining Figure 4.22b, HS-SCC does not correlate to a reduction in shear strength as tests conducted by Sozen et al. (1959) exhibited lower shear strength ratios with conventional concrete.

Figure 4.23 displays the results plotted with the effective level of prestressing, defined as the effective prestressing force divided by the cross-sectional area of the concrete section. This parameter was investigated as not all prestressed members are prestressed to the same extent. The plots show a slight decrease in the conservativeness of the ACI 318 estimates. However, the specimens with high prestressing levels also were cast with high strength concrete (Elzanaty et al., 1986). This difference could explain the observed trend. There is significant scatter in the results when compared to AASHTO LRFD estimates. Unlike ACI 318 which directly accounts for the level of prestressing, AASHTO LRFD indirectly takes into account the degree of prestressing through the diagonal cracking term,  $\beta$ . Thus, the prestressing force does not contribute as heavily to the predicted shear strength of the AASHTO LRFD specifications. Neither figure shows a clear distinction in the prestressing level between CC and HS-SCC.

Of the five references used to construct the shear database, only three provided information on the coarse aggregate content. The tests conducted by Elzanaty et al. (1986), Sozen et al. (1959), and Myers et al. (2012) are included with the NU test girders in Figure 4.24 to evaluate the impact of varying coarse aggregate contents by total weight of aggregate. Neither ACI 318 nor AASHTO LRFD show definitive trends of the shear strength ratio as a function of the coarse aggregate content. Myers et al. (2012) reported coarse aggregate contents as low as 30% at select precast manufacturers across the United States; outliers of this magnitude would need to be tested to completely assess the impact of coarse aggregate content on shear strength. For the given range of data, other factors including concrete strength and member geometry contribute more heavily to the shear strength of prestressed concrete members.

Figure 4.25 displays the shear strength ratio as a function of the coarse aggregate content by total weight of the mix. The coarse aggregate content by weight of the mix is calculated as the weight of coarse aggregate divided by the coarse aggregate, fine aggregate, cementitious materials, admixtures, and water. Similar to Figure 4.24, only 3 other references listed the CA content, and both ACI 318 and AASHTO LRFD show significant scatter in the data with no discernible trends. Additional data points with lower CA contents as reported by Myers et al. (2012) could yield different results.

Alternatively, the coarse aggregate content could be reported by the paste volumetric fraction. Since the paste is typically the weak link in the concrete, a larger volume of paste could provide a better indication of the impact of coarse aggregate on the shear strength of concrete members. However, of the 5 references in the database, only Myers et al. (2012) reported specific gravities of the investigated coarse and fine aggregates, and so the shear strength ratio was not plotted against this variable. The specific gravities could be used to calculate the paste volumetric fraction based on the batch weights per cubic yard. Future studies should report the specific gravities of the mix design constituents to investigate this variable.

The final plot in evaluating the impact of HS-SCC in shear was the shear span to depth ratio (Figure 4.26). This term,  $a/d$ , is specific to laboratory testing, yet can be crudely related to the span length of a field member. The valley of the shear failure, described in Section 2.2.4, is evident in Figure 4.26a. When examining the 2012

AASHTO LRFD provisions, the shear strength is greatly overestimated for low shear span ratios; for this reason, only 3 of the 11 tests of Teng et al. (1998b) are shown in Figure 4.26b. The remaining tests had shear strength ratios in excess of 3. Many of Teng et al.'s (1998b) tests included a/d ratios less than or equal to 1.6. For short shear span to depth ratios, the member fails due to crushing of the compression strut between the point of applied load and the support rather than a diagonal tension failure as with larger a/d values. For short shear spans, the strut and tie model has been found to be more accurate to predict the shear strength (ACI-ASCE 445, 1999). Bentz (2000) identified this conservatism in the MCFT for short a/d ratios during the development of Response 2000. As observed in the previous database figures, there is not a discernible difference in the test-to-predicted shear strength ratio for HS-SCC. Even the Myers et al. (2012) tests including lower strength SCC mixtures show no difference among the collected database.

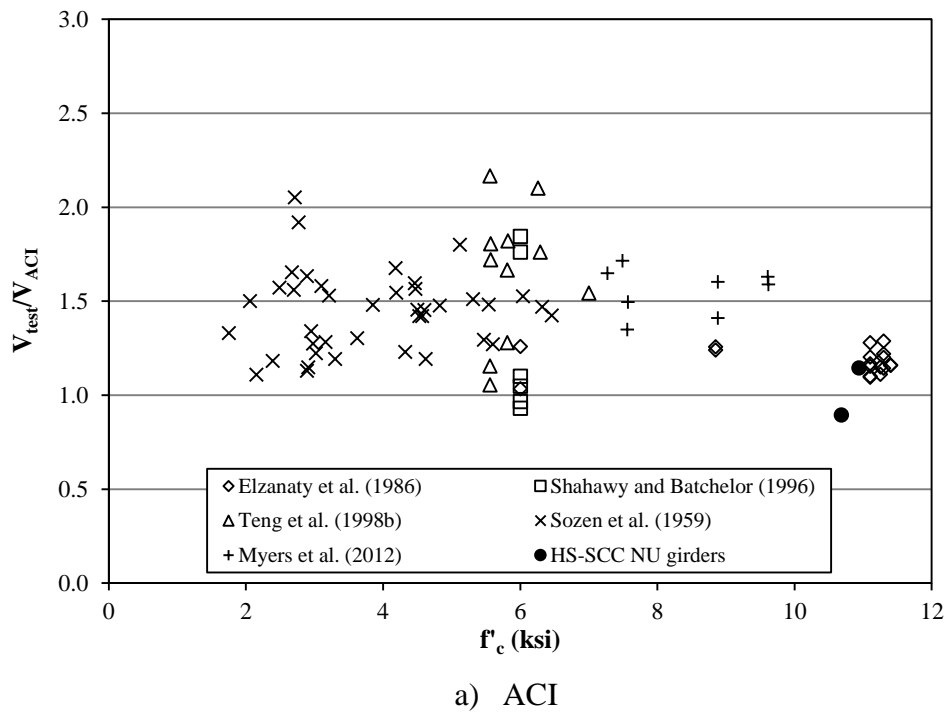
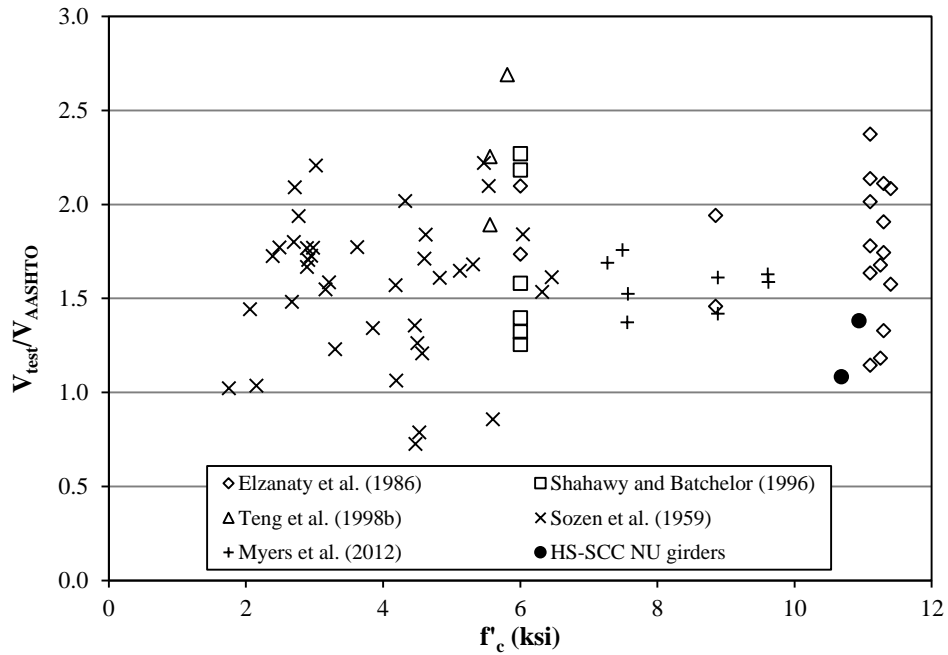


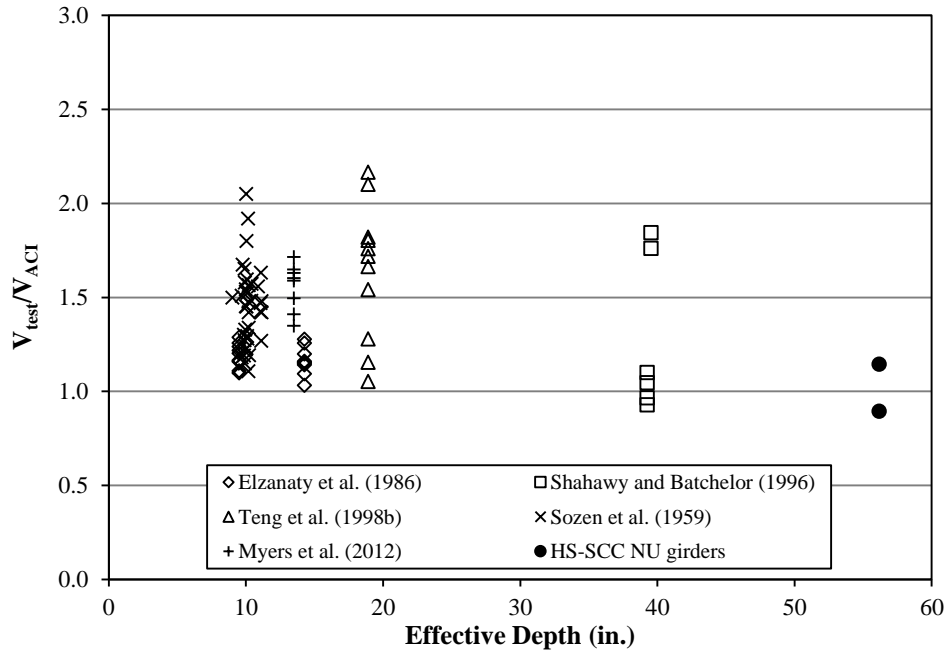
Figure 4.21. Shear Strength Ratio vs. Compressive Strength



b) AASHTO LRFD

Conversion: 1 ksi = 6.895 MPa

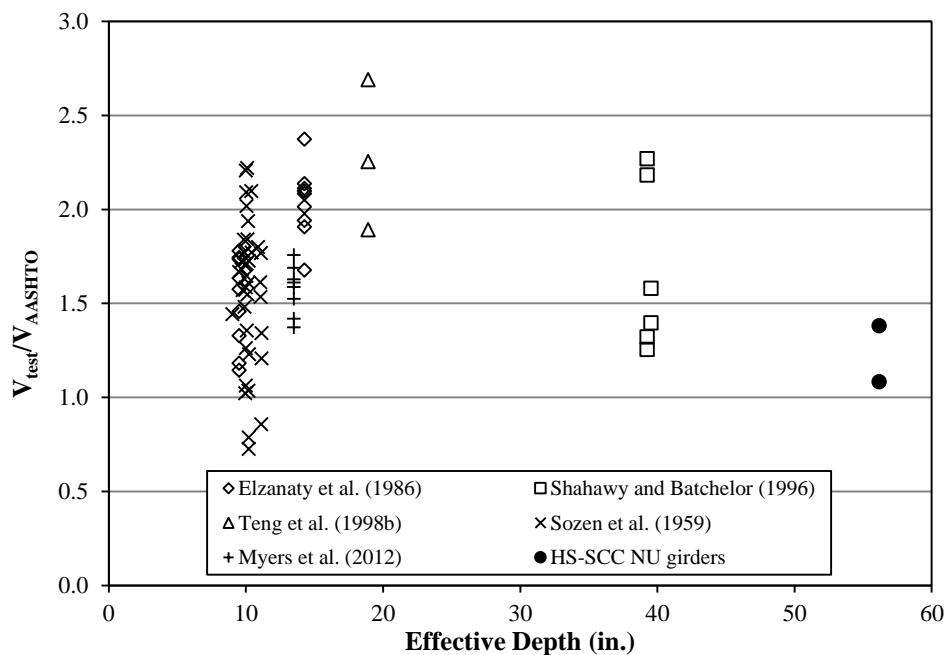
Figure 4.21. Shear Strength Ratio vs. Compressive Strength (cont.)



a) ACI

Figure 4.22. Shear Strength Ratio vs. Effective Depth

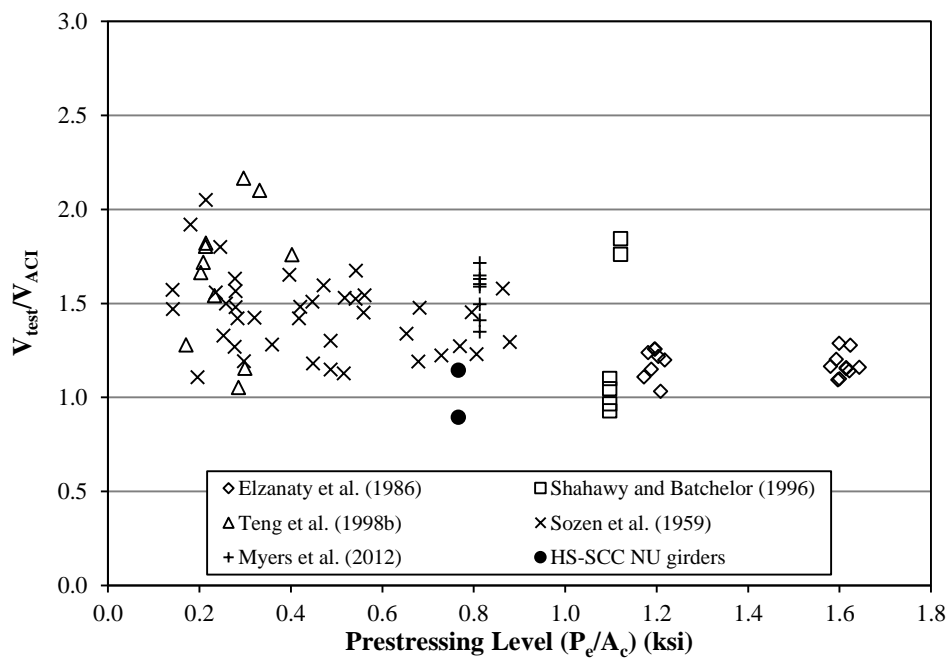




b) AASHTO LRFD

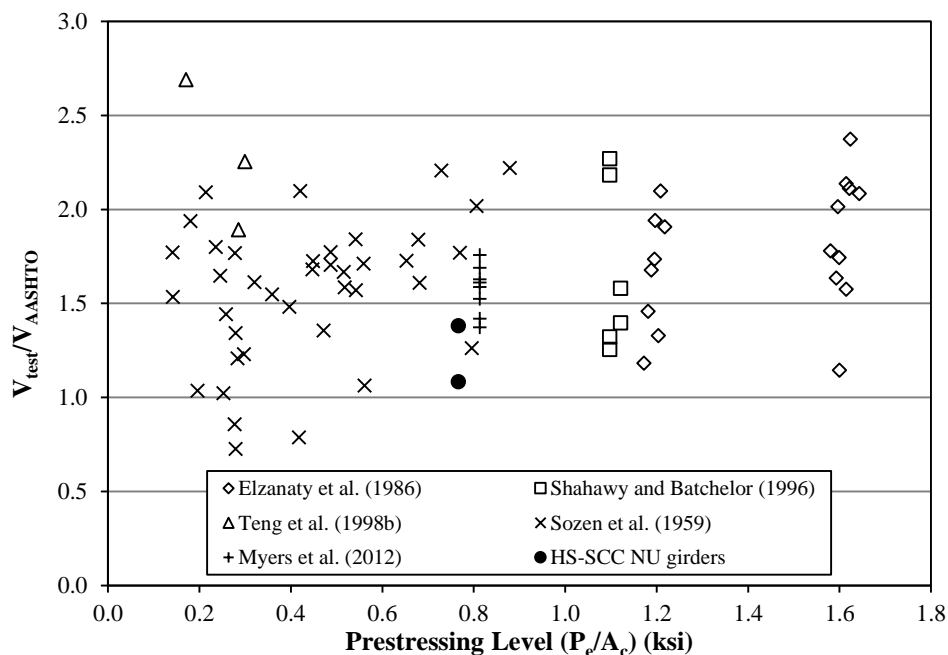
Conversion: 1 in. = 25.4 mm

Figure 4.22. Shear Strength Ratio vs. Effective Depth (cont.)



a) ACI

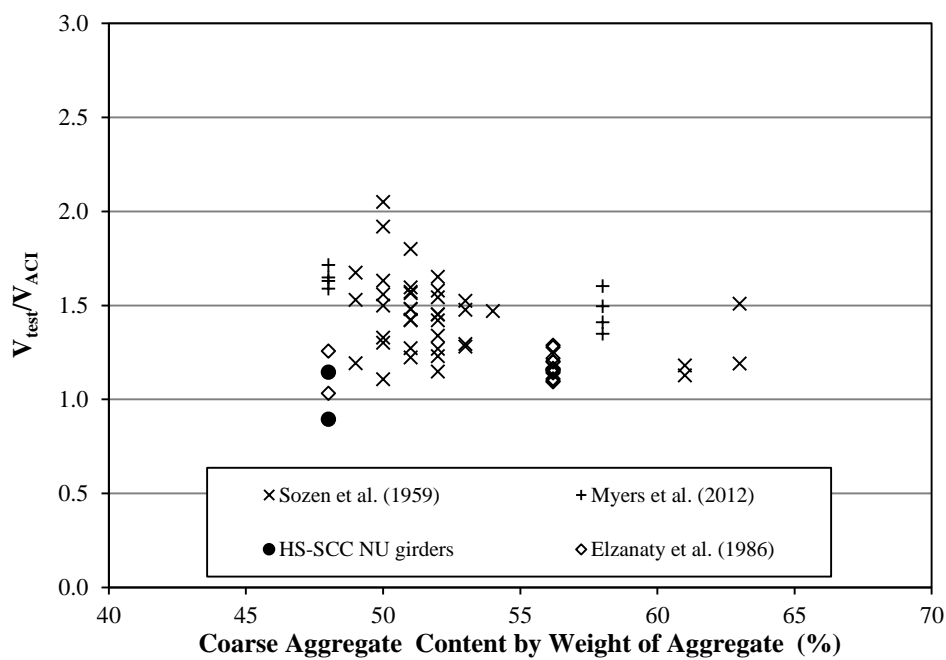
Figure 4.23. Shear Strength Ratio vs. Prestress Level



b) AASHTO LRFD

Conversion: 1 ksi = 6.895 MPa

Figure 4.23. Shear Strength Ratio vs. Prestress Level (cont.)



a) ACI

Figure 4.24. Shear Strength Ratio vs. CA Content by Total Weight of Aggregate

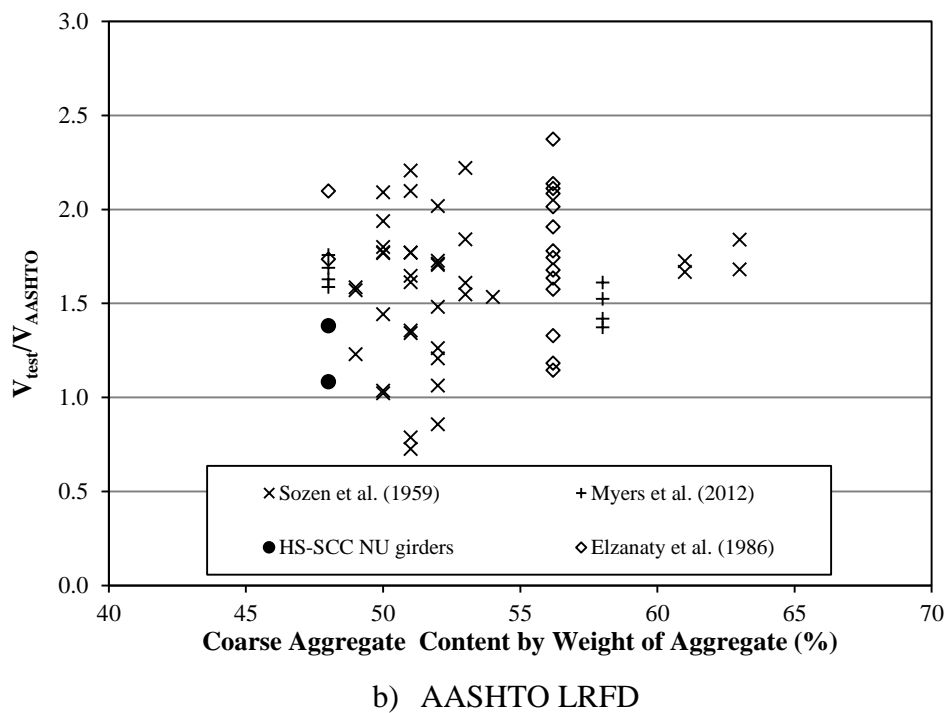


Figure 4.24. Shear Strength Ratio vs. CA Content by Total Weight of Aggregate (cont.)

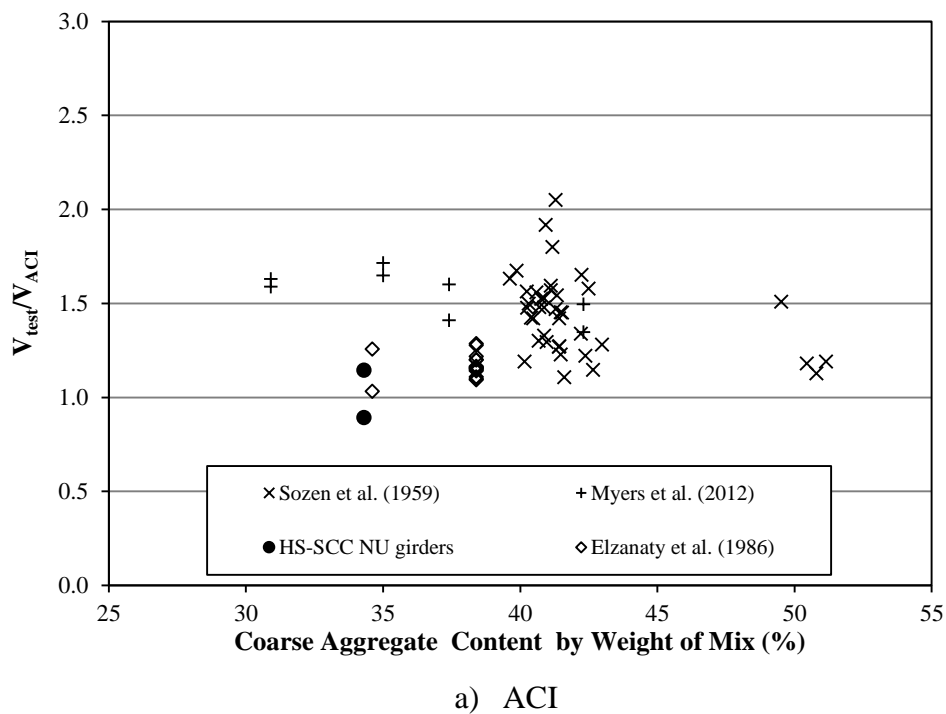


Figure 4.25. Shear Strength Ratio vs. CA Content by Total Weight of Mix

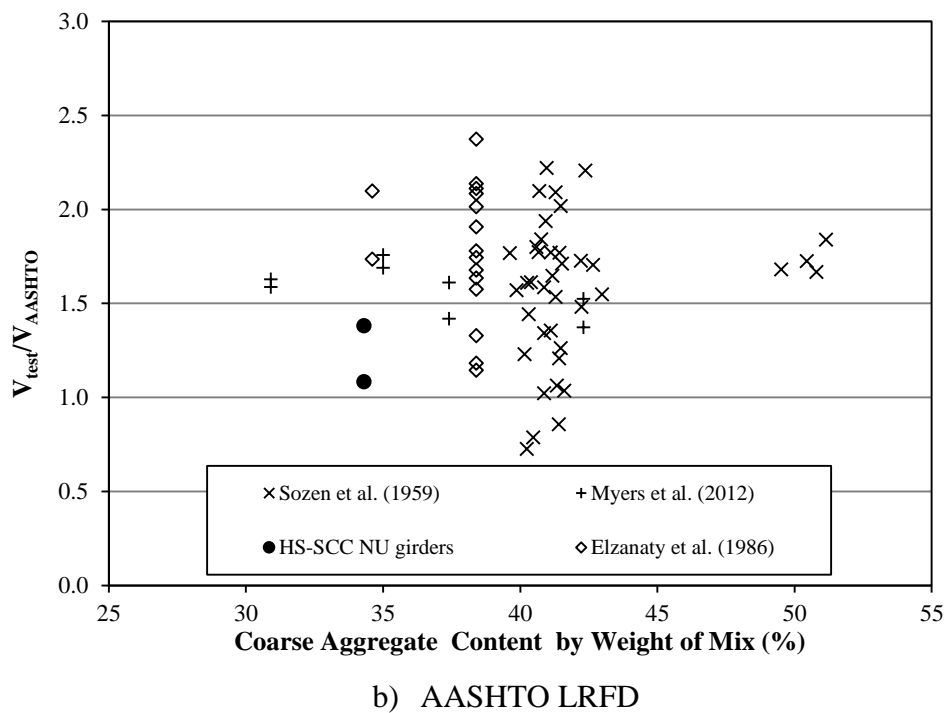


Figure 4.25. Shear Strength Ratio vs. CA Content by Total Weight of Mix (cont.)

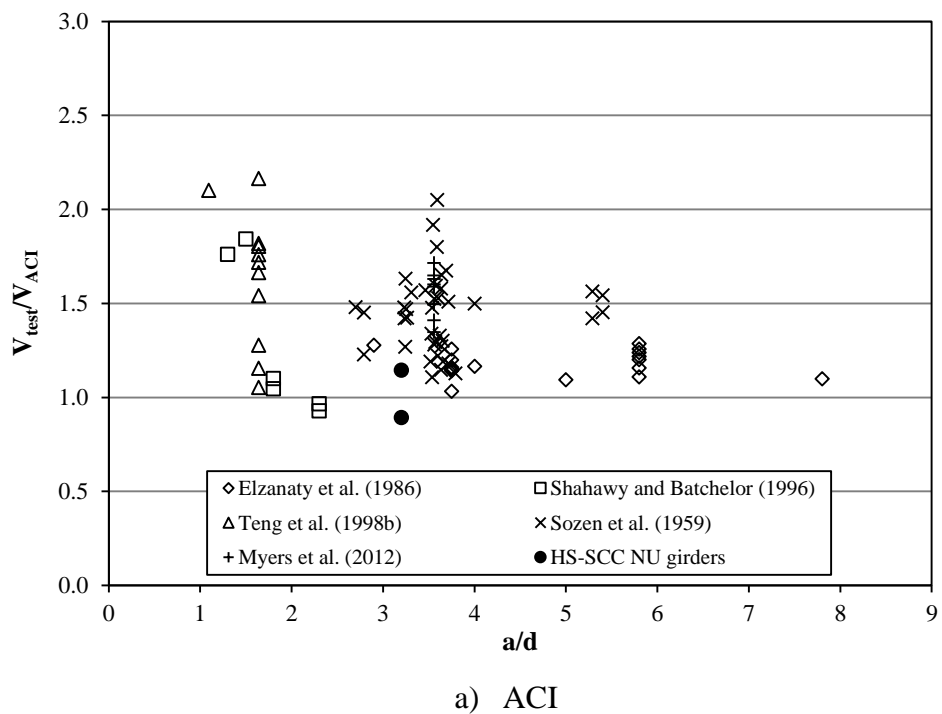
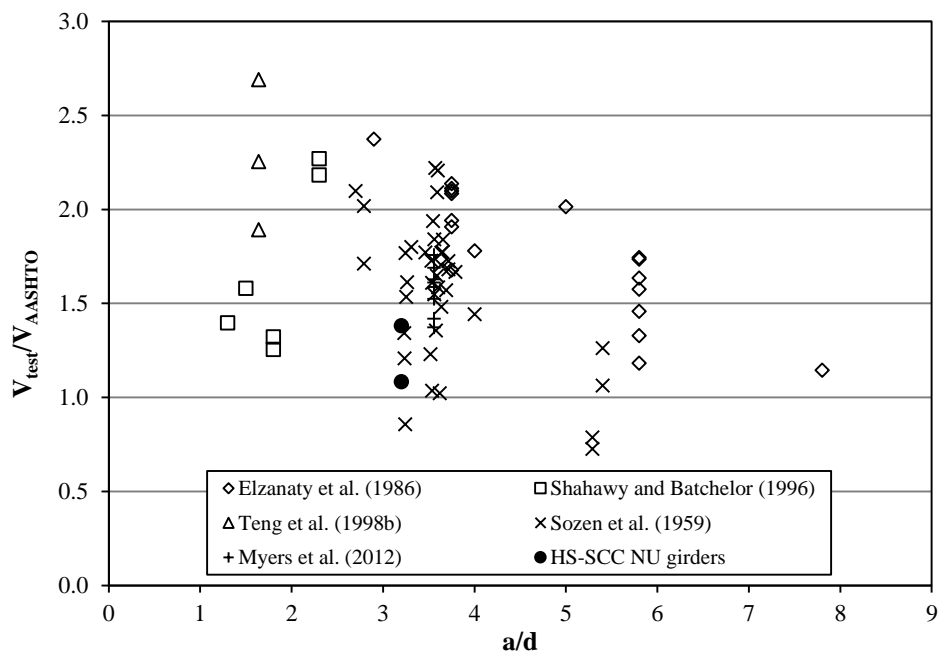


Figure 4.26. Shear Strength Ratio vs. Shear Span to Depth Ratio



b) AASHTO LRFD

Figure 4.26. Shear Strength Ratio vs. Shear Span to Depth Ratio (cont.)

**4.5.3. Summary of Database Results.** The shear strength ratios were plotted for 85 shear specimens against compressive strength, effective depth, prestressing level, coarse aggregate content by weight of aggregate and weight of mix, and shear span to depth ratio. The NU test girders exceeded the 2012 AASHTO LRFD specifications and, on average, exceed the 2011 ACI 318 predicted shear strength. The shear strength ratio appears to be on the low end of the test results in the collected database. This could be attributed to various factors. First, the reduction in coarse aggregate could contribute to the lower ratio. However, this trend was not clearly observed based on the collected data. Second, the wide, flat upper and lower flanges of the NU girder leads to a more efficient section for flexure; however, this corresponds to a greater shear depth,  $d_v$ , relative to the overall height. This physical difference could reduce the shear strength ratio. The CIP deck also leads to an increase in the shear depth relative to the overall height. Other sections in the database have stockier flanges, thus reducing the proportion of the shear depth to the overall height. Third, the effective web width,  $b_v$ , is not constant for the same proportion of the overall height. In the AASHTO Type II girders, the web width

used in shear computations only spans 42% of the overall height. In contrast, the NU series effective web width is constant for 48% of member's overall height. Lastly, as mentioned in Section 3.5.4, there was minor hairline cracking in the unreinforced shear region when testing was conducted on the opposite end of the beam. This initial damage in addition to the aforementioned geometrical and material differences could attribute to the lower observed shear strength ratios in the database.

Based on the presented data, the results of the NU girders in this study and the HS-SCC and SCC shear beams of Myers et al. (2012) indicate no discernible differences between self-consolidating concrete and conventional concrete despite the material differences in size and content of coarse aggregate. This conclusion is based on only 6 SCC shear tests against 79 tests of conventional or high strength concrete. Additional shear tests on SCC mixtures with varying coarse aggregate contents and compressive strengths are necessary to more effectively evaluate the shear strength of SCC. Myers et al. (2012) reported precast manufacturers using SCC mixtures with coarse aggregate contents by weight as low as 30%. Perhaps, by widening the band of CA content data, a more comprehensive understanding of the shear strength of SCC could be achieved. The tests carried out in this study aim to contribute to the universal acceptance of the shear behavior of SCC with respect to CC in precast applications.

#### **4.6. SUMMARY**

The mechanical properties of the HS-SCC were documented. The tested shear strength of the NU 53 girder without shear reinforcement was compared to ACI 318 and AASHTO LRFD code estimates. The results of these two tests were compared with Response 2000 and evaluated with ATENA Engineering. These tests without shear reinforcement were gauged against other non-shear reinforced prestressed girders and beams via a database. Testing observations and conclusions were discussed regarding the shear behavior of the NU 53 composite PC/PS girder both with and without web reinforcement.

The ultimate failure loads of the NU girders without shear reinforcement were compared to ACI 318 (2011), AASHTO LRFD (2012), and Response 2000. Table 4.14 lists the experimental and predicted values (in kips) along with the shear strength ratio.

Aside from ACI 318, which can overestimate the shear capacity for larger members, Response 2000 modeled the test results to a reasonable combination of accuracy and conservativeness. The initial hairline cracking that occurred in the unreinforced region during the first tests (Section 3.5.4) did not appear to have any adverse effects on the end results as both girders experienced this initial damage, yet produced different failure shear loads.

Table 4.14. Summary Table of Shear Testing without Web Reinforcement

	$V_{\text{test}}$	$V_{\text{ACI}}$	$V_{\text{AASHTO}}$	$V_{\text{R2K}}$	$V_{\text{test}}/V_{\text{ACI}}$	$V_{\text{test}}/V_{\text{AASHTO}}$	$V_{\text{test}}/V_{\text{R2K}}$
TG1	228.1	196	159.7	172.2	1.17	1.43	1.32
TG2	176.7			169.6	0.91	1.11	1.04

Conversion: 1 kip = 4.448 kN

The first tests with web reinforcement provided valuable insight into the behavior for two different types of reinforcement bars: welded wire reinforcement and mild steel bars. The experimental results and modeling with ATENA Engineering indicate that to maintain and maximize the shear capacity for a given section, a larger number of smaller reinforcement bars should be considered when web reinforcement is required by design. This finding is based on the collected data, and is analogous to controlling flexural cracking through ACI 318 (2011) Section 10.6.4.

Conclusions from the constructed prestressed concrete database were previously discussed (Section 4.5.3), indicating that the coarse aggregate content appears to have a negligible effect on the shear strength for the given CA contents. The traditional scatter observed in shear testing results possibly shadows any trends regarding the coarse aggregate content. Additional testing with lower coarse aggregate contents is necessary to observe the outer limits of mix designs.

## 5. SUMMARY & CONCLUSIONS

### 5.1. SUMMARY

The objective of this study was to evaluate the shear capacity of a composite NU 53 girder composed of high strength self-consolidating concrete and compare it to code estimates. After completion and evaluation of the tests, construction began on Bridge A7597 near Linn, Missouri, to serve as an implementation test bed to showcase HS-SCC, SCC, and HVFAC.

Two test girders were fabricated at County Materials Corporation in Bonne Terre, Missouri, and transported to the Butler-Carlton Hall SERL at Missouri University of Science and Technology for destructive testing. The test set-up and preparation were documented including fabrication of a 6 in. (152 mm) thick cast-in-place slab to simulate a road deck. Each girder design allowed for two shear tests, one at each end to evaluate the performance both with and without web reinforcement. The shear behavior containing web reinforcement was observed and analyzed, followed by the destructive testing of the NU section without transverse reinforcement. Cylinders and beams were collected from the fabrication process to assess the mechanical properties of HS-SCC including compressive strength, modulus of elasticity, and modulus of rupture.

The results of the hardened mechanical properties of the HS-SCC mix were documented and compared to existing empirical equations from ACI and AASHTO LRFD documents and specifications. Crack patterns and widths were extensively documented and discussed. The ultimate capacity without web reinforcement was compared against ACI 318 (2011) and AASHTO LRFD (2012) specifications. Response 2000, a sectional analysis software based on the MCFT, and ATENA Engineering, a non-linear finite element analysis program, were included to evaluate the capacity and response of the girders, respectively. Lastly, a prestressed concrete shear database was developed, focusing on both I-shaped and larger members. The shear strength ratio with respect to both the 2011 ACI 318 and the 2012 AASHTO LRFD was evaluated against the compressive strength, effective depth, level of prestressing, two approaches to defining the coarse aggregate content, and shear span to depth ratio. The effectiveness of



HS-SCC in shear was gauged against previous laboratory shear tests containing both lower and higher strength concretes.

## 5.2. FINDINGS & CONCLUSIONS

**5.2.1. HS-SCC Mechanical Properties.** Compressive strength, modulus of elasticity, and modulus of rupture tests were performed on representative specimens of the HS-SCC. The following conclusions were reached regarding the mechanical properties of HS-SCC with locally available Missouri aggregates. These findings are based on the specific mix design of this HS-SCC mix, most notably the size, content, and type of the coarse aggregate.

- The compressive strength met the required design strength of 10,000 psi (68.9 MPa) before the 28 day test. A peak average compressive strength of 11,020 psi (76.0 MPa) was observed at a maturity age of 77 days.
- The modulus of elasticity was overestimated by ACI 318 (2011), and accurately predicted by the Martinez et al. equation in ACI 363R (2010). Alternatively, the Tomosawa et al. proposed equation in ACI 363R (2010) should be used as a lower bound predictor.
- The modulus of rupture was most accurately predicted by the ACI 318 (2011) equation and overestimated by ACI 363R (2010), which can be attributed to the stiffness and content of the aggregate. Scatter on the order of 40% was observed among the test results for the modulus of rupture.

**5.2.2. Shear Tests.** The results of the shear testing were documented along with comparisons to code estimates and software analysis programs. Conclusions documented below are representative of the HS-SCC mix investigated and the 85 specimens in the constructed shear database. The following conclusions were made:

- Shear crack widths in TG1-T1 were 23% of those in TG2-T1, a result of the spacing of shear reinforcement. A recommendation based on this observation is provided in the subsequent section.
- The shear force provided by the uncracked concrete in the presence of transverse reinforcement increased by 48% and 23% in test girders 1 and 2, respectively. In

these tests, the shear reinforcement limited both the formation and widths of the cracks.

- The concrete contribution to shear not in the presence of transverse reinforcement exceeded the factored shear capacity predicted by ACI 318 (2011). The average load at failure exceeded the nominal predicted capacity by a factor of 1.02 when the actual concrete compressive strength was used. This value increased to 1.04 when the ACI 318 maximum limit on  $f'_c$  of 10,000 psi (68.9 MPa) is included.
- The shear load at failure exceeded both the nominal and the factored shear resistance predicted by the 2012 AASHTO LRFD Bridge Design Specifications for the concrete contribution to shear without web reinforcement. The size effect parameter included in the AASHTO provisions led to more conservative estimates than ACI 318 (2011).
- Response 2000 predicted the shear capacity of the NU test girders to a reasonable degree of accuracy. However, the level of conservativeness is greatly affected by the input tensile strength of concrete, which can vary significantly for a given compressive strength.
- ATENA Engineering v5.0.3 showed a general decrease in the shear capacity as the coarse aggregate content reduces to zero. However, there were mixed results when the aggregate size was increased to 1 in. (25.4 mm). Based on the analysis, the presence of aggregate (rather than the size) influenced the results. The predicted crack patterns aligned with the tested observations when shear reinforcement is placed at 12 in. (305 mm) on center.
- Based on the constructed shear database, the shear strength ratio of the HS-SCC tests girders was similar to the shear strength ratios of other specimens, specifically when analyzed with the 2012 AASHTO LRFD specifications. The test results appear to be on the lower end of the data points when compared with the 2011 ACI 318 estimations; however this trend occurs from the size effect not accounted for in the ACI 318 provisions. Based on the data collected, there were no distinguishable trends of the shear strength ratio with respect to the coarse aggregate content as other factors contribute more heavily to the shear capacity of prestressed concrete members.

### 5.3. RECOMMENDATIONS

The results and testing observations of the NU girders were recorded and documented. Based on the results obtained, the high strength self-consolidating concrete mix investigated is a viable alternative for precast prestressed concrete elements. When designing HS-SCC elements in shear, the transverse reinforcement should be designed to minimize the spacing. By reducing the spacing of web reinforcement, the diagonal shear crack widths are minimized such that the interface shear transfer mechanism of the shear carried by the concrete is maximized even when cracks propagate through the aggregate. The shear test observations containing web reinforcement support this recommendation.

### 5.4. FUTURE WORK

The results of this study embody the unique cross-section and material constituents of the concrete mix. To obtain a more comprehensive understanding of the shear behavior and capacity of HS-SCC, additional tests are necessary. Additional test data will fuel the everyday use of SCC in both CIP and precast applications. Full-scale shear testing on SCC girders with web reinforcement was documented in Section 2.4.2 of this thesis, all with similar results. However, there is limited data on the shear behavior of SCC without web reinforcement. To gain a more comprehensive understanding of the shear response of self-consolidating concrete, parametric studies of prestressed self-consolidating concrete beams without web reinforcement should encompass:

1. Varying concrete compressive strength in excess of 12,000 psi (82.7 MPa). This will support the inevitable advancements in concrete technology.
2. Varying the coarse aggregate content while still maintaining mix stability and robustness. The mix investigated was limited to a minimum CA content by total weight of aggregate of 48%. Additional full-scale testing with lower CA contents is necessary. It is advisable for future studies to report the specific gravities of the investigated coarse and fine aggregates as well. This information could assist in comparisons of the paste volumetric fraction between test results of different mix designs. This could serve as an alternate method to analyze the reduction in coarse aggregate in SCC mixtures.

3. Various types of coarse aggregate. Local geographical rock formations dictate the strength of the coarse aggregates in reinforced and prestressed concrete elements. Research institutions across the continent must contribute to the objective to obtain a more representative test bed with diverse mixture constituents.
4. Substitution of Portland cement with varying levels of fly ash and other cementitious materials as the push for more sustainable materials expands.

APPENDIX A.  
DESIGN DRAWINGS

Concrete for Test Girder No. 1 shall be self-consolidating concrete with  $f'_c = 10,000$  psi and  $f'_t = 8000$  psi. (See Special Provisions)

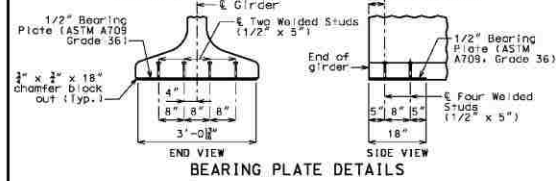
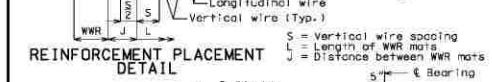
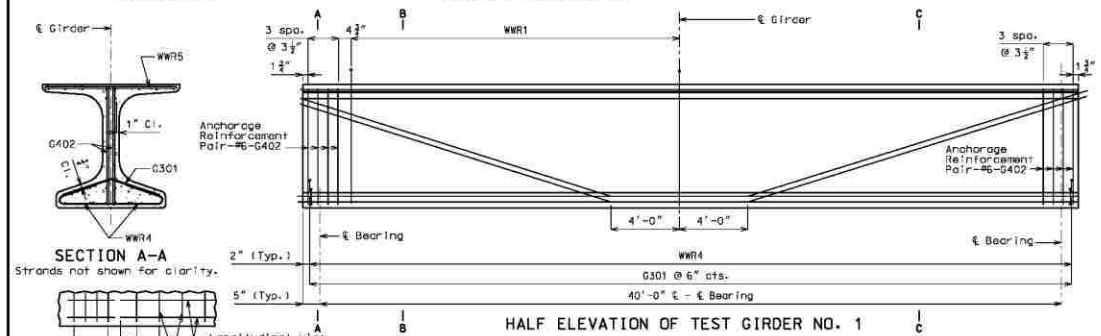
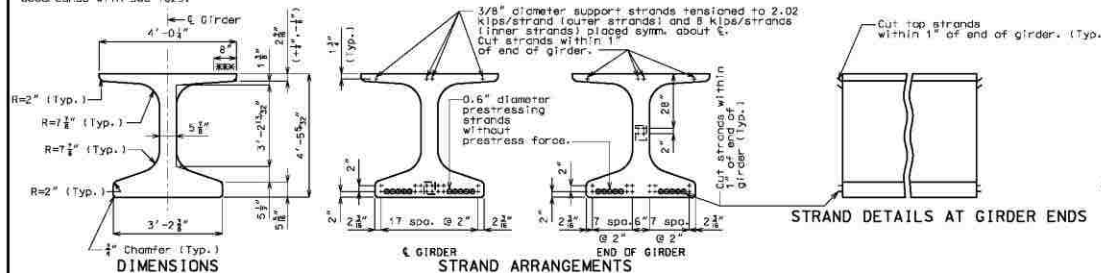
(+) Indicates prestressing strand.

Use 16 strands with an initial prestress force of 704 kips.

Prestressing tendons shall be uncoated, seven-wire, low-relaxation strands, 0.6 inch diameter in accordance with AASHTO M 203, Grade 270. Prestressing members shall be in accordance with Sec 1029.

Girders shall be lifted by devices designed by the fabricator.

\*\*Girder top flange shall be steel troweled to a smooth finish for 8" at the edges, as shown. Bond breaker shall be applied to this region only. The center portion shall be rough finished by scuffing the surface transversely with a wire brush, and no tolerance shall remain on the surface.



Galvanize the 1/2" bearing plate (ASTM A709 Grade 36) in accordance with ASTM A123.  
 Cost of furnishing, galvanizing, and installing the 1/2" bearing plate (ASTM A709 Grade 36) and welded studs in the prestressed girder will be considered completely covered by the contract unit price for Prestressed Concrete NU-Girder.

Detailed Feb. 2012  
 Checked Apr. 2012

Note: This drawing is not to scale. Follow dimensions.

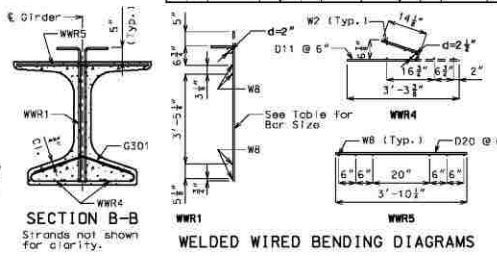
Sheet No. 15a of 44

BILL OF REINFORCING STEEL - EACH GIRDER					
NO.	SHAPE	QUANTITY	UNIT	WEIGHT	REMARKS
82	3 G301	2'-11 1/2"	15		SHAPE 15 (G301)
16	6 G402	4'-3"	20		SHAPE 20 (G402)

\*THIS MEDIA SHOULD NOT BE CONSIDERED A CERTIFIED DOCUMENT.\*

EST. NUMBER: 8/6/2012  
 COUNTY: OSAGE  
 JOB NO.: JSP0951B  
 CONTRACT ID: 15A

WELDED WIRE REINFORCEMENT											
(WWR4 & WWR5 as shown in Welded Wire Bending Diagrams)											
BAR	SIZE	U1	U2	U3	U4	U5	U6	U7	U8	U9	U10
D2012	19	0									



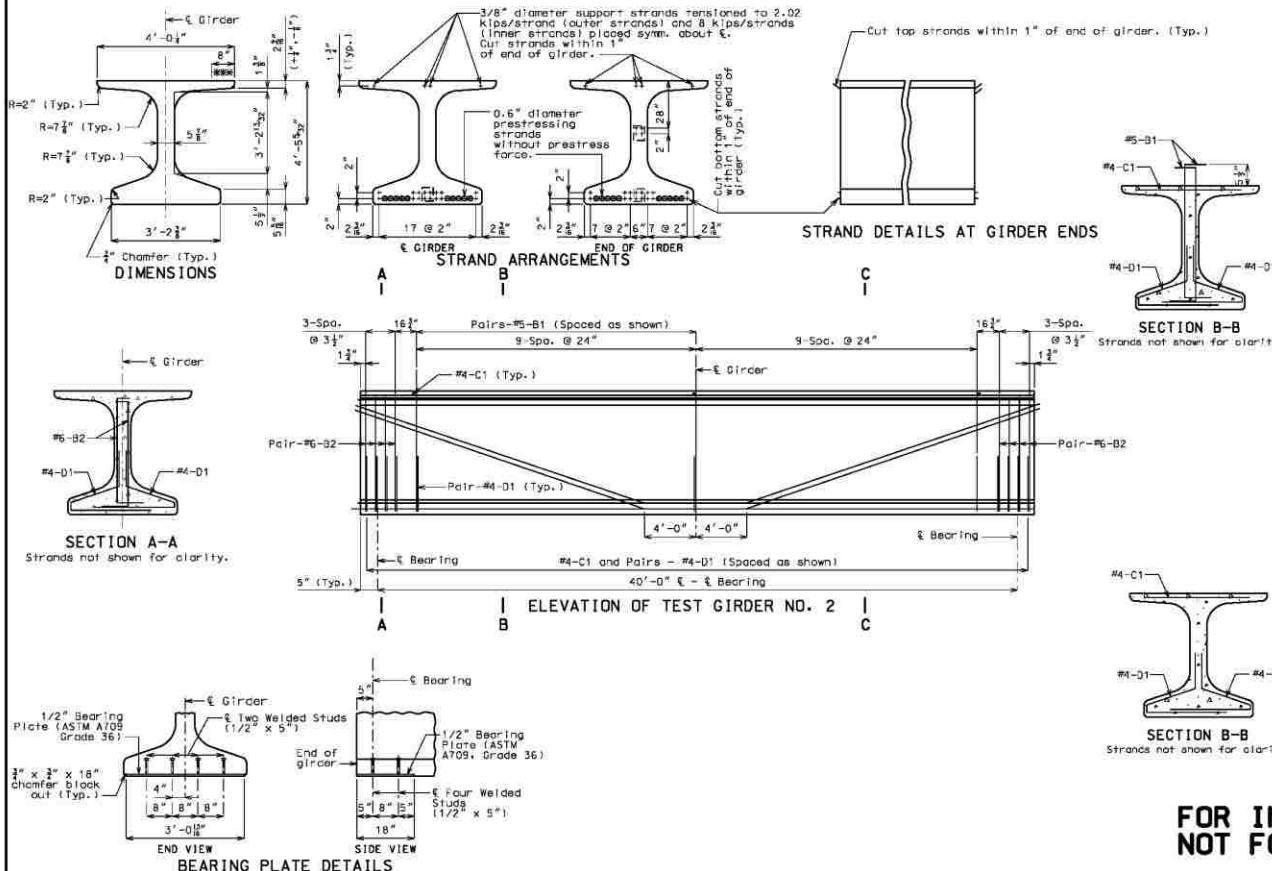
**REINFORCING STEEL NOTES:**  
 Reinforcing steel shall conform to the requirements of AASHTO M 31, Grade 60, Welded Wire Reinforcement (WWR) shall conform to the requirements of AASHTO M 221.  
 WWR shall not be epoxy coated.  
 All dimensions are out to out.  
 Hooks and bends shall be in accordance with the CRSI Manual of Standard Practice for Detailing Reinforced Concrete Structures, Stirrup and Tie Dimensions.  
 Minimum clearance to reinforcing shall be 1", unless otherwise shown.  
 Actual bar lengths are measured along centerline of bar.  
 Drilling is not allowed.

**FOR INFORMATION ONLY  
 NOT FOR CONSTRUCTION**

Sheet Added 8/06/2012

Concrete for Test Girder No. 2 shall be self-consolidated with  $f'_c = 10,000 \text{ psi}$  and  $f'_ci = 8000 \text{ psi}$ . (See Special Provisions)  
 (+) indicates prestressing strand.  
 Use 16 strands with an initial prestress force of 704 kips.  
 Prestressing tendons shall be uncoated, seven-wire, low-relaxation strands, 0.6 inch diameter in accordance with AASHTO M 203, Grade 270. Prestressing members shall be in accordance with Sec 1029.

Girders shall be luffed by devices designed by the fabricator.  
 \*\*\* Girder top flange shall be steel troweled to a smooth finish for 8" at the edges, as shown. Bond breaker shall be applied to this region only. The center portion shall be rough finished by scrubbing the surface transversely with a wire brush, and no laitance shall remain on the surface.



NO.	SIZE & SHAPE	LENGTH	QUANTITY	REMARKS
38	5 B1	5'-9"	16	SHAPE 20 (C1)
16	6 B2	5'-2"	16	
27	4 C1	3'-10"	20	SHAPE 9
34	4 D1	4'-2"	9	SHAPE 19

All dimensions are out to out.  
 Hooks and bends shall be in accordance with the CRSI Manual of Standard Practices for Detailing Reinforced Concrete Structures, Stirrup and Tie Dimensions.  
 Actual lengths are measured along centerline of bar to the nearest inch.  
 Minimum clearance to reinforcing shall be 1".  
 All reinforcement shall be Grade 60.  
 The two D1 bars may be furnished as one bar at the fabricator's option.  
 All B1 bars shall be epoxy coated.  
 At fabricator's option WWR5 bars may be used to replace C1 bars.  
 Drilling is not allowed.

"THIS MEDIA SHOULD NOT BE CONSIDERED A CERTIFIED DOCUMENT."

EXT. REVISION 8/6/2012  
 COUNTY OSAGE  
 PROJECT BR 17A

JOB NO. J5P0951B  
 CONTRACT ID.  
 PROJECT NO.  
 BRIDGE NO. A7957

DATE	DESCRIPTION

MISSOURI HIGHWAYS AND TRANSPORTATION COMMISSION

105 WEST CAPITAL  
 JEFFERSON, MO 64601  
 1-800-ARK-MODOT 1-888-275-6638

**FOR INFORMATION ONLY  
 NOT FOR CONSTRUCTION**

Sheet Added 8/06/2012

APPENDIX B.  
MIX DESIGNS





**Missouri Department of Transportation-Construction and Materials Division**

**Concrete Mix Design Submittal Form**

Date: 03/07/12

Concrete Supplier: County Materials Corp., Bonne Terre (Egyptian) Plant Location: \_\_\_\_\_

Designer Name: Larry Johnson Designer Phone No.: (573) 358-2773

Version 3.45

Print Pages 1 and 2

Print Pages 1 & 2 and mix analysis

Note: This form should be submitted with a cover letter acknowledging which MoDOT contracts a mix is planned to be used on if any are known.

**Components**

Mineral	Producer	Type	Unit Wt (lb/cf)	Sp. Gravity	Abs.	Ledges	Enter Sample ID
Fine Agg.	Weber, Crystal City Sand	Natural Sand for Conc Class A	113.00	2.62	0.4	Mississippi River	116R3M199
Intern. Agg.							
Coarse Agg.	Lead Belt, Park Hills Stone	PCCP 0 1/2" Max LS/DO	101.00	2.66	1.5	4 - 1	110MA0304
Cement	Holcim, Ste. Genevieve Plant	Portland Cement Type I		3.15			10MRSM305
Fly Ash							
GGBFS							

**Admixtures**

	Source	Type	Brand Name	Enter Sample ID
#1	W. R. Grace, (IL) W 51 st. St.	@ Air Entraining Agent for Concrete @	DARAVAIR 1400	106DAJ065
#2	W. R. Grace, (IL) W 51 st. St.	@ Type D Water Reduce & Retard Admix Con @	RECOVER	04MNP04023
#3	W. R. Grace, (TX)	@ Type F High Range Water Reduce Agent @	ADVA CAST 575	07MNP0724
#4				

**Proportions and Properties (for up to five mixes)**

MoDOT Mix ID (to be filled in by MoDOT)	Class	Water / Cement Factor				Dry Yield for 27.0 cf	Cubic Yard Batch Rates (lbs)						Range				Enter Full Mix Type	
		gal/bk	sks/cy	Sharp	% Air		Cement	Fly Ash	GGBFS	F.A. (CA#2)	C.A.	Water	Admix #1 oz/cwt	Admix #2 oz/cwt	Admix #3 oz/cwt	Admix #4 oz/cwt		
13SECSPE001		3.72	9.04	8	5.0	21.16	850			1433		1340	280	1-5	1-3	9-17		Concrete, Special
13SECSPE002		3.91	7.98	8	5.0	21.48	750			1433		1476	260	1-5	1-3	9-17		Concrete, Special
3																		
4																		
5																		



Grace Construction Products  
 6000 W. 51st Street  
 Chicago, IL 60638  
 Jim Kolakowski  
 708-203-5210  
 james.a.kolakowski@grace.com

## Mix Design Submittal

**Date:** 11/2/2012  
**Project:** Fred Weber Project (MO DOT)  
**Customer:** County Materials Corp  
**Location:**  
**Design PSI:** 10000  
**Mix Design ID:** SCC 10K  
**Plant:** Bonne Terre, MO

**W/cm ratio:** 0.329  
**Sand / Total Agg:** 0.52  
**Design Unit Weight:** 144.6  
**Design Slump Range:** 20 - 30"  
**Design Air % Range:** 4 - 6%  
**Placement Method:** PC

	(%)	Wt. Lb	Sp.Gr.	Ft <sup>3</sup>	Source	Spec.
Cementitious: Type I Cement	100%	850	3.15	4.32	Holcim St Gen	ASTM C 150

	(%)	Wt. Lb		Ft <sup>3</sup>	Source	Spec.
Aggregates: Leadbelt 1/2" Dolomite	48%	1340	2.66	8.07	Ladbelt, Park Hills Stone	
Mississippi River Sand	52%	1433	2.62	8.77	Weber, Crystal City	

<b>Air: (%) Design Air</b>	5.0%			1.35		
<b>Water (Gal - lbs - Vol)</b>	33.6	280		4.49		
<b>Fiber / Color</b>						
<b>Totals</b>		3903		27.00		

	Oz/cwt	Oz/yd <sup>3</sup>	Source	Spec.
Admixtures: Daravair 1400	2.00	17.0	Grace	ASTM C-260
Adva Cast 575	9.00	76.5	Grace	ASTM C 494
Recover	3.00	25.5	Grace	ASTM C 494

*We hope the information here will be helpful. It is based on data and knowledge considered to be true and accurate and is offered for the user's consideration, investigation, and verification, but we do not warrant the results to be obtained. Please read all statements, recommendations, or suggestions in conjunction with our conditions of sale, which apply to all goods supplied by us. No statement, recommendation, or suggestion is intended for any use which would infringe any patent or copyright.*

**W.R. Grace & Co.-Conn., 62 Whittemore Avenue, Cambridge, MA 02140**

APPENDIX C.  
EXCEL SPREADSHEETS

INPUT			
	TG1	TG2	
$f'_c$	10.393	11.029	ksi
$f'_{ci}$	7.942	7.942	ksi
$E_{ci}$	4712	4712	ksi
$E_c$	5445	5857	ksi
$E_{psi}$	28500	28500	ksi
$A_{ps}$	3.472	3.472	in <sup>2</sup>
$A_g$	743.88	743.88	in <sup>3</sup>
H	70	70	%
Age at transfer	3	3	days
Age at deck	20	63	days
Age at first test	45	77	days
$P_j$	704	704	k
$f_j$	202.5	202.5	ksi
$e_{pg}$	20.71	20.71	in
I	297512	297512	in <sup>4</sup>
$M_g$	155.2	155.2	k-ft
V/S	3.048	3.048	
$I_c$	429579	429579	in <sup>4</sup>
$A_e$	894.18	894.18	in
$e_{pc}$	26.165	26.165	
$M_{dab}$	52.3	52.3	k-ft
$A_d$	259.5	259.5	in <sup>2</sup>
$E_{cd}$	3154	2841	ksi
V/S (deck)	4.697	4.697	
$f'_{cd}$	3.061	2.485	ksi
$e_d$	26.99	26.99	in

Prestress Losses (AASHTO 2012 - Section 5.9.5)							
Elastic Losses							
Anch losses est.	0	%	Insignificant for long tendons				
$E_p$	28500	ksi					
$E_{ct}$	4712	ksi					
$f_{sp}$	1.73	ksi					
$\Delta f_{eS}$	10.45	ksi	⇒ 5.16 %				
Long term losses							
	Before Deck		After Deck				
	TG1	TG2	TG1	TG2			
$\epsilon_{b,d}$	0.000127	0.000232772	$\epsilon_{b,d}$	0.00016	0.000112		
$k_j$	1.05376	1.05376	$k_j$	1.05376	1.05376		
$k_{hr}$	1.02	1.02	$k_{hr}$	1.02	1.02		
$k_F$	0.559	0.559	$k_F$	0.559	0.559		
$k_{cd}$	0.368	0.672	$k_{cd}$	0.461	0.324		
$K_{cd}$	0.923	0.919	$K_{cd}$	0.925	0.921		
$k_j$	1.05376	1.05376	$k_j$	1.05376	1.05376		
$k_{hc}$	1	1	$k_{hc}$	1	1		
$k_F$	0.559	0.559	$k_F$	0.559	0.559		
$k_{cd}$	0.606	0.725	$k_{cd}$	0.606	0.725		
$\psi_b(t_b, t_i)$	0.596	0.713	$\psi_b(t_b, t_i)$	0.596	0.713		
$\Delta f_{pSR}$	3.350	6.099	ksi	$\Delta f_{pSD}$	4.208	2.944	ksi
$k_{cd}$	0.406	0.683		$P_\Delta$	-30.36	-48.92	k
$\psi_b(t_b, t_i)$	0.399	0.672		$\Delta f_{cd}$	-0.128	-0.180	ksi
$\Delta f_{pCR}$	3.855	6.453	ksi	$\psi_b(t_b, t_i)$	0.477	0.498	
$f_{jt}$	192.1	192.1		$\Delta f_{pCD}$	1.605	-0.006	ksi
$K_T$	30	30		$\Delta f_{pR2}$	1.539	1.539	ksi
$f_{py}$	243	243		$k_j$	1	1	
$\Delta f_{pS1}$	1.539	1.539	ksi	$k_{hr}$	1.02	1.02	
				$k_F$	1.231	1.435	
				$k_{cd}$	0.339	0.215	
				$\epsilon_{d,d}$	0.000204	0.000151	
				$\psi_d(t_b, t_i)$	0.542	0.430	
				$\Delta f_{c,d}$	-0.064	-0.045	ksi
				$\Delta f_{pSS}$	-0.411	-0.272	ksi

	TG1	TG2	
Total Losses ⇒	26.13	28.74	ksi
$f'_e$	176	173	ksi

Stiffener Schedule

Line (From Support)	Location (T/B)	Channel							Plates (w = 480 lb/ft)					Plates (stiffener to girder connection, w = 480 lb/ft)					Total Weight		
		Number	Length (in)	Height (in)	Flange width (in)	Flange thickness (in)	Designation	Weight (lb/ft)	Total weight (lb)	No.	Length (in)	Width (in)	Thickness (in)	Weight (lb)	Total weight (lb)	No.	Length (in)	Width (in)			Thickness (in)
1	T	2	120	15	3.75	0.875	C15x50	.50	1000	4	14	3	0.5	23.3	90.8	1	12	6	0.5	10.0	1100.8
	B	2	120	15	3	0.875	C15x33.9	.33.9	678	18	9	3	0.5	67.5		1	12	4	0.5	6.7	
2	T	2	120	15	3.75	0.875	C15x50	.50	1000	4	14	3	0.5	23.3	90.8	1	12	6	0.5	10.0	1100.8
	B	2	120	15	3.75	0.875	C15x50	.50	1000	18	9	3	0.5	67.5		1	12	6	0.5	10.0	
3	T	2	61	10	3	0.5	C10x30	.30	305	4	9	6	0.5	30.0	117.7	1	12	6	0.5	10.0	432.7
	B	2	63	12	3	0.5	C12x25	.25	262.5	18	9	2.75	0.5	61.9		1	12	6	0.5	10.0	
4	T	2	48	10	3	0.5	C10x30	.30	240	8	8	3	0.5	26.7	92.6	1	8	8	0.5	8.9	341.5
	B	2	48	12	3	0.5	C12x25	.25	200	10	10.5	3	0.5	43.8		1	12	8	0.5	13.3	
5	T	2	48	10	3	0.5	C10x30	.30	240	2	10	8	0.5	22.2	53.1	1	8	8	0.5	8.9	301.9
	B	2	48	12	3	0.5	C12x25	.25	200	2	12	8.5	0.5	28.3		1	12	8	0.5	13.3	
6	T	2	60	10	3	0.5	C10x30	.30	300	8	8	3	0.5	26.7	73.0	1	8	8	0.5	8.9	381.9
	B	2	60	12	3	0.5	C12x25	.25	250	2	8.5	5.5	0.5	13.0		1	12	8	0.5	13.3	
7	T	2	48	12	3	0.5	C12x25	.25	200	2	12	8.5	0.5	28.3	108.9	1	8	8	0.5	8.9	317.8
	B	2	50	10	3	0.5	C10x30	.30	250	1	8	8	0.5	8.9		1	12	8	0.5	13.3	

Dwydadg Bars

Line (From Support)	Location (E/W)	Bars (w = 5.70 lb/ft)			Splices (w = 10 lbs)		Washers (w = 25 lbs)		Nuts (w = 3.5 lbs)		
		No.	Length (in)	Width (in)	Weight (lb)	No.	Weight (lb)	No.	Weight (lb)	No.	Weight (lb)
1	E	1	120	1.5	.57	0	0	2	.50	2	.7
	W	1	120	1.5	.57	0	0	2	.50	2	.7
2	E	1	168	1.5	.79.8	0	0	2	.50	2	.7
	W	1	168	1.5	.76	1	10	2	.50	2	.7
3	E	1	102	1.5	48.5	0	0	2	.50	2	.7
	W	1	108	1.5	51.3	0	0	2	.50	2	.7
4	E	1	112	1.5	53.2	0	0	2	.50	2	.7
	W	1	111	1.5	52.7	0	0	2	.50	2	.7
5	E	1	120	1.5	.57	1	10	2	.50	2	.7
	W	1	132	1.5	62.7	1	10	2	.50	2	.7
6	E	1	120	1.5	.57	0	0	2	.50	2	.7
	W	1	114	1.5	54.2	0	0	2	.50	2	.7
7	E	1	168	1.5	.79.8	1	10	2	.50	2	.7
	W	1	168	1.5	.79.8	1	10	2	.50	2	.7

Line	Location	Total Weight (lb)
1	E	114
	W	114
2	E	136.8
	W	143
3	E	105.5
	W	108.3
4	E	110.2
	W	109.7
5	E	124
	W	139.7
6	E	114
	W	111.2
7	E	146.8
	W	146.8

Stiffener Weights (per line)	
Line No.	Weight (lb-ft)
1	2088.5
2	2640.6
3	1019.3
4	861.7
5	872.7
6	985.4
7	971.0
<b>Total</b>	<b>9439.1 lbs</b>

Input	
<b>Composite Section Properties</b>	
L	40 ft
L <sub>k</sub>	16 ft
A <sub>c</sub>	894 in <sup>2</sup>
I <sub>c</sub>	429579 in <sup>4</sup>
y <sub>b</sub>	29.165 in
y <sub>t</sub>	29.99 in
b <sub>w</sub>	6 in
h	59.15625 in
e <sub>e</sub>	15.420 in
e <sub>m</sub>	20.71 in
f <sub>c</sub>	10000 psi
f <sub>ci</sub>	8000 psi
A <sub>ps</sub>	0.217 in <sup>2</sup>
N	16
A <sub>pe</sub>	3.472 in <sup>3</sup>
f <sub>ps</sub>	270 ksi
f <sub>py</sub>	202.5 ksi
initial losses	5.16 %
total losses	14.5 %
f <sub>si</sub>	192.1 ksi
f <sub>pe</sub>	173.1 ksi
<b>Loads</b>	
w <sub>concrete</sub>	145 pcf
w <sub>a</sub>	1037.0 lb/ft

x (ft)	e (in)	d <sub>p</sub> (in)	V <sub>i</sub> (lb)	M <sub>D</sub> (k-ft)	f <sub>i</sub> (ksi)	f <sub>pe</sub> (ksi)	M <sub>cre</sub> (k-ft)	V <sub>i</sub> (lb)	M <sub>max</sub> (k-ft)	V <sub>ci</sub> (k)	φV <sub>ci</sub> (k)
0.0	15.423	50.87	20730	0.2	0.000	1.41	2468.3	20730	0.2	246809.7	185107.2
0.5	15.585	51.04	20222	10.2	0.010	1.42	2466.1	20222	10.2	4907.9	3680.9
1.0	15.751	51.20	19703	20.2	0.019	1.43	2464.1	19703	20.2	2438.7	1829.0
1.5	15.916	51.37	19185	29.9	0.029	1.43	2462.4	19185	29.9	1614.9	1211.2
2.0	16.081	51.53	18666	39.4	0.038	1.44	2461.0	18666	39.4	1202.6	901.9
2.5	16.247	51.70	18148	48.6	0.046	1.45	2459.9	18148	48.6	954.7	716.1
3.0	16.412	51.86	17629	57.6	0.055	1.46	2459.1	17629	57.6	789.2	591.9
3.5	16.577	52.03	17111	66.2	0.063	1.47	2458.7	17111	66.2	670.6	502.9
4.0	16.743	52.19	16592	74.7	0.071	1.47	2458.5	16592	74.7	581.3	436.0
4.5	16.908	52.36	16074	82.8	0.079	1.48	2458.6	16074	82.8	511.6	383.7
5.0	17.073	52.52	15555	90.7	0.087	1.49	2459.1	15555	90.7	455.6	341.7
5.5	17.238	52.69	15037	98.4	0.094	1.50	2459.8	15037	98.4	409.5	307.2
6.0	17.404	52.85	14518	105.8	0.101	1.51	2460.9	14518	105.8	370.9	278.2
6.5	17.569	53.02	14000	112.9	0.108	1.51	2462.2	14000	112.9	338.0	253.5
7.0	17.734	53.18	13481	119.8	0.115	1.52	2463.9	13481	119.8	309.5	232.2
7.5	17.900	53.35	12963	126.4	0.121	1.53	2465.8	12963	126.4	284.7	213.5
8.0	18.065	53.52	12444	132.7	0.127	1.54	2468.1	12444	132.7	262.7	197.0
8.5	18.230	53.68	11926	138.8	0.133	1.55	2470.7	11926	138.8	243.1	182.3
9.0	18.396	53.85	11407	144.7	0.138	1.55	2473.5	11407	144.7	225.4	169.1
9.5	18.561	54.01	10889	150.2	0.144	1.56	2476.7	10889	150.2	209.4	157.1
10.0	18.726	54.18	10370	155.6	0.149	1.57	2480.2	10370	155.6	194.8	146.1
10.5	18.892	54.34	9852	160.6	0.154	1.58	2484.0	9852	160.6	181.4	136.0
11.0	19.057	54.51	9333	165.4	0.158	1.59	2488.1	9333	165.4	168.9	126.7
11.5	19.222	54.67	8815	169.9	0.163	1.59	2492.5	8815	169.9	157.4	118.0
12.0	19.388	54.84	8296	174.2	0.167	1.60	2497.2	8296	174.2	146.5	109.9
12.5	19.553	55.00	7778	178.2	0.170	1.61	2502.2	7778	178.2	136.4	102.3
13.0	19.718	55.17	7259	182.0	0.174	1.62	2507.5	7259	182.0	126.7	95.0
13.5	19.883	55.33	6741	185.5	0.177	1.62	2513.1	6741	185.5	117.6	88.2
14.0	20.049	55.50	6222	188.7	0.180	1.63	2519.0	6222	188.7	108.8	81.6
14.5	20.214	55.66	5704	191.7	0.183	1.64	2525.2	5704	191.7	100.5	75.3
15.0	20.379	55.83	5185	194.4	0.186	1.65	2531.8	5185	194.4	92.4	69.3
15.5	20.545	55.99	4667	196.9	0.188	1.66	2538.6	4667	196.9	84.6	63.4
16.0	20.710	56.16	4148	199.1	0.190	1.66	2545.7	4148	199.1	77.0	57.7
16.5	20.710	56.16	3630	201.0	0.192	1.66	2543.4	3630	201.0	69.3	52.0
17.0	20.710	56.16	3111	202.7	0.194	1.66	2541.5	3111	202.7	61.9	46.4
17.5	20.710	56.16	2593	204.2	0.195	1.66	2539.8	2593	204.2	56.1	42.1
18.0	20.710	56.16	2074	205.3	0.196	1.66	2538.4	2074	205.3	56.1	42.1
18.5	20.710	56.16	1556	206.2	0.197	1.66	2537.4	1556	206.2	56.1	42.1
19.0	20.710	56.16	1037	206.9	0.198	1.66	2536.6	1037	206.9	56.1	42.1
19.5	20.710	56.16	519	207.3	0.198	1.66	2536.1	519	207.3	56.1	42.1
20.0	20.710	56.16	0	207.4	0.198	1.66	2536.0	0	207.4	56.1	42.1

f <sub>pe</sub> (psi)	V <sub>p</sub> (lb)	V <sub>crw</sub> (k)	φV <sub>crw</sub> (k)	V <sub>c</sub> (k)	φV <sub>c</sub> (k)
808.1	16046.9	193.1	144.8	193.1	144.8
808.1	16046.9	193.7	145.3	193.7	145.3
808.1	16046.9	194.3	145.7	194.3	145.7
808.1	16046.9	194.8	146.1	194.8	146.1
808.1	16046.9	195.4	146.6	195.4	146.6
808.1	16046.9	196.0	147.0	196.0	147.0
808.1	16046.9	196.6	147.4	196.6	147.4
808.1	16046.9	197.1	147.8	197.1	147.8
808.1	16046.9	197.7	148.3	197.7	148.3
808.1	16046.9	198.3	148.7	198.3	148.7
808.1	16046.9	198.9	149.1	198.9	149.1
808.1	16046.9	199.4	149.6	199.4	149.6
808.1	16046.9	200.0	150.0	200.0	150.0
808.1	16046.9	200.6	150.4	200.6	150.4
808.1	16046.9	201.2	150.9	201.2	150.9
808.1	16046.9	201.7	151.3	201.7	151.3
808.1	16046.9	202.3	151.7	202.3	151.7
808.1	16046.9	202.9	152.2	202.9	152.2
808.1	16046.9	203.5	152.6	203.5	152.6
808.1	16046.9	204.0	153.0	204.0	153.0
808.1	16046.9	204.6	153.5	194.8	146.1
808.1	16046.9	205.2	153.9	181.4	136.0
808.1	16046.9	205.8	154.3	168.9	126.7
808.1	16046.9	206.3	154.8	157.4	118.0
808.1	16046.9	206.9	155.2	146.5	109.9
808.1	16046.9	207.5	155.6	136.4	102.3
808.1	16046.9	208.1	156.0	126.7	95.0
808.1	16046.9	208.6	156.5	117.6	88.2
808.1	16046.9	209.2	156.9	108.8	81.6
808.1	16046.9	209.8	157.3	100.5	75.3
808.1	16046.9	210.4	157.8	92.4	69.3
808.1	16046.9	210.9	158.2	84.6	63.4
808.1	0.0	195.5	146.6	77.0	57.7
808.1	0.0	195.5	146.6	69.3	52.0
808.1	0.0	195.5	146.6	61.9	46.4
808.1	0.0	195.5	146.6	56.1	42.1
808.1	0.0	195.5	146.6	56.1	42.1
808.1	0.0	195.5	146.6	56.1	42.1
808.1	0.0	195.5	146.6	56.1	42.1
808.1	0.0	195.5	146.6	56.1	42.1
808.1	0.0	195.5	146.6	56.1	42.1
808.1	0.0	195.5	146.6	56.1	42.1
808.1	0.0	195.5	146.6	56.1	42.1

Input		
Composite Section Properties		
L	40	ft
L <sub>h</sub>	16	ft
f <sub>c</sub>	10	ksi
A <sub>ps</sub>	3.472	in <sup>2</sup>
E <sub>ps</sub>	28500	ksi
A <sub>s</sub>	2.17	in <sup>2</sup>
E <sub>s</sub>	29000	ksi
b <sub>v</sub>	5.875	in
d <sub>v</sub>	51.01	in
a <sub>g</sub>	0.5	in
f <sub>pu</sub>	270	ksi
f <sub>pj</sub>	202.5	ksi
initial losses	5.16	%
total losses	14.5	%
f <sub>pi</sub>	192.1	ksi
f <sub>pe</sub>	173.1	ksi
α	6.130	degrees

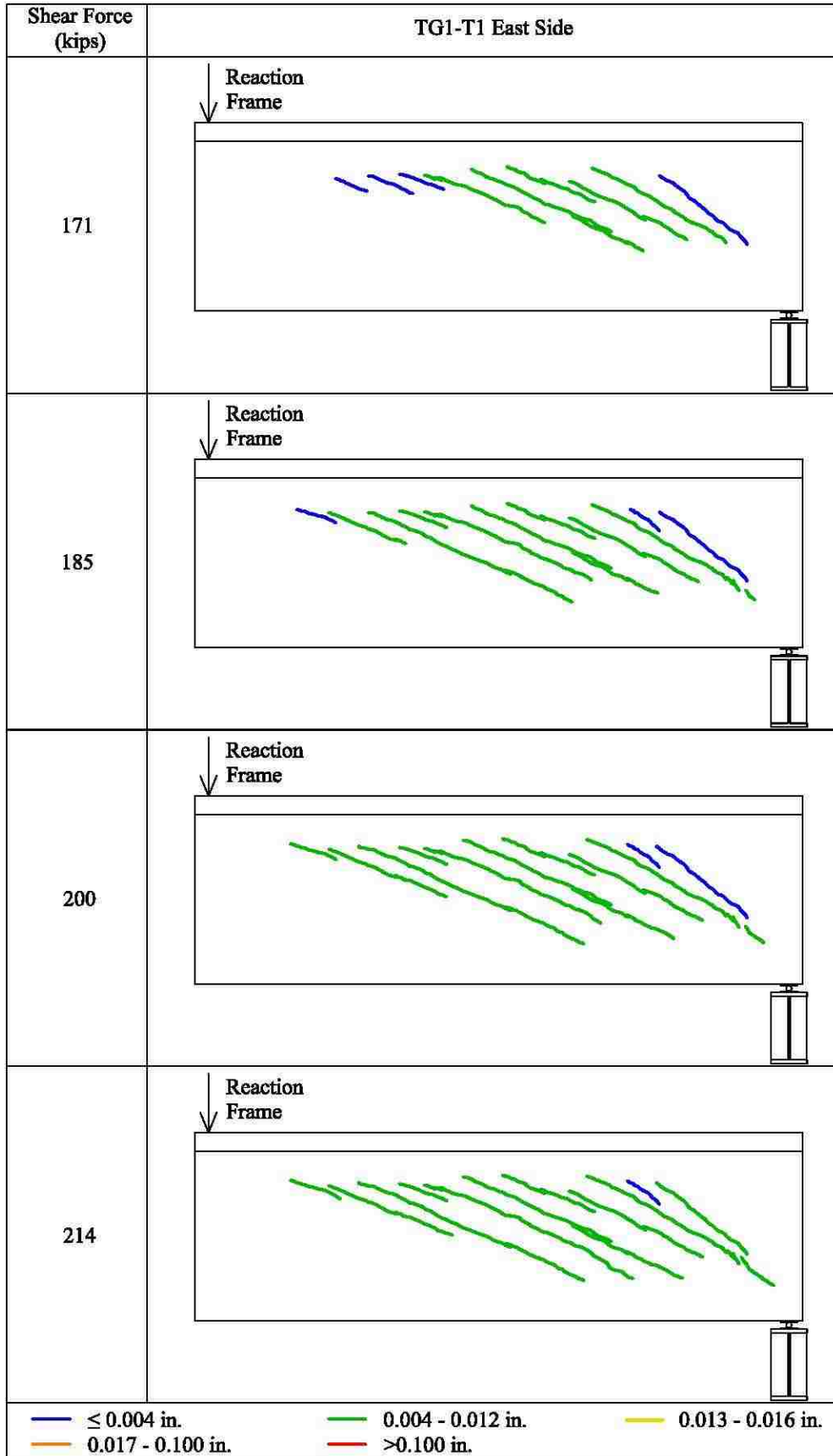
Loads		
w <sub>concrete</sub>	145	pcf
w <sub>u</sub>	1037.0	lb/ft
P <sub>u</sub>	336.1	k

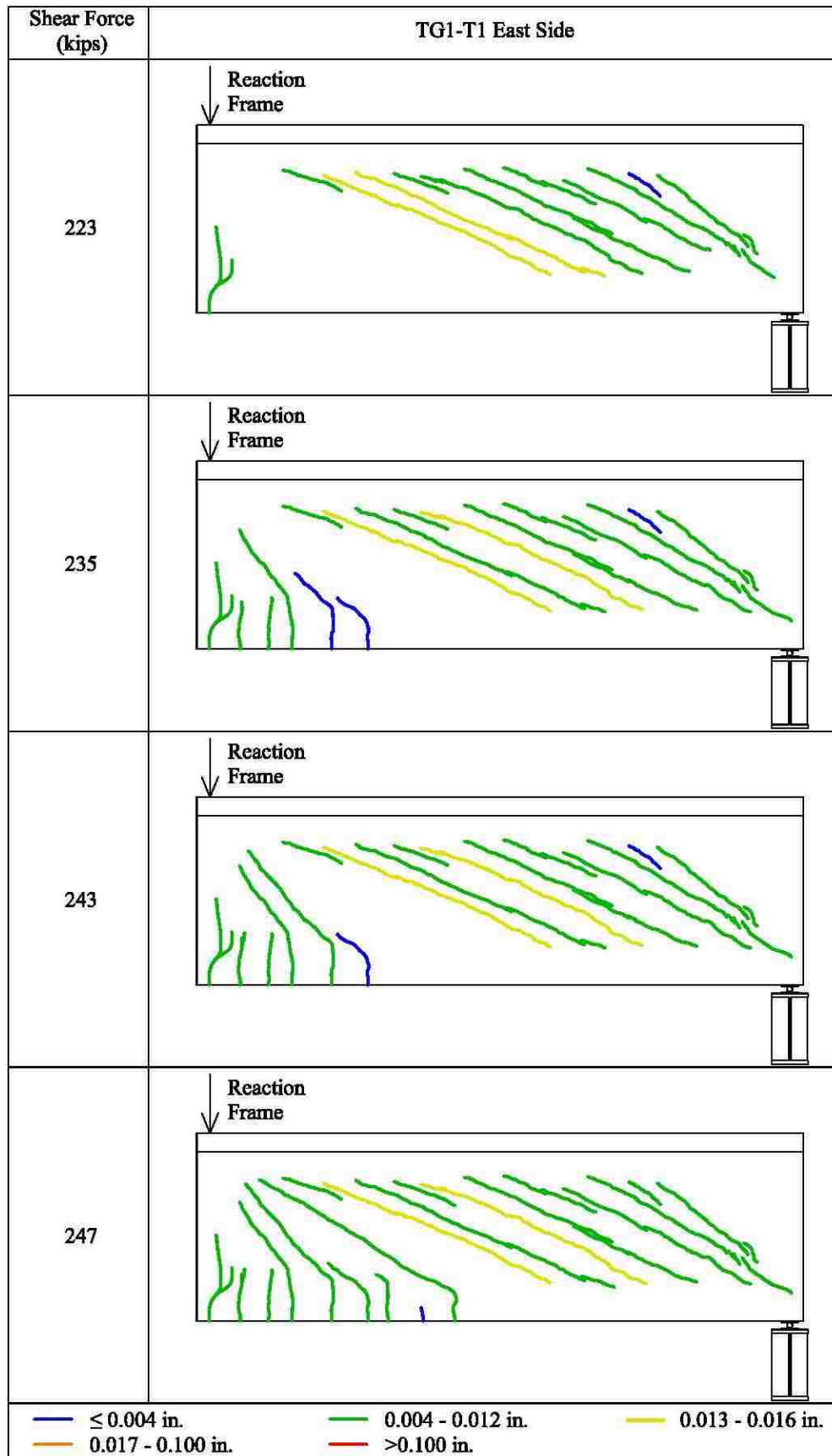
x (ft)	s <sub>x</sub> (in)	s <sub>xe</sub> (in)	V <sub>u</sub> (k)	M <sub>u</sub> (k-ft)	V <sub>p</sub> (k)	ε <sub>s</sub>	θ	β	V <sub>c</sub> (k)	V <sub>n</sub> (k)	φV <sub>n</sub> (k)
0.0	2.0	12.0	230.8	0.0	16.05	0.00E+00	29	4.8	143.7	159.8	143.8
0.5	2.0	12.0	230.3	115.3	16.05	0.00E+00	29	4.8	143.7	159.8	143.8
1.0	2.0	12.0	229.8	230.3	16.05	0.00E+00	29	4.8	143.7	159.8	143.8
1.5	2.0	12.0	229.2	345.0	16.05	0.00E+00	29	4.8	143.7	159.8	143.8
2.0	2.0	12.0	228.7	459.5	16.05	0.00E+00	29	4.8	143.7	159.8	143.8
2.5	2.0	12.0	228.2	573.8	16.05	0.00E+00	29	4.8	143.7	159.8	143.8
3.0	2.0	12.0	227.7	687.7	16.05	0.00E+00	29	4.8	143.7	159.8	143.8
3.5	2.0	12.0	227.2	801.5	16.05	0.00E+00	29	4.8	143.7	159.8	143.8
4.0	2.0	12.0	226.7	914.9	16.05	0.00E+00	29	4.8	143.7	159.8	143.8
4.25	2.0	12.0	226.4	971.5	16.05	0.00E+00	29	4.8	143.7	159.8	143.8
4.5	2.0	12.0	226.1	1028.1	16.05	0.00E+00	29	4.8	143.7	159.8	143.8
5.0	2.0	12.0	225.6	1141.1	16.05	0.00E+00	29	4.8	143.7	159.8	143.8
5.5	2.0	12.0	225.1	1253.7	16.05	0.00E+00	29	4.8	143.7	159.8	143.8
6.0	2.0	12.0	224.6	1366.1	16.05	0.00E+00	29	4.8	143.7	159.8	143.8
6.5	2.0	12.0	224.1	1478.3	16.05	0.00E+00	29	4.8	143.7	159.8	143.8
7.0	2.0	12.0	223.5	1590.2	16.05	0.00E+00	29	4.8	143.7	159.8	143.8
7.5	2.0	12.0	223.0	1701.9	16.05	0.00E+00	29	4.8	143.7	159.8	143.8
8.0	2.0	12.0	222.5	1813.2	16.05	0.00E+00	29	4.8	143.7	159.8	143.8
8.5	2.0	12.0	222.0	1924.4	16.05	0.00E+00	29	4.8	143.7	159.8	143.8
9.0	2.0	12.0	221.5	2035.2	16.05	1.08E-04	29	4.4	133.0	149.1	134.2
9.5	2.0	12.0	221.0	2145.8	16.05	2.65E-04	30	4.0	119.9	136.0	122.4
10.0	2.0	12.0	220.4	2256.2	16.05	4.22E-04	30	3.6	109.2	125.2	112.7
10.5	2.0	12.0	219.9	2366.3	16.05	5.79E-04	31	3.3	100.2	116.3	104.6
11.0	2.0	12.0	219.4	2476.1	16.05	7.35E-04	32	3.1	92.6	108.7	97.8
11.5	2.0	12.0	218.9	2585.7	16.05	8.91E-04	32	2.9	86.1	102.2	92.0
12.0	2.0	12.0	218.4	2695.0	16.05	1.05E-03	33	2.7	80.5	96.6	86.9
12.5	2.0	12.0	217.8	2804.0	16.05	1.20E-03	33	2.5	75.6	91.6	82.5
13.0	2.0	12.0	217.3	2912.8	16.05	1.36E-03	34	2.4	71.2	87.3	78.6
13.5	2.0	12.0	216.8	3021.3	16.05	1.51E-03	34	2.2	67.4	83.4	75.1
14.0	2.0	12.0	216.3	3129.6	16.05	1.67E-03	35	2.1	63.9	80.0	72.0
14.5	2.0	12.0	215.8	3237.6	16.05	1.82E-03	35	2.0	60.8	76.8	69.2
15.0	2.0	12.0	215.2	3345.4	16.05	1.97E-03	36	1.9	58.0	74.0	66.6

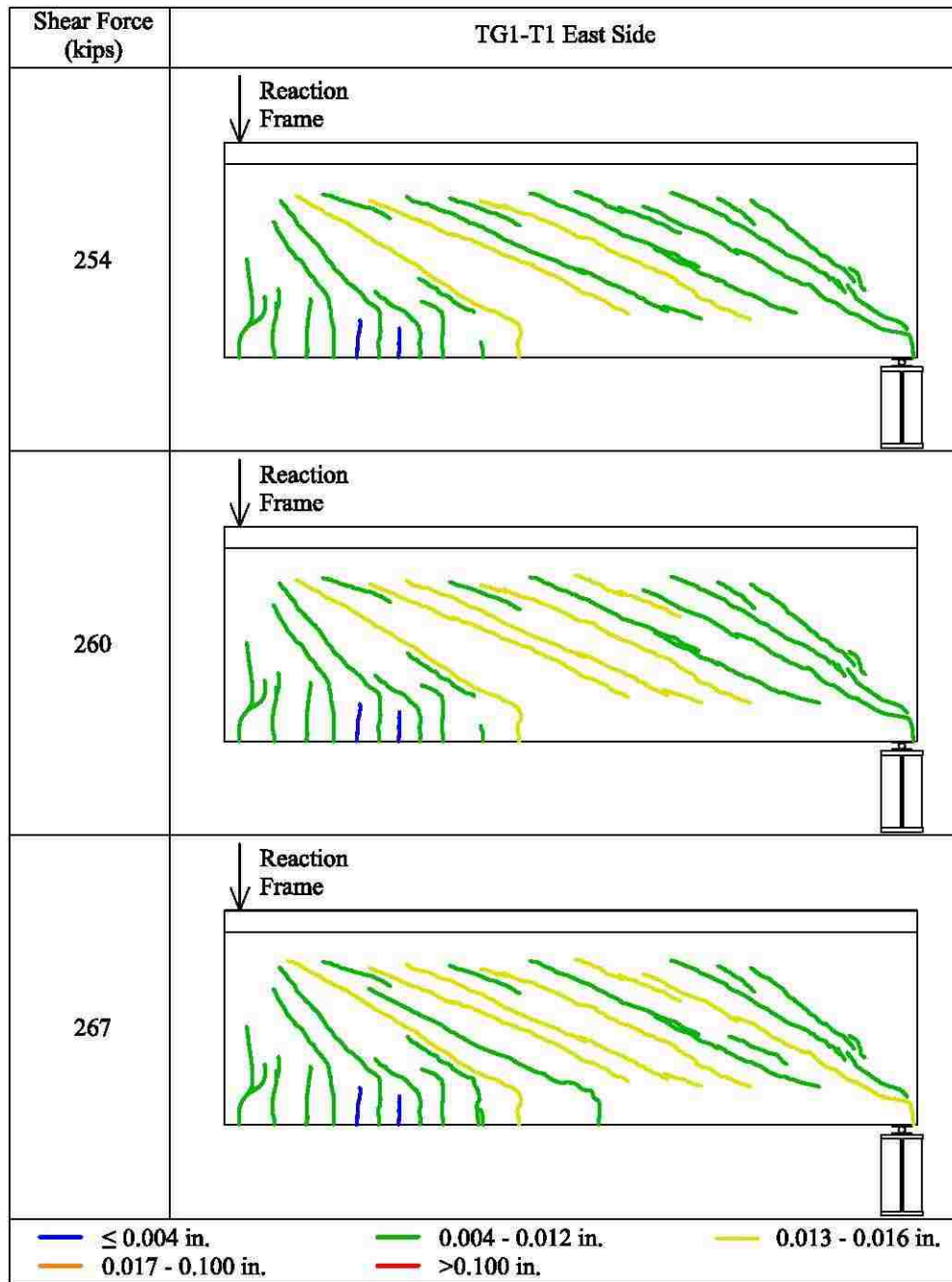
Response 2000 Input Parameters								
Data		Flexure	TG1-T1	TG1-T2	TG2-T1	TG2-T2		
$A_{ps}$	3.472 in <sup>2</sup>	Critical section <sup>1</sup> (ft)	20	12.3	11.3	12.3	11.3	
$W_{g+slab}$	1.037 k/ft	Effective prestress (ksi)	173	176	175	173	172	
$W_{ext. str.}$	9.44 k	Effective prestrain (ms)	6.070	6.175	6.140	6.070	6.035	
$A_g$	743.88 in <sup>2</sup>	1 - closest support						
$y_t$	29.45 in	Strain Discontinuity Calculations						
$y_b$	23.71 in	$e$ (in)	20.71	19.49	19.16	19.49	19.16	
$I$	297512 in <sup>4</sup>	$M_{self}$ (k-ft)	207.4	176.7	168.2	176.7	168.2	
$E_{28}$	5200 ksi	Stresses due to prestress and self weight (ksi)	Top of girder	0.178	0.148	0.136	0.142	0.130
$\alpha$	6.13 degrees	Bottom of girder	-1.600	-1.602	-1.584	-1.571	-1.554	
		Strains due to prestress and self weight <sup>2</sup> (ms)	Top of girder	0.0341	0.0284	0.0261	0.0272	0.0250
		Bottom of girder	-0.3078	-0.3080	-0.3046	-0.3022	-0.2988	
		Extrapolated strains for Response 2000 (ms)	Top of deck	-0.0727	-0.0664	-0.0634	-0.0644	-0.0616
			Bottom of deck	-0.0341	-0.0284	-0.0261	-0.0272	-0.0250
			Top of girder	0	0	0	0	0
			Bottom of girder	0	0	0	0	0
		2 - Calculated using MCE at 28 days						
		Concrete Properties						
		$f'_c$ girder (psi)	10000	10393	10941	11029	10680	
		$f'_c$ slab (psi)	3000	3061	3103	2485	2392	
		Harped Tendon Distances <sup>3</sup>						
		Top row (in)	N/A	8.769	10.057	8.769	10.057	
		Bottom row (in)	N/A	6.769	8.057	6.769	8.057	
		3 - measured from soffit of girder						
		Loading						
		$V_{initial}$ (k)	N/A	9.56	10.60	9.56	10.60	
		$M_{initial}$ (k-ft)	N/A	196.1	186.0	196.1	186.0	
		$\Delta M$ (k-ft)	1.0	12.3	11.3	12.3	11.3	
		$\Delta V$ (k)	0.0	1.0	1.0	1.0	1.0	

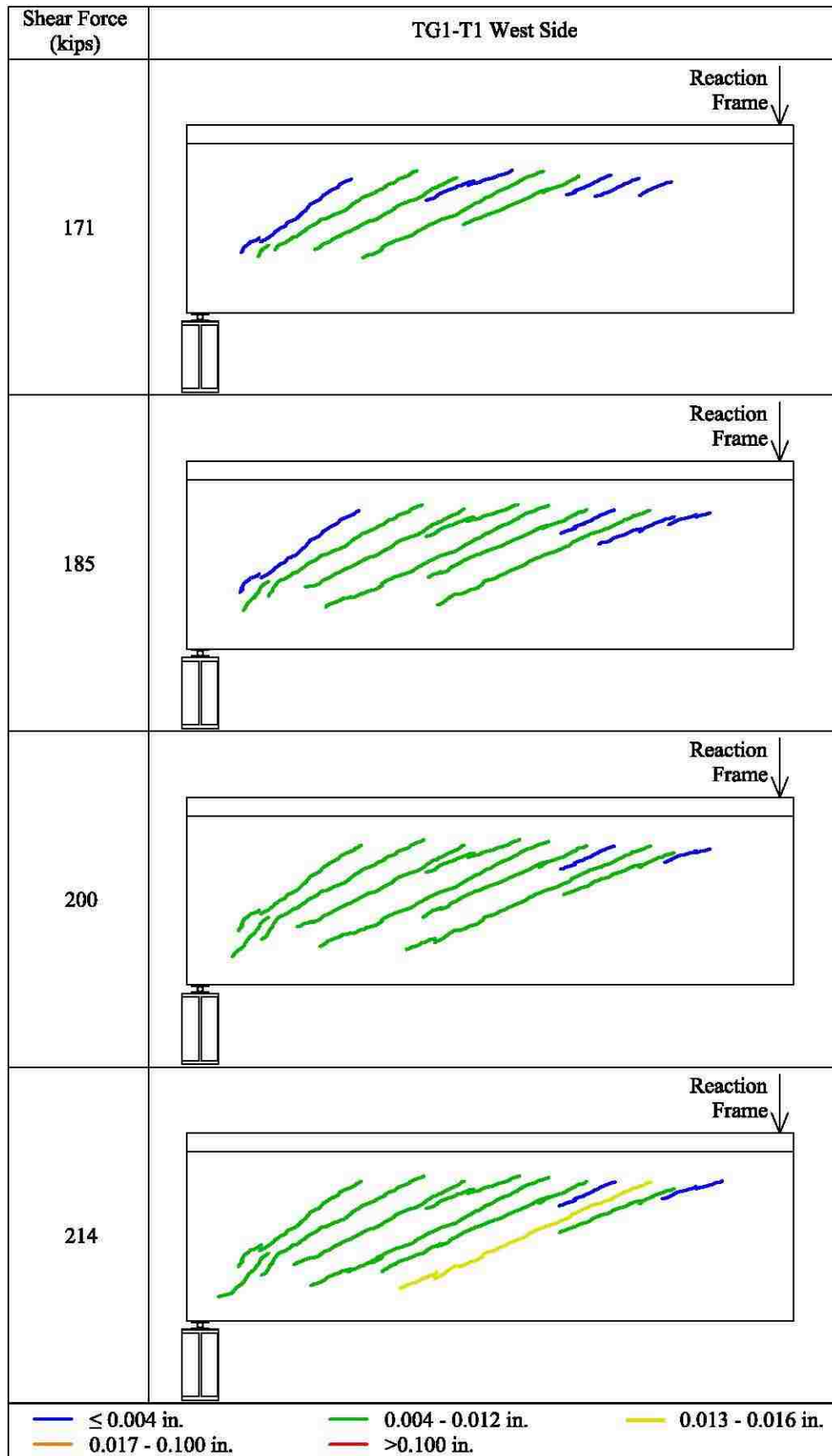


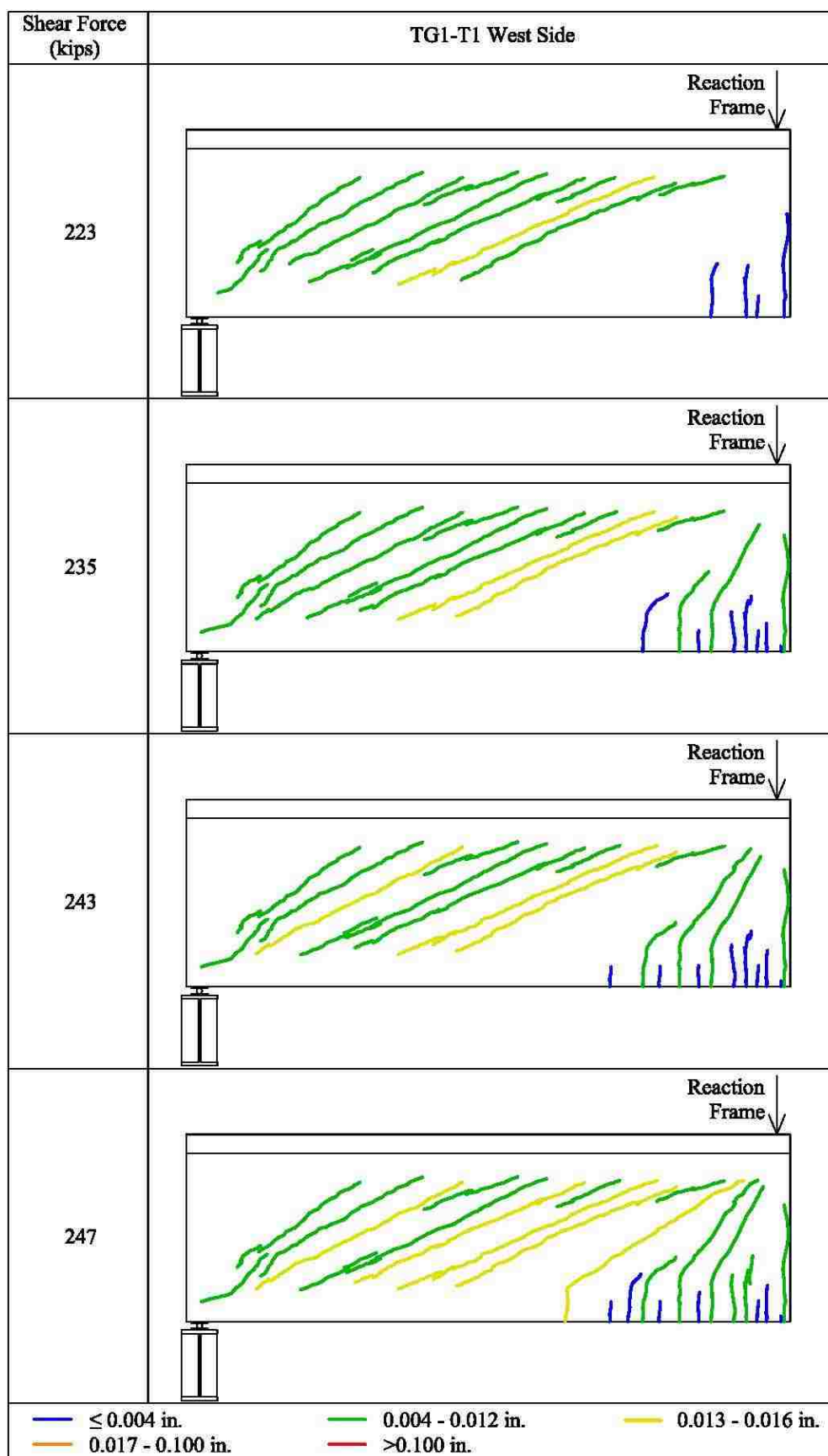
APPENDIX D.  
CRACK PATTERNS AND DOCUMENTATION

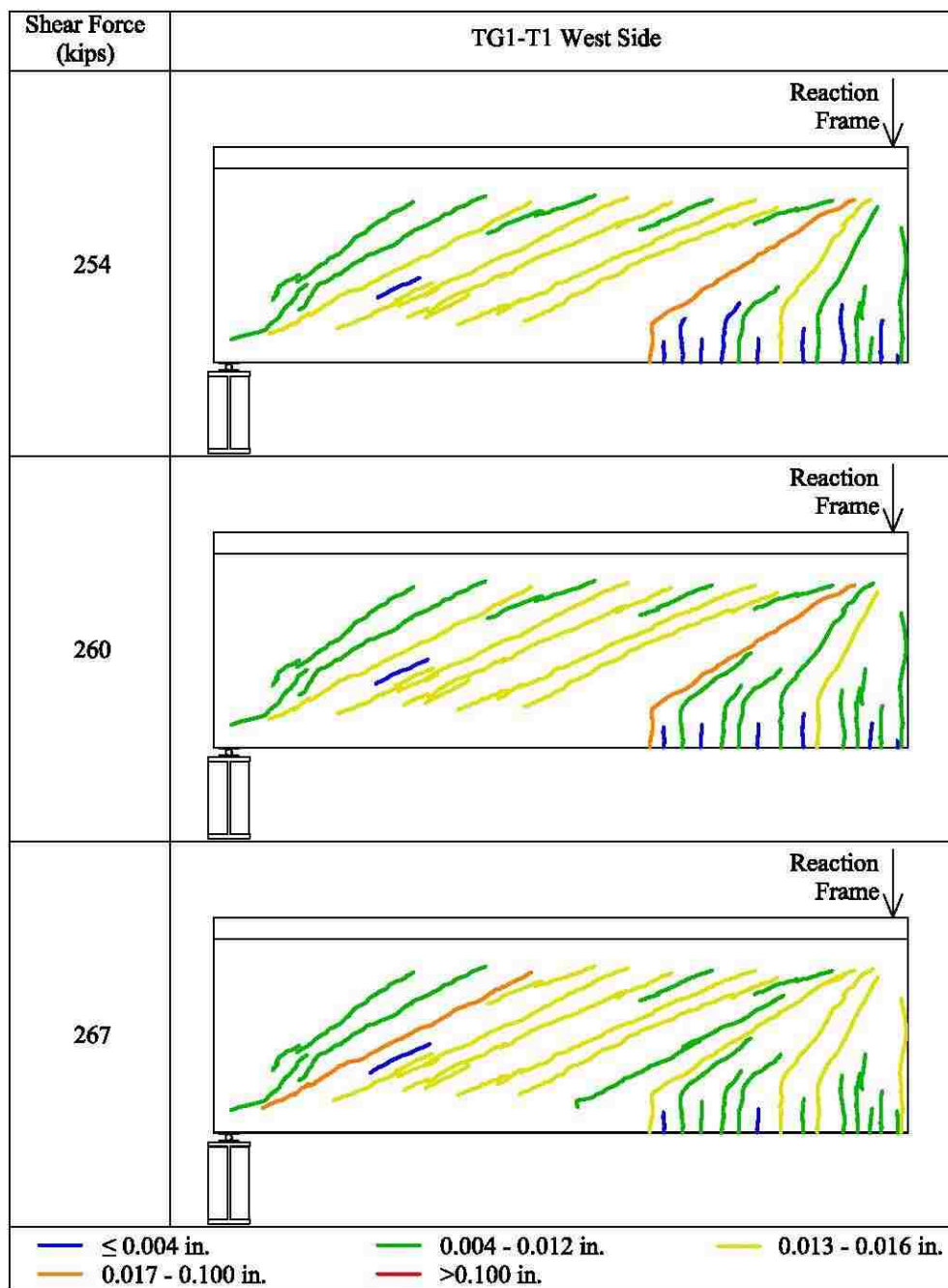


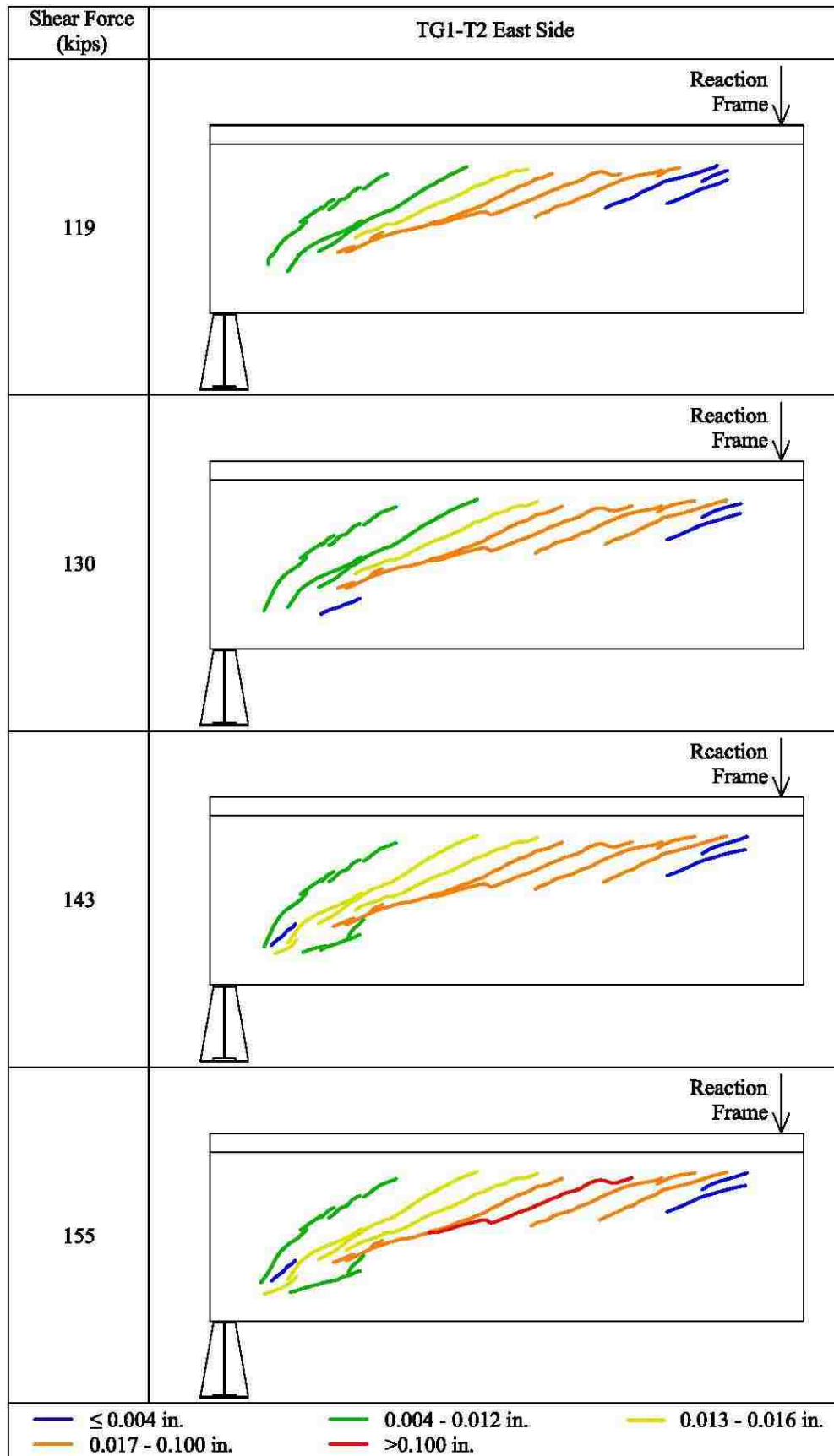




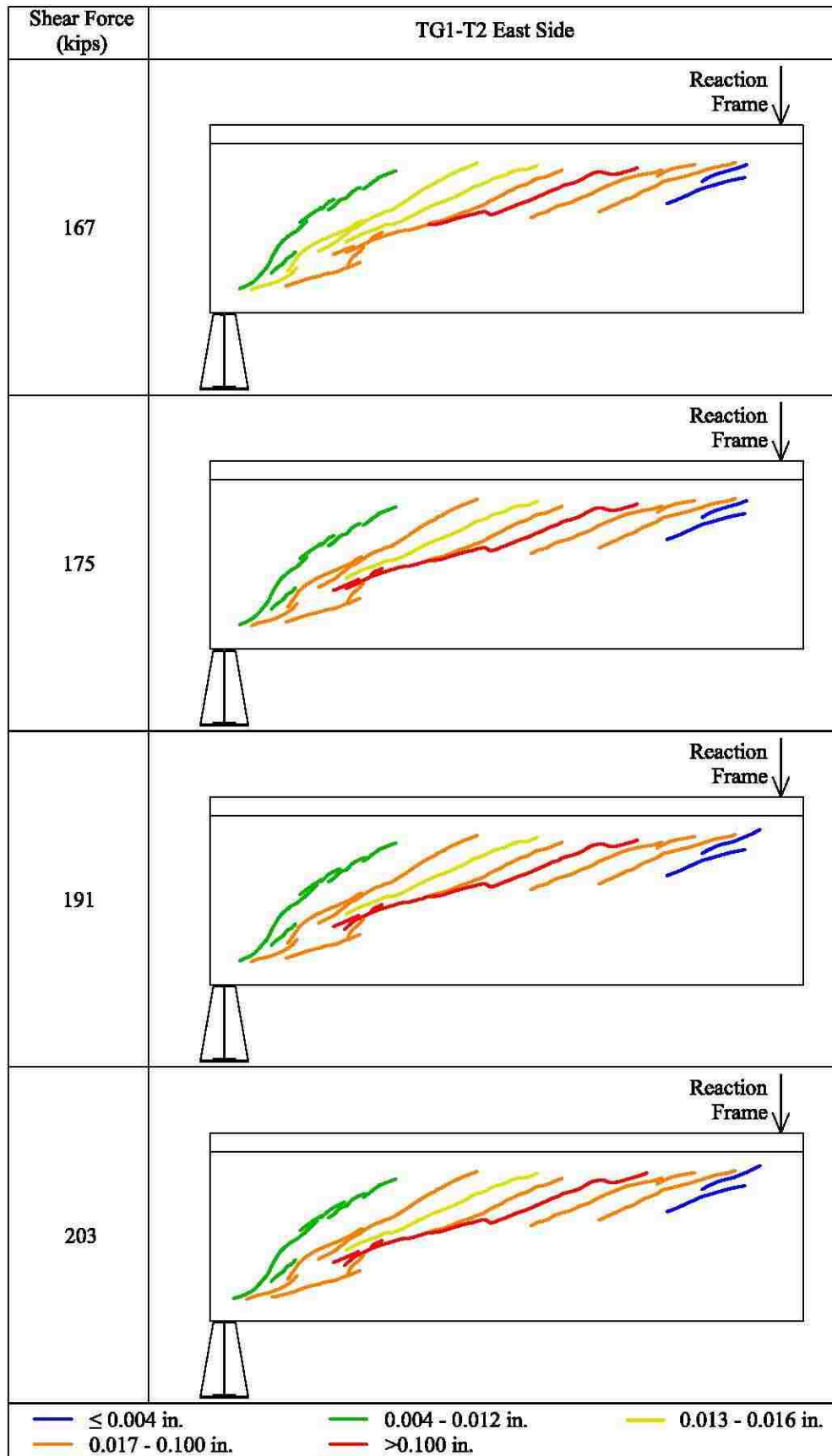


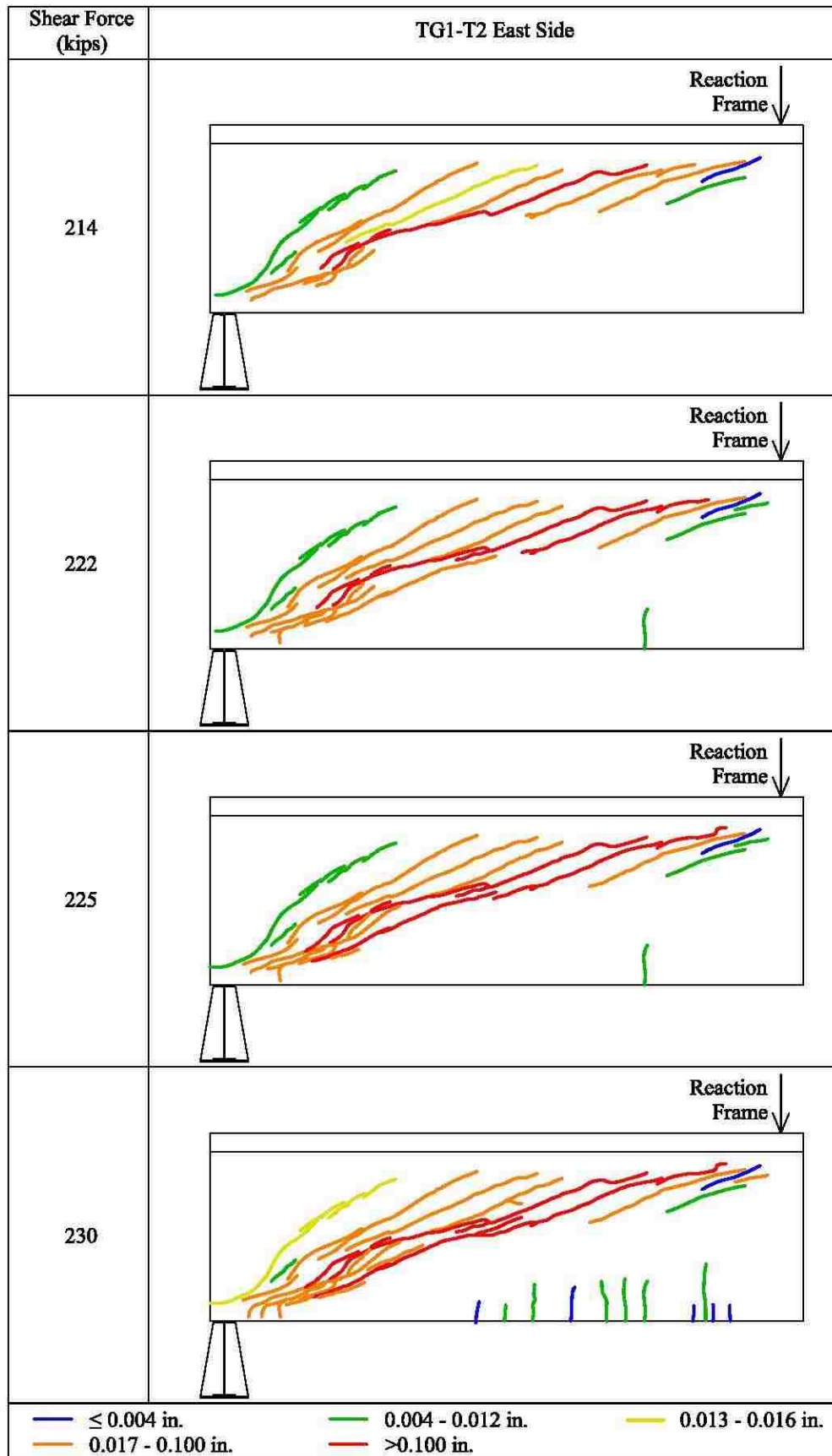


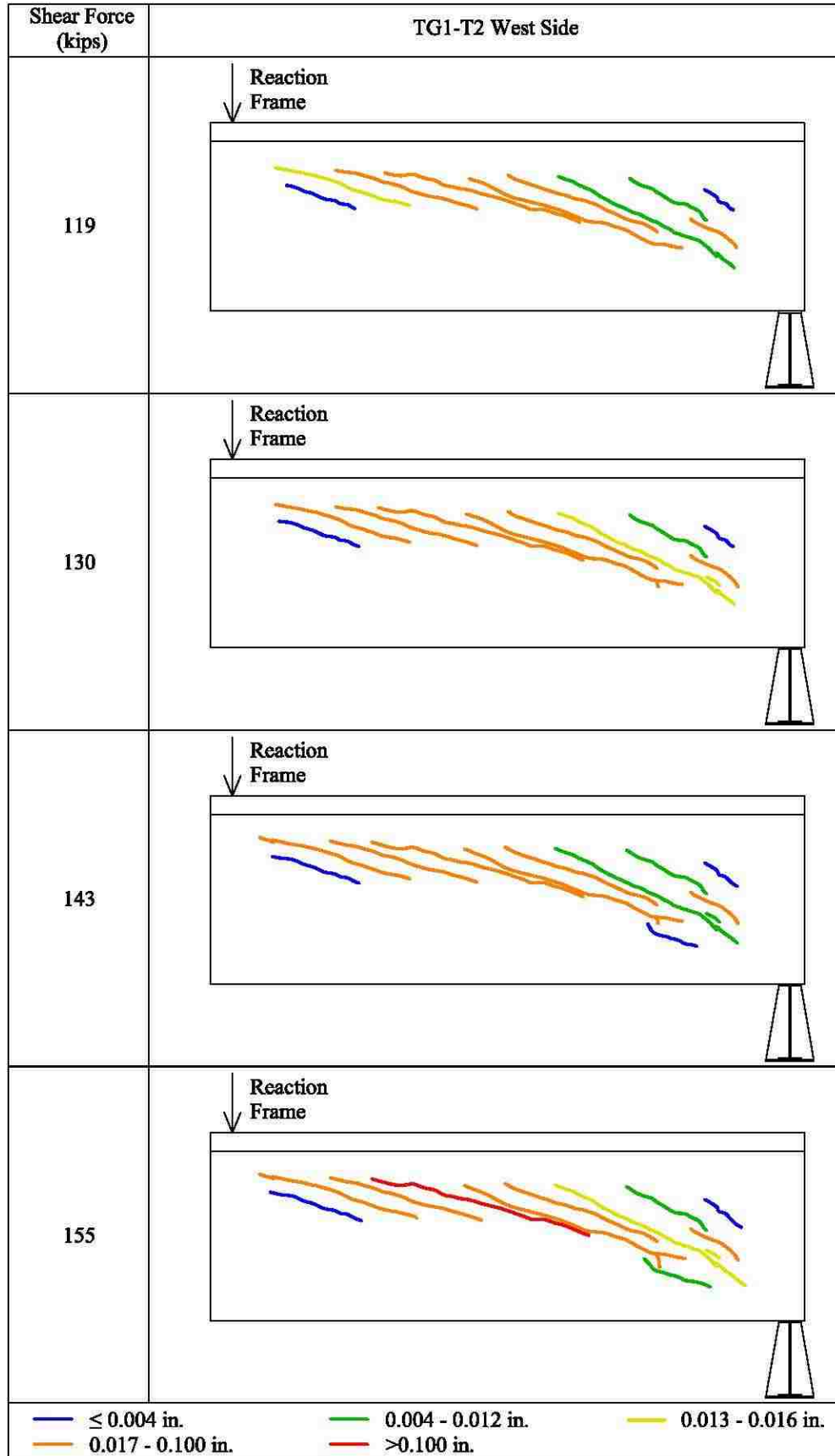


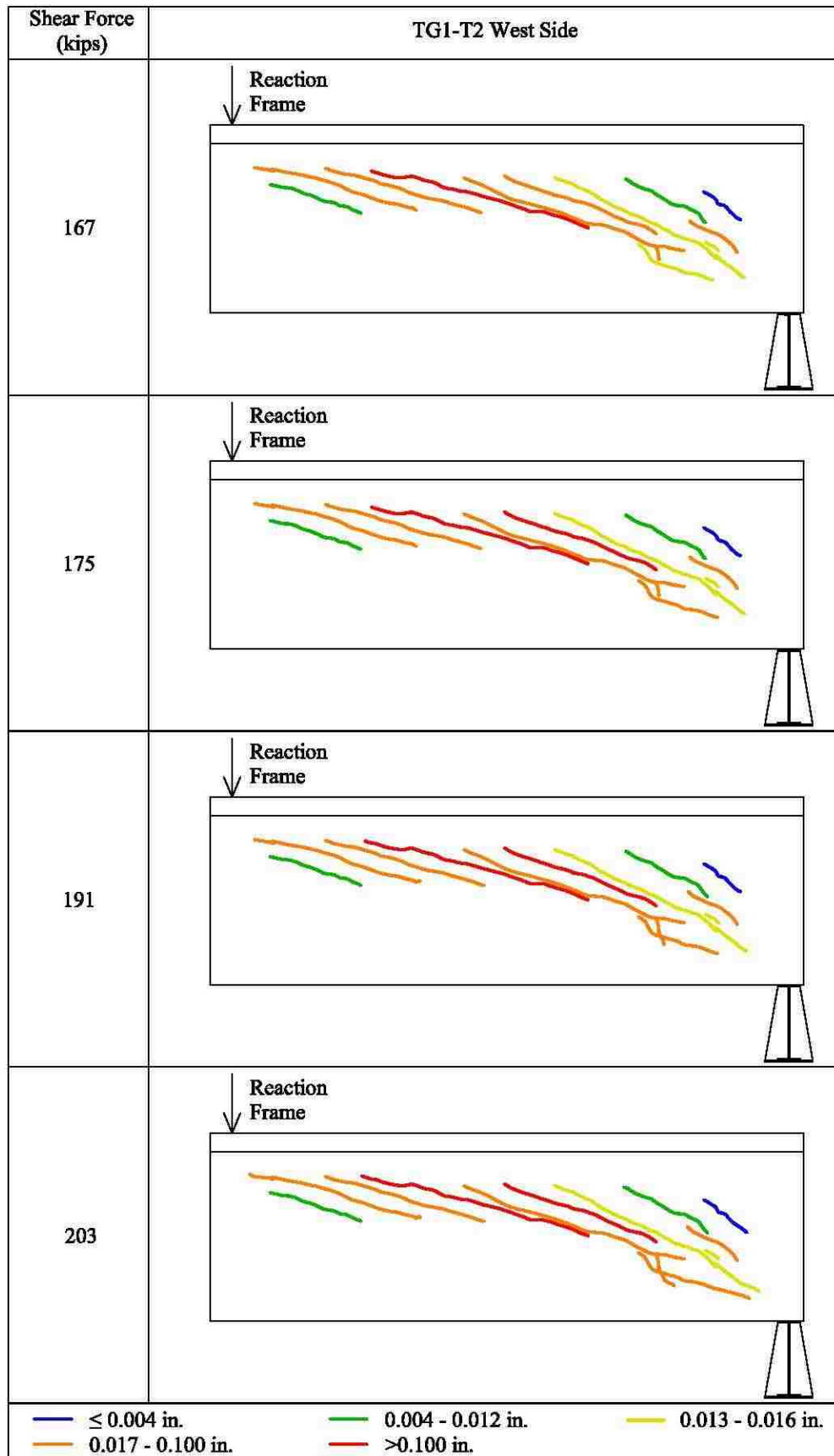


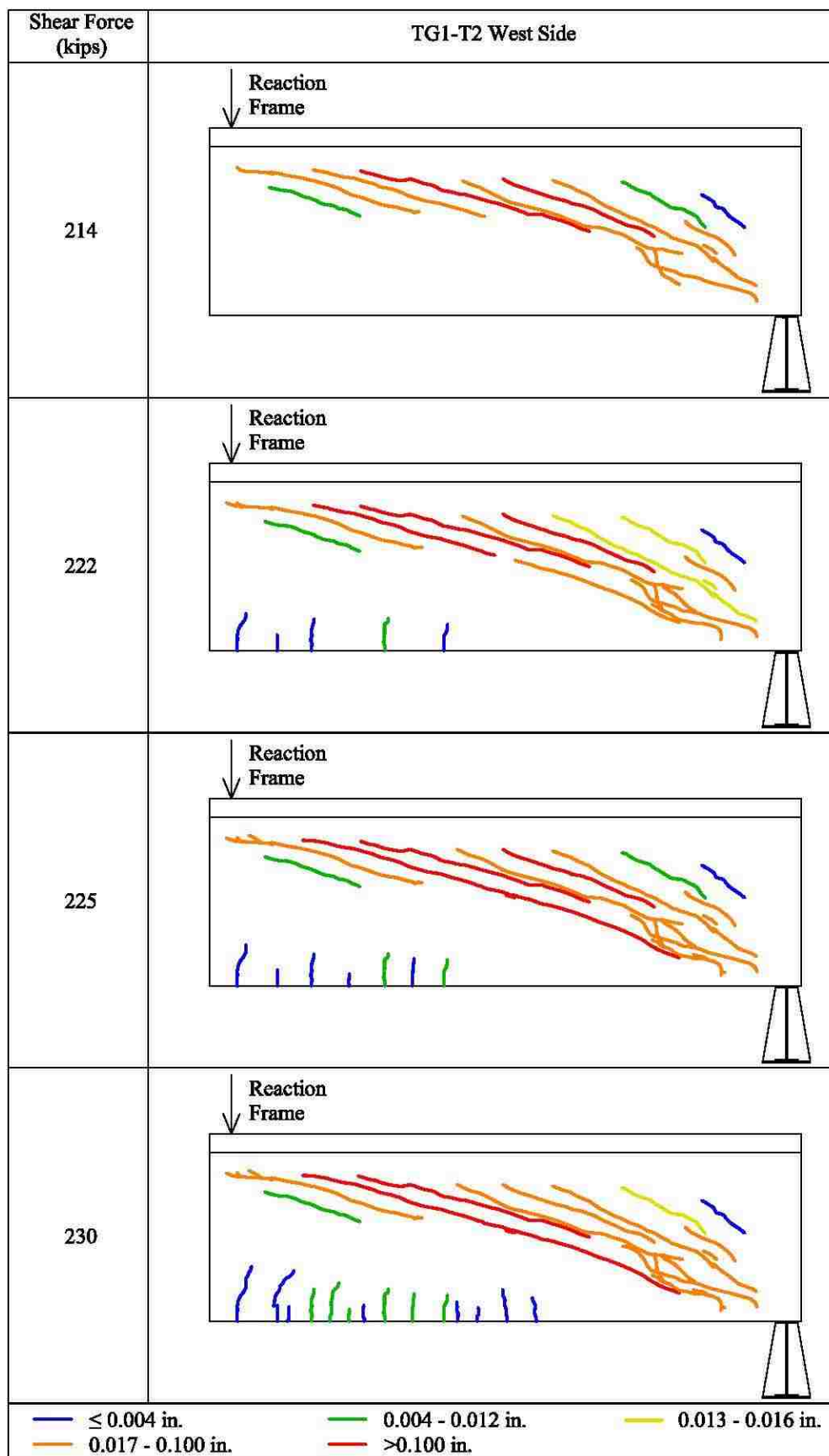


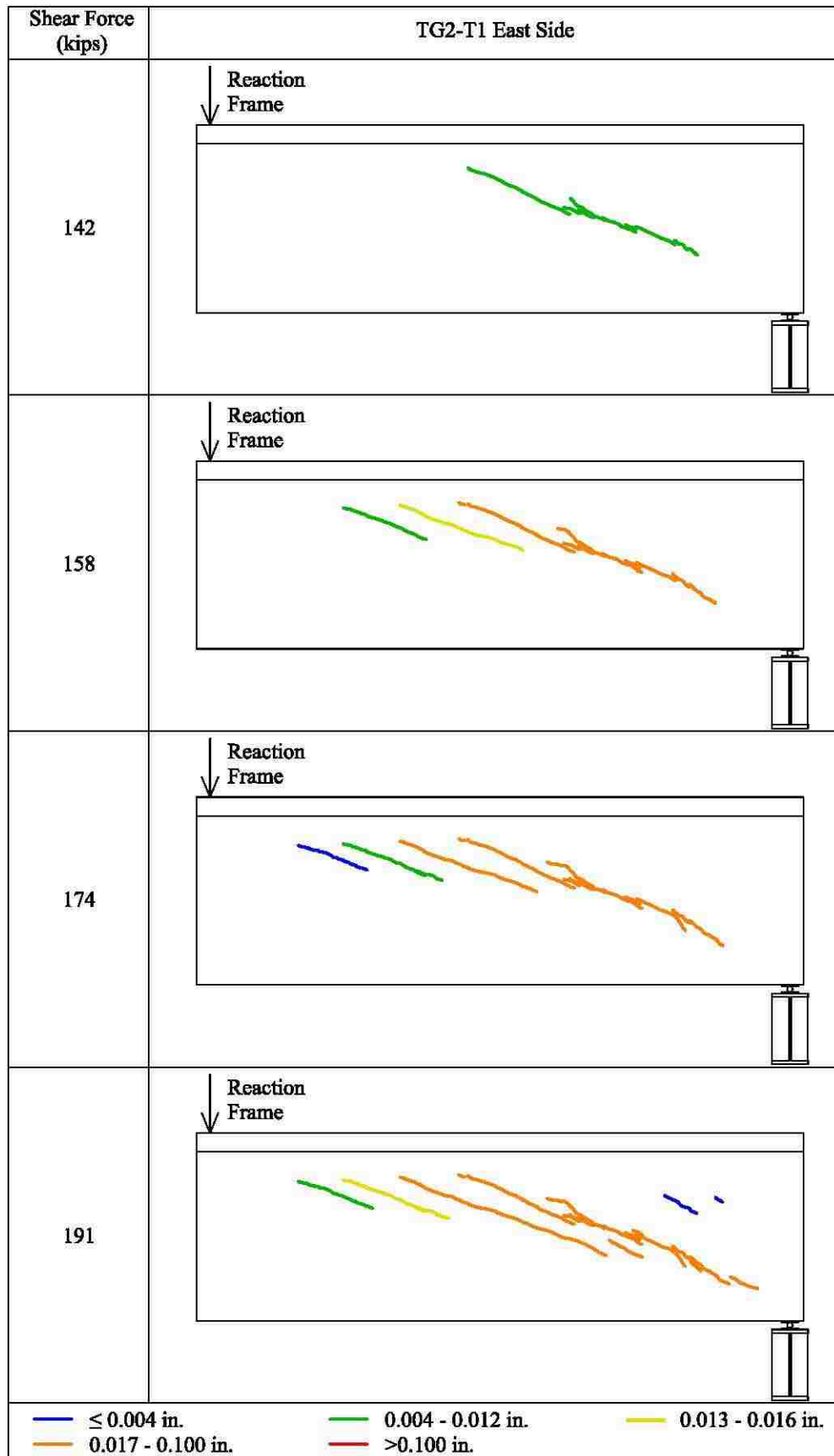


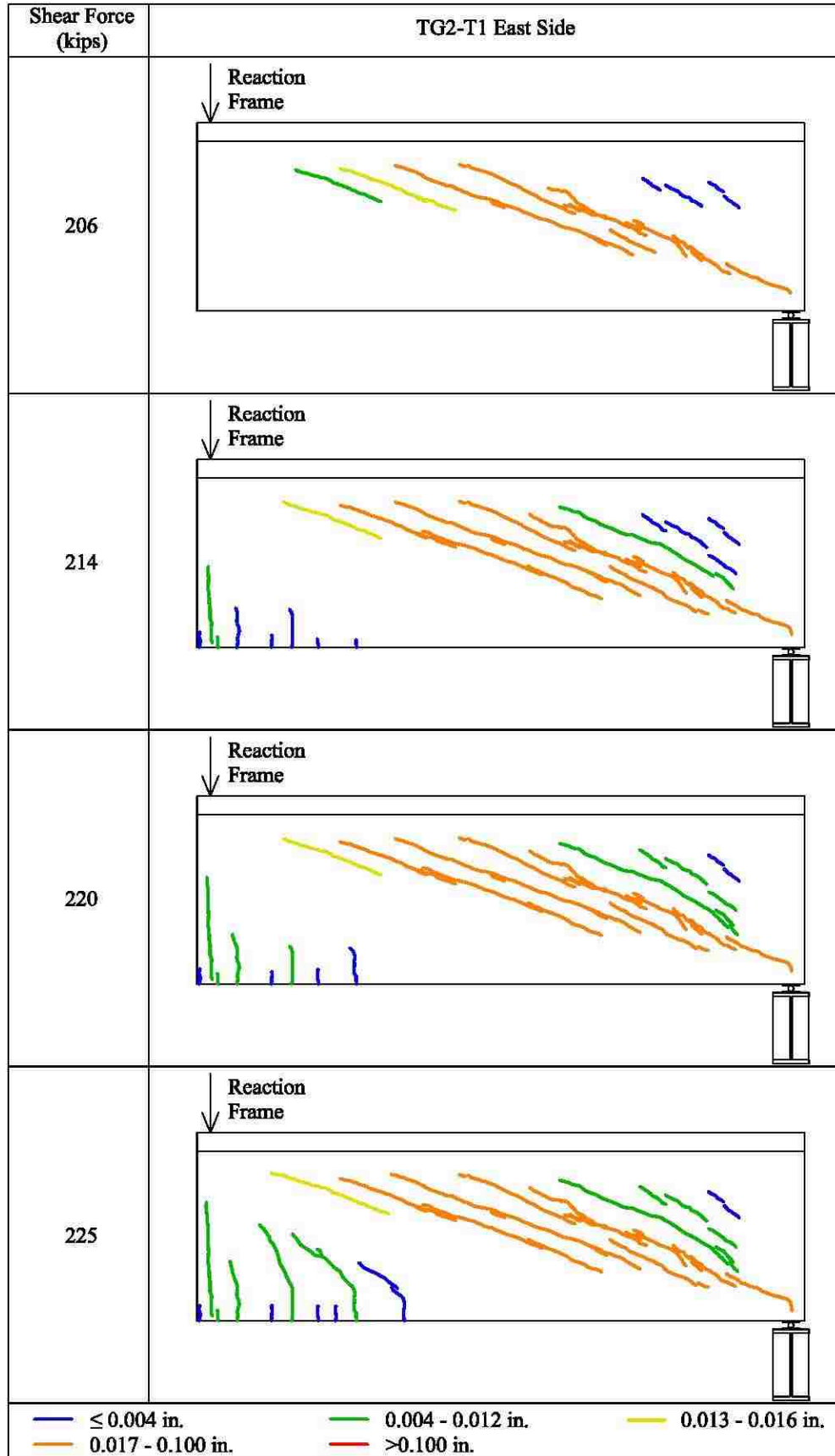


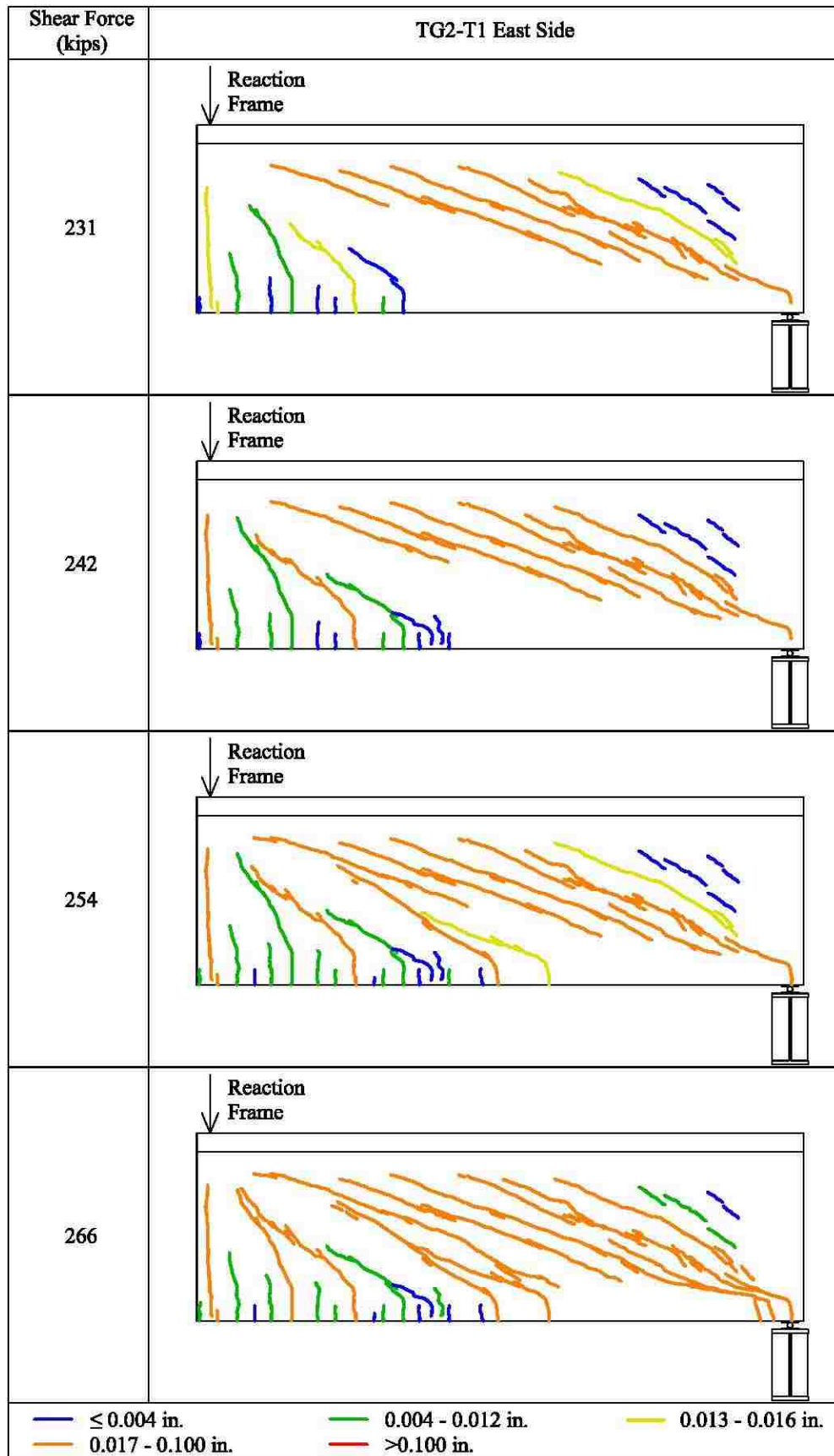




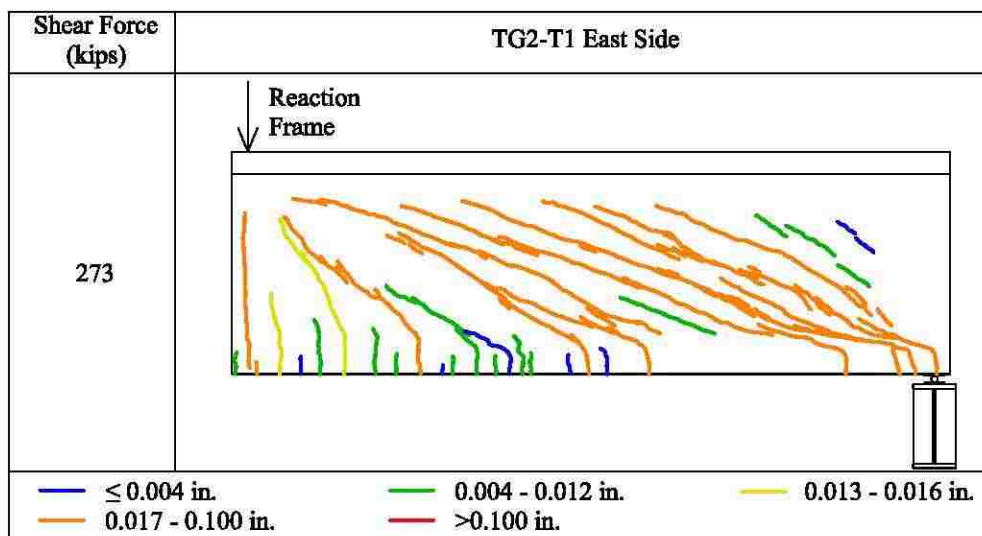


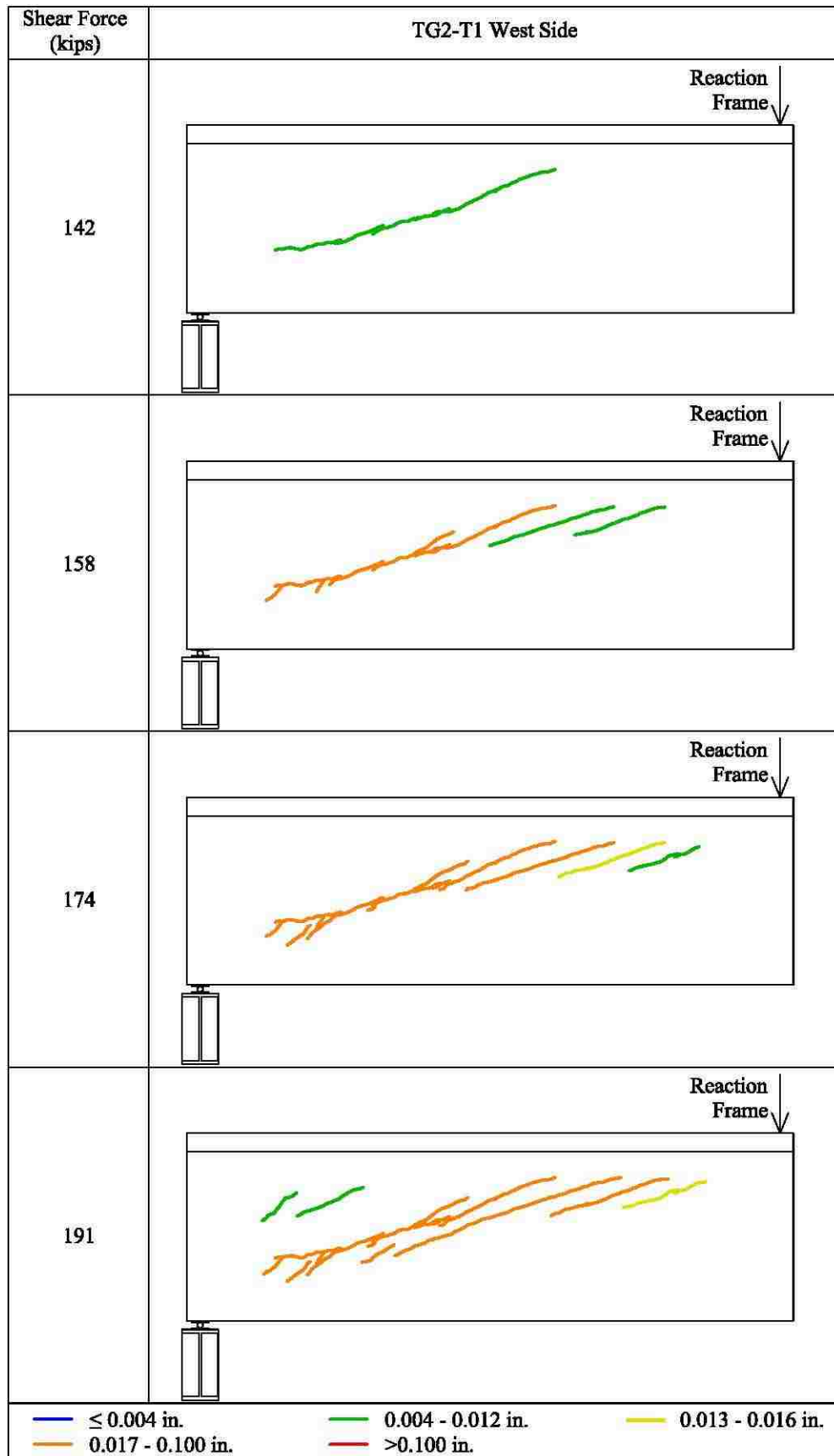


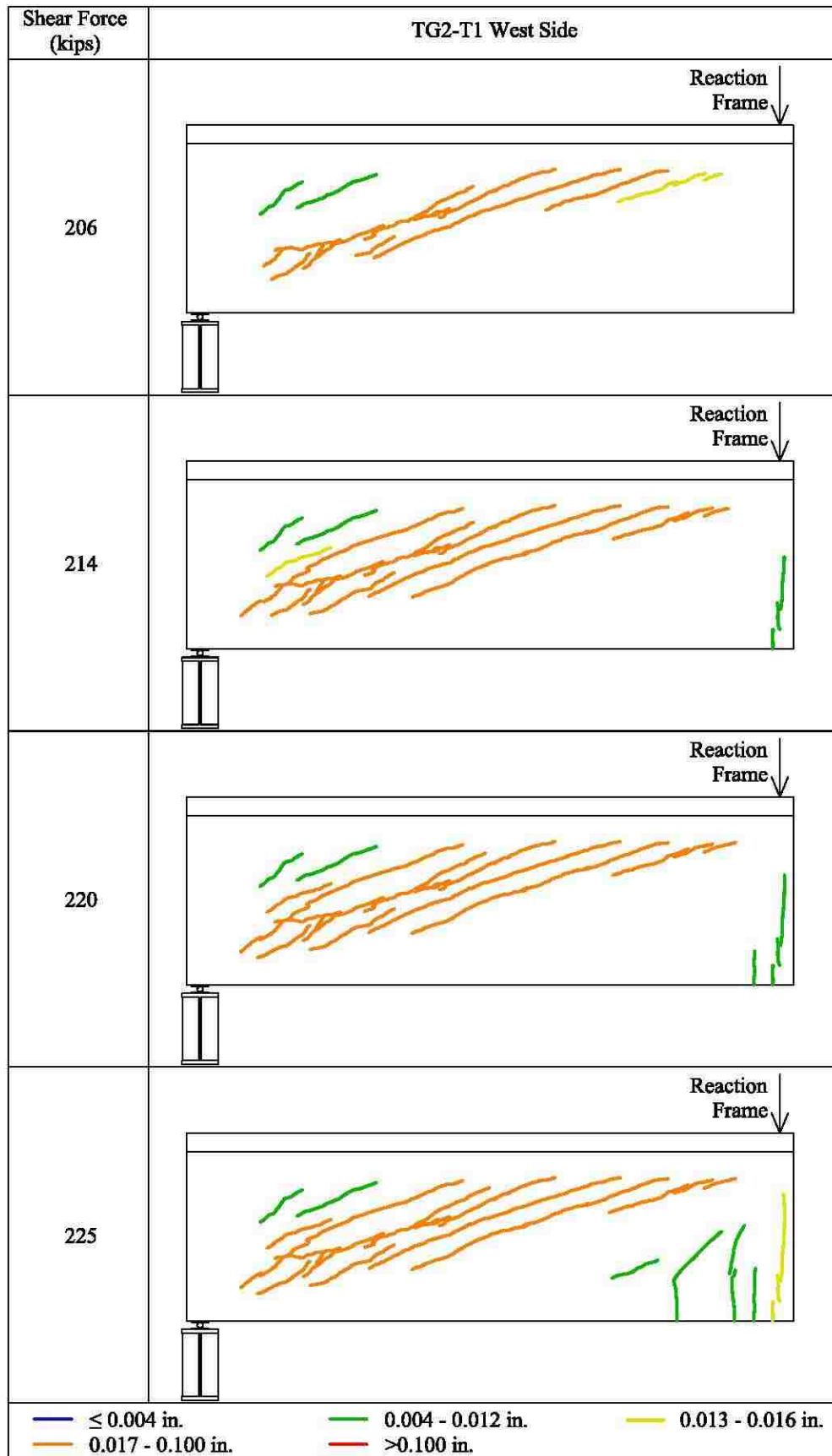


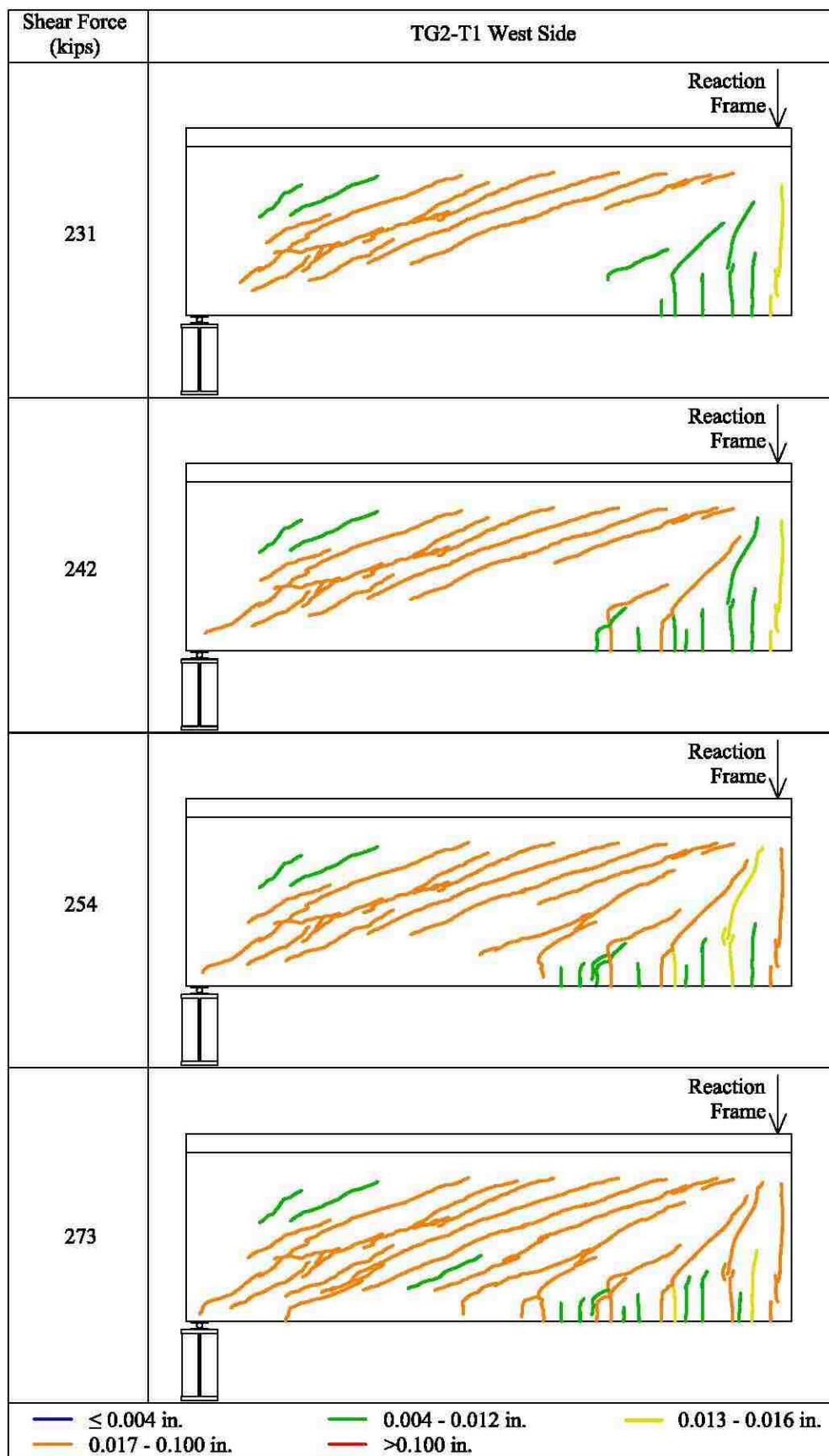


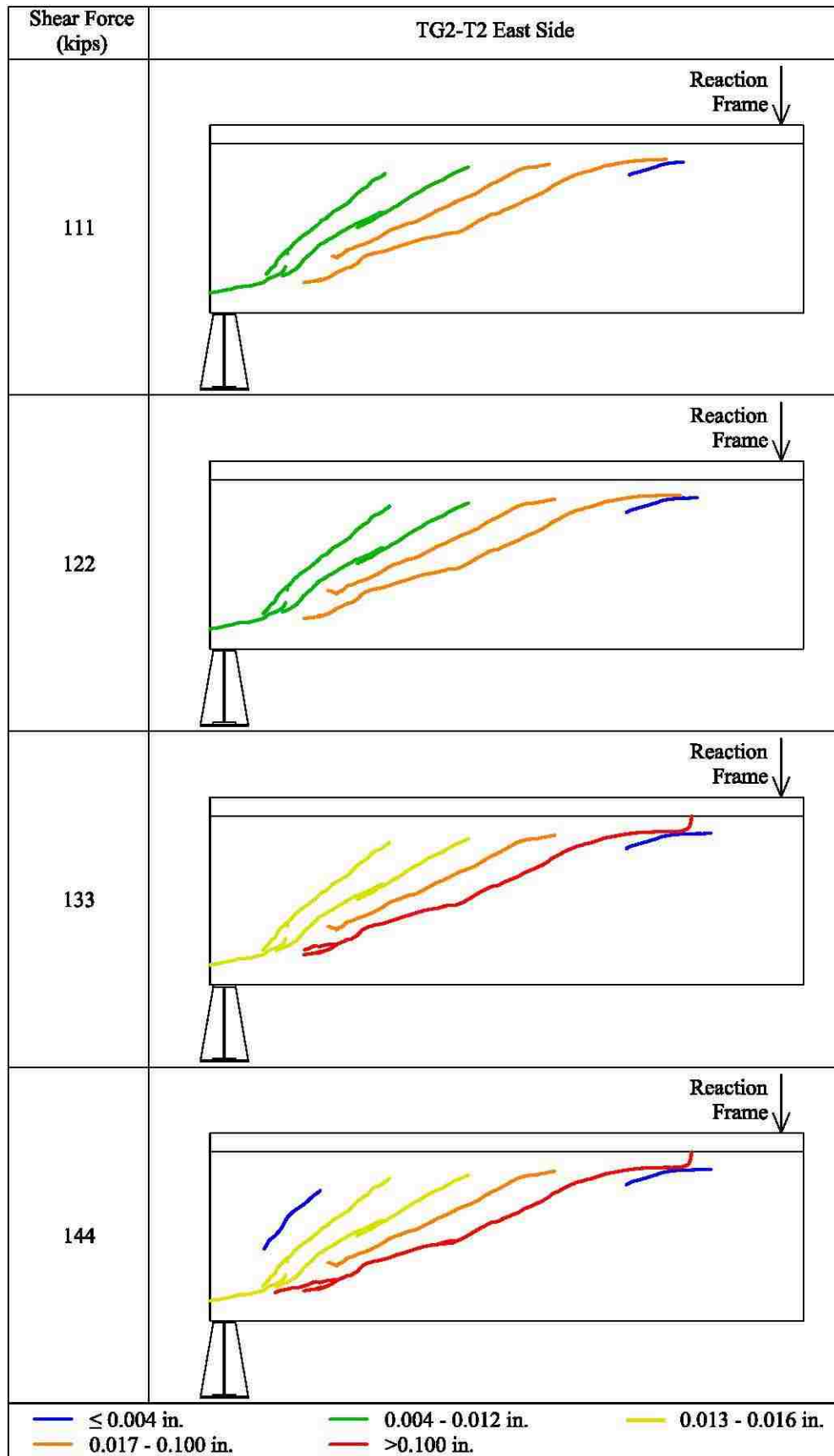


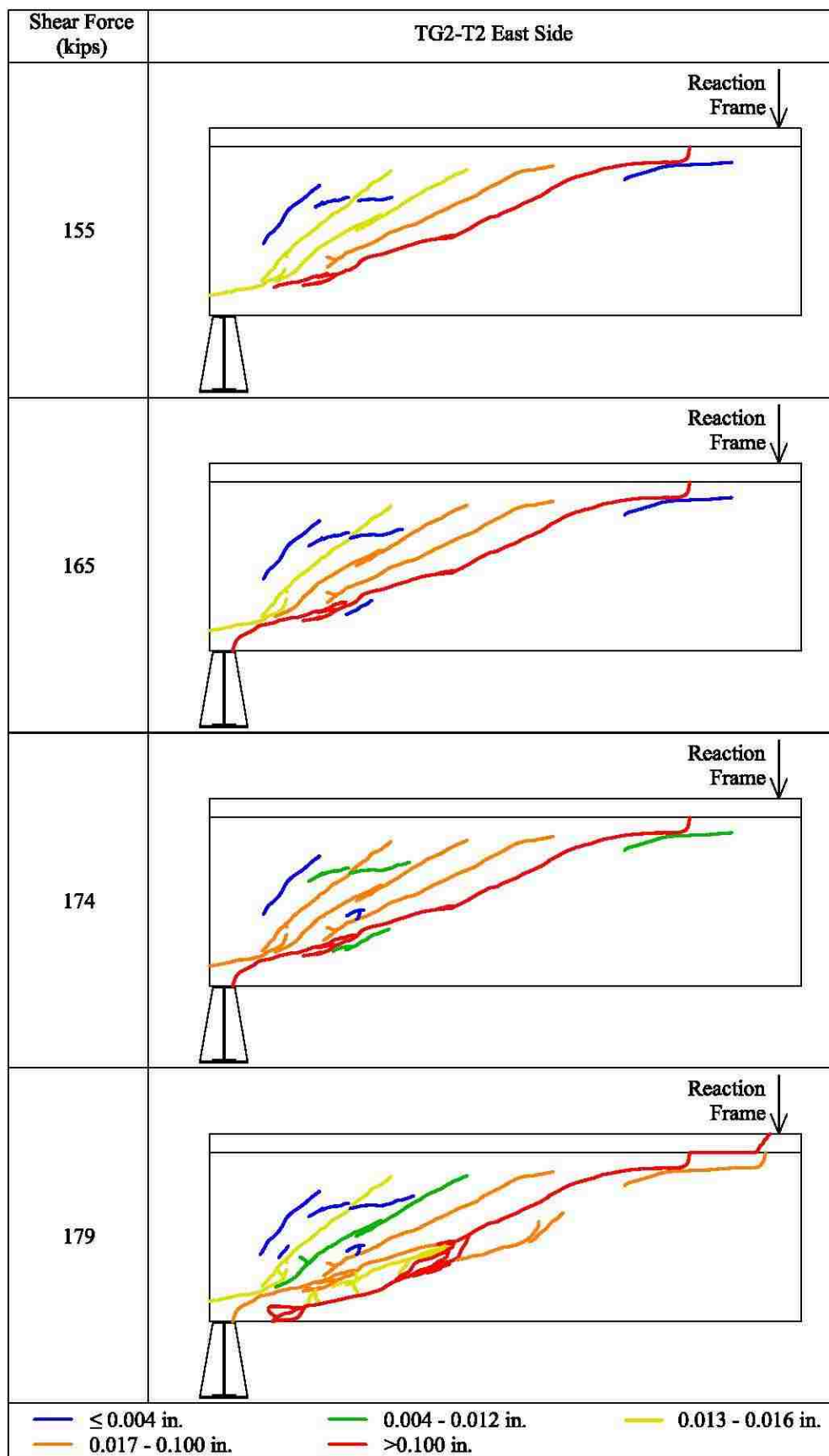


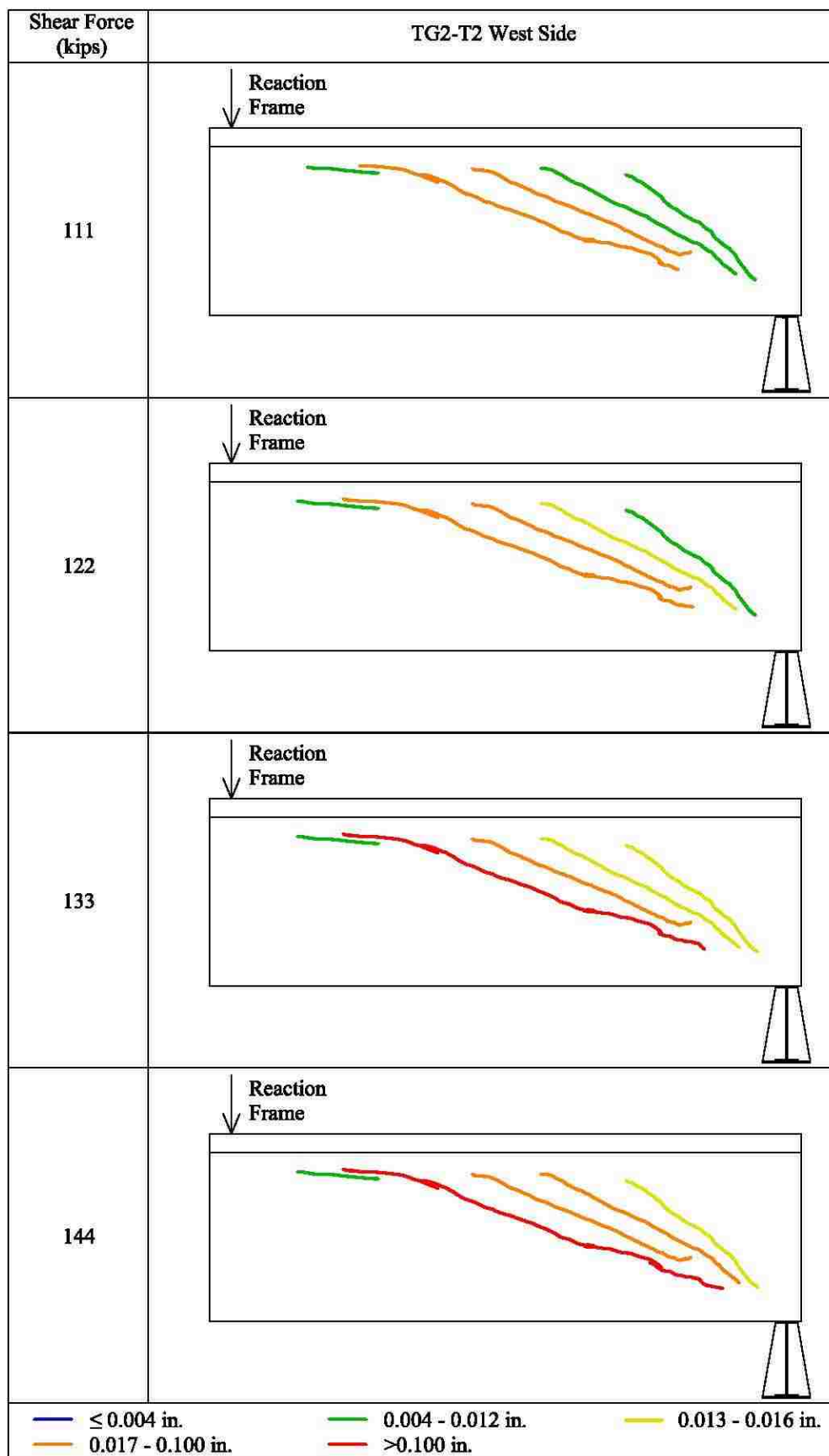


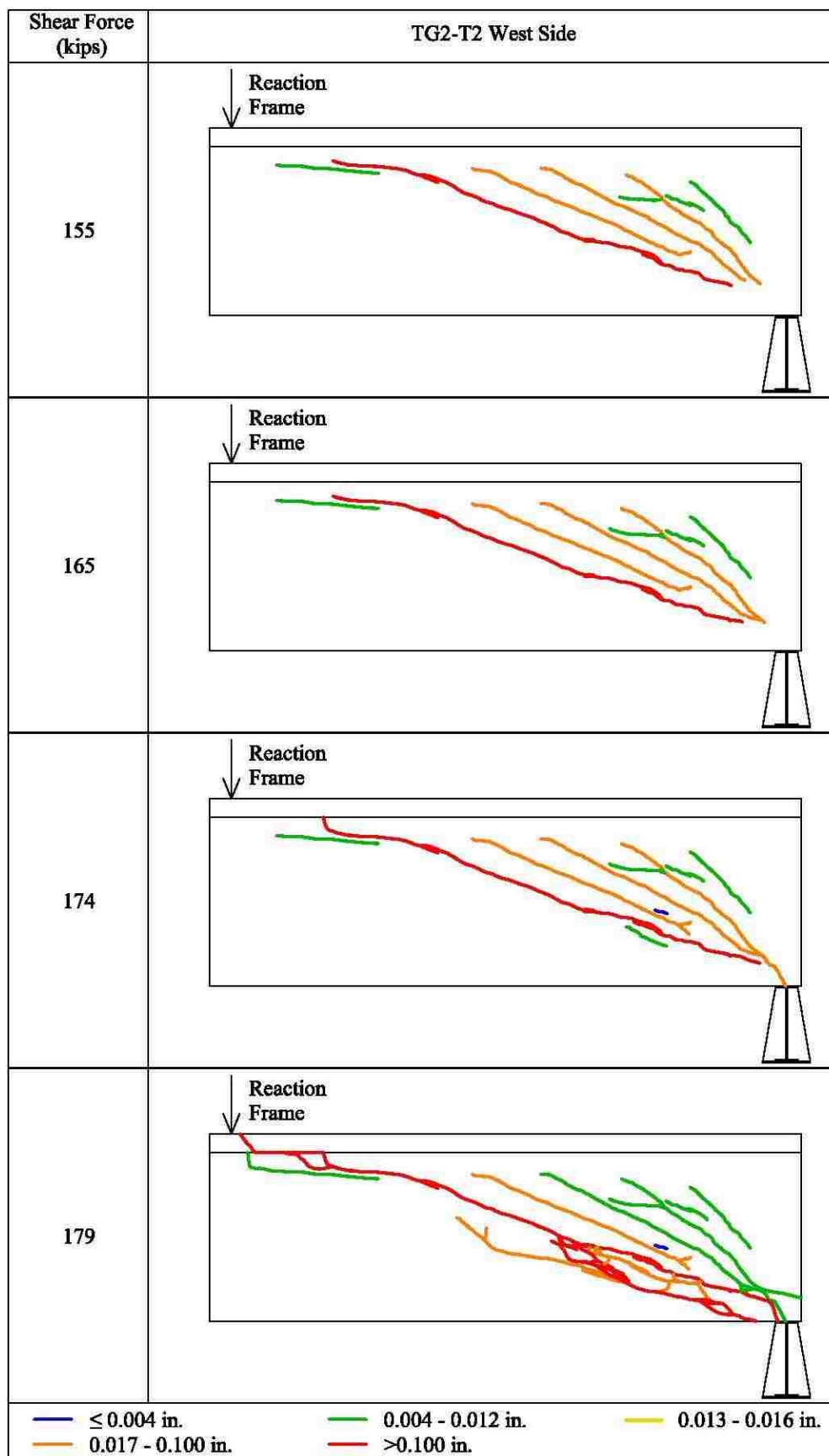
















TGI - T1 West Side

Crack Label	Shear Force (kips)										
	171	185	200	214	223	235	243	247	254	260	267
Shear Cracks											
1	0.002	0.004	0.008	0.008	0.006	0.008	0.008	0.008	0.006	0.008	0.008
1'	0.006	0.006	0.008	0.008	0.006	0.008	0.010	0.010	0.010	0.010	0.012
2	0.008	0.010	0.012	0.012	0.012	0.012	0.014	0.016	0.016	0.016	0.018
3	0.004	0.005	0.006	0.006	0.007	0.008	0.010	0.010	0.012	0.012	0.014
4	0.006	0.008	0.010	0.010	0.012	0.012	0.012	0.012	0.014	0.016	0.016
5	0.006	0.006	0.011	0.012	0.012	0.012	0.012	0.014	0.014	0.014	0.014
6	0.004	0.004	0.004	0.004	0.006	0.006	0.008	0.006	0.008	0.008	0.010
7	0.002	0.006	0.012	0.014	0.014	0.014	0.014	0.016	0.016	0.016	0.016
8	0.001	0.004	0.008	0.010	0.012	0.014	0.015	0.014	0.016	0.016	0.014
9	--	0.002	0.002	0.004	0.006	0.006	0.008	0.008	0.008	0.010	0.010
10	--	--	--	--	--	--	--	--	0.004	0.004	0.002
11	--	--	--	--	--	--	--	--	--	--	0.012

Crack Label	Shear Force (kips)										
	171	185	200	214	223	235	243	247	254	260	267
Flexure/Flexure-Shear Cracks											
F1	--	--	--	--	0.004	0.008	0.010	0.010	0.012	0.016	0.014
F2	--	--	--	--	0.004	0.004	0.004	0.006	0.006	0.006	0.008
F3	--	--	--	--	0.002	0.002	0.002	0.004	0.006	0.004	0.006
F4	--	--	--	--	0.004	0.008	0.010	0.010	0.012	0.010	0.014
F5	--	--	--	--	0.002	0.002	0.004	0.004	0.004	0.002	0.006
F6	--	--	--	--	0.002	0.004	0.010	0.012	0.014	0.014	0.014
F7	--	--	--	--	0.002	0.002	0.004	0.004	0.006	0.004	0.006
F8	--	--	--	--	--	0.004	0.008	0.008	0.012	0.012	0.010
F9	--	--	--	--	--	0.006	0.010	0.012	0.014	0.012	0.014
F10	--	--	--	--	--	0.001	0.002	0.004	0.004	0.004	0.006
F11	--	--	--	--	--	0.002	0.002	0.006	0.004	0.006	0.006
F12	--	--	--	--	--	0.002	0.004	0.004	0.004	0.006	0.006
F13	--	--	--	--	--	0.001	0.002	0.004	0.004	0.004	0.006
F14	--	--	--	--	--	0.004	0.004	0.006	0.006	0.008	0.008
F15	--	--	--	--	--	0.002	0.004	0.004	0.006	0.006	0.006
F16	--	--	--	--	--	0.006	0.012	0.012	0.014	0.014	0.012
F17	--	--	--	--	--	0.001	0.002	0.002	0.002	0.002	0.002
F18	--	--	--	--	--	--	0.002	0.004	0.004	0.004	0.006
F19	--	--	--	--	--	--	0.001	0.002	0.002	0.002	0.002
F20	--	--	--	--	--	--	0.002	0.004	0.004	0.004	0.004
F21	--	--	--	--	--	--	0.001	0.002	0.002	0.002	0.006
F22	--	--	--	--	--	--	--	0.014	0.018	0.018	0.016
F23	--	--	--	--	--	--	--	0.004	0.004	0.006	0.006
F24	--	--	--	--	--	--	--	--	0.002	0.002	0.002
F25	--	--	--	--	--	--	--	--	0.004	0.008	0.010
F26	--	--	--	--	--	--	--	--	0.004	0.004	0.004
F27	--	--	--	--	--	--	--	--	0.004	0.006	0.004
F28	--	--	--	--	--	--	--	--	0.002	0.006	0.010
F29	--	--	--	--	--	--	--	--	--	0.002	0.008
F30	--	--	--	--	--	--	--	--	--	0.002	0.004

\* F27 and 11 connected at 254 k







TG2 - T1 West Side

Crack Label	Shear Force (kips)												
Shear Cracks	142	158	174	191	206	214	220	225	231	242	254	266	273
1	0.010	0.020	0.035	0.040	0.040	0.035	0.035	0.035	0.035	0.035	0.035	0.045	0.050
2	--	0.010	0.025	0.035	0.035	0.035	0.035	0.040	0.040	0.040	0.040	0.040	0.080
3	--	0.005	0.015	0.020	0.025	0.035	0.035	0.035	0.040	0.040	0.040	0.035	0.040
4	--	--	0.010	0.015	0.015	0.020	0.020	0.020	0.025	0.030	0.040	0.045	0.050
5	--	--	--	0.010	0.010	0.010	0.010	0.005	0.005	0.005	0.005	0.005	0.005
6	--	--	--	0.005	0.010	0.010	0.010	0.010	0.010	0.010	0.010	0.010	0.010
7	--	--	--	--	--	0.015	0.020	0.020	0.020	0.025	0.025	0.030	0.030
8	--	--	--	--	--	--	--	0.005	0.010	0.020	0.025	0.025	0.025
9	--	--	--	--	--	--	--	--	--	--	0.025	0.035	0.045
10	--	--	--	--	--	--	--	--	--	--	--	--	0.010

Crack Label	Shear Force (kips)												
Flexure/Flexure-Shear Cracks	142	158	174	191	206	214	220	225	231	242	254	266	273
F1	--	--	--	--	--	0.005	0.010	0.015	0.015	0.015	0.020	0.020	0.020
F2	--	--	--	--	--	0.005	0.010	0.010	0.010	0.010	0.015	0.020	0.020
F3	--	--	--	--	--	0.005	0.005	0.005	0.005	0.005	0.005	0.010	0.010
F4	--	--	--	--	--	0.010	0.010	0.010	0.015	0.015	0.015	0.010	0.015
F5	--	--	--	--	--	0.005	0.010	0.015	0.015	0.020	0.025	0.030	0.030
F6	--	--	--	--	--	--	0.005	0.005	0.010	0.010	0.010	0.010	0.015
F7	--	--	--	--	--	--	0.010	0.010	0.015	0.020	0.020	0.020	0.020
F8	--	--	--	--	--	--	0.005	0.005	0.005	0.005	0.005	0.010	0.010
F9	--	--	--	--	--	--	--	0.005	0.005	0.010	0.010	0.005	0.010
F10	--	--	--	--	--	--	--	0.010	0.010	0.010	0.015	0.015	0.015
F11	--	--	--	--	--	--	--	0.010	0.010	0.005	0.005	0.005	0.005
F12	--	--	--	--	--	--	--	0.005	0.005	0.010	0.015	0.015	0.020
F13	--	--	--	--	--	--	--	0.005	0.005	0.005	0.005	0.010	0.005
F14	--	--	--	--	--	--	--	0.005	0.010	0.005	0.010	0.010	0.010
F15	--	--	--	--	--	--	--	--	0.005	0.020	0.035	0.035	0.050
F16	--	--	--	--	--	--	--	--	0.005	0.005	0.005	0.005	0.010
F17	--	--	--	--	--	--	--	--	0.005	0.005	0.005	0.010	0.010
F18	--	--	--	--	--	--	--	--	0.005	0.005	0.005	0.005	0.005
F19	--	--	--	--	--	--	--	--	0.010	0.015	0.020	0.020	0.020
F20	--	--	--	--	--	--	--	--	--	0.005	0.005	0.005	0.010
F21	--	--	--	--	--	--	--	--	--	0.005	0.005	0.005	0.010
F22	--	--	--	--	--	--	--	--	--	--	0.010	0.005	0.005
F23	--	--	--	--	--	--	--	--	--	--	0.005	0.010	0.010
F24	--	--	--	--	--	--	--	--	--	--	0.010	0.010	0.020
F25	--	--	--	--	--	--	--	--	--	--	0.005	0.005	0.010
F26	--	--	--	--	--	--	--	--	--	--	0.005	0.005	0.005
F27	--	--	--	--	--	--	--	--	--	--	0.005	0.005	0.005
F28	--	--	--	--	--	--	--	--	--	--	0.005	0.010	0.010
F29	--	--	--	--	--	--	--	--	--	--	0.005	0.005	0.005
F30	--	--	--	--	--	--	--	--	--	--	0.005	0.010	0.005
F31	--	--	--	--	--	--	--	--	--	--	0.005	0.005	0.005
F32	--	--	--	--	--	--	--	--	--	--	0.005	0.005	0.005

TG2 - T2 East Side

Crack Label	Shear Force (kips)							
Shear Cracks	111	122	133	144	155	165	174	179
1	0.012	0.012	0.014	0.014	0.014	0.016	0.020	0.014
2	0.010	0.012	0.014	0.016	0.016	0.018	0.022	0.008
3	0.024	0.030	0.030	0.030	0.032	0.032	0.032	0.026
4	0.075	0.100	0.125	0.125	0.188	0.188	0.250	0.938
5	0.002	0.002	0.002	0.004	0.004	0.004	0.008	0.020
6	--	--	--	0.004	0.004	0.004	0.004	0.004
7	--	--	--	--	0.002	0.004	0.006	0.004
8	--	--	--	--	--	0.004	0.012	0.016
9	--	--	--	--	--	--	--	0.750

Crack Label	Shear Force (kips)							
Flexure/Flexure-Shear Cracks	111	122	133	144	155	165	174	179
F1	No flexural cracks							

TG2 - T2 West Side

Crack Label	Shear Force (kips)							
Shear Cracks	111	122	133	144	155	165	174	179
1	0.010	0.012	0.014	0.016	0.018	0.022	0.022	0.012
2	0.012	0.014	0.016	0.020	0.022	0.022	0.022	0.010
3	0.026	0.028	0.030	0.032	0.035	0.040	0.040	0.026
4	0.075	0.100	0.125	0.125	0.156	0.188	0.219	0.969
5	0.006	0.006	0.006	0.008	0.010	0.010	0.010	0.012
6	--	--	--	--	0.008	0.008	0.010	0.010
7	--	--	--	--	0.006	0.010	0.010	0.006
8	--	--	--	--	--	--	0.002	0.001
9	--	--	--	--	--	--	0.006	0.040
10	--	--	--	--	--	--	--	0.600

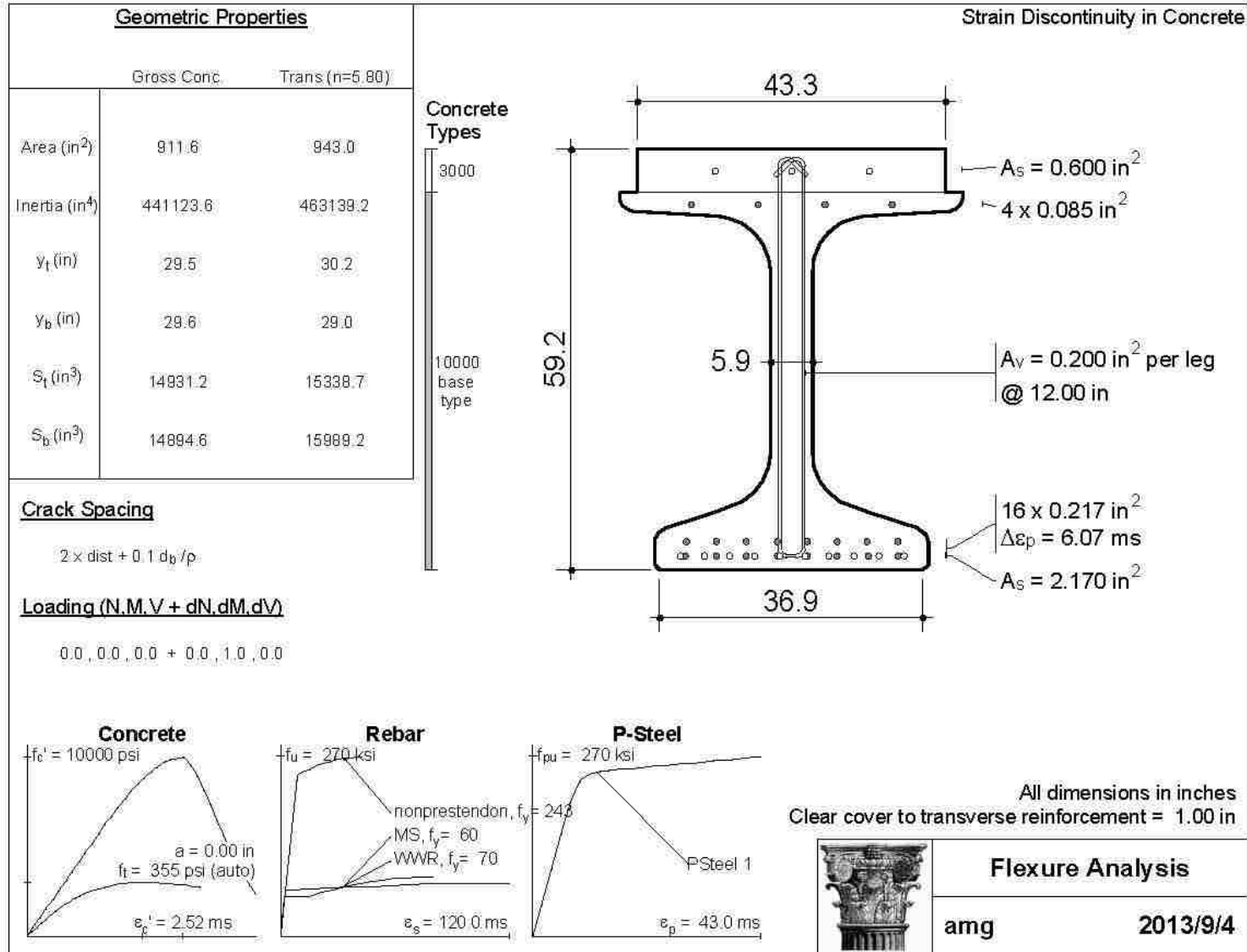
Crack Label	Shear Force (kips)							
Flexure/Flexure-Shear Cracks	111	122	133	144	155	165	174	179
F1	No flexural cracks							

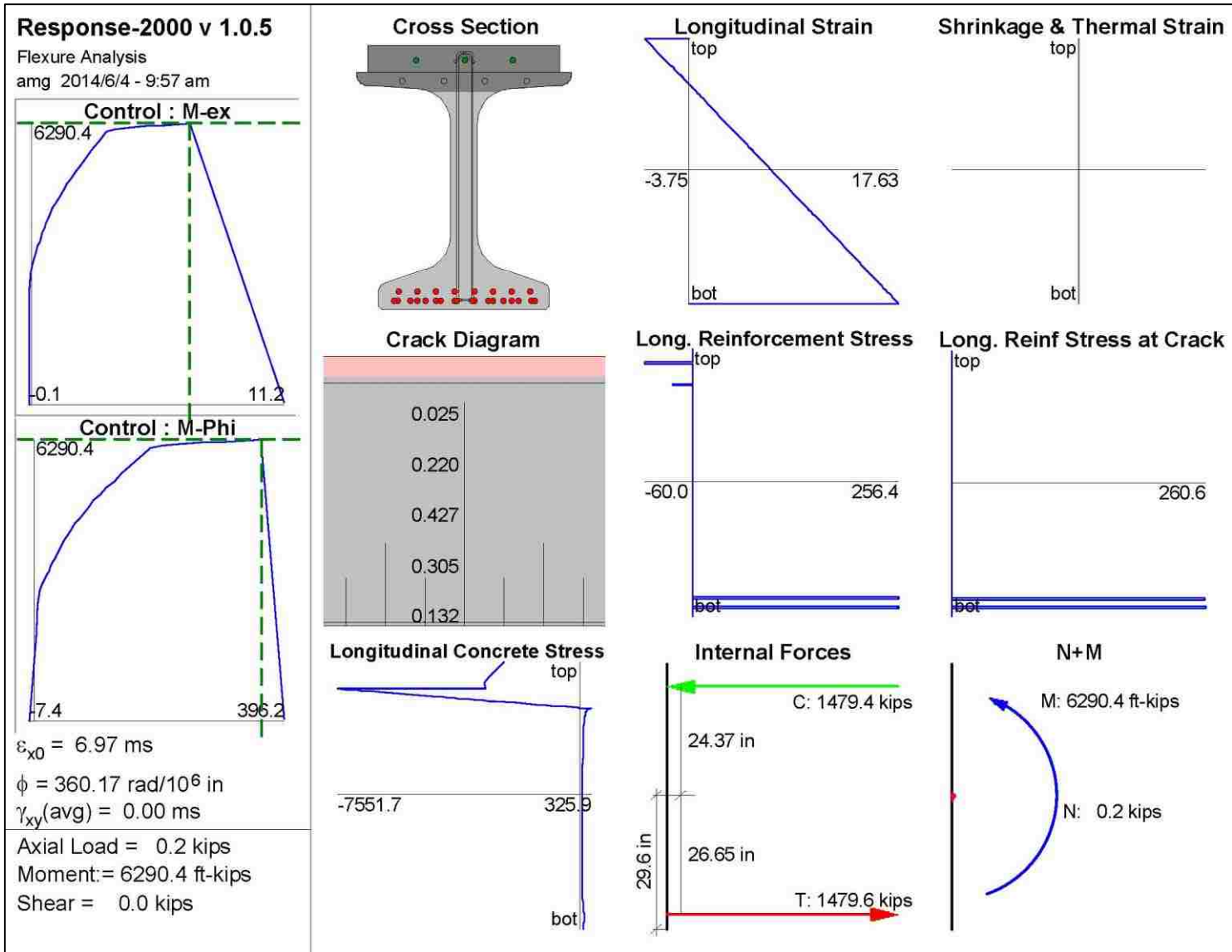
APPENDIX E.  
SHEAR DATABASE

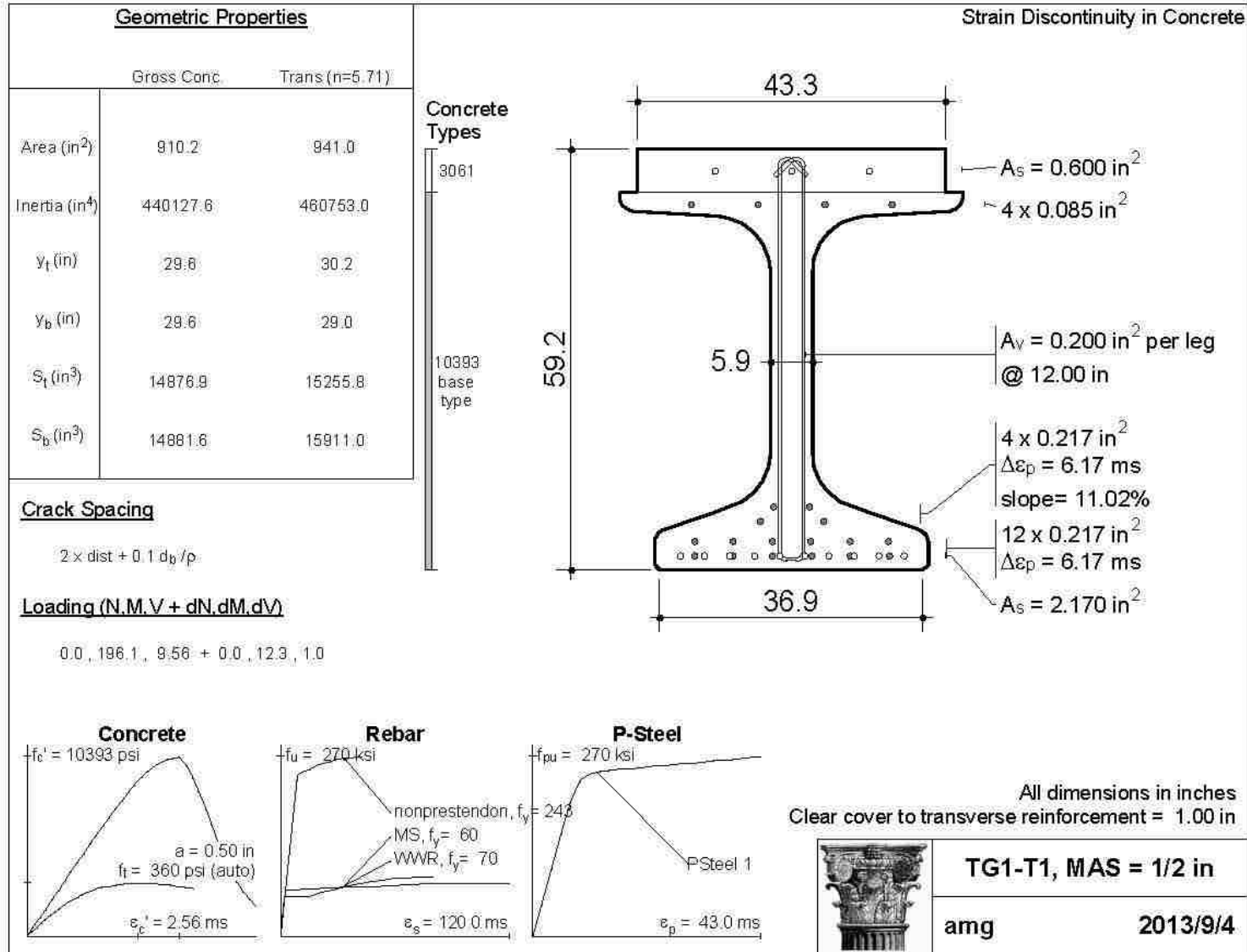


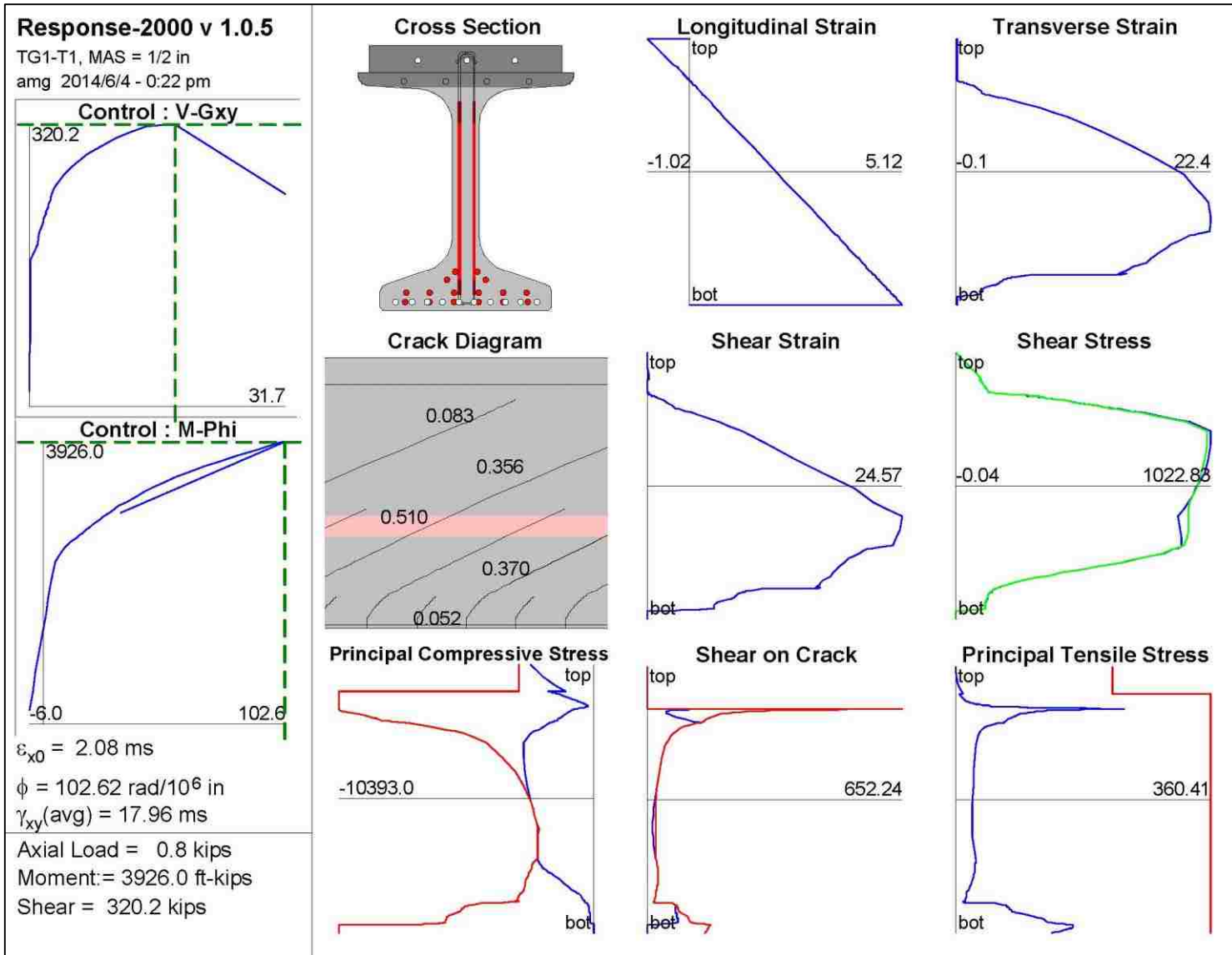


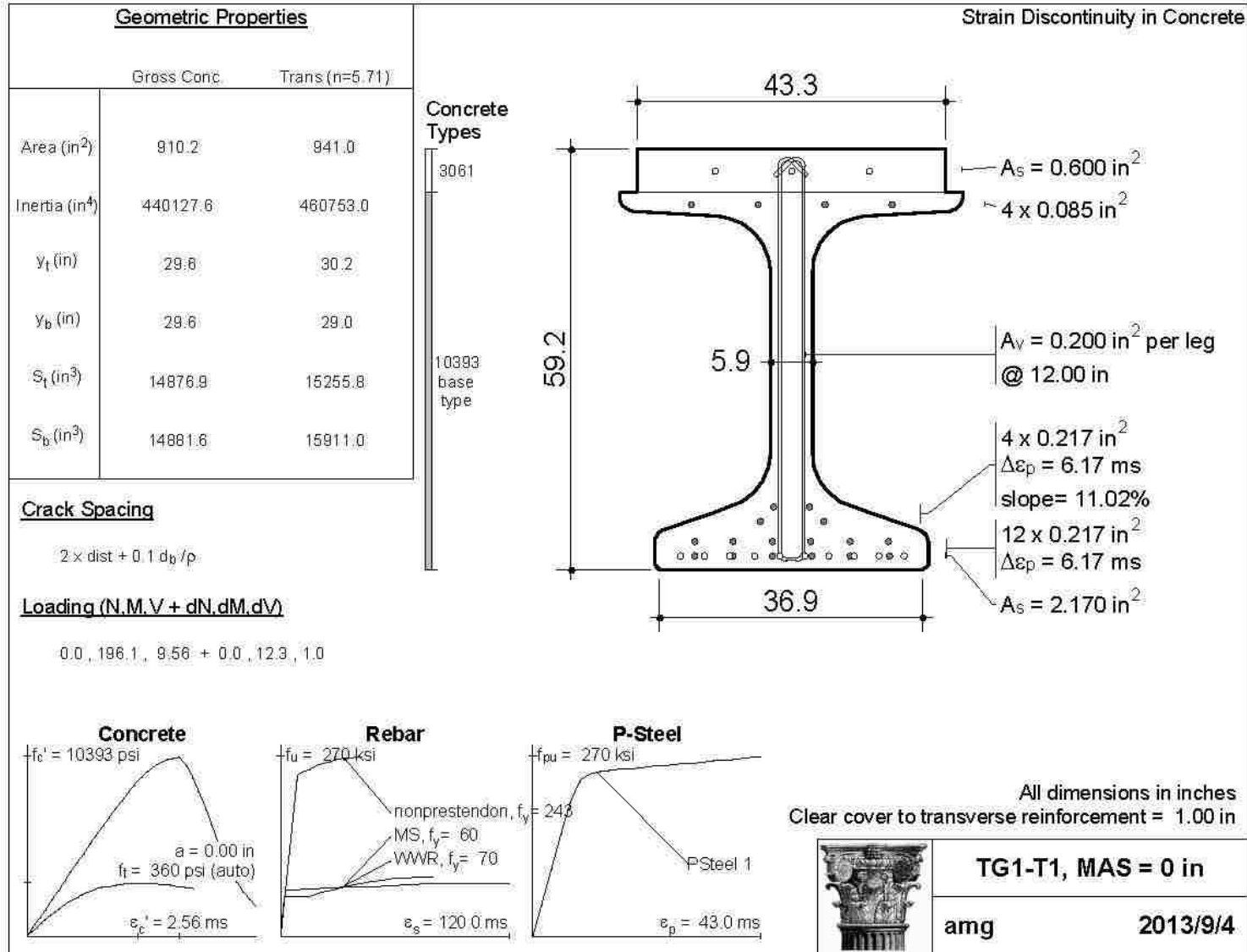
APPENDIX F.  
RESPONSE 2000

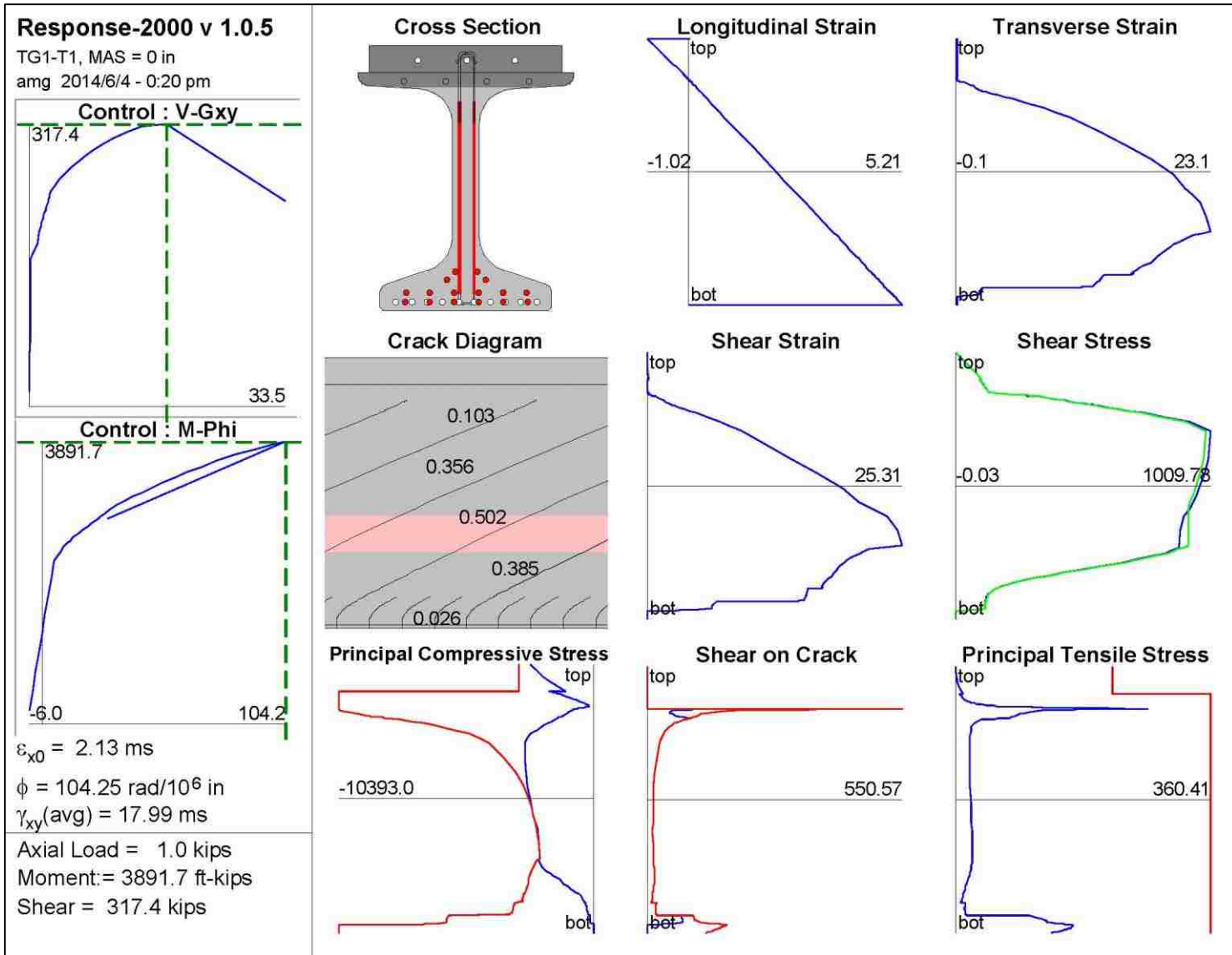




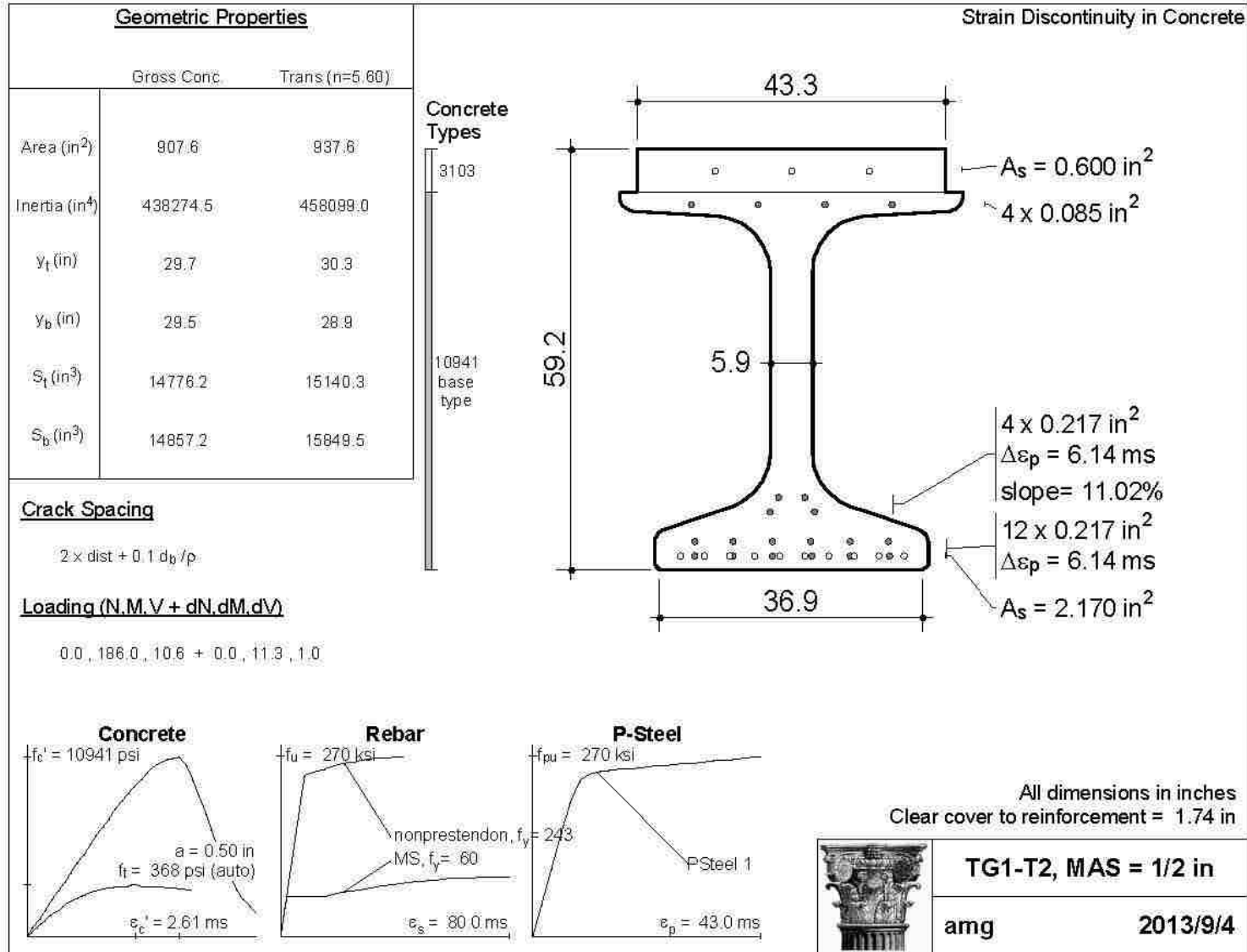






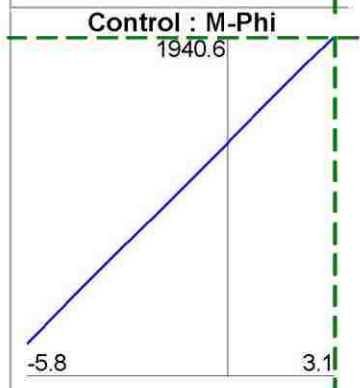
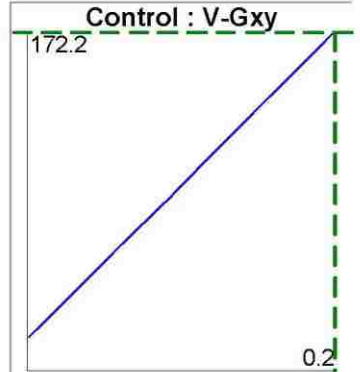




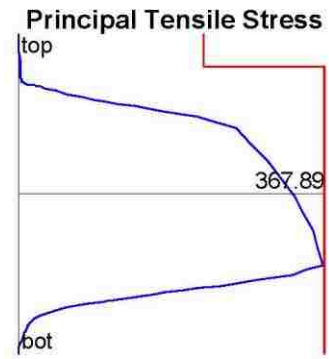
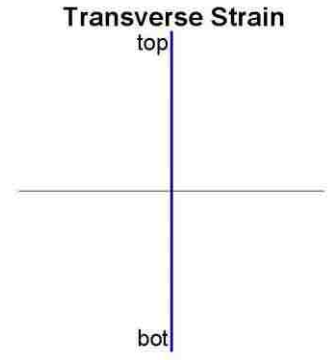
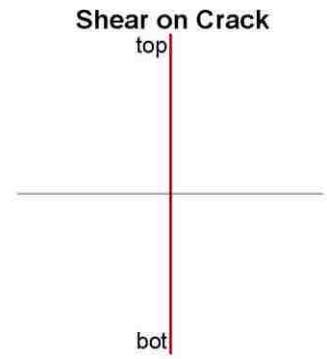
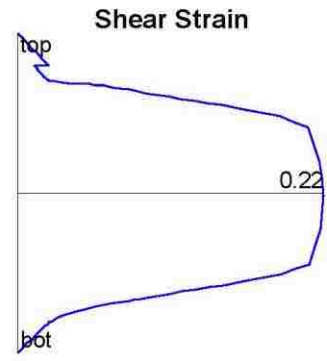
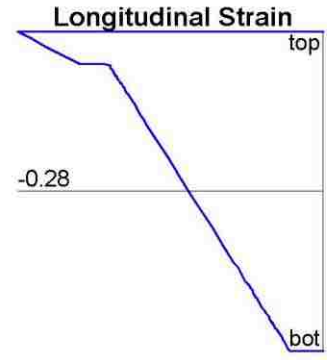
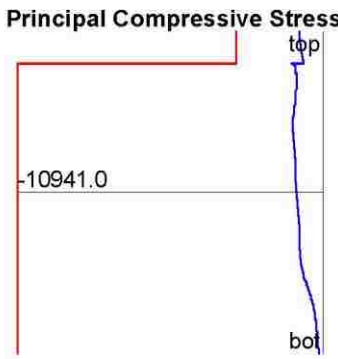
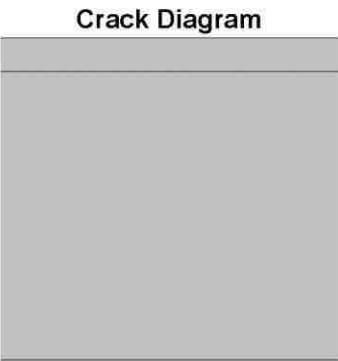
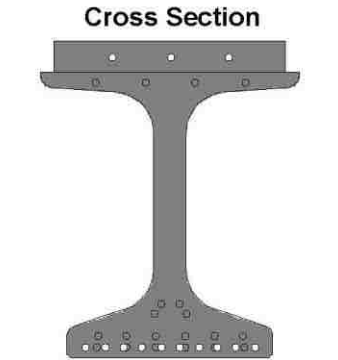


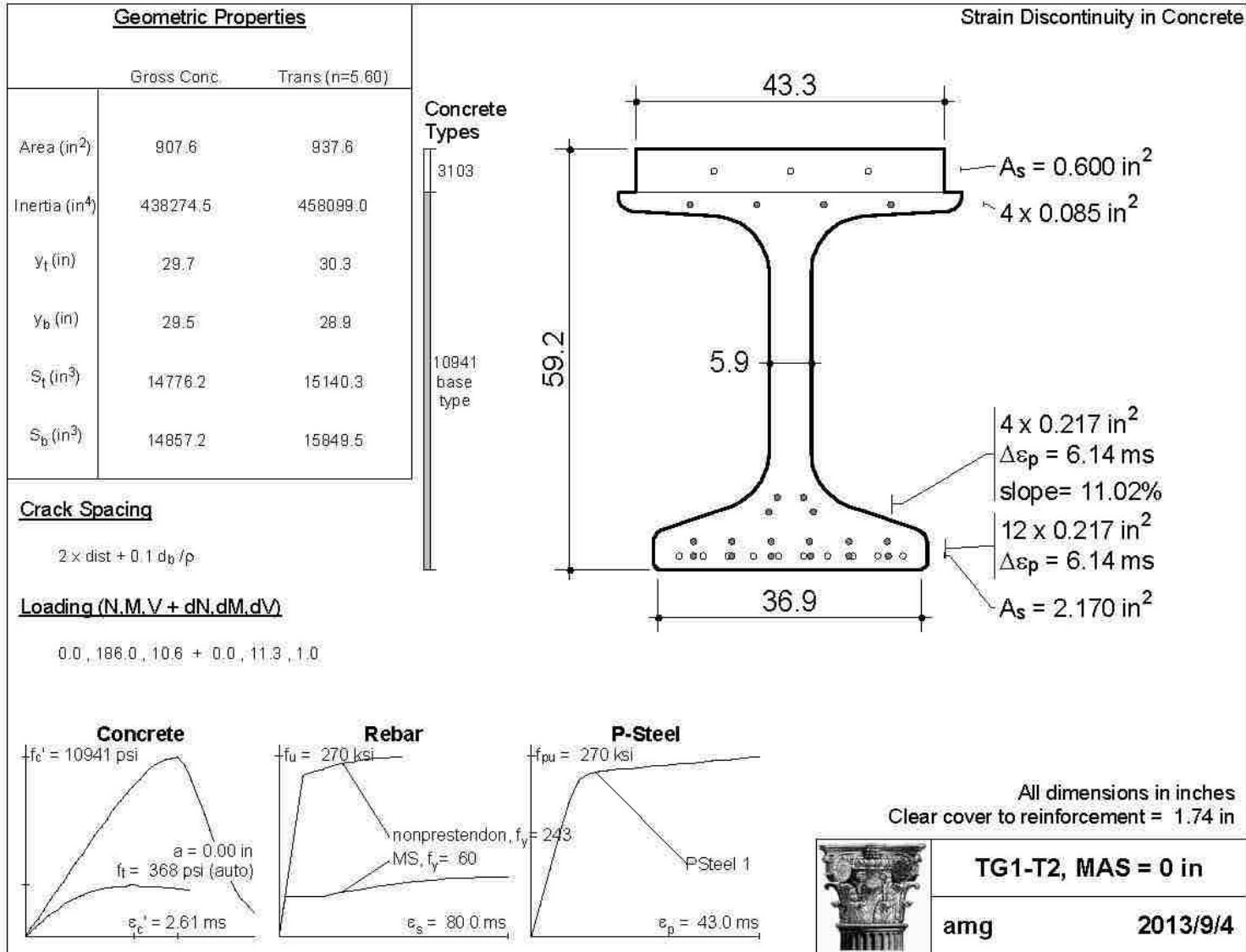
**Response-2000 v 1.0.5**

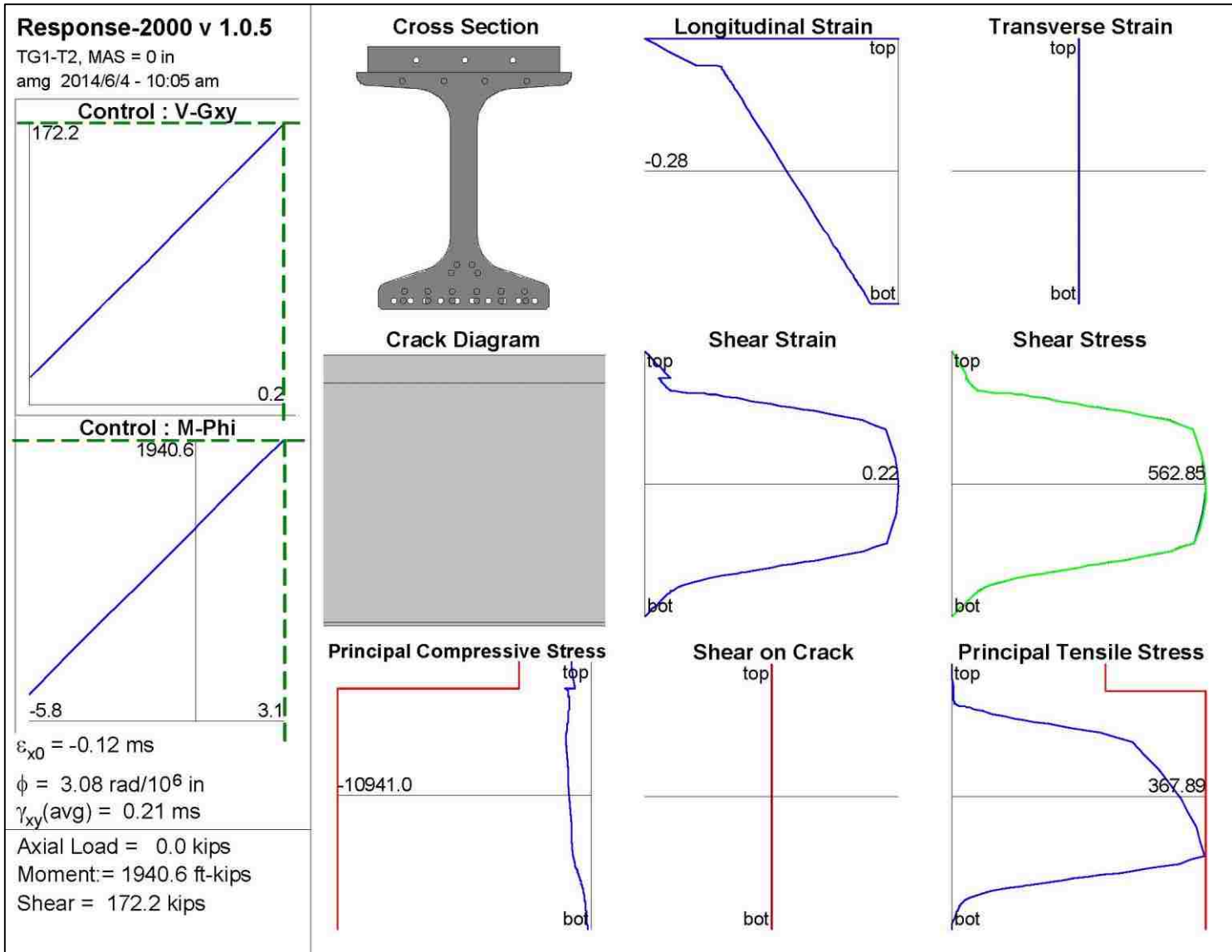
TG1-T2, MAS = 1/2 in  
 avg 2014/6/4 - 10:08 am

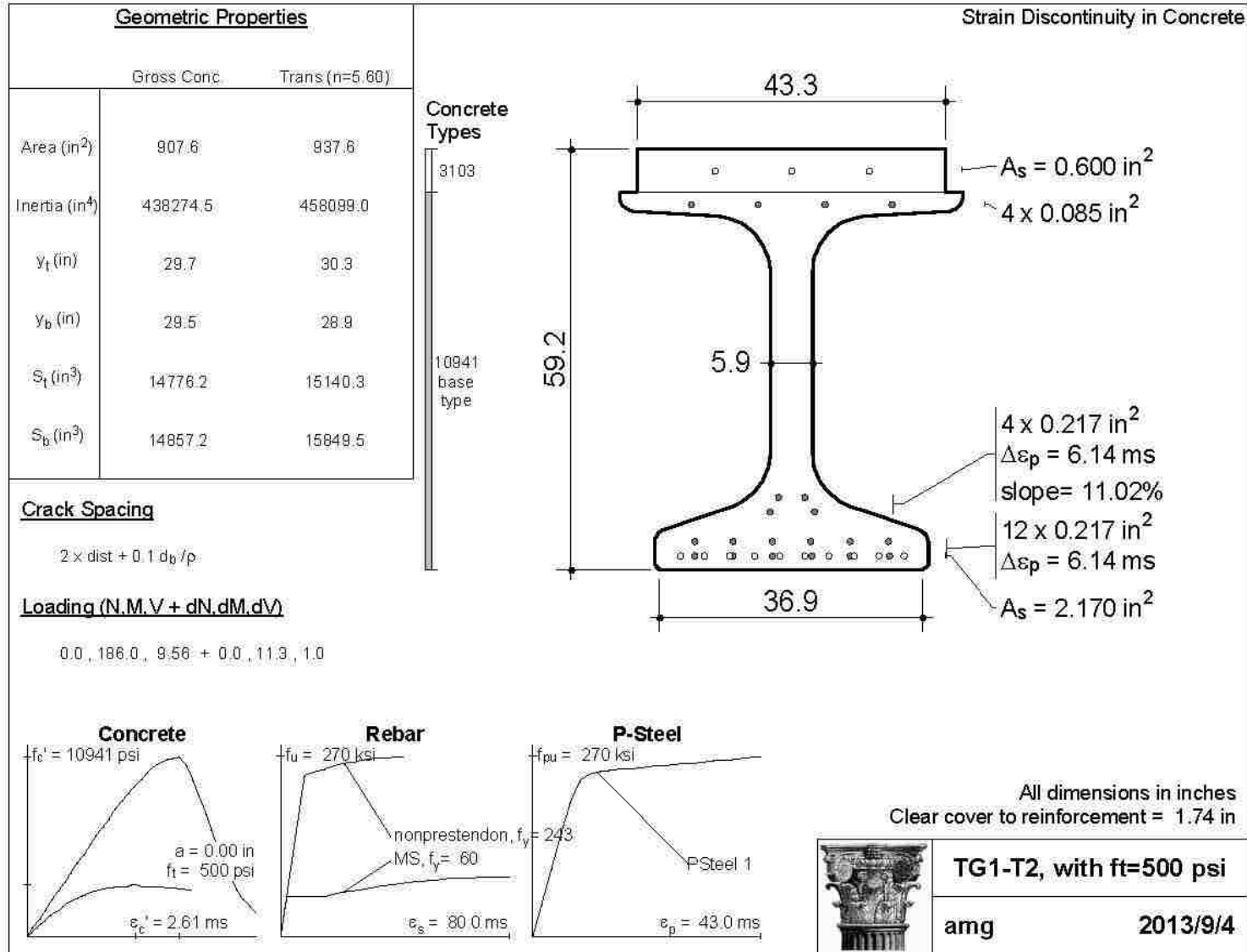


$\epsilon_{x0} = -0.12$  ms  
 $\phi = 3.08$  rad/ $10^6$  in  
 $\gamma_{xy}(avg) = 0.21$  ms  
 Axial Load = 0.0 kips  
 Moment = 1940.6 ft-kips  
 Shear = 172.2 kips



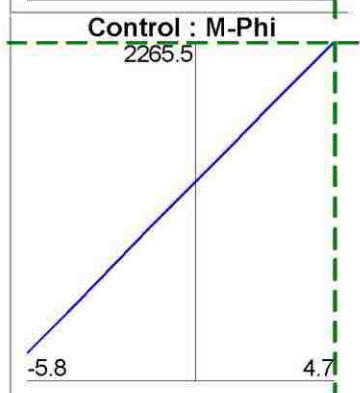
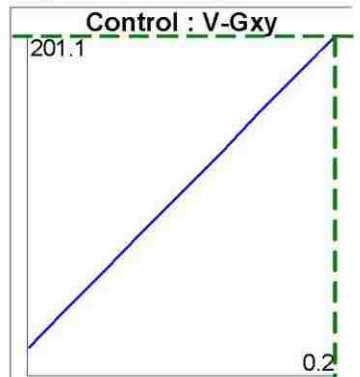




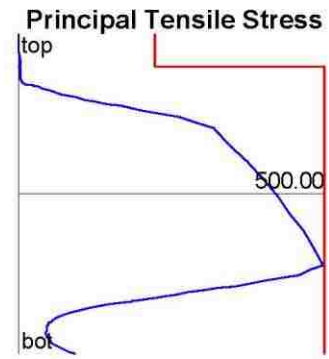
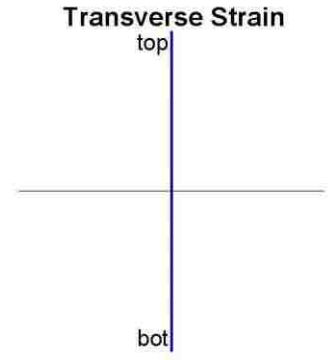
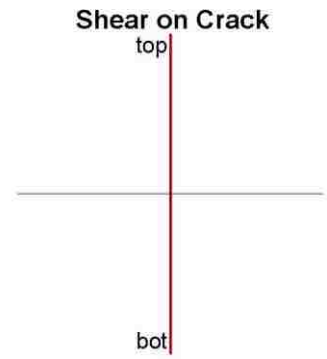
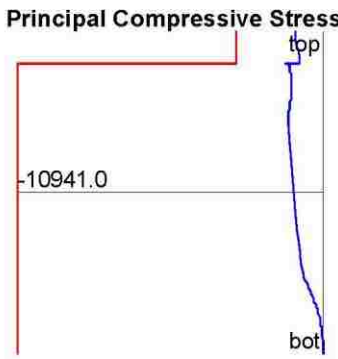
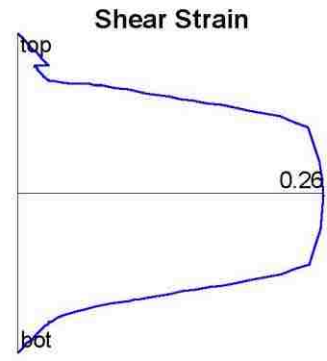
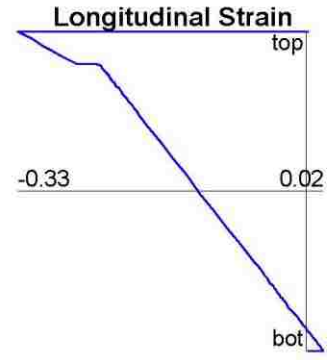
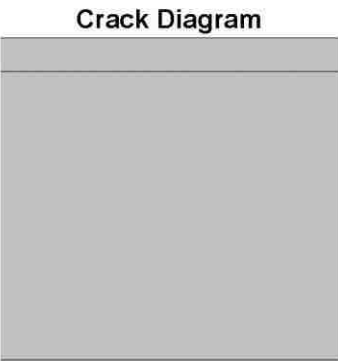
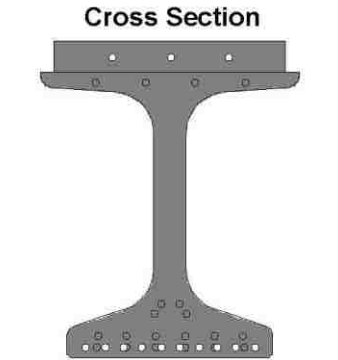


**Response-2000 v 1.0.5**

TG1-T2, with ft=500 psi  
 amg 2014/6/5 - 3:59 pm



$\epsilon_{x0} = -0.12$  ms  
 $\phi = 4.75$  rad/ $10^6$  in  
 $\gamma_{xy}(avg) = 0.25$  ms  
 Axial Load = 0.0 kips  
 Moment = 2265.5 ft-kips  
 Shear = 201.1 kips



<u>Geometric Properties</u>		
	Gross Conc.	Trans (n=5.58)
Area (in <sup>2</sup> )	895.4	825.3
Inertia (in <sup>4</sup> )	429436.3	448998.2
y <sub>t</sub> (in)	30.0	30.6
y <sub>b</sub> (in)	29.1	28.5
S <sub>t</sub> (in <sup>3</sup> )	14302.8	14663.5
S <sub>b</sub> (in <sup>3</sup> )	14739.4	15732.3

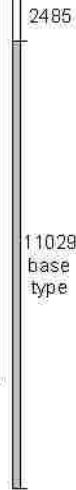
**Crack Spacing**

$2 \times \text{dist} + 0.1 d_b / \rho$

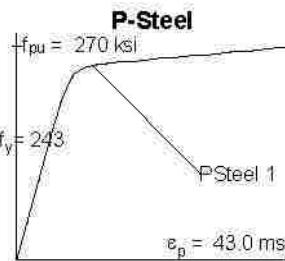
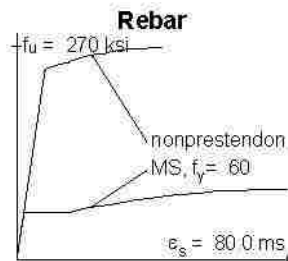
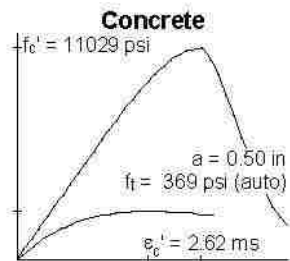
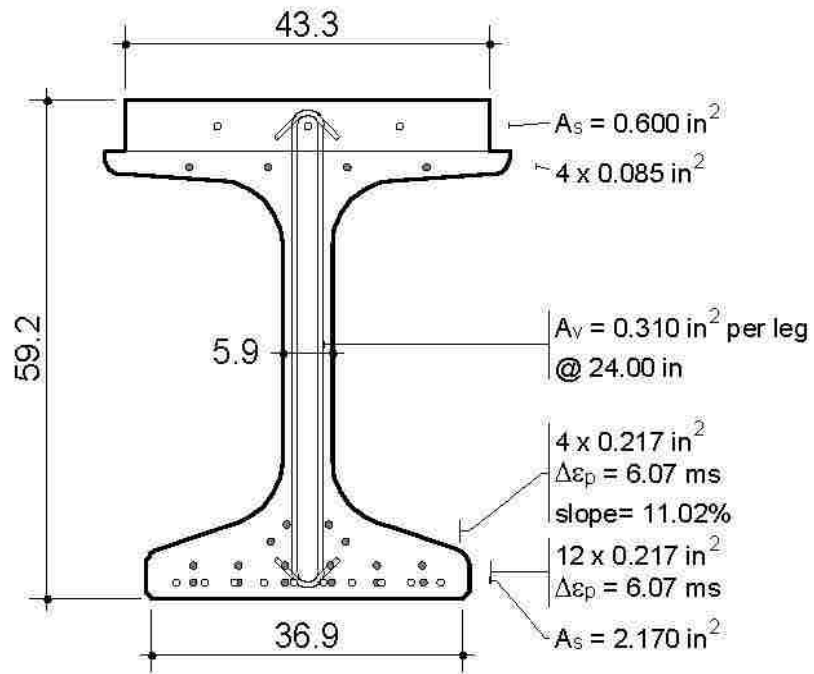
**Loading (N.M.V + dN,dM,dV)**

0.0, 196.1, 9.56 + 0.0, 12.3, 1.0

**Concrete Types**



**Strain Discontinuity in Concrete**



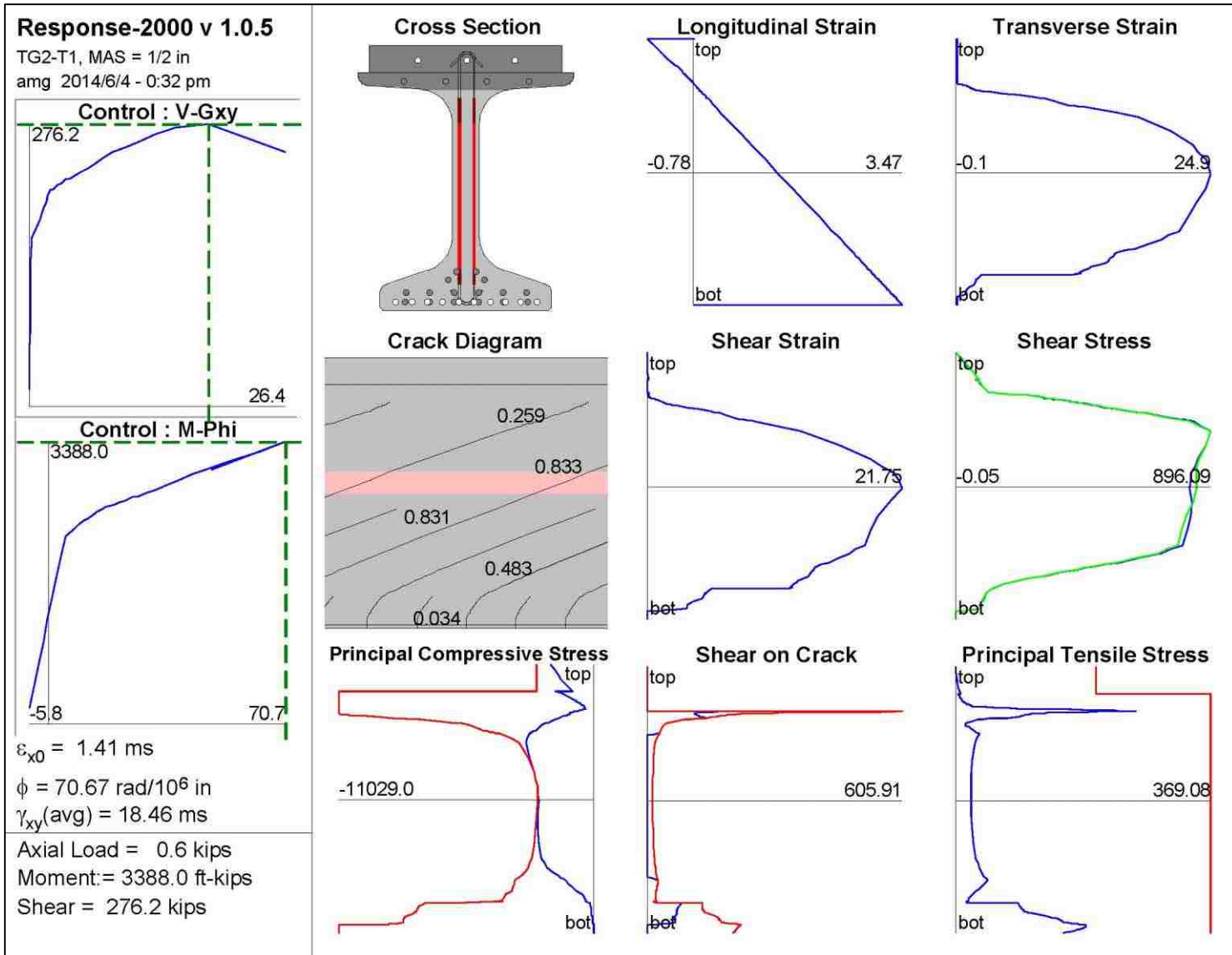
All dimensions in inches  
Clear cover to transverse reinforcement = 1.00 in



**TG2-T1, MAS = 1/2 in**

amg

2013/9/4





<u>Geometric Properties</u>		
	Gross Conc.	Trans (n=5.58)
Area (in <sup>2</sup> )	895.4	825.3
Inertia (in <sup>4</sup> )	429436.3	448998.2
y <sub>t</sub> (in)	30.0	30.6
y <sub>b</sub> (in)	29.1	28.5
S <sub>t</sub> (in <sup>3</sup> )	14302.8	14663.5
S <sub>b</sub> (in <sup>3</sup> )	14739.4	15732.3

**Crack Spacing**

$2 \times \text{dist} + 0.1 d_b / \rho$

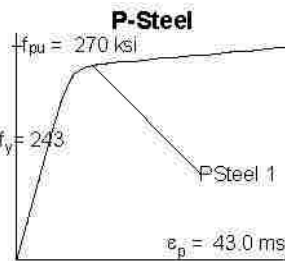
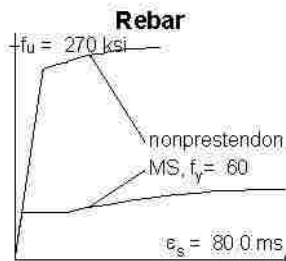
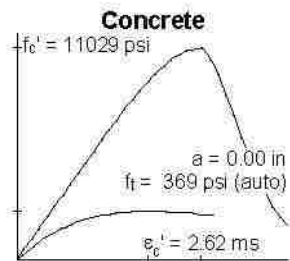
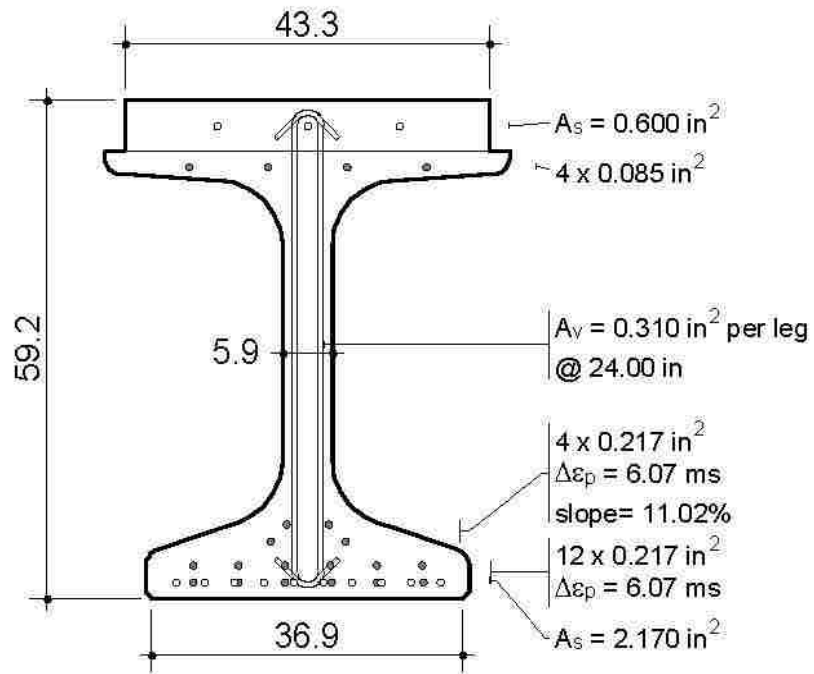
**Loading (N.M.V + dN,dM,dV)**

0.0, 196.1, 9.56 + 0.0, 12.3, 1.0

**Concrete Types**



**Strain Discontinuity in Concrete**



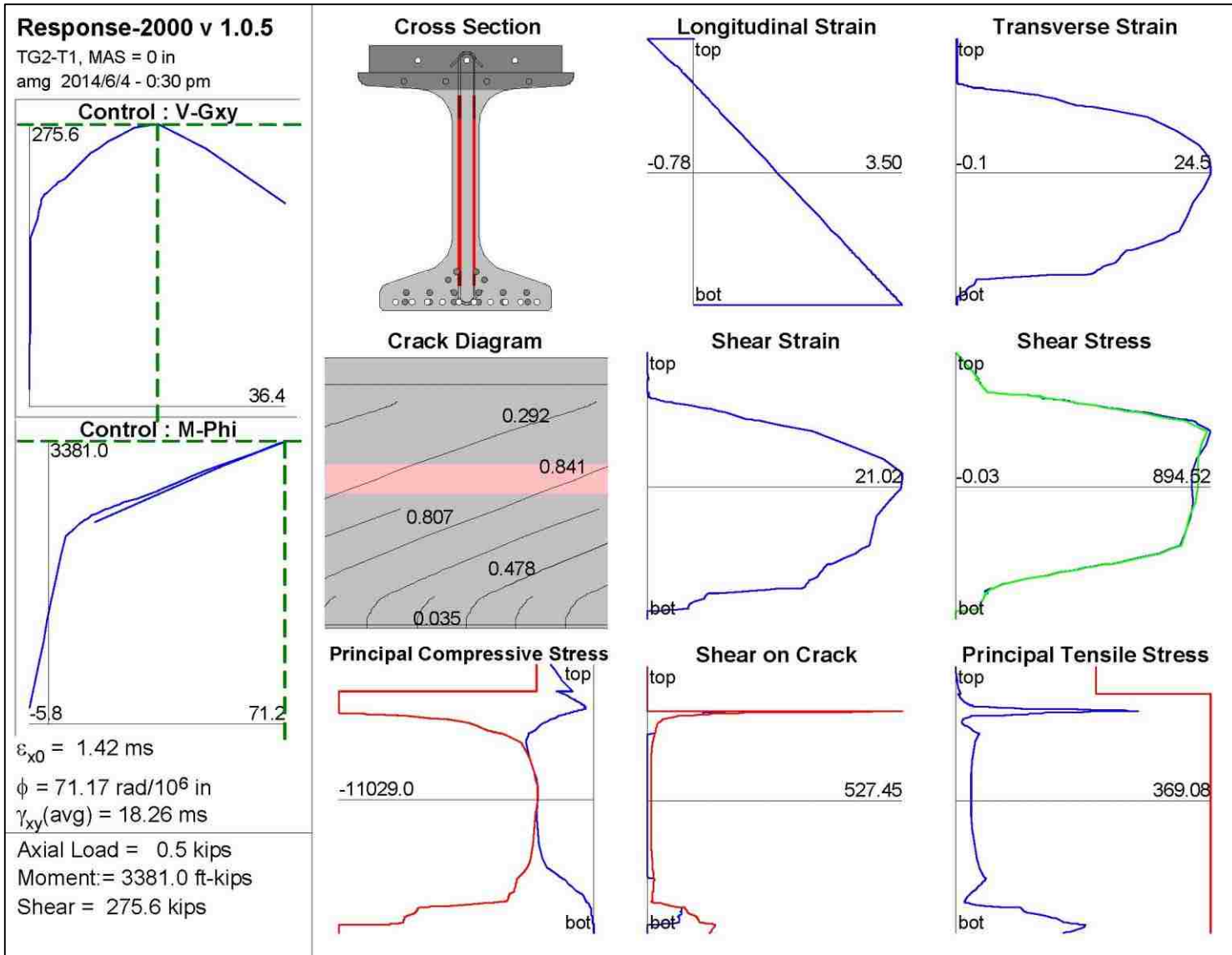
All dimensions in inches  
Clear cover to transverse reinforcement = 1.00 in

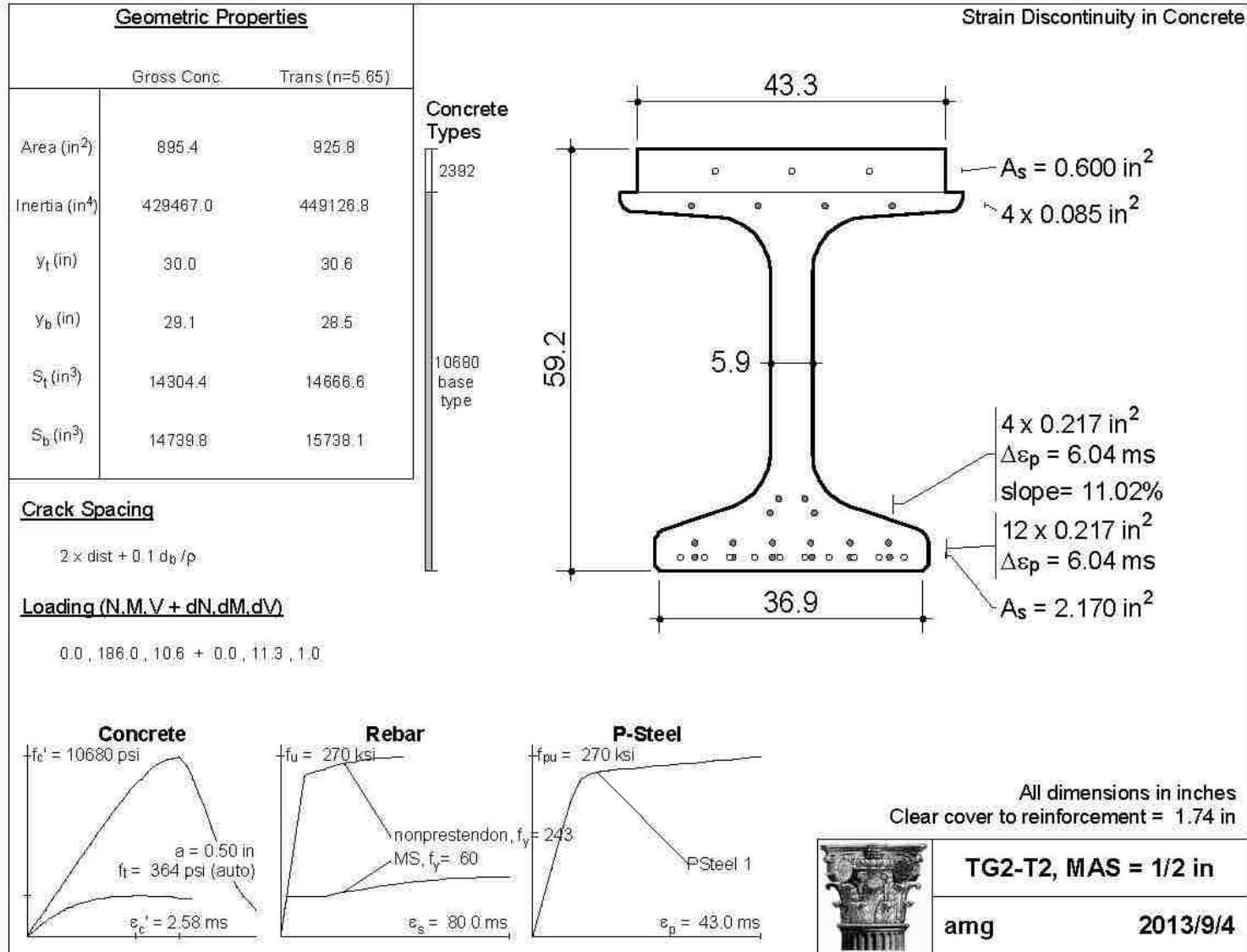


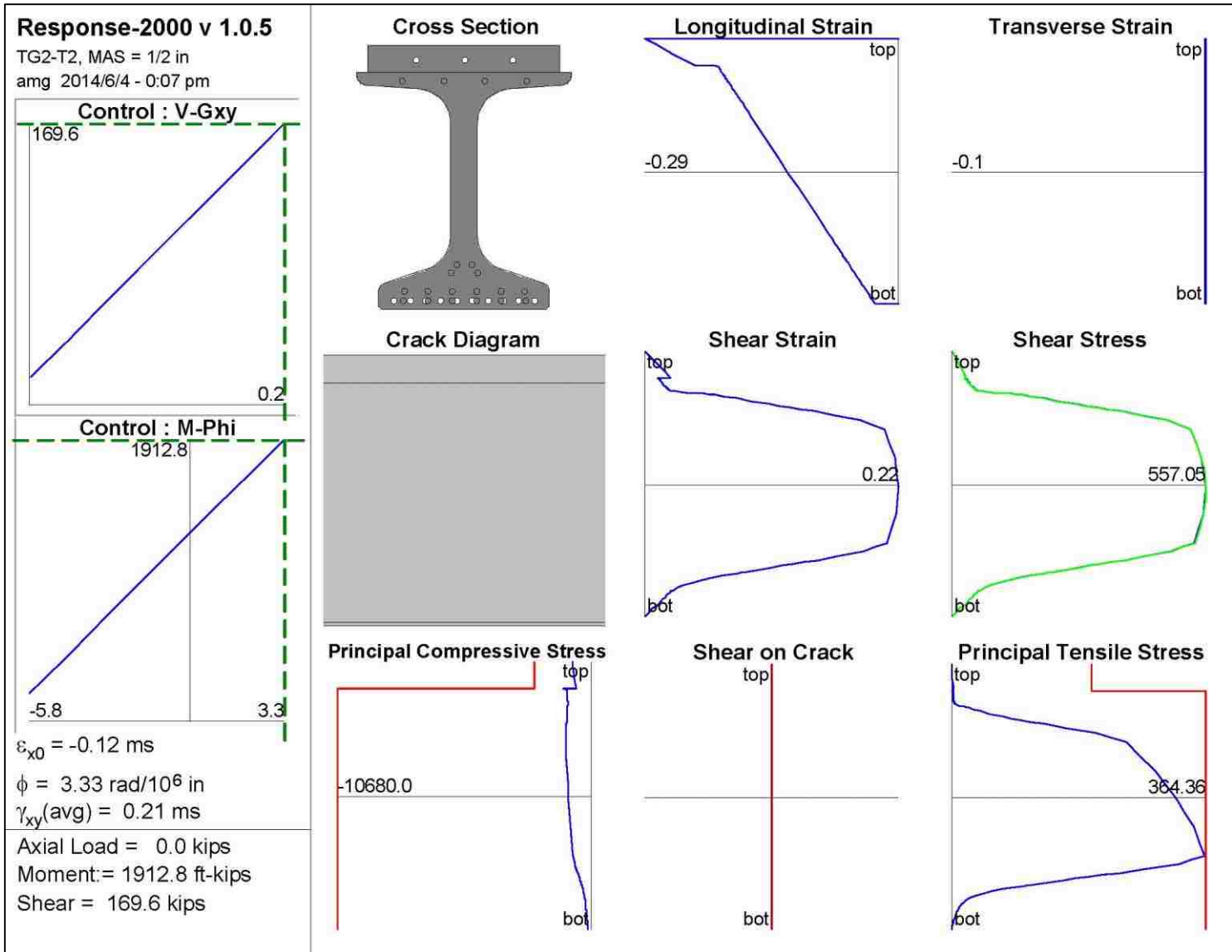
**TG2-T1, MAS = 0 in**

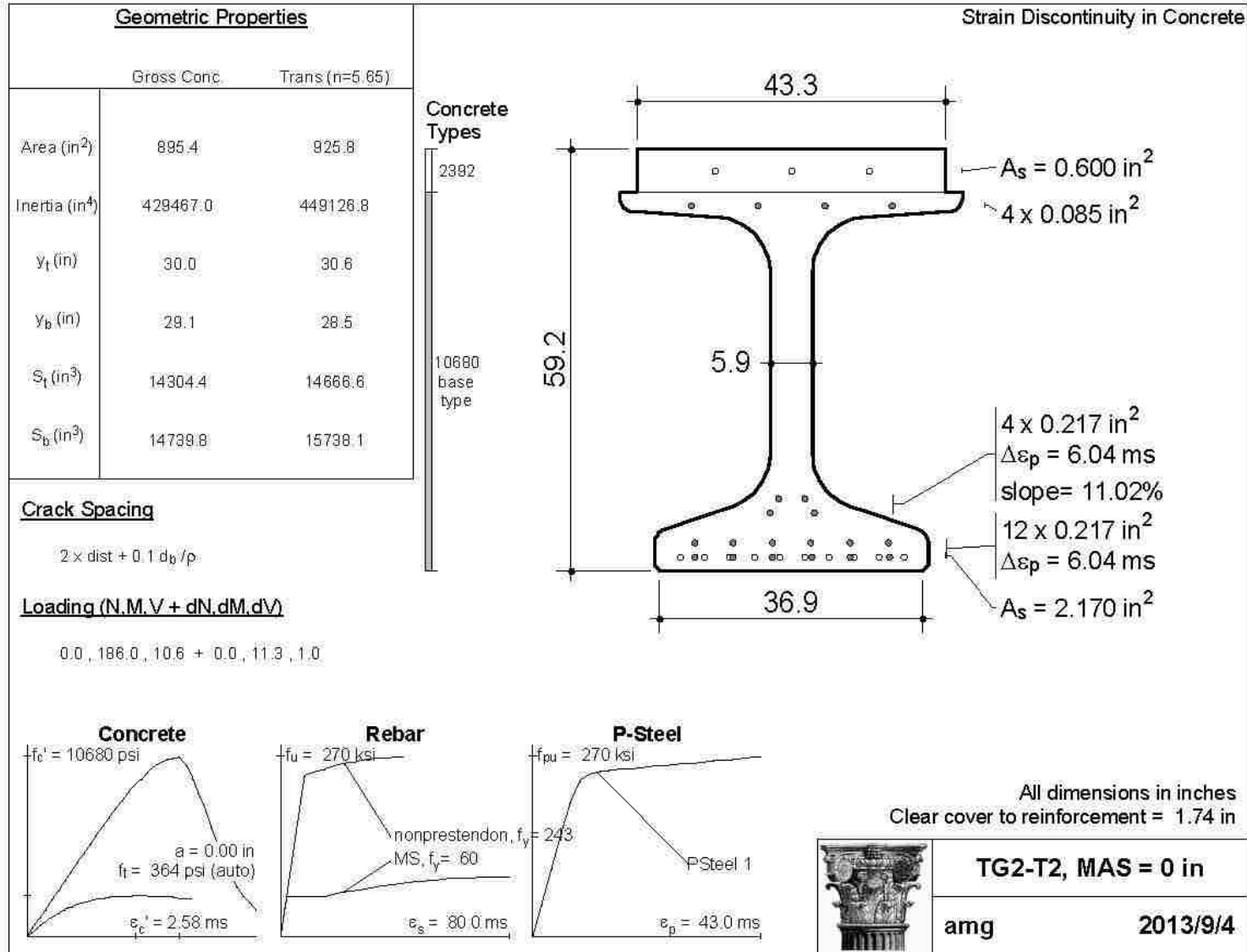
amg

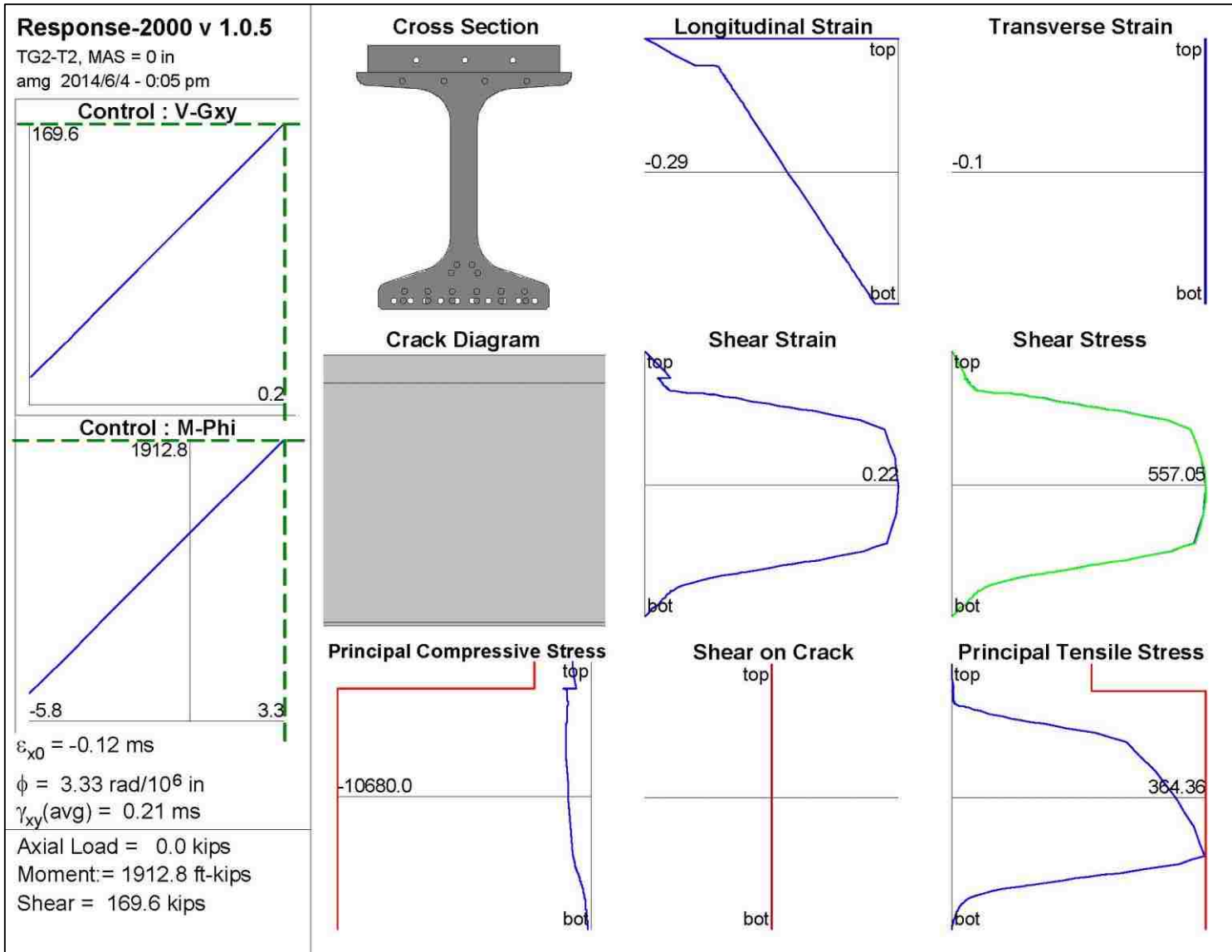
2013/9/4





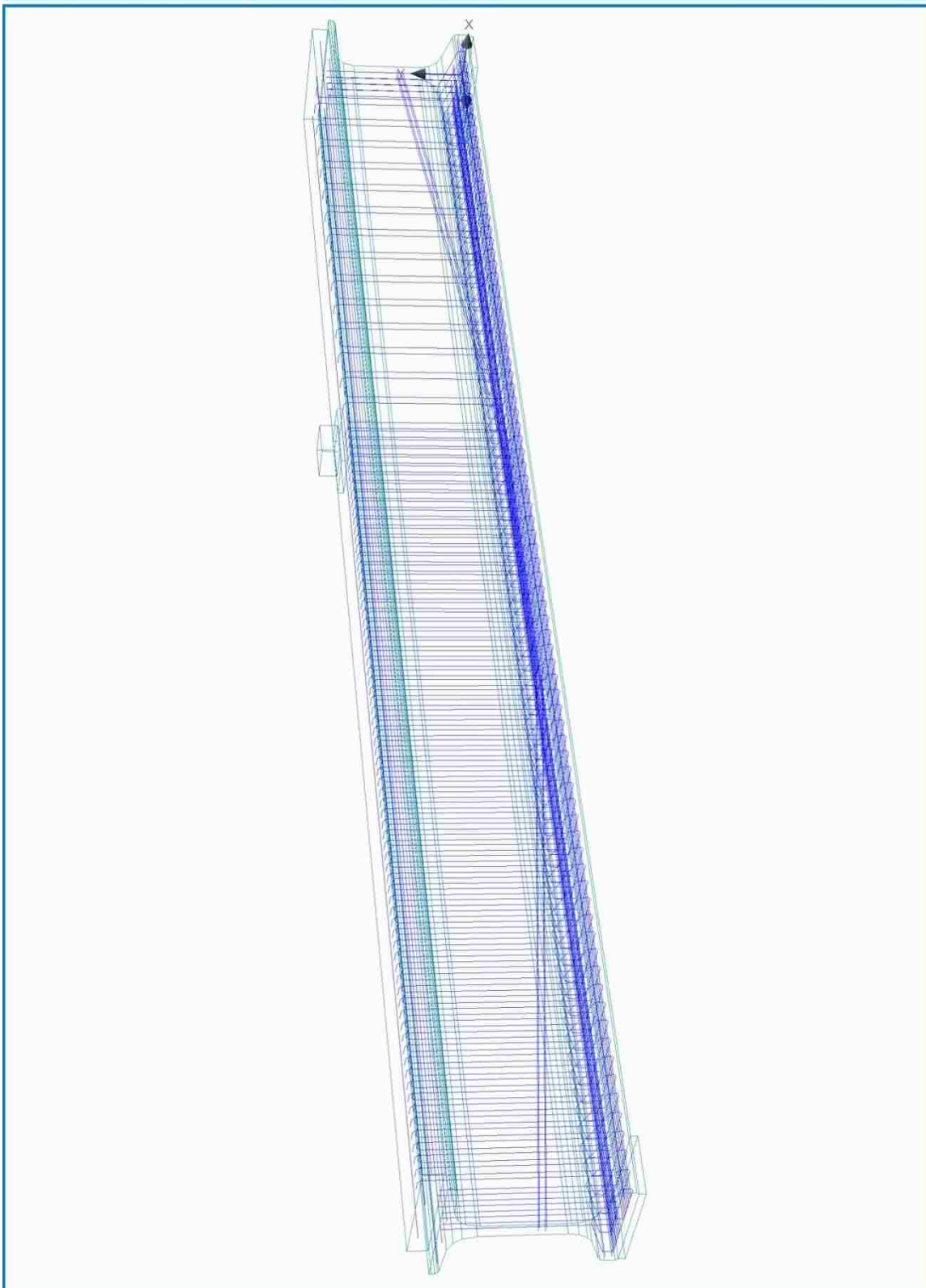







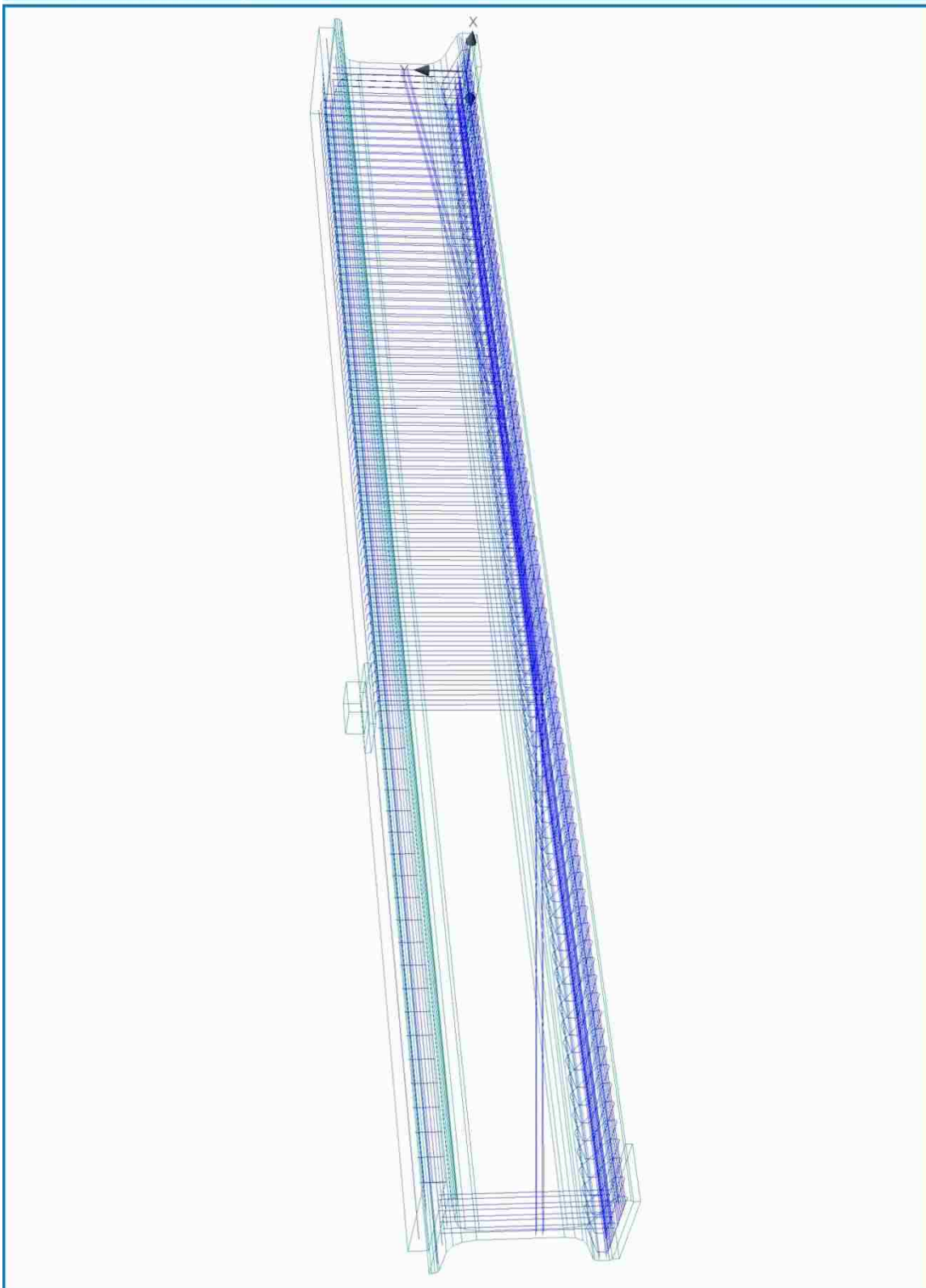
APPENDIX G.  
ATENA ENGINEERING

	Description:	TG1-T1	Unit system:	Metric
	Note:	Shear Reinforcement		

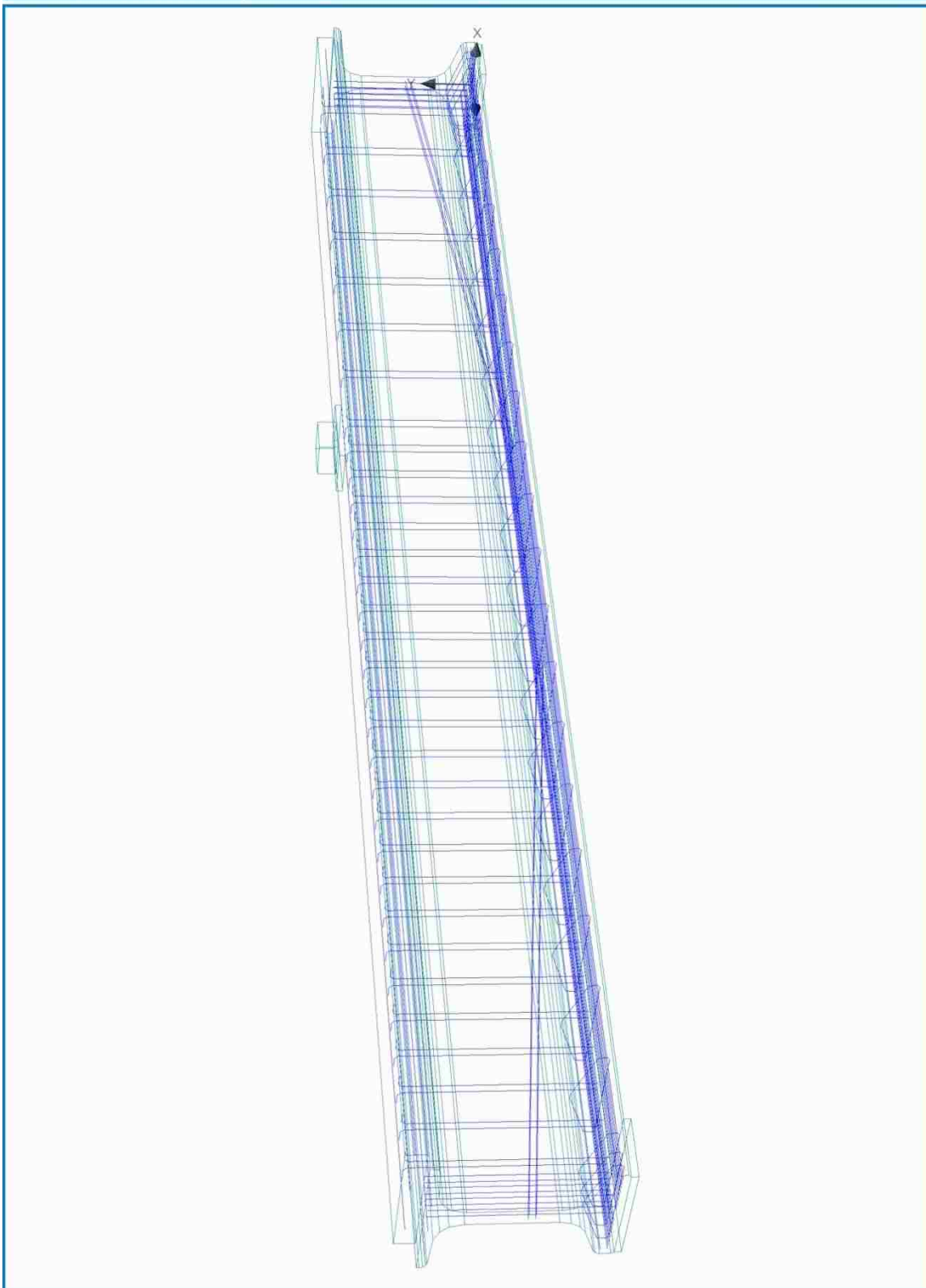





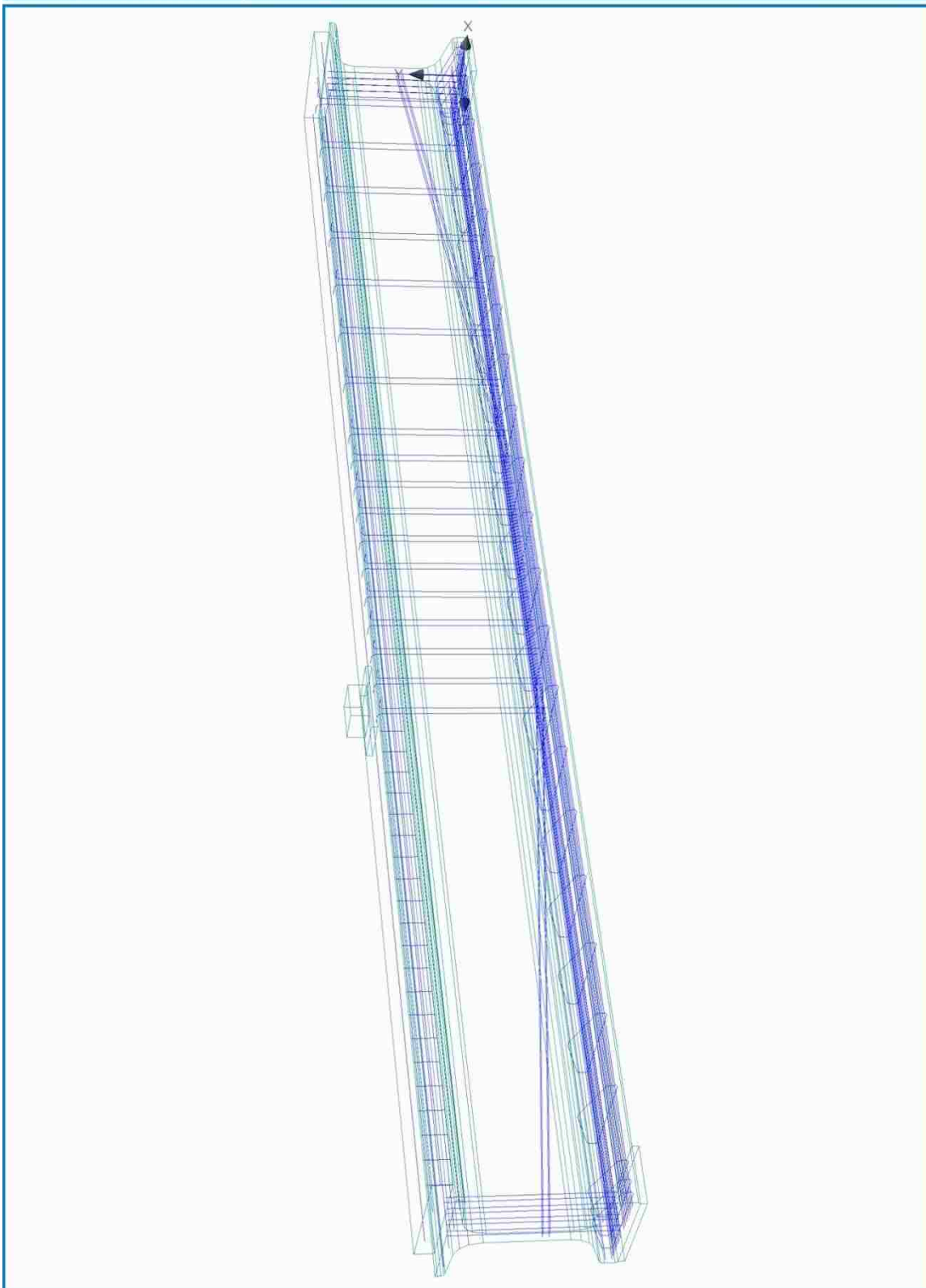
	Description:	TG1-T2	Unit system:	Metric
	Note:	No Shear Reinforcement		



	Description:	<b>TG2-T1</b>	Unit system:	Metric
	Note:	Shear Reinforcement		



	Description:	<b>TG2-T2</b>	Unit system:	Metric
	Note:	No Shear Reinforcement		



## REFERENCES

- AASHTO M 31 (2007). "Standard Specification for Deformed and Plain Carbon-Steel Bars for Concrete Reinforcement." *American Association of State Highway and Transportation Officials (AASHTO)*. Washington, D.C.
- AASHTO M 203 (2012). "Standard Specification for Steel Strand, Uncoated Seven-Wire for Concrete Reinforcement." *American Association of State Highway and Transportation Officials (AASHTO)*. Washington, D.C.
- AASHTO M 221 (2009). "Standard Specification for Steel Welded Wire Reinforcement, Deformed, for Concrete." *American Association of State Highway and Transportation Officials (AASHTO)*. Washington, D.C.
- ACI Committee 224 (2001). "Control of Cracking in Concrete Structures." *American Concrete Institute*, Farmington Hills, Michigan.
- ACI Committee 237 (2007). "Self-Consolidating Concrete." *American Concrete Institute*, Farmington Hills, Michigan.
- ACI Committee 318 (2011). "Building Code Requirements for Structural Concrete and Commentary." *American Concrete Institute*, Farmington Hills, Michigan.
- ACI Committee 363 (2010). "State of the Art Report on High Strength Concrete." *American Concrete Institute*, Farmington Hills, Michigan.
- ACI-ASCE Committee 326 (1962). "Shear and Diagonal Tension." *American Concrete Institute*, Farmington Hills, Michigan.
- ACI-ASCE Committee 426 (1973). Shear strength of reinforced concrete members. *Journal of the Structural Division, ASCE*, 99(ST6), 1091-1187.
- ACI-ASCE Committee 445 (1999). "Recent Approaches to Shear Design of Structural Concrete." *American Concrete Institute*, Farmington Hills, Michigan.
- Alejandro, R., Avendano, V., and Bayrak, O. (2008). *Shear Strength and Behavior of Prestressed Concrete Beams* (Report IAC-88-5DD1A003-3). University of Texas at Austin, Austin, Texas.
- American Association of State Highway and Transportation Officials (2012). "AASHTO LRFD Bridge Design Specifications, 6<sup>th</sup> Edition." *American Association of State Highway and Transportation Officials*, Washington, D.C.

- ASTM A 416 (2012a). “Standard Specification for Steel Strand, Uncoated Seven-Wire for Prestressed Concrete.” *American Society for Testing and Materials (ASTM) International*, West Conshohocken, Pennsylvania.
- ASTM A 615 (2012). “Standard Specification for Deformed and Plain Carbon-Steel Bars for Concrete Reinforcement.” *American Society for Testing and Materials (ASTM) International*, West Conshohocken, Pennsylvania.
- ASTM A 1064 (2012). “Standard Specification for Carbon-Steel Wire and Welded Wire Reinforcement, Plain and Deformed, for Concrete.” *American Society for Testing and Materials (ASTM) International*, West Conshohocken, Pennsylvania.
- ASTM C 31 (2012). “Standard Practice for Making and Curing Concrete Test Specimens in the Field.” *American Society for Testing and Materials (ASTM) International*, West Conshohocken, Pennsylvania.
- ASTM C 39 (2012). “Standard Test Method for Compressive Strength of Cylindrical Concrete Specimens.” *American Society for Testing and Materials (ASTM) International*, West Conshohocken, Pennsylvania.
- ASTM C 78 (2010). “Standard Test Method for Flexural Strength of Concrete.” *American Society for Testing and Materials (ASTM) International*, West Conshohocken, Pennsylvania.
- ASTM C 143 (2012). “Standard Test Method for Slump of Hydraulic-Cement Concrete.” *American Society for Testing and Materials (ASTM) International*, West Conshohocken, Pennsylvania.
- ASTM C 231 (2010). “Standard Test Method for Air Content of Freshly Mixed Concrete by the Pressure Method.” *American Society for Testing and Materials (ASTM) International*, West Conshohocken, Pennsylvania.
- ASTM C 469 (2010). “Standard Test Method for Static Modulus of Elasticity and Poisson’s Ratio of Concrete in Compression.” *American Society for Testing and Materials (ASTM) International*, West Conshohocken, Pennsylvania.
- ASTM C 496 (2011). “Standard Test Method for Splitting Tensile Strength of Cylindrical Concrete Specimens.” *American Society for Testing and Materials (ASTM) International*, West Conshohocken, Pennsylvania.
- ASTM C 1610 (2010). “Standard Test Method for Static Segregation of Self-Consolidating Concrete using Column Technique.” *American Society for Testing and Materials (ASTM) International*, West Conshohocken, Pennsylvania.

- ASTM C 1611 (2009). "Standard Test Method for Slump Flow of Self-Consolidating Concrete." *American Society for Testing and Materials (ASTM) International*, West Conshohocken, Pennsylvania.
- ASTM C 1621 (2009). "Standard Test Method for Passing Ability of Self-Consolidating Concrete by J-Ring." *American Society for Testing and Materials (ASTM) International*, West Conshohocken, Pennsylvania.
- Baali, L. (2009). "Self-Consolidating Concrete for Precast, Prestressed Concrete Bridge Elements." Master's Thesis, McGill University, Montreal, Quebec.
- Bentz, E. (2000). "Sectional Analysis of Reinforced Concrete Members." Doctoral Dissertation, University of Toronto, Toronto, Ontario.
- Bentz, E. and Collins, M. (2000). Response 2000 [Software]. Available from: [www.ecf.utoronto.ca/~bentz/r2k.htm](http://www.ecf.utoronto.ca/~bentz/r2k.htm).
- Bhide, S. and Collins, M. (1989). Influence of axial tension on the shear capacity of reinforced concrete members. *ACI Structural Journal*, 86(5), 570-581.
- Brewe, J. and Myers, J. (2010). High strength self-consolidating concrete girders subjected to elevated compressive fiber stresses; part 1: Prestress loss and camber behavior. *PCI Journal*, 55(4), 59-77.
- Cervenka Consulting (2013). ATENA Engineering 3-D (v. 5.0.3) [Software]. Prague, Czech Republic. [www.cervenka.cz](http://www.cervenka.cz).
- Collins, M., Mitchell, P., Adebar, P., and Vecchio, F. (1996). A general shear design method. *ACI Structural Journal*, 93(1), 36-45.
- De Silva, S., Mutsuyoshi, H., and Witchukreangkrai, E. (2008). Evaluation of shear crack width in I-shaped prestressed reinforced concrete beams. *Journal of Advanced Concrete Technology* 6(3), 443-458.
- Domone, P. (2007). A review of hardened mechanical properties of self-compacting concrete. *Cement and Concrete Composites*, 29(1), 1-12.
- EFNARC (2005). "The European Guidelines for Self-Compacting Concrete." Retrieved from <http://www.efnarc.org> (Feb. 4. 2014).
- Elzanaty, A., Nilson, A., and Slate, F., (1987). Shear capacity of prestressed concrete beams using high-strength concrete. *ACI Structural Journal*, 83(2), 359-368.
- Elzanaty, A., Nilson, A. and Slate, F. (1985). *Shear-Critical High-Strength Concrete Beams* (Report 85-1). Cornell University, Ithaca, New York.

- EN206-1 (2000). "Concrete – Part 1: Specification, Performance, Production, and Conformity." *European Committee for Standardization*, Brussels, Belgium.
- Frosch, R. and Wolf, T. (2003). *Simplified Shear Design of Prestressed Concrete Members* (Report FHWA/IN/JTRP-2003/5). Purdue University, West Lafayette, Indiana.
- Garber, D., Gallardo, J., Deschenes, D., Dunkman, D., and Bayrack, O. (2013). *Effect of New Prestress Loss Estimates on Pretensioned Concrete Bridge Girder Design*, (Report FHWA/TX-12/0-6347-2). University of Texas at Austin, Austin, Texas.
- Haines, R. (2005). "Shear Testing of Prestressed High Performance Concrete Bridge Girders." Master's Thesis, Civil Engineering, Georgia Institute of Technology, Atlanta, Georgia.
- Hanna, K., Morcou, G., and Tadros, M. (2010). *Design Aids of NU I-Girders Bridges*, (Report SPR-P1(09)P322). University of Nebraska-Lincoln, Lincoln, Nebraska.
- Hartman, D., Breen, J., and Kreger, M. (1988). *Shear Capacity of High Strength Prestressed Concrete Girders* (Report FHWA/TX-88+381-2). University of Texas at Austin, Austin, Texas.
- Hassan, A., Hossain, K., and Lachemi, M. (2010). Strength, cracking and deflection performance of large-scale self-consolidating concrete beams subjected to shear failure. *Engineering Structures*, 32, 1262-1271.
- Hawkins, N., Kuchma, D., Mast, R., Marsh, M., and Reineck, K. (2005). *Simplified Shear Design of Structural Concrete Members* (NCHRP 549). Transportation Research Board, Washington, D.C.
- Hawkins, N. and Kuchma, D. (2007). *Application of LRFD Bridge Design Specifications to High-Strength Structural Concrete: Shear Provisions* (NCHRP 579). Transportation Research Board, Washington, D.C.
- Heckman, C. and Bayrak, O. (2008). *Effects of Increasing the Allowable Compressive stress at Release on the Shear Strength of Prestressed Concrete Girders* (Report FHWA/TX-09/0-5197-3). University of Texas at Austin, Austin, Texas.
- Kani, G. (1967). How safe are our large reinforced concrete beams? *ACI Journal*, 64 (3), 128-141.
- Khayat, K., and Mitchell, D. (2009). *Self-Consolidating Concrete for Precast, Prestressed Concrete Bridge Elements* (NCHRP 628). Transportation Research Board, Washington, D.C.

- Kim, Y., Hueste, M., Trejo, D. and Cline, D. (2010). Shear characteristics and design for high-strength self-consolidating concrete. *ASCE Journal of Structural Engineering*, 136 (8), 989-1000.
- Kim, Y. H. (2008). "Characterization of Self-Consolidating Concrete for the Design of Precast, Pretensioned Bridge Superstructure Elements." Doctoral Dissertation, Texas A&M University, College Station, Texas.
- Labib, E., Dhonde, H., Howser, R., Mo, Y., Hsu, T., and Ayoub, A. (2013). *Shear in High Strength Concrete Bridge Girders: Technical Report* (Report FHWA/TX-13/0-6152-2). University of Houston, Houston, Texas.
- Labonte, T. (2004). "Construction and Testing of AASHTO Type II Girders Using Self-Consolidating Concrete." Master's Thesis, Civil Engineering, University of Florida, Gainesville, Florida.
- Lachemi, M., Hossain, K., and Lambros, V. (2005). Shear resistance of self-consolidating concrete beams – experimental investigations. *Canadian Journal of Civil Engineering*, 32(6), 1103-1113.
- Lin, C. and Chen, J. (2012). Shear behavior of self-consolidating concrete beams. *ACI Structural Journal*, 109(3), 307-315.
- Long, W. and Khayat, K. (2011). Creep of prestressed self-consolidating concrete. *ACI Materials Journal*, 108(5), 476-484.
- Long, W., Khayat, K., and Hwang, S (2013). Mechanical properties of prestressed self-consolidating concrete. *Materials and Structures*, 46, 1473-1487.
- Martinez, S., Nilson, A. and Slate, F. (1984). *Spirally-Reinforced High-Strength Concrete Columns* (Report 82-10). Cornell University, Ithaca, New York.
- McSaveney, L., Khrapko, M., and Papworth, F. Self-Compacting Concrete Enhances Tauranga's New Harbour Link. Retrieved from <http://www.goldenbay.co.nz/mainmenu35/page163/Recent+Projects.html> (3 June 2014).
- McSaveney, L., Papworth, F., and Khrapko, M. (2011). Self compacting concrete for superior marine durability and sustainability. *Concrete in Australia*, 37(2), 59-64.
- Missouri Department of Transportation (MoDOT) (2011). "Engineering Policy Guide, Category 751 LRFD Bridge Design Guidelines." MoDOT, Jefferson City, Missouri.



- Myers, J. and Bloch, K. (2011) Accelerated Construction for Pedestrian Bridges: A Comparison between High Strength Concrete (HSC) and High-Strength Self-Consolidating Concrete (HS-SCC). *Design, Construction, Rehabilitation, and Maintenance of Bridges*: 129-136. doi: 10.1061/47630(409)17.
- Myers, J., and Carrasquillo, R. (1998). *Production and Quality Control of High Performance Concrete in Texas Bridge Structures* (Report 9-580/589-1). University of Texas at Austin, Austin, Texas.
- Myers, J., Volz, J., Sells, E., Porterfield, K., Looney, T., Tucker, B., & Holman, K. (2012). *Self-Consolidating Concrete (SCC) for Infrastructure Elements*, (Report cmr 13-003). Missouri University of Science and Technology, Rolla, Missouri.
- Nagle, T. and Kuchma, D. (2007). *Nontraditional Limitations on the Shear Capacity of Prestressed Concrete Girders* (Report NSEL-003). University of Illinois, Urbana-Champaign, Illinois.
- Nakamura, E., Avendano, A., and Bayrak, O. (2013). Shear database for prestressed concrete members. *ACI Structural Journal*, 100(6), 909-918.
- Nawy, E. (2009). *Prestressed Concrete: A Fundamental Approach*. Upper Saddle River, New Jersey: Pearson Education, Inc.
- Nilson, A. (1987). *Design of Prestressed Concrete*. Ithaca, New York: John Wiley and Sons.
- Okamura, H. and Ouchi, M. (2003). Self-compacting concrete. *Journal of Advanced Concrete Technology*, 1(1), 5-15.
- Ouchi, M., Nakamura, S., Osterberg, T., Hallberg, S., and Lwin, M. (2003). "Applications of Self-Compacting Concrete in Japan, Europe, and the United States." Federal Highway Administration. ISHPC.
- Pauw, A. (1960). Static modulus of elasticity of concrete as affected by density. *Journal of the American Concrete Institute*, 32(6), 769-687.
- Price, W. (1951). Factors influencing concrete strength. *Journal of the American Concrete Institute*, 22(6), 417-432.
- Reineck, K., Kuchma, D., Kim, K., and Marx, S. (2003). Shear database for reinforced concrete members without shear reinforcement. *ACI Structural Journal*, 100(2), 240-249.
- Runzell, B., Shield, C., and French C., (2007). *Shear Capacity of Prestressed Concrete Beams* (Report MN/RC 2007-47). University of Minnesota, Minneapolis, Minnesota.

- Schindler, A., Barnes, R., Roberts, J., and Rodriguez, S. (2007). Properties of self-consolidating concrete for prestressed members. *ACI Materials Journal*, 104(1), 53-61.
- Sells, E. (2012). "Self-Consolidating Concrete for Infrastructure Elements Shear Characterization." Master's Thesis, Civil Engineering, Missouri University of Science and Technology, Rolla, Missouri.
- Shahawy, M. A., and Batchelor, B. (1996). Shear behavior of full-scale prestressed concrete girders: comparison between AASHTO specifications and LRFD Code. *PCI Journal*, 41(3), 48-62.
- Takagi, Y., Umetsu, K., Taira, Y., and Mizuno, K. (2000). Shear resisting behavior of prestressed concrete beams with inner and external cables. *Transactions of the Japan Concrete Institute*, 22(3), 685-690.
- Teng, S., Kong, F. K., and Poh, S. P. (1998b). Shear strength of reinforced and prestressed concrete deep beams. *Proceedings of the Institution of Civil Engineers, Structures and Buildings*, 128(2), 112-143.
- Trejo, D., Hueste, M., Kim, Y., and Atahan, H. *Characterization of Self-Consolidating Concrete for Design of Precast Prestressed Bridge Girders (Report 0-5134-2)*. Texas A&M University, College Station, Texas.
- Vecchio, F. and Collins, M. (1986). The modified compression-field theory for reinforced concrete elements subjected to shear. *ACI Journal*, 83(2), 219-231.
- Wang, H., Qi, C., Farzam, H., & Turici, J. (2006). Interaction of materials used in concrete. *Concrete International*, 28(4), 47-52.
- Wight, K. and MacGregor, J. (6<sup>th</sup> ed.). (2009). *Reinforced Concrete Mechanics and Design*. Upper Saddle River, New Jersey: Pearson Education, Inc.

## VITA

Alexander Michael Griffin was born in Laguna Hills, California. Alex spent the majority of his childhood growing up in Chesterfield, Missouri, a suburb of Saint Louis, Missouri. His interest in his high school physics class led him to pursue a degree in Civil Engineering at Missouri University of Science and Technology (Missouri S&T).

Alex went on to attend Missouri S&T and was a member of the varsity swim team. He joined the Missouri S&T American Society of Civil Engineers student chapter as a freshman, obtaining the position of President in the spring of 2013, and was inducted into the civil engineering honor society, Chi Epsilon. After experiencing a taste of both the structural engineering and geotechnical engineering fields through summer internships, he aspired to become a structural engineer. In May of 2013, he graduated summa cum laude with a Bachelors of Science degree in Civil Engineering.

In the summer of 2013, Alex continued his education at Missouri S&T, later earning his Masters of Science degree in Civil Engineering with an emphasis in Structural Engineering in December of 2014. He chose to start his professional career at Burns and McDonnell in Kansas City, Missouri, and is very grateful for his time spent at Missouri S&T in Rolla, Missouri.

